Interfaces haptiques non fondées pour le guidage et le rendu d'interaction

Lisheng Kuang

COLLEGE DOCTORAL BRETAGNE
MATHS, TELECOMS
INFORMATIQUE, SIGNAL
SYSTEMES, ELECTRONIQUE

Université de Rennes

THÈSE DE DOCTORAT DE

L'UNIVERSITÉ DE RENNES

ÉCOLE DOCTORALE N° 601
Mathématiques, Télécommunications, Informatique, Signal, Systèmes, Électronique
Spécialité : *Automatique, Productique et Robotique*

Par
Lisheng KUANG

Ungrounded Haptic Interfaces for Guidance and Interaction Rendering

Thèse présentée et soutenue à Rennes, le 23-06-2023
Unité de recherche : IRISA

Rapporteurs avant soutenance :

Nathanaël JARRASSÉ — CR CNRS, Sorbonne Université, ISIR
Lorenzo MASIA — Professeur, Heidelberg University

Composition du Jury :

Président :	Marie BABEL	Professor, INSA Rennes, France
Examinateurs :	Christine CHEVALLEREAU	DR CNRS, LS2N Nantes, France
	Nathanaël JARRASSÉ	CR CNRS, Sorbonne Université, Paris, ISIR, France
	Lorenzo MASIA	Professeur, Heidelberg University, Germany
Dir. de thèse :	Claudio PACCHIEROTTI	CR CNRS, IRISA/Inria Rennes, France
Co-dir. de thèse :	Paolo ROBUFFO GIORDANO	DR CNRS, IRISA/Inria Rennes, France

Résumé en français

Le terme *"haptique"* provient du mot grec haptikós, qui signifie "capable de toucher". Depuis le siècle dernier, l'haptique est définie comme la science de la transmission et de l'interprétation de l'information par le sens du toucher. Elle étudie le mécanisme, en termes de neurosciences, de perception et de technologie, qui stimule les récepteurs tactiles intégrés dans notre peau pour susciter des sensations tactiles. L'interaction haptique a toujours été considérée comme une forme d'interaction importante, mais elle est souvent sous-étudiée et sous-exploitée : Dans la Chine ancienne, Confucius a décrit la sensation tactile et l'a associée à la valeur sociale : Depuis la Chine ancienne, où Confucius a décrit et associé la sensation tactile à la valeur sociale : "Contempler le bien et le poursuivre, comme si vous ne pouviez pas plonger la main dans l'eau bouillante", en passant par les années 1960, où le professeur Frank Geldard considérait le sens du toucher comme un sens de la communication important mais "négligé", jusqu'à la dernière décennie, où les technologies haptiques ont montré leur grande capacité à aider les humains à effectuer un large éventail de tâches d'exploration et de manipulation.

De nos jours, les applications potentielles de l'haptique augmentent à mesure que les technologies d'interaction jouent un rôle de plus en plus important dans la communication, la formation, le travail et le divertissement. L'haptique s'est déjà révélée très prometteuse dans l'industrie, l'éducation et les jeux, bien que son expressivité et sa facilité d'utilisation dans de nombreux dispositifs haptiques commerciaux soient encore limitées. En particulier, comme on s'y attendait, l'haptique a un impact considérable dans les domaines où le sens du toucher est essentiel pour la tâche et le scénario considérés (télémanipulation, palpation, prothèses), où les indices visuels ou auditifs peuvent être efficacement remplacés (navigation et communication mobile) et où le toucher peut augmenter l'immersivité de l'interaction (réalité virtuelle et augmentée, VR/AR).

Pour recréer la sensation de toucher des objets virtuels ou distants de manière convaincante, les technologies haptiques recréent artificiellement ces sensations en stimulant la partie cible du corps (par exemple, le bout du doigt, la paume de la main, le bras)

par l'intermédiaire de différents types d'effecteurs. Cette interaction médiatisée stimule les récepteurs tactiles intégrés dans notre peau, recréant ainsi la sensation de toucher les environnements cibles. Le retour d'information haptique est fourni à l'utilisateur humain par une combinaison de stimuli cutanés et kinesthésiques. Les sensations cutanées sont détectées par les mécanorécepteurs de la peau, ce qui permet à l'homme de reconnaître les propriétés locales des objets telles que la forme, les bords et la texture. Les sensations kinesthésiques, en revanche, fournissent à l'homme des informations sur la position et la vitesse des parties du corps voisines, ainsi que sur la force et le couple appliqués. Ces informations sont principalement perçues au moyen de récepteurs situés dans les muscles, la peau et les articulations. Les sensations haptiques peuvent donc être considérées comme une combinaison de stimulations cutanées et kinesthésiques transmises par la peau de l'utilisateur [1]. À cet égard, l'utilisation du retour d'information cutané a récemment fait l'objet d'une grande attention de la part des chercheurs qui cherchent une alternative à la substitution sensorielle du retour d'information de force standard dans la téléopération robotique [2]. En effet, il a été prouvé que la substitution d'un retour haptique complet (c'est-à-dire cutané et kinesthésique) par des sensations cutanées uniquement fournissait des sensations riches tout en garantissant la sécurité de la boucle de téléopération [1]. En général, il a été prouvé que les dispositifs de retour cutané fournissaient des informations riches dans un facteur de forme beaucoup plus compact et peu coûteux que les interfaces kinesthésiques plus populaires [3], ce qui ouvre la voie à l'utilisation de ces technologies dans des applications quotidiennes.

Les interfaces haptiques, c'est-à-dire les systèmes artificiels capables de fournir des sensations haptiques à un utilisateur humain, peuvent être classées dans de nombreuses catégories différentes, notamment le type de stimulation qu'elles fournissent, leur amplitude de mouvement, leur largeur de bande, leur force maximale, la partie du corps qu'elles ciblent, leur coût et leur mise à la terre. En ce qui nous concerne, il est particulièrement intéressant de classer les interfaces haptiques en fonction de leur mise à la terre. Les dispositifs haptiques mis à la terre sont des interfaces dont la base est fixée à un support externe, tel qu'un bureau ou une chaise ; en revanche, les dispositifs haptiques non mis à la terre sont des interfaces qui peuvent être portées ou tenues par l'utilisateur, sans attache ou support externe, tels que des gants, des bracelets, des poignées ou des gilets. Les dispositifs haptiques mis à la terre ont été utilisés pour un large éventail d'applications, de l'espace à la robotique chirurgicale, de la rééducation à la formation industrielle. Ils comprennent des systèmes haptiques commerciaux populaires tels que Virtuose (Haption,

FR), Omega.x (Force Dimension, CH), Falcon (Novint, USA) et la série Phantom (3D Systems, USA), mais aussi des objets tangibles auto-reconfigurables mis à la terre, des interfaces de type rencontre, des dispositifs à changement de forme et des systèmes haptiques de table. Des dispositifs haptiques non mis à la terre ont été mis au point pour restituer diverses sensations sur l'ensemble du corps, en fournissant des sensations haptiques kinesthésiques, de pression, d'étirement de la peau, de douceur et/ou vibratoires aux doigts, à la paume, à la main et au bras. Ces dispositifs permettent aux utilisateurs de se déplacer librement tout en recevant un retour haptique, ce qui les rend idéaux pour les applications de réalité virtuelle, la formation dans de grands environnements et les jeux. La diffusion des technologies de prototypage rapide a favorisé le développement de ces types de dispositifs, rendant le développement des technologies haptiques possible pour un large éventail de chercheurs et d'ingénieurs. Les dispositifs haptiques sans contact avec le sol présentent divers facteurs de forme, en fonction de la stimulation haptique requise et de la position du corps sur laquelle ils agissent. L'haptique sans contact avec le sol est un sujet récent et brûlant dans ce domaine. Elle a récemment suscité l'intérêt de la communauté internationale et de grandes entreprises. Par exemple, la conférence 2018 de l'IEEE Haptics Symposium sur l'haptique a consacré sa première journée à ce sujet, et Meta a organisé un atelier sur l'haptique sans contact avec le sol au cours de l'édition 2019 de l'IEEE World Haptics à Tokyo, au Japon. Le principal avantage de l'haptique sans contact avec le sol est bien sûr son facteur de forme et son coût réduits par rapport aux solutions avec contact avec le sol, une caractéristique qui ouvre la possibilité de s'engager facilement dans des interactions multi-points (ou multi-contacts) pour les activités quotidiennes. Avec de tels dispositifs, le retour haptique multipoint ne nécessite plus de systèmes encombrants et complexes, mais plutôt de multiples instances de dispositifs plus petits et plus simples répartis sur l'ensemble du corps de l'utilisateur.

Les limites et les défis

Il n'existe pas d'interface haptique "parfaite" ou "idéale", car chaque situation, tâche et environnement requiert un ensemble différent de caractéristiques. Par exemple, une interface peut bien rendre la courbure d'un objet, mais elle peut être un moins bon choix que d'autres si cette caractéristique n'est pas importante pour la tâche considérée. De même, la pertinence perceptuelle des sensations haptiques restituées par rapport à l'application en question doit également être prise en compte pour décider quels types de stimuli haptiques

sont les plus importants à transmettre. Indépendamment des caractéristiques spécifiques requises, chaque dispositif haptique ne peut généralement transmettre qu'un (petit) sous-ensemble du spectre complet des sensations haptiques, ce qui limite considérablement la gamme d'interactions qu'ils peuvent restituer ainsi que leur applicabilité dans de nombreux scénarios. En effet, comme la fourniture de différents types de signaux haptiques implique généralement des interfaces plus volumineuses (et plus coûteuses), il est rare de trouver des dispositifs haptiques capables de transmettre un large éventail de sensations haptiques [4]. Cette limitation est particulièrement gênante en réalité virtuelle (RV), où les capacités d'actionnement limitées du dispositif haptique utilisé ne doivent pas limiter les choix de conception du contenu virtuel. C'est pourquoi les approches modulaires et personnalisées, dans lesquelles il est facile de modifier, d'améliorer et d'adapter le système haptique pour répondre aux besoins du scénario, sont de plus en plus populaires [5]–[7].

L'une des principales caractéristiques des systèmes de retour haptique est qu'ils peuvent fournir plusieurs informations à la fois (par exemple, des sensations de contact de force/couple, des contraintes actives rigides/compliantes, des informations sur la présence de singularités, des limites de l'espace de travail et des zones dangereuses à éviter). Cela est possible car notre sens du toucher est réparti sur tout notre corps et est composé de différents récepteurs (kinesthésiques, tactiles/cutanés, thermiques). Les éléments d'information représentatifs comprennent les sensations de contact de force et de couple, les contacts rigides ou souples, la présence d'obstacles ou de zones dangereuses à éviter. Le même résultat ne peut être obtenu en utilisant, par exemple, la modalité visuelle ou audio. Cette caractéristique importante a fait du retour d'information haptique l'une des caractéristiques les plus attendues et les plus recherchées dans de nombreux domaines, y compris la robotique et la RV, promettant de fortes augmentations de performance dans un large éventail de scénarios - ce qui n'est toutefois pas le cas actuellement.

Malgré ces avantages avérés, les systèmes d'interaction actuels ne fournissent qu'un retour d'information haptique très limité. Pacchierotti [8] a identifié trois principaux obstacles qui bloquent (ou du moins ralentissent) l'adoption des technologies haptiques dans les technologies interactives et robotiques actuelles : (b1) la difficulté de concevoir des politiques de rendu haptique efficaces, viables et générales ; (b2) l'effet négatif du retour d'information kinesthésique au sol sur la sécurité du système ; (b3) le coût élevé et la complexité des consoles haptiques disponibles à l'heure actuelle.

Pour surmonter ces obstacles, dans le domaine de la robotique et de l'interaction homme-robot, la recherche sur l'haptique se concentre sur la perception du toucher, la conception

mécanique des interfaces haptiques, le contrôle et le rendu haptiques, et l'interaction avec les systèmes cyberphysiques. L'objectif général est de permettre à divers systèmes distants et cybernumériques de communiquer efficacement, intuitivement et confortablement avec leurs utilisateurs humains par le biais du sens du toucher. Je résume ci-dessous une série de défis scientifiques et technologiques que j'estime pertinents pour ce domaine.

* Perception haptique: il est important d'étudier comment le sens du toucher code et interprète les interactions environnementales, afin de comprendre quels éléments d'information tactile sont les plus pertinents pour l'application et l'interaction en question, ainsi que d'apprendre comment exploiter les effets multimodaux et illusoires pour susciter des sensations riches avec un matériel limité, par exemple avec un dispositif haptique non relié à la terre.
* Conception de systèmes haptiques: il est important de concevoir des dispositifs haptiques capables de fournir des sensations tactiles haptiques multisensorielles, diversifiées et distribuées dans un emballage petit et confortable, facile à adapter à l'évolution rapide des besoins des utilisateurs et de l'application considérée.
* Rendu: il est important de développer des algorithmes de rendu capables de combiner, de manière intuitive, la signification perceptuelle du retour d'information et leur congruence sémantique au cours de l'interaction.

Contributions de cette thèse

Cette thèse présente ma contribution au domaine de la conception et du rendu haptique, en rassemblant tous les travaux que j'ai réalisés dans le cadre de mon doctorat à l'IRISA et lors d'un séjour de six mois à l'université d'Aarhus.

Dans cette thèse, j'ai présenté le développement de plusieurs dispositifs haptiques non mis à la terre, capables de fournir divers retours haptiques pour l'interaction homme-robot et homme-environnement. Nous avons mené des études sur des sujets humains afin d'évaluer le confort, la facilité d'utilisation et l'efficacité des dispositifs, et d'identifier les domaines dans lesquels des améliorations peuvent être apportées. Nous avons évalué les dispositifs proposés afin de mesurer leur exactitude et leur précision et d'identifier leurs limites ou leurs faiblesses. Nous avons validé les conceptions pour une gamme assez large d'applications, en nous concentrant particulièrement sur le guidage de la navigation.

En particulier, l'une des premières contributions de cette thèse a été le développement d'un dispositif cutané portable non relié à la terre avec un retour d'information sur la

position et l'emplacement pour la navigation. Ce travail a présenté un dispositif 2-DoF portable (sur l'avant-bras, la main, le front) à étirement cutané pour la navigation en intérieur. Ce travail a contribué à l'étude sur l'interprétation des stimuli de guidage cutanés portables [9].

Une autre contribution a été le développement de dispositifs de la main avec des effecteurs finaux interchangeables, appliquant diverses sensations tactiles à la paume. Nous avons présenté le prototypage et le contrôle d'une structure exosquelette non fondée de 4-DoF pour la manipulation d'effecteurs finaux sur la paume. Nous avons évalué des effecteurs rigides, déformables, élastiques, en forme d'origami et à grain pour rendre la forme, la douceur et la dureté de divers objets dans des environnements virtuels. Ce travail est très prometteur pour améliorer la présence dans l'exploration spatiale, la détection d'objets, et améliorer l'expérience immersive et réaliste dans l'environnement virtuel.

En outre, nous avons présenté un ensemble de structures cylindriques changeant de forme pour fournir un retour d'information kinesthésique pendant le guidage des mouvements de la main, la téléopération bilatérale et les interactions de type rencontre [10].

Enfin, grâce à nos collaborateurs de l'université d'Aarhus, nous avons également étudié la relation entre l'entraînement à la motricité fine dans la RV, le retour haptique et l'excitation physiologique. Nous avons révélé que l'entraînement avec un retour d'information kinesthésique au sol entraînait un niveau d'excitation plus élevé que l'entraînement avec un retour d'information vibrotactile au sol, et que l'inclusion d'un retour d'information haptique présentait donc un potentiel pour l'entraînement des habiletés motrices dans la RV.

La thèse commence par un examen des dispositifs haptiques portables et portatifs non fixés au sol pour la navigation (chapitre 1) - présentant les travaux connexes, les limites et les défis du développement, de l'évaluation et de l'application des dispositifs. Nous concluons par une réflexion sur les caractéristiques de perception des parties du corps, de la tête à l'épaule, en passant par les bras, les doigts et jusqu'aux pieds. En outre, nous étudions l'application de divers retours haptiques (vibrotactile, étirement de la peau, kinesthésique et pression) pour générer des indices directionnels et restituer l'environnement. Après l'examen du chapitre 1, le chapitre 2 présente notre conception d'un dispositif cutané portable à étirement de la peau fournissant un retour d'information sur la position et l'emplacement pour la navigation. Le chapitre 3 présente l'ensemble des dispositifs kinesthésiques de changement de forme pour le guidage du mouvement, la téléopération bilatérale et l'interaction de type rencontre. Le chapitre 4 présente un dispositif portable

monté sur la paume de la main pour le rendu des sensations de contact, qui est ensuite étendu au chapitre 5 avec l'utilisation d'effecteurs terminaux interchangeables pour le rendu des courbures, de la texture et de la rigidité. Enfin, le chapitre 6 présente la conception d'une poignée vibrotactile et étudie la relation entre l'entraînement de la motricité fine dans la RV, le retour haptique et l'excitation physiologique.

Publications connexes

1. **L. Kuang**, F. Chinello, P. Robuffo Giordano, M. Marchal, C. Pacchierotti. "Haptic Mushroom: a 3-DoF shape-changing encounter-type haptic device with interchangeable end-effectors." *Proc. IEEE World Haptics Conference*, 2023.
   Video available at: https://youtu.be/vpC5s7-xXA8.
2. **L. Kuang**, M. Ferro, M. Malvezzi, D. Prattichizzo, P. Robuffo Giordano, F. Chinello, C. Pacchierotti. "A Wearable Haptic Device for the Hand with Interchangeable End-Effectors." *IEEE Transactions on Haptics*, 2023.
   Video available at: https://youtu.be/1rs0s9UN2fI.
3. **L. Kuang**, M. Malvezzi, M. Ferro, D. Prattichizzo, P. Robuffo Giordano, F. Chinello, C. Pacchierotti. "A 4-DoF Wearable Hand Device for Haptic Rendering of Surfaces and Edges." *Submitted to Elsevier Mechatronics*, 2023.
   Video available at: https://youtu.be/ZuB_JxwbB9s.
4. U. Radhakrishnan, **L. Kuang**, K. Koumaditis, F. Chinello, C. Pacchierotti. "Haptic Feedback, Performance and Arousal: A Comparison Study in an Immersive VR Motor Skill Training Task." *Submitted to IEEE Transactions on Haptics*, 2023.
   Video available at: https://youtu.be/qZ6fBP-poAs?t=106.
5. E. Bouzbib, **L. Kuang**, P. Robuffo Giordano, A. L´ecuyer, C. Pacchierotti, "Survey of Wearable Haptic Technologies for Navigation Guidance." *Submitted to IEEE Transactions on Haptics*, 2023.
6. **L. Kuang**, M. Aggravi, P. Robuffo Giordano. "Wearable cutaneous device for applying position/location haptic feedback in navigation applications." *Proc. IEEE Haptics Symposium (HAPTICS)*, Santa Barbara, USA, 2022.
   Video available at: https://youtu.be/38BHsYCQ6uM.
7. **L. Kuang**, M. Marchal, P. Robuffo Giordano, C. Pacchierotti. "Rolling handle for hand motion guidance and teleoperation." *Short paper at Eurohaptics*, Hamburg,

Germany, 2022.
Video available at: https://youtu.be/vc6B-OOj590.

8. **L. Kuang**, M. Marchal, P. Robuffo Giordano, C. Pacchierotti. "Design of a 2-dof haptic device for motion guidance." *Proc. Eurohaptics*, Hamburg, Germany, 2022.
Video Video available at: https://youtu.be/vc6B-OOj590

Table of Contents

Acknowledgments

First and foremost, I would like to express my sincere appreciation to my supervisors, Dr. Claudio Pacchierotti and Dr. Paolo Robuffo Giordano, for their tremendous support throughout my research and training journey. Claudio has been shaping my academic path and personal growth as well as introducing me to the vibrant haptic community. His motivation and enthusiasm have guided me throughout the years, and I am truly grateful for his guidance, patience, and encouragement. Paolo provided us the protection under his umbrella within the Rainbow Team.

I was attracted by the robotics in the second year of my undergraduate, when in the China CNC Machine Tool Exhibition in Nanjing, I got the chance, for the first time, to see a robot, the orange-colored FANUC robotic arm, manipulating objects in a magical way. I was deeply shocked, and since that day, I made my mind to delve deeper into the world of robotics, a world of endless possibilities, hope, and ambitious goals unfolded ahead of me. Motivated by this passion, I made the decision to pursue control engineering for my master's degree. I designed a robotic hand (three-finger gripper) in my master thesis, from that I got to understand that doing research on robot is not like designing a Atlas robot of everything on you own from scratch, it's a team work of a group of researchers from multidisciplinary fields, such as mechanical engineering, computer science and electronics.

I do what I like but also like what I do. I did not expect that I would come to France and do a PhD here in Rennes, until the day I got in contact with Claudio. It was a bit hard from the beginning, and it became harder when my PhD started exactly the very first day of the Covid lockdown in March 2020. The vision is still in my mind that at that day Claudio, Marco Aggravi and I, in the cold and windy Bretagne weather in the Plages de Baud, discussing how to design a skin stretch device. But I was lucky, even in the lockdown, I still got companied by Claudio and Marco, we had meetings every week to keep me 'alive' and stay active, Claudio helped a lot not only in the study but also the daily life, Marco also played an important role in the advisory, teaching me a lot of robotic skills.

During my third year of PhD, I got the opportunity to visit Extended Reality and Robotics Lab at Aarhus University for a brief and significant period in the collaboration with Prof. Francesco Chinello and Prof. Konstantinos Koumaditis, whom I thank for the support and hospitality. I had a very happy time during the five months working with Francesco and Unnikrishnan Radhakrishnan, which reshaped my altitude to research and life. I am also happy to circulate the friendship with Francesco, he has contributed significantly to my work in the lab and to my PhD training, as well as my personal growth. The colleagues in Aarhus university are way more warm-hearted and welcoming than I expected and they irradiated the dark side of me induced by the language barriers living in France. Doing research (PhD) and being a student the same time, immersed in a real university, was a wonderful experience in Aarhus University. I Hereby also acknowledge the support of the Brittany region during my research visit at the Aarhus University. I would like to thank Prof. Monica Malvezzi for the collaboration through my PhD, the interdisciplinary nature of our projects enriched my knowledge of robotics and haptics.

A special thank you goes out to my lab mates at the Rainbow team, whose support and assistance have been instrumental during these years. They have made a difference in my research experience. I also express my appreciation to our collaborators in INSA Rennes, the group lead by Marie Babel gave me lots of inspiration in the work, Frédéric Marie and Thomas voisin did a great work in the fabrication of the mechanical parts for our haptic devices, they have made our work more efficient.

I would thank my parents who have encouraged me to pursue my academic aspirations. Additionally, I am grateful to my brothers and sister for taking care of our family, the limitations imposed by the Covid pandemic made it impossible for me to return to my hometown. Great thanks to my wife for the accompany and the incoming of our daughter, they all give me strength to march ahead.

Introduction

"Haptics" originates from the Greek word *haptikós*, meaning "able to touch". Since the last century, "haptics" has been defined as the science of transmitting and interpreting information through the sense of touch. It studies the mechanism, in terms of neuroscience, perception, and technology, that stimulates the tactile receptors embedded in our skin to elicit touch sensations. Haptic interaction has always been considered an important form of interaction, yet so often under-researched and under-exploited: From ancient China, where Confucius described and linked the touch sensation to social value: "*Contemplating good and pursuing it, as if you could not reach hand into boiling water*". Through the 1960s, when Professor Frank Geldard considered the sense of touch as a important yet "neglected sense of communication", to the last decade, where haptic technologies have shown their broad capability of enhancing humans in performing a wide range of exploration and manipulation tasks.

In modern times, the potential applications of haptics grows as interaction technologies play an increasingly prominent role in communication, training, work, and entertainment. Haptics has already shown significant promise in industry, education, and gaming, despite the fact that its expressiveness and usability in many commercial haptic devices are still limited. Especially, as expected, haptics show great impact in areas where the sense of touch is critical to the considered task and scenario (e.g., telemanipulation, palpation, prosthetics), where visual or auditory cues can be effectively replaced (e.g., navigation and mobile communication), and where touch can augment immersiveness in the interaction (e.g., Virtual and Augmented Reality, VR/AR).

To recreate the sensation of touching virtual or remote objects in a compelling manner, haptic technologies artificially recreate these sensations by stimulating the target part of the body (e.g., the fingertip, the palm, the arm) through different types of end-effectors. This mediated interaction stimulate the touch receptors embedded in our skin, recreating the sensation of touching the target environments. Haptic feedback is provided to the human user through a combination of cutaneous and kinesthetic stimuli. Cutaneous sensations

are detected by mechanoreceptors in the skin, enabling humans to recognize the local properties of objects such as shape, edges, and texture. Kinesthetic sensations, instead, provide humans with information about the position and velocity of neighboring body parts, as well as the applied force and torque. This information is mostly sensed by means of receptors in the muscles, skin, and joints. Haptic sensations can therefore be considered as a combination of cutaneous and kinesthetic stimulations mediated by the user's skin [1]. In this respect, the use of cutaneous feedback has recently received great attention from researchers looking for an alternative to sensory substitution of standard force feedback in robotic teleoperation [2], [11]. Indeed, substituting full haptic feedback (i.e., cutaneous and kinesthetic) with cutaneous-only sensations has been proven to provide rich sensations while guaranteeing the safety of the teleoperation loop [1], [12], [13]. In general, cutaneous feedback devices have been proven to provide rich information in a much more compact and inexpensive form factor with respect to more popular kinesthetic interfaces [3], [14], opening to the use of these technologies in everyday applications.

Haptic interfaces, i.e., artificial systems able to provide haptic sensations to a human user, can be categorized in many different ways, including the type of stimulation they provide, their range of motion, bandwidth, peak force, part of the body they target, cost, grounding. For our purposes, categorizing haptic interfaces according to their grounding is particularly relevant. Grounded haptic devices are those interfaces that have their based fixed to an external support, such as a desk or chair; on the other hand, ungrounded haptic devices are those interfaces that can be worn or held by the user, without any external attachment or support, such as gloves, bracelets, handles, or vests. Grounded haptic devices have been employed for a wide range of applications, from space to surgical robotics, from rehabilitation to industrial training. They include popular commercial haptic systems such as the Virtuose (Haption, FR), Omega.x (Force Dimension, CH), Falcon (Novint, USA) and the Phantom (3D Systems, USA) series, but also grounded self-reconfiguring tangibles, encounter-type interfaces, shape-changing devices, and table-top haptic systems. Ungrounded haptic devices have been developed for rendering diverse sensations across the body, providing kinesthetic, pressure, skin stretch, softness, and/or vibratory haptic sensations to the fingers, palm, hand, and arm. These devices allow users to move around freely while receiving haptic feedback, making them ideal for virtual reality applications, training in large environments, and gaming. The spread of fast prototyping technologies have boosted a great development of these types of devices, making the development of haptic technologies possible to a broad range of researchers and engineers. Ungrounded

haptic devices have diverse form factor, depending on the haptic stimulation required and the body position they act on. Ungrounded haptics is a recent and hot topic in the field. It has attracted the interest of the international community as well as that of large companies in the recent past. For example, the 2018 IEEE Haptics Symposium conference on haptics dedicated its first day to this very topic, and Meta has organized a workshop on wearable ungrounded haptics during the 2019 IEEE World Haptics in Tokyo, Japan. The primary advantage of ungrounded haptics is of course the reduced form factor and cost compared to grounded solutions, a feature that opens the possibility of easily engaging in multi-point (or multi-contact) interactions for everyday activities. With such devices, multi-point haptic feedback does not require cumbersome and complex systems anymore, but rather multiple instances of smaller and simpler devices, spread throughout the user's body.

Limitations and challenges

There exists no "perfect" or "ideal" haptic interface, as each situation, task, and environment requires a different set of features. For example, an interface might perform well at rendering an object's curvature, but it may be a worse choice than others if such a feature is not important for the considered task. Similarly, the perceptual relevance of the rendered haptic sensations with respect to the application at hand also needs to be considered for deciding which types of haptic stimuli are more important to convey. Regardless the specific features needed, each haptic device can usually convey a (small) subset of the full spectrum of haptic sensations, severely limiting the range of interactions they can render as well as their applicability in many scenarios. Indeed, as providing different types of haptic cues usually means bulkier (and more expensive) interfaces, it is rare to find haptic devices able of convey a large set of haptic sensations [4]. This limitation is particularly daunting in Virtual Reality (VR), where the limited actuation capabilities of the haptic device in use should not limit the design choices for the virtual content. For this reason, modular and personalized approaches, where it is easy to modify, upgrade, and adapt the haptic system to fit the scenario's needs are increasingly popular [5]–[7], [15].

One of the most prominent features of haptic feedback systems is that they can provide several pieces of information at once (e.g., force/torque contact sensations, stiff/compliant active constraints, information on the presence of singularities, workspace limitations,

and dangerous areas to avoid). This is possible as our sense of touch is spread across our body and it is composed of different receptors (kinesthetic, tactile/cutaneous, thermal). Representative pieces of information include force and torque contact sensations, stiff or compliant contacts, presence of obstacles or dangerous areas to avoid. The same result cannot be achieved using, e.g., the visual or audio modality. This important characteristic has made haptic feedback one of the most anticipated and wanted feature in many fields, including robotics and VR, promising steep performance increases in a wide range of scenarios – however, this is not currently the case.

Despite these well-proven benefits, current interaction systems provide very limited haptic feedback. Pacchierotti [8] identified three main barriers blocking (or at least slowing down) the adoption of haptic technologies in nowadays interactive and robotics technologies: (b1) the challenge of devising effective, viable, and general haptic rendering policies; (b2) the negative effect grounded kinesthetic feedback has on the safety of the system; (b3) the high cost and complexity of currently-available haptic-enabled consoles.

To overcome these barriers, within robotics and human-robot interaction, research on haptics focuses on touch perception, mechanical design of haptic interfaces, haptic control and rendering, and interaction with cyberphysical systems. The general intent is to enable diverse remote and cyberdigital systems to effectively, intuitively, and comfortably communicate with their human users through the sense of touch. Below I summarize a series of scientific and technological challenges that I believe relevant for the field.

* Haptic perception: it is relevant to study how the sense of touch encodes and interprets environmental interactions, so as to comprehend which pieces of tactile information are most relevant for the application and interaction at hand, as well as to learn how to exploit cross-modal and illusory effects to elicit rich sensations with limited hardware, e.g., with an ungrounded haptic device.
* Design of haptic systems: it is important to design haptic devices that can provide multisensory, diverse, and distributed tactile haptic sensations in a small and comfortable package, easy to adapt to the fast-changing needs of the users and the considered application.
* Rendering: it is important to develop rendering algorithms able to combine, in an intuitive manner, the perceptual meaning of the feedback with their semantic congruence during the interaction.

These are the objectives and insights that have driven my research in the past three years during my PhD studies.

Contributions of this thesis

This thesis presents my contribution to the field of haptic design and rendering, collecting all the work I have done toward my Ph.D. degree at IRISA and during a 6-months visit at Aarhus University.

In this thesis, I have presented the development of multiple ungrounded haptic devices, which are able to provide diverse haptic feedback for human-robot and human-environment interaction. We conducted human-subject studies, assessing the comfort, usability, and effectiveness of the devices, as well as identifying any areas where improvements can be made. We evaluated the proposed devices so as to measure their accuracy and precision, as well as identifying any limitations or weaknesses. We validated the designs for a rather broad range of applications, especially focusing on navigation guidance.

In particular, one of the first contributions of this thesis was the development of a wearable ungrounded cutaneous device with position/location feedback for navigation. This work presented a wearable (on the forearm, hand, forehead) skin stretch 2-DoF device for indoor navigation. This work contributed to the study on the interpretation of wearable cutaneous guidance stimuli [9].

Another contribution was the development of hand devices with interchangeable end-effectors, applying diverse touch sensations to the palm. We presented the prototyping and control of a 4-DoF ungrounded exoskeleton-like structure for manipulating end-effectors on the palm. We evaluated rigid, deformable, elastic, origami-shaped, and grained end-effectors in rendering shape, softness, and hardness of various objects in virtual environments. This work has great promise to improve presence in spatial exploration, objects detection, and enhance the immersive and realistic experience in virtual environment.

In addition, we presented a set of cylindrical shape changing structures for providing kinesthetic feedback during hand motion guidance, bilateral teleoperation, and encounter-type interactions [10], [16], [17].

Finally, thanks to our collaborators from Aarhus University, we also studied the relationship between fine motor skill training in VR, haptic feedback, and physiological arousal. We revealed that training with kinesthetic grounded feedback resulted in higher arousal compared to training with vibrotactile ungrounded feedback, and that the inclusion of haptic feedback thus holds potential for motor skill training in VR.

The thesis starts with a review on wearable and handheld ungrounded haptic devices for navigation (Chapter 1) – introducing the related works, limitations, and challenges

of the devices development, evaluation and applications. We conclude with some consideration about the perception characteristics of the body parts from head, down to the shoulder, arms, fingers, and all the way to the feet. In addition, we study the application of diverse haptic feedback (vibrotactile, skin stretch, kinesthetic, and pressure) for generating directional cues and rendering the environment. Following this review work in Chapter 1, Chapter 2 presents our design of a wearable skin stretch cutaneous device providing position/location feedback for navigation. Chapter 3 presents the set of kinesthetic shape-changing devices for motion guidance, bilateral teleoperation, and encounter-type interaction. Chapter 4 presents a wearable palmar-mounted device for contact sensation rendering[18], which is then extended in Chapter 5 with the use of interchangeable end-effectors for rendering curvatures, texture, and stiffness. Finally Chapter 6 presents the design of vibrotactile handle and investigates the relationship between fine motor skill training in VR, haptic feedback, and physiological arousal.

Related Publications

1. **L. Kuang**, F. Chinello, P. Robuffo Giordano, M. Marchal, C. Pacchierotti. "Haptic Mushroom: a 3-DoF shape-changing encounter-type haptic device with interchangeable end-effectors." *Proc. IEEE World Haptics Conference*, 2023.
   Video available at: https://youtu.be/vpC5s7-xXA8.
2. **L. Kuang**, M. Ferro, M. Malvezzi, D. Prattichizzo, P. Robuffo Giordano, F. Chinello, C. Pacchierotti. "A Wearable Haptic Device for the Hand with Interchangeable End-Effectors." *IEEE Transactions on Haptics*, 2023.
   Video available at: https://youtu.be/1rs0s9UN2fI.
3. **L. Kuang**, M. Malvezzi, M. Ferro, D. Prattichizzo, P. Robuffo Giordano, F. Chinello, C. Pacchierotti. "A 4-DoF Wearable Hand Device for Haptic Rendering of Surfaces and Edges." *Submitted to Elsevier Mechatronics*, 2023.
   Video available at: https://youtu.be/ZuB_JxwbB9s.
4. U. Radhakrishnan, **L. Kuang**, K. Koumaditis, F. Chinello, C. Pacchierotti. "Haptic Feedback, Performance and Arousal: A Comparison Study in an Immersive VR Motor Skill Training Task." *Submitted to IEEE Transactions on Haptics*, 2023.
   Video available at: https://youtu.be/qZ6fBP-poAs?t=106.
5. E. Bouzbib, **L. Kuang**, P. Robuffo Giordano, A. L´ecuyer, C. Pacchierotti, "Survey of Wearable Haptic Technologies for Navigation Guidance." *Submitted to IEEE*

Transactions on Haptics, 2023.

6. **L. Kuang**, M. Aggravi, P. Robuffo Giordano. "Wearable cutaneous device for applying position/location haptic feedback in navigation applications." *Proc. IEEE Haptics Symposium (HAPTICS)*, Santa Barbara, USA, 2022.
   Video available at: https://youtu.be/38BHsYCQ6uM.
7. **L. Kuang**, M. Marchal, P. Robuffo Giordano, C. Pacchierotti. "Rolling handle for hand motion guidance and teleoperation." *Short paper at Eurohaptics*, Hamburg, Germany, 2022.
   Video available at: https://youtu.be/vc6B-OOj590.
8. **L. Kuang**, M. Marchal, P. Robuffo Giordano, C. Pacchierotti. "Design of a 2-dof haptic device for motion guidance." *Proc. Eurohaptics*, Hamburg, Germany, 2022.
   Video Video available at: https://youtu.be/vc6B-OOj590

Chapter 1

Ungrounded Haptics for Navigation

Contents

1.1 Introduction

In this chapter, we provide an overview of wearable and handheld haptics interfaces designed for guidance and tested with subjects in both indoor and outdoor scenarios. These haptic devices instantiate physical contacts with users, either to confirm actions or to communicate a surrounding information - over a worn-type and in-hand interface. We focused our state of the article on this topic as it is the most important subject of research of my thesis.

We classify the existing literature through two dimensions: (1) the body part they stimulate and (2) the haptic stimulation they provide through their actuation technology. We then analyze the navigation guidance strategies they adopt for communicating with the user, to finally identify challenges and limitations reflected in their evaluation protocols. Compromises are to be drawn when eliciting navigation through wearable haptics, between acceptability, cognitive workload, usability and accuracy. Human-robot and human-machine interaction technologies have led to great improvements in our lives, enabling radically new ways to interact and exchange information with artificial machines in a natural and effective way. Yet, communicating information between humans and machines requires an effective mediating tool. In these regards, wearable and handheld haptic interfaces - haptic systems that users can literally "wear" and held in hand - are considered crucial [3], [19]

Wearable and handheld haptics enhance such interactions, enabling users to feel remote and virtual worlds as well as perform a wide variety of exploration and manipulation tasks.

They stimulate the human body (e.g. hands, arm, leg, head) to convey rich touch sensations, in an intuitive and understandable manner, delivered through small, lightweight, and often inexpensive packages [3]. These promising features justify the recent burst of available wearable devices communicating through haptics, which have successfully been employed in a wide range of scenarios, including robotic teleoperation [2], [20]–[22], virtual and augmented reality [23]–[28], motor rehabilitation and augmentation [29]–[34], surgical interventions [35]–[42], assistive robotics [43]–[45], communication [46]–[48], and navigation.

Wearable haptics have been proven particularly useful and effective in providing navigation guidance information, mostly thanks to their distributed and private rendering capabilities [3], [19]. Handheld interfaces also attracted the interest of industry and academia, where typical work are smartphones and smartwatches [19], [49] which are widely commercialized for both indoor and out door navigation, researchers in the academia explore other autonomous design with diverse mechanical structures, materials

and stimuli (vibrotactile, skin stretch, kinesthetic...) [19]. Haptic cues have been used to communicate turn-by-turn navigation [50], guidance in industrial teleoperation [20], [51]–[57], medicine [58], [59], rehabilitation, or assembly tasks [60], and support people with sensory disabilities [61].

In this chapter, we analyze the existing literature according to (1) the body part the wearable haptic devices and technologies stimulate, and (2) the type of haptic stimulation they provide. We then describe the navigation guidance strategies they adopt for communicating with the wearer, and finally discuss the challenges and limitations highlighted through wearable haptics for navigation guidance evaluation protocols.

This Chapter is a revised version of the works under revision as

* E. Bouzbib, **L. Kuang**, P. Robuffo Giordano, A. Lécuyer, C. Pacchierotti, "Survey of Wearable Haptic Technologies for Navigation Guidance." *Submitted to IEEE Transactions on Haptics*, 2023.

1.2 Definitions, Background and Scope

In this section, we first define *haptics*, *wearables*, *handhelds* and *navigation*. We provide background on the current work in these fields to then present our scope and highlight our motivations.

1.2.1 Definitions & Background

We provide some definitions and background on haptics, wearables, handhelds, navigation, and describe our scope at these fields' intersection.

1.2.1.1 Haptics - Perception and Experience

"Haptics" is a generic term used for both of the sense of touch and the science studying the sense of touch. Haptics, on a perception perspective, is usually gathering two types of cues: cutaneous - through the skin, and kinesthetic - through proprioception, muscles and tendons. Cutaneous and kinesthetic cues are actually enabling different types of perception. Indeed, each haptic feature (e.g. shape, weight etc) we perceive is dependent on the cell it stimulates, and its frequency.

Cutaneous sensations are elicited by receptors and corpuscles embedded in the skin, which are present in different densities and types throughout our bodies. On a perception

perspective, they enable us to identify local properties of the environment, such as the shape, temperature, and texture of an object we touch. Cutaneous perception for exploration and manipulation principally relies on measures of the location, intensity, direction, and timing of contact forces on the hands [62]–[64]. On the other hand, kinesthetic sensations originate from the muscles, joints, and skin. They enable us to identify the position and velocity of our limbs, as well as the forces they apply [62], [63]. Kinesthesia is indeed strictly intertwined with proprioception. We can define the former as the cognizance of joint movement and the latter as the awareness of our own joints positions [65].

Haptics extends from the design of external stimulation simulating haptic features to the experience it provides on a user perspective. The *Haptic Experience* was defined in these regards [66], discussing design parameters and usability requirements of a haptic stimulation as well as their potential impact on the experiential dimensions influencing the user experience.

With the growth of haptic technologies, many surveys in haptics are being drawn, from various perspectives. They have focused on haptic interaction techniques [67], haptic rendering technologies [68]–[70], or on specific applications such as medical/surgery training [71]–[73], virtual or augmented realities [74]–[76], telemanipulation [77], industry training [78], active walking [19], or a combination of them [79]. In this chapter, we only focus on two class of haptic technology: wearable and handheld haptics (see below), as they are the two types of haptic technologies I considered in my thesis.

1.2.1.2 Wearable Technologies

Wearables are a group of interfaces that can be worn onto the user's body. This class of devices includes flexible garments (e.g. gloves, t-shirts) and rigid accessories (e.g., watch, glasses, bracelet) [80]–[82]. They can be defined as "small electronic and mobile devices, or computers with wireless communications capability that are incorporated into gadgets, accessories, or clothes, which can be worn on the human body, or even invasive versions such as micro-chips or smart "tattoos" [83]. They are mainly used for body-tracking, e.g., in sports applications [84], rehabilitation/health monitoring [85], [86] or motion capture, and gained a global popularity as tools for the Internet of Things (IoT) [83]. A wearable therefore provides information about the users and/or its vicinity to an external display. In this chapter, we focus on *wearable haptics*: the wearable device itself communicates an information to the users through haptic cues, which includes notifications about the users, their physical environment, or a remote/virtual one. They are defined by Pacchierotti et

al. as haptic "interfaces capable of communicating with the human wearers during their interaction with the environment they share" [3].

Wearable haptic technologies have been presented and analyzed according to their field of application (e.g., sensory replacement [87], rehabilitation [88]), the technology they exploit (e.g., exoskeletons [89]), their form factor (e.g., gloves [90]), or the body part they stimulate (e.g., fingertip and hand [3]). In this chapter, we provide a classification of wearable haptics technologies according to the body part(s) they stimulate and the applied stimulation. However, we only focus on a single application: indoor/outdoor navigation.

1.2.1.3 Handheld Technologies

Handheld devices are peripherals or mobile connectivity devices that can be hold on the hand of the user, such as handles or controllers. A handheld haptic interface is therefore a display that can be hold by the user and, at the same time, provide haptic sensation, e.g., a vibrating handle providing directional cues. Handheld devices are interesting to study because of their portable format. They are also often considered more flexible than wearables, which need do-on do-off effort.

Handheld haptic devices stimulate the palm with mechanical stimuli such as skin stretch [91], vibration [92], [93], pressure and shape changing [94]–[99], thermal [100], and kinesthetic [101]–[103]. The pattern mapping from the mechanical stimuli to the directional cues varies from the mechanism the stimuli was provided. Pressure is well developed in generating linear/continuous pressure vectors to the fingertip and palm [94], while vibrotactile is more popular in generating discrete cues [104], for turn-by-turn navigation scenarios. Kinesthetic cues use the pseudo-attraction force technique [101] and asymmetric torques [102] to generate a force sensation and deliver directional information.

1.2.1.4 Navigation

Navigation is defined as a "goal-directed travel through space" [105]. It refers to one's ability to displace in a remote, virtual, or physical environment. The literature has often focused on the means to provide users with navigation capabilities in different environments. For instance, users in a virtual environment can be teleported, walk in place, or walk naturally [106]. Using these interaction techniques, users choose their arrival and displace themselves towards it. Nonetheless, in psychology, an entire field of research is devoted to navigation in itself, through spatial cognition, the *knowledge of oneself in relation to our surroundings* [107]. Taxonomies in this area classify navigation as either *locomotion* or

way-finding [108]. While these terms often refer to the same task outside of the spatial cognition field, they are to be differentiated as they do not rely on the same cognition maps on a user perception perspective. To understand them, three spatial representations are available: (a) landmarks, unique configurations of perceptual events; (b) routes, as a sequence of landmarks; (c) survey or map, as sequences of routes [109].

Locomotion Locomotion refers to "the guidance of oneself through space in response to **local** sensorimotor information in the immediate surrounds" (i.e. obstacle avoidance, moving towards a target) [105]. It therefore only relies on (a) and (b), i.e. the local landmarks in the visible space around self. It does not require an entire mental model or cognitive map of the environment.

Way-Finding Way-finding refers to "the planning and decision making that allows one to reach a destination not in the immediate sensory field" [105] (i.e. choosing the shortest route, orientating to non-local landmarks). Way-finding therefore relies on (a), (b) and (c); and requires memorizing the environment and creating a cognitive map of it. To reduce this cognitive load, way-finding can be aided (using signage, maps, navigation assistant) or directed, when the destination is specific [108].

Navigation Guidance In this chapter, the wording "navigation guidance" refers to the spatial cognition's **locomotion**: information provided to the users are in their direct vicinity. Navigation guidance "helps the user to find, locate, and reach a target without having to perform an exhaustive search within the space" [110]. More specifically, techniques providing aided way-finding giving information about the users' surroundings and requiring decision making (presence of stairs, doors, toilets etc. [111]); or unaided directed way-finding for target approximation or path finding (e.g. [112]) are not included in this chapter. Similarly, papers on guidance outside of the navigation field (rehabilitation [113], teleoperation/guided manipulation tasks [114]) are also out of the scope of this chapter.

This navigation guidance information can be provided through external tools (e.g., GPS) or be directly connected to the user. For instance, visually-impaired people are guided through their white cane, physically discovering their vicinity when moving along an unencumbered pathway.

Guidance can also be provided without conveying explicit feedback to the user. Users navigating an environment can be subject to visual illusions and be physically redirected

towards a destination without noticing a trajectory alteration [115]. This chapter addresses navigation guidance systems providing explicit feedback to the users.

1.2.2 Scope

This chapter focuses on **wearable and handheld haptics for navigation applications**, regardless of the type of information they provide to the wearer (e.g., trajectory tracking, obstacle avoidance). Technologies only providing visual feedback for navigation (such as non-vibrating glasses) are out of the scope of this chapter, as to wearable haptics that *could* be employed for navigation but have never suggested to be used in such an application (e.g., a vibrotactile bracelet used for VR contact rendering), or systems whose purpose is to only render some environment properties (e.g., a haptic watch rendering the map of an environment for non-navigational purposes). We analyze the state of the art in the following aspects: (1) a classification of wearable and handheld haptics for navigation through two dimensions: body area and stimulation type; (2) an overview of wearable haptics technologies for navigation; (3) an analysis of the strategies to provide navigation information; (4) a summary of current challenges and limitations highlighted from the devices' evaluation protocols.

1.3 Stimulated Body Parts

This section analyzes the body parts most often stimulated through wearable haptics for navigation . We describe them according to two dimensions: comfort and sensitivity (see Figure 1.1) . Comfort relates to the "wearability" of the device (i.e. weight, size, shape, ergonomics) [3], while sensitivity relates to its acuity and related expected performance for communicating guidance during navigation. Indeed, wearables have the benefit of being directly attached to the body in an often non-invasive, non-obtrusive, and convenient way. Wearable haptics usually rely on rigid controllers or PCBs that therefore need to be worn without compromising the users' comfort and freedom of movement [3]. For instance, a rigid link should not be placed on a body joint, as it would prevent or impair potential limb displacements and rotations.

Prior design guidelines for wearable haptics indicate that absolute characteristics (e.g., the weight and size of a device) might be misleading in measuring its "wearability" [3]. Instead, such characteristics should be evaluated considering the part of the body where

the interface is worn. As an example, a device too heavy for a fingertip might be perfectly comfortable if worn on the forearm.

Handheld haptic devices have a straightforward criteria that the sensitive part of the device, which is in contact with the volar part of the end (e.g., the palm, fingertips), should fit the dimension of the hand size. It is also necessary to shape the surface of the in-contact part to provide a comfortable usability.

In terms of sensitivity, and as per Penfield's homunculus [122], a given artificial haptic stimulation is interpreted differently depending on its location, according to density of mechanoreceptors in the skin [123]–[125].

There are many ways to measure and describe sensitivity, according to the target stimulation and information to convey. In general, we define an absolute perceptual threshold as the smallest amount of stimulus energy necessary to produce a sensation, and a differential perceptual threshold, or Just Noticeable Difference (JND), as the smallest amount of stimulus change necessary to achieve some criterion level of performance in a discrimination task [126]. For example, the vibrotactile absolute perceptual threshold (or vibrotactile sensitivity) can be defined as the lowest vibratory frequency/amplitude for which a vibration is perceived. Similarly, kinesthetic sensitivity can be defined as the minimal physical stimulus eliciting a kinesthetic perception, and its acuity defines the accuracy of the estimation of a limb position after having been moved by an external person [127]. Other representative examples for our purposes are the "tactile sensitivity", also referred to as *tactile acuity* or two-point threshold, which has been defined as the distance threshold for which users are able to discriminate a two-point stimulus [128]; the "error of localization" (or "point localization" [128], [129]), which is defined as the

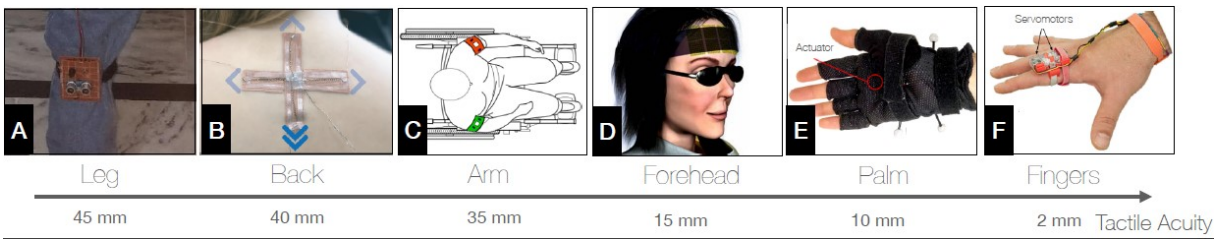

Figure 1.1 – Body areas for wearable haptics. A trade-off is often made between *comfort* and *sensitivity*. This continuum shows devices for navigation guidance - worn on various body parts according to their respective cutaneous sensitivity, or *acuity*. (A) Leg-worn device [116]; (B) Back wearable [117], (C) Armbands for wheelchair navigation aid [118]; (D) Forehead headband [119]; (E) Palm device integrated through a glove [120]; (F) Finger rings integrated through a glove [121].

separation between a reference point and what is identified by the user as the reference point [130]; and the tactile directional sensitivity (or *shift*), which is defined as the threshold distance for which users are able to tell the direction of a movement [130]. We note that the wording *acuity* in the common vocabulary usually refers to a resolution; though when used in haptics, it often refers to a spatial tactile sensitivity rather than other stimulation (kinesthetic, thermal etc.).

1.3.1 Head

The head is a human body part which assembles many receptors in charge of collecting important external information, including vision (eyes), smell (nose), hearing (ears), taste (mouth). It also includes lots of sensitive neurons distributed around the skin of the neck and cheeks. Most of the head parts (neck, ears, forehead, cheeks) also have a high sensitivity to thermal variations, which can be leveraged to provide further information to the user [131].

In this section, we gather systems stimulating the head, including the neck, ears, back of the head, forehead, mouth, and tongue.

Neck. We are already familiar with wearing headbands, necklaces, and earrings; yet, as most wearable haptic devices and technologies require to be in firm contact with the skin, neck devices are usually considered to be too uncomfortable or even dangerous [132]. Sensitivity-wise, the area of stimulation can easily be determined from a single point stimulus [133]. In this respect, the neck was shown to be one of the most effective body part to detect vibratory frequencies (absolute threshold of 0.72 Hz) [134] (see Figure 1.2.A); however, this refers to the back of the neck, as the front has a lesser tactile spatial acuity [133].

Ears. Most glasses-like haptic interfaces usually stimulate the user at the ears [136], [138], [139] and have the benefit to be able to also easily stimulate the user's vision (see Figure 1.2.B), which makes it promising for Augmented Reality applications. More generally, ears can be stimulated through earrings-like devices, which seem like a convenient location for wearable haptics [117], providing high sensitivity and comfort. One benefit is their symmetry around the users' head: an independent stimulation of two haptic-enabled earrings can easily indicate the direction to follow.

Back of the head. Many wearables are already available for covering the users' head, often attached to its back. In this regard, we see wearable haptic solutions for guidance with helmets [137], [140]–[142] (see Figure 1.2.C), wigs [143], hats [144], and caps [145],

[146], stimulating mostly the back of the head, in spite of its usually lesser sensitivity due to the presence of hair. This can be seen as a compromise, as the back of the head provides the largest head area and therefore can be stimulated to provide spatially more information.

Forehead. The forehead provides a convenient stimulation location as it guarantees an area of application spanning 360° [147]. Moreover, it is rarely employed for other purposes. Headbands such as [9], [119], [148], [149] are therefore quite popular for wearable haptic guidance applications exploiting on the head. Sensitivity-wise, the forehead has a tactile acuity of 15 mm [128] and a 10 mm directional sensitivity (see Figure 1.1.d). It has been indicated as the best body locus for pressure sensitivity [128], [129] and as the second best area for detecting vibratory frequencies [134].

Mouth. Within the head, the mouth, lips, and tongue are the most sensitive areas to thermal cues [150], yet mostly vibrations cues are currently explored. These areas also are the most sensitive parts of the head according to Penfield's homunculus [122]. They have been exploited by Tang et al. [151] for the delivery of guidance information to blind users. Yet, they are still not popular body areas to stimulate, as they are quite inaccessible and inconvenient: humans swallow their saliva, speak, or eat, and therefore cannot be often encumbered by a tongue device. Moreover, their respective areas are quite limited and do not allow to leverage their high sensitivity (e.g. the upper lip for instance displays a 5 mm tactile acuity [128]).

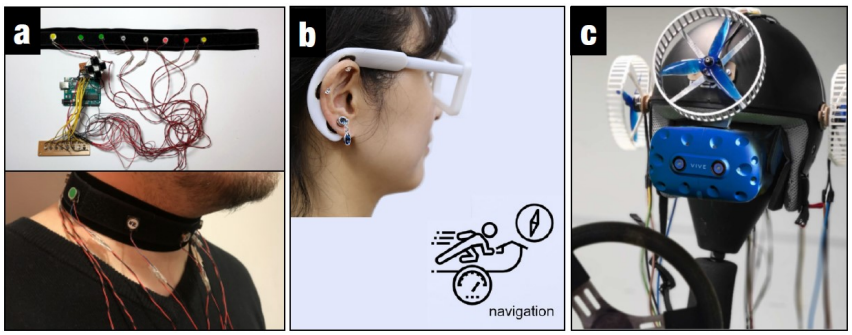

Figure 1.2 – Examples of wearable haptic systems for the head: (A) Neck collar [135], providing guidance through vibrotactile feedback; (B) Earring [136], associated with AR glasses, communicating guidance information through vibrotactile feedback; (C) Head helmet (back of the head and forehead) [137], providing guidance in VR through kinesthetic feedback.

1.3.2 Torso

The torso, defined as the central part of the body, including the front and the back sides, is a large and convenient area for wearable feedback, as the stimulation can occur in a garment such as a jacket or a belt [152]. Even though its sensitivity is quite limited compared to other high-sensitive body areas, Piateski and Jones [153] showed that the torso is capable of accommodating twice the information received at the fingertips thanks to its significantly larger area. Sensitivity-wise, the potential presence of fat makes it the worst body locus to detect vibratory frequencies (0.91 Hz) [134]. It features a 30 mm tactile acuity and a 10 mm directional sensitivity for the front, as well as 40 mm tactile acuity (see Figure 1.1.b) and over 5 mm directional sensitivity for the back [130], [154]. It also displays a 10 mm error of localization [130], similar on the belly and the back - which is almost twice as much as the forehead one. Yet, the torso is the second most sensitive body locus to pressure (after the forehead/face) [128], [129], therefore a large class of pressure-based stimulation exploits this spacious body area.

1.3.3 Arm

The arm is a very popular and comfortable area for a wearable, that can be integrated in sleeves [155] or arm bands [118], [156], [157]. A large amount of skin is available for stimulation, in various directions (proximal-distal - through its length, e.g. with a sleeve, or lateral-medial - through its circumference, e.g. with an arm band). Arms are also often used for wearing exoskeletons able to provide kinesthetic feedback to the elbow and/or shoulder. In this respect, kinesthetic sensitivity is dependent on both the limb displacement and its velocity. In fact, a movement over the shoulder would have an impact over the entire arm (upper arm, forearm and hand), as a movement on the elbow would directly impact the forearm (and ultimately the wrist would directly impact the hand). For instance, with the hypothesis of a straight 65-cm-long arm, a 1° rotation on the shoulder would cause a 23 mm displacement on a fingertip. The same rotation applied on the wrist joint would only move it by 5 mm, if we consider a hand of 15 cm. Second, regarding speed, the same displacement for a faster movement is detected more easily than a slower one. For instance, at a $10 - 80°/s$ velocity range, the kinesthetic sensitivity threshold is at 1°; for a $1.25°/s$ velocity it goes up to 8° [158].

In terms of tactile acuity, the global arm sensitivity falls in $35 - 40$ mm (see Figure 1.1.c) [128]. A *gap detection* task was also performed on this body area, using a two-*surface*

discrimination threshold - as opposed to two-*point* discrimination threshold (what we call tactile acuity here). For this task, the stimulus orientation was shown to have a significant impact on the threshold detection. Indeed, this threshold is above 20 mm for a proximal-distal stimulation (forearm: 23 mm, upper arm: 20.1 mm), and decreases up to approximately 10 mm for a lateral-medial one (forearm: 9.75 mm, upper arm: 12.21 mm) [159]. Frequency-wise, the vibratory threshold is 0.83 Hz [134].

No data was found regarding the upper arm and forearm directional sensitivities. Yet, using the previous information, we can already assume that a wearable can be easily placed on an arm band to provide a lateral-medial stimulation. A kinesthetic stimulation can also be sent to the upper arm for the entire arm to be stimulated, as seen in [160].

Similarly to the ears, the symmetry of the arms (and ultimately of the hands, wrists, legs, and feet) make them great candidate for guidance applications: a direction can be communicated to the appropriate limb whenever required.

1.3.4 Hands and Wrist

The wrist, hands, and fingers are the most stimulated body areas when considering wearable haptic interfaces. They regroup bracelets, watches [161], [162], gloves [120] (see Figure 1.1.e), rings [121] (see Figure 1.1.f), that however can potentially encumber and impair their use during important grasping and manipulation tasks.

Hands are our main mean of communicating with the environment: we most often explore and manipulate our surroundings using hands, when the fingertips and palm receive the sensations. They are the most represented body areas in Penfield's homunculus: as opposed to the back being represented by the same brain part, each finger has a dedicated brain part, discriminating their respective signals. The wrist has registered a vibratory frequency threshold of 0.83 Hz [134]. As opposed to the arm (see previous subsection), proximal-distal and lateral-medial stimuli are quite similar for gap detection, with ratios (proximal to lateral) around 1 [159]. The palm tactile acuity is around 10 mm and the fingers about $2-3$ mm, which make them the most sensitive areas of the entire body. The fingers also display a 0.1 mm directional sensitivity [130], which is therefore more than 40 times higher than the one on the back and makes it a really promising locus for guidance applications. The high acuity in the fingers is also practical as their small areas would not allow for a stimulation otherwise.

1.3.5 Legs and Feet

The lower trunk (legs and feet) is a usually comfortable area for wearables. They can be designed as leggings/leg bands [23], [116], [163], [164] (see Figure 1.1.a), ankle bracelets [165]–[167] or shoes [168]–[171]. When a human moves in the environment, these limbs are the most concerned and are therefore less sensitive to external stimuli compared to other body loci, i.e., the movement itself might partially mask the external stimulation provided by a wearable device. We should also consider that the calf, thigh, and gluteal region have a reduced tactile sensitivity ($42 - 45$ mm [128]) and are less sensitive to vibrations than other body areas [172].

Finally, the ankle and feet seem to have similar sensitivities as the wrist and hands, compared to their attached limb (respectively, legs and arms). The ankle and wrist absolute frequency detection thresholds are also similar (0.83 Hz). The tactile acuity of the feet is around 20 mm. It is the second best area for vibration sensitivity (after the hands) [172]. Similarly, as the fingers in the upper trunk, the toes' tactile acuity is the highest among the lower trunk [173]. Finally, thighs, glutes, and calves are less sensitive to temperature changes than soles and feet.

The advantage of using wearable haptics on this part of the body, despite its lesser sensitivity, is its comfort, its large area, its global symmetry on the body, and the fact that it is rarely used for other activities or devices.

1.3.6 Summary

This section analysed the different body parts most often used for interacting with haptic devices during navigation guidance, focusing on their comfort and sensitivity. Machida et al. [132] proposed these two dimensions to evaluate which body parts are the most convenient for communicating information through a haptic device. Results showed that, comfort-wise, the ears and wrists (e.g. earrings and watches) are the most appropriate locations to stimulate, while the neck and ankle (e.g. necklace, ankle bracelet) lack comfort from the user's perspective. Sensitivity-wise, signals are easier to perceive on the hands than on the chest or waist. It is also important to consider the function of each body part and how wearing a device can affect them. Indeed, some parts of the human body are usually covered and their skin is not so often exploited for touch (e.g. torso, legs), while others are meant to be left free and commonly employed in exploration and manipulation tasks (e.g. hands). For this reason, choosing the body part most suited for a

certain interface and task should consider multiple aspects, going well beyond the mere tactile acuity, also considering its comfort and wearability with respect to its everyday use.

	Comfort	Size	Tactile acuity (2-point stimulus)	Shift	Error of Localization	Vibratory Acuity	Kinesthetic Acuity	Pressure	Thermal
Head	- -	-	+	+	++	-	/	+++	+++
Torso/Back	++	+++	- - -	- - -	- - -	+	/	++	+++
Arm	+	++	+	+	- -	+	+++	+	++
Hands	-	- - -	+++	+++	+++	+++	+	++	+
Wrist	+	- -	++	+	++	++	++	++	+
Legs	- - -	+++	- -	/	- - -	- - -	+++	-	- -
Feet	- -	+	-	/	- -	++	+	- -	- - -

Table 1.1 – Subjective qualitative overview of relative characteristics of target body parts (+++: best, ---: worst, /: not found or not applicable). Information is notably extracted from [128], [129], [134], [150], [172], [173].

We summarize our quantitative analysis in Table 1.1, as a function of the considered parameters and with respect to each other (+++: best, ---: worst). This table aims at offering a subjective qualitative overview of the compromises to consider when designing a wearable technology for each part of the body. While we reviewed them considering our target application of navigation guidance, this information is useful for most designs of wearable haptics.

1.4 Stimulation Types and Actuation Technology

This section examines the different techniques for generating haptic stimuli during navigation guidance. We categorize what stimuli are generated, how they are exploited to communicate navigation guidance information, and which wearable haptics systems leverage them.

1.4.1 Kinesthetic

Exploiting kinesthetic feedback to generate directional cues involve applying external forces and/or torques to a joint or limb (see Section 1.2.2). Yet, proprioceptive sensations

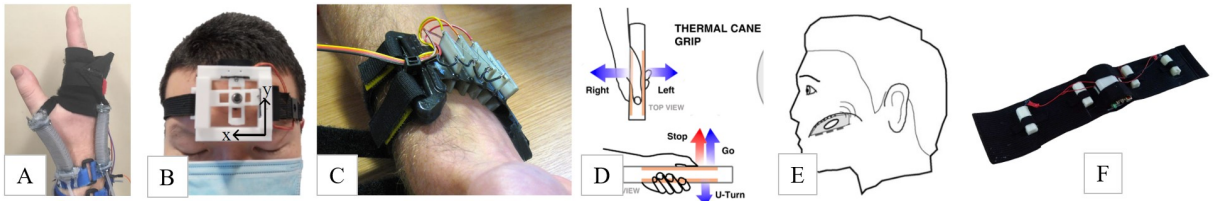

Figure 1.3 – Our second dimension classifies the stimulation types for wearable and handheld haptics. Seven types of haptic stimulation for navigation guidance exist in the literature. We also associate the stimulated body parts in this figure to illustrate their variety from our first dimension. (A) Kinesthetic feedback using *reverse-Pneumatic Artificial Muscles* on the wrist [174]; (B) Skin stretch waist-belt device guiding blinded users [9]; (C) Skin stroke device using brushes to wear on the arm [175]; (D) Thermal feedback provided directional cues on cane-grip for non-visual navigation [100]; (E) Electric signals sent to a mouth-piece worn on the tongue, to guide blind users [151]; (F) Vibrations on the bracelet to provide guidance [176].

can also be elicited by locally deforming the skin around the joints, as it replicates a joint deformation caused by a limb displacement [177]–[179].

A kinesthetic stimulation relies on muscles and tendons configurations, and can take advantage of a "reconfiguration" to directly guide the users through their environment. For instance, lower-body *exoskeletons* can literally move the users' limbs to follow the target guidance trajectory [180]. A similar effect can be achieved by directly stimulating the muscles using *Electro Muscle Stimulation* (EMS). It consists of small electrodes attached to the users' skin, which generate an electric signal activating the users muscles to achieve a target motion [181], [182]. In these two techniques, users have thus no say in whether to follow the target direction or not. Their limbs are moved by the system to induce the wanted motion. This physical redirection approach is of course only available when wearing such systems on the lower trunk, e.g., actuating the users legs and feet through an exoskeleton to make them walk towards a target. Handheld haptic devices can use "pseudo-attraction force" technique to provide guidance information. It exploits the nonlinear relationship between perceived and physical acceleration to generate a force sensation [101], which can be then interpreted as, e.g., a direction to follow. Examples of handheld devices for this purpose are those of one hand [102] and two hands [103].

Kinesthetic feedback can also provide information to be interpreted. A promising approach consists of a haptic sleeve using *Pneumatic Artificial Muscles* (PAMs), to provide pronation, supination, and abduction guidance feedback [155]. The advantages of PAMs are their safety, light weight, and flexibility. Indeed, they can be easily integrated into a garment suitable for different limbs, generating large forces while providing an easily

interpretable guidance information. A PAM, or any other general pneumatic interface attached to a garment (e.g., [183]) can inflate on a side of a limb to indicate the direction to follow, though this inflation is tricky to fully achieve around joints such as the wrist. *Reversed PAMs* (rPAMs) are therefore often preferred on joints. They can be deflated to indicate the direction to follow [174] (see Figure 1.3.A).

1.4.2 Skin Stretch

Skin stretch feedback refers to the deformation of the skin caused by an end-effector moving over its surface. The movement causes no relative displacement within the contact area and hence creates shear and normal stimuli to the skin [3]. Skin stretch offers many possibilities but was also recognized as potentially painful for users [184]. We consider three types of skin stretch for wearable and handheld haptics, shear, pressure, and twist, which depend on the direction of the external force generated by the considered device. When the displacement of the stimulation is parallel to the contact surface, it generates shear force; when the displacement is normal to the skin, it generates pressure; when the applied force is twisted with respect to the normal direction of contact [185], [186], it generates a twist.

A common approach to provide skin stretch through shear forces is through *belt haptic devices*. They consist of an elastic belt fitted around a circular limb (e.g., waist [187], see Figure 1.3.B) and actuated through one or more motors. The actuated belt moves around the limb delivering skin stretch sensations, which direction is exploited to guide users. The intensity of the stretch can be dynamically adjusted by controlling the motor position and speed, so as to map the appropriate target trajectory angle [188]. If two motors are available, the belt can provide skin stretch at different pressure skin levels, which can exploited for guidance in collision avoidance scenarios. In general, skin stretch does not require large stretches to provide rich and understandable stimuli, which makes it a very promising approach for small parts of the body, e.g., the fingers. For example, Gleeson et al. [189] placed the users' fingertips on a solid plate and performed guidance through micro displacements of the fingertips skin using a *shear tactor*, Koslover et al. [91] generated 2-axis directional cues on a horizontal plane into a handheld display. Pressure sensations induced through a skin stretch interface providing, e.g., tapping [190], are currently explored but still rarely used for navigation guidance applications. They can be instantiated through *solenoid actuators*, placed as an array in a wrist band, and generate discrete and binary skin hitting sensations, interpreted as "left" or "right" by the user [191];

or using *shape memory alloys* - SMAs, integrated in flexible ergonomic on-skin stickers [117]. Their contraction provides skin stretch, stretch-induced pressure and motion perception - used for guidance. Finally, twist sensations are not (yet) represented in wearable haptics for navigation guidance.

1.4.3 Skin Stroke

An alternative to the above skin stretch stimulation is providing light skin stroking, which can elicit "tactile apparent motion" effects. Discrete skin stroking signals can indeed be perceived as single smooth continuous signal across the skin [192], [193], "as if a rabbit were hopping on it" [194]. These discrete strokes can therefore communicate a continuous direction to the navigating user. Skin stroking was instantiated in [184] using *brushes* moving (anti-)clockwise, and integrated in a wearable bracelet. The signals are apparently well interpreted for assistance guidance [184] (see Figure 1.3.C) and wayfinding [195], on top of being comfortable and pleasant to receive.

1.4.4 Thermal

Thermal cues are not very popular in the literature for guidance applications. Indeed, they show many drawbacks for providing guidance information to the users. First, only a small range of temperatures ($24°C - 40°C$) is considered as appropriate, safe, and comfortable to send to the users [196] (see Figure 1.3.D). The thermal resolution of the skin also shows a lower resolution and a longer response time than most visual, audio, or mechanical sensations. Whenever stimulated through temperatures, the skin also requires to be reset back to a neutral state, which therefore induces some potential delays between signals and undermines the detection of new stimuli [197].

Thermal cues are often stimulated through *thermo-electric devices* (most often including Peltier modules), which temperature is a function of the electrical current. They can be integrated into headbands [198], wristbands [199], armbands [197], or earmuff-like devices [131], [200], and white cane [100] for guidance purposes. For example, Narumi et al. [200] designed an ear device providing location-dependent thermal information to move in an existing space, which was divided into several thermal fields. People were then guided through the space by distinguishing the different thermal areas. A literal heat-map can also be mapped to the available space, as a gradient of the users' distance to target [197]. A more direct approach consists in designing patterns of thermal modules to provide

guidance information using three stimuli variables: location (where the stimulus starts), number (of consecutive spatio-temporal stimuli) and direction ((counter-)clockwise stimuli) [196], [199]. Thermal stimulation is thus subtle to discriminate and its main advantage is its simple integration in wearable haptics, e.g., Peltier elements can be easily embedded in most end-effectors with very little footprint.

While LEDs or other techniques could be used to generate heat in wearable devices, Peltier elements are currently the most popular, as they guarantee a good efficiency with a relatively low voltage, and they ensure no burning sensations when touching the skin.

1.4.5 Electric (electrotactile)

In Section 1.4.1, we already discussed Electro-Muscle Stimulation. Apart from contracting the users' muscles and tendons, electric signals can also be sent through the users' skin so as to directly stimulate the nerve endings and provide tactile sensations. These systems are called *electrotactile interfaces* and provide low-level current pulses to the skin [201]. These interfaces rely on electrodes, which are often flexible and very thin, facilitating their integration in wearable haptics technologies. They can be used as collision avoidance notifiers, for instance to inform users of potential obstacles or landmarks [202], or directly send a direction to follow [203] (see Figure 1.3.E).

1.4.6 Vibratory

Vibrotactile cues are the most often employed to provide guidance information, mostly thanks to their cost-effectiveness and simplicity of implementation.

The human skin is sensitive to vibrotactile stimulation, at different frequencies or amplitudes depending on body loci (see Section 1.3), making vibrations easily noticeable and reliable perception-wise. This justifies why most wearable haptics devices use vibrations, no matter the body area or form factor. However, sustained and prolonged vibrations are known to be uncomfortable [118], [204]. The most popular actuation technologies among them are *Eccentric Rotating Mass* (ERM) [205], [206] (see Figure 1.3.F), where the mass is subject to a rotational force, *Linear Resonant Actuator* (LRA) [149], [207], where the mass is moved up and down along a line with a spring, *voice-coil actuators*, where a permanent magnet is suspended in an electromagnetic coil to produce vibrations [208] and *piezo-electric actuators*, which consist in beams deforming to vibrate against the users' skin [209]. Using the same principle, *electro-active polymers* can also provide vibrations

against the user's skin [210]. Indeed, these materials deform as a function of the received voltage; at an adequate frequency, they therefore provide a vibratory feedback [82]. Their flexible materials (e.g., electro-active textiles, dielectric elastomers [82]) seem adapted for wearable applications, though these have not been developed for guidance applications yet. Vibratory haptics in handheld devices is mainly found in the format of a smartphones [19], generating vibrations, e.g., whenever the device is pointed to the direction to follow, or activating the vibration motor towards the direction to follow [211].

1.4.7 Summary

This section described the different types of feedback for navigation guidance and the technologies enabling them.

Although each of them has its pros and cons with regard to navigation guidance, we can see some interesting and inspiring patterns. For example, compact and easy-to-use solutions such as ERM vibrators are largely the most popular actuation technology for the considered application. This is due to multiple reasons. First, they are inexpensive and trivial to use, which makes them straightforward to employ, even for novice designers. Second, their associated stimuli is familiar (e.g. smartphones notifications), noticeable and understandable. Third, they can be easily integrated into garments, for instance exploiting the symmetry of the human body and providing intuitive guidance cues. However, it is known that sustained vibrations become uncomfortable very quickly. Also, vibrotactile actuators need to be spaced out to be recognizable, preventing their use for navigation guidance in smaller parts of the body. In this respect, skin stretch and skin stroke devices seem very promising, as they need little space to convey rich information, they are not as complicated and cumbersome as, e.g., kinesthetic exoskeletons, and they are faster to react and convey changes in the stimulation than, e.g., thermo-electric devices. However, to provide effective information, skin stretch and stroke devices need to be well fastened to the body, which can make them uncomfortable to wear in some areas, especially for prolonged times. This aspect is also relevant for electrotactile interfaces, where small changes in the position of the electrode with respect to the skin can lead to significant changes in the delivered sensation [212]. This limitation complicates the integration of skin stretch, skin stroke, and electrotactile interfaces in garments or wearable structures. Indeed, the adaptation and customisation of wearable interfaces targeting panels of different users is an open problem in the community [5].

1.5 Navigation Guidance Strategies

We distinguish two methods for navigation guidance through wearable and handheld haptics: either the user is literally physically guided by the interface, or she receives information about her surroundings (e.g. landmarks, routes [105], [109]). In this latter case, stimulation can be either interpreted as a **where** notification (Section 1.5.1), and a **when** direction (Sections 1.5.2-1.5.3). As mentioned in [110], "guidance systems generally have two characteristics: 1) they orient the user's body movement, perhaps iteratively, to reach the target location, and 2) they indicate the target location". This section discusses the different stimulation strategies providing guidance navigation information. As per the Haptic Experience [66], we define the haptic signal *intensity* as the overall perceived strength of feedback and the *density* as its rate or frequency, i.e., the number of noticeable stimuli per a given time.

1.5.1 Directions

Navigation information provides directions to orient users, often coupled with some additional strategies described later in Sections 1.5.2 and 1.5.3. When providing a direction information, we rely on the *angle to the target trajectory* [188]. To interpret the direction correctly, we can exploit the *causality* feature [66] of the feedback, i.e., the user is required to relate the haptic feedback she receives from its source, identify the direction, and then follow it. Beyond causality, direction is also shown to be better interpreted using *density* than *intensity* [213] (see Fig. 1.4). In all cases, it is important to ensure that the considered directional sensations are understandable and perceived as different by the user, considering the tactile acuity of each part of the body with respect to the chosen type of stimulation (see Secs. 1.3 and 1.4).

1.5.1.1 Binary direction: 1D Direction

A binary direction can be seen as a 1D direction: it communicates a direction, and provides a *"sense"* (left or right). A straightforward strategy for providing directional guidance is to leverage the symmetry within the body (e.g., one actuator per arm, leg, or hand). For instance, a wearable device on each wrist can be worn to indicate left and right directions, and a simultaneous actuation of both of them indicates a "stop" signal [213]. Similarly, an array of four actuators can be designed, with binary cues to interpret (e.g. left/right, forward/backward [121], [168]), or absolute cardinal directions [195].

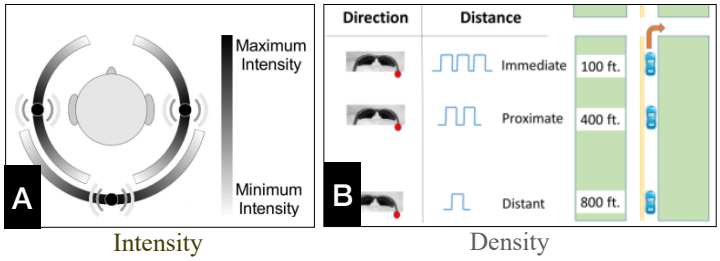

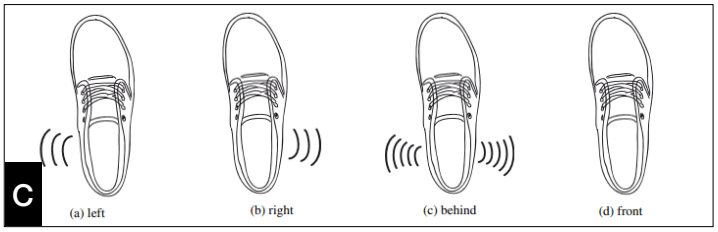

Figure 1.4 – Examples of haptic feedback parameters from providing strategies to convey navigation guidance, from [66]. (A) Intensity: the stimulation intensity indicates the direction to follow, e.g., [157]. (B) Density: the rate of stimuli per a given time indicates when to take a turn, e.g., [138]. (C) Causality: the user needs to identify the source of the feedback to choose the correct guidance direction, e.g., [168].

1.5.1.2 2D direction

A 2D direction navigation strategy provides more information than a binary direction one: it is more precise regarding the angles and trajectories to follow. It provides a more accurate *angle information* than a simple sense. A first method is to increase the number of stimulation points: it allows for less interpretation and more intuitiveness, e.g., it can directly communicate the direction to follow in the transverse plane of the human user.

The number of actuators and their spatial distance can be used to provide the directional information. For instance, and as a function of the local sensitivity, discrete or continuous signals can be provided [141]. Changing the distance between actuators has been proven to significantly affect the interpreted information: a smaller one conveyed the user with the sensation of a continuous stimulation, exploiting the "apparent motion" illusion - also called "funneling" [214], which was considered better for understanding directions to follow [141]. The sequences of actuation provide different types of directional information: arrays of actuators can be updated regularly to keep the user in the right direction (e.g., every 0.3 s

in [203]). Sequences can also indicate all of the wrong directions of an intersection [215]. These "directional interfaces" are defined as "aiding users to orient themselves to find a way-point during navigation tasks" [152].

1.5.1.3 3D direction

Finally, there exists techniques to provide 3-dimensional direction information, with a *height or depth* perception on top on a 2D angle. Spatial and dynamic haptic illusion can be obtained by varying the time and spatial sequence of the multi vibrations [148]. As opposed to previous techniques, the directions are updated regularly to guide the user in "real-time". A good synchronisation between actuators can also provide 3D directions (translation, rotation). For instance, simultaneously stimulating the fingers in opposite directions can indicate hand supination, pronation or flexion, and can be then exploited for navigation guidance [208].

1.5.2 Turn-by-Turn (GPS-like)

Guiding a user with a turn-by-turn strategy consists in providing a stimulation *when* she is required to take a turn, similarly to GPS guiding systems. In this case, the navigation information to modulate is the *delay* or *distance before turning*, in addition to the direction to turn to (see Section 1.5.1). The frontier between delay and distance is thin in navigation guidance applications: Kiss et al. [216] provide patterns to "turn far" and "turn near" (*distance information*) to eventually communicate to "turn now" (*delay information*).

Whether they rely on thermal [199] or vibratory cues [217]–[219], turn-by-turn information are represented as (a) a change of intensity in the stimulus [157], [217] or (b) a change of density [120], [138]. As an example of intensity change, a thermo-electric haptic device can correlate its temperature to the delay before making a turn [131], [197]. A density change is instantiated with symmetric vibrators in [138], where the frequency varies from 1 to 3 stimuli per 50 ms. With a higher density, the skin can consider the stimuli as continuous, as above the discrimination threshold (see Section 1.3).

1.5.3 Obstacle Avoidance

Differently from the previous strategy, a haptic system exploiting an obstacle avoidance strategy relies on the *distance to obstacles*. The user is free to choose her trajectory while avoiding obstacles on her way. This approach is similar to using a white cane: it provides

haptic feedback whenever a collision might occur [202], [220], [221]. This rationale is also developed in handheld device for hand motion guidance in Chapter 6 of this thesis, in which the vibrotactile stimulation indicates the the presence of obstacles.

Once again, the feedback can be altered in intensity or density – the closer the obstacle, the stronger or the more frequent the stimulus. This strategy is adapted for vibratory [140], [144], [222], [223] and skin stroke [224] stimuli. In the same regards, a continuous signal can provide a "stop" signal [213], [225], or indicates all the wrong directions to redirect the users and avoid a trajectory deviation [215], [226]. In the same line of observations, this strategy can also be adapted for *target attraction*, therefore relying on the *distance to target*.

1.6 Challenges & Limitations

Providing guidance through haptic signals seems straight-forward – a direction, delay, or obstacle is indicated and the user interprets it. Taking advantage of the variety of cues available for stimulation, this information can potentially be very rich. Cues can be intertwined and/or complex patterns can be drawn to provide specific information. Though, wearable and handheld haptics for navigation guidance still show limitations - which are usually expressed in the devices' evaluation protocols.

1.6.1 Conceptual User Expectations and Acceptability

Extensive interviews and surveys have been conducted to define (1) user expectations [227], (2) their prospective acceptability [228], as well as to evaluate (3) wearable or handheld devices and technology usability [144], [227] and (4) their requirements [229] for navigation guidance.

Using conceptual prototypes over a 600-participant panel, a survey showed that user expectations for guidance were preferably using visual (over 60%) and cartographic information (over 50%) than haptics (under 10%) [227]. Similarly, acceptability criteria included *utility*, *ease of use*, *ease of learning*, *safety*, *pleasantness* and *self-esteem* and also displayed significantly negative feedback compared to maps [227]. Conceptual vignettes evaluating sensory preferences were also evaluated using the UMUX questionnaire [230] and wearable acceptability questionnaire from [228] (see also Section 1.6.3). This acceptability is evaluated from an external point of view: the interviewed participants rate their perception

of user wearing a head-mounted wearable interface [228]. On a user perspective, they communicate whether the wearable or handheld device user seemed independent, needed help or the device, looked cool or nerdy. On an interaction perspective, they rate whether the interaction made them feel uncomfortable, if the user seemed awkward, normal, rude, distracting, or if the interaction seemed appropriate. On a device perspective, they evaluate whether the device seemed useful or unnecessary. Users once again preferred navigation guidance through auditory feedback than haptic [144].

Prior to designing a (wearable or handheld haptic)-device or technology, identifying user experience dimensions through interviews and experts opinions helps identifying requirements. In these regards, Gustafson et al. [229] defined that wearable haptic devices (1) should be hidden, (2) should not impede on senses working to full capacity, (3) should be easy to use, and (4) should leave the hands free. Another approach consists in identifying the device's principal functions and potential failures, in order to mitigate their risks and/or occurrences and thus optimize the user experience [231].

User expectations are important to consider as they enable the early identification of requirements and provide guidelines regarding the interfaces design. Indeed, even though haptics might not always seem like a promising and/or accepted approach for navigation guidance - we are more used to follow visual and auditory navigation cues than haptics - experimental evaluations highlight a great potential for this type of application. Also, although in questionnaires participants were often positive about the navigation aid, it remains to be seen whether they would actually use such devices on a regular basis [19].

1.6.2 Cognitive Load

On a user perspective, the signal provided by the haptic devices and technologies during navigation is required to be intuitive and easy to interpret. This requirement is usually reflected through cognition load quantification, for instance using the NASA TLX questionnaire [232]. This questionnaire evaluates mental, physical and temporal demands, performance, effort and frustration [232]. Haptics for guidance are shown to be cognitively less demanding than vision [139], [141], auditory feedback, or both [138], [144] and guidance through haptics is displayed as intuitive and effective [233].

This cognitive load is also expressed through time for completion, which is shown to be significantly faster with haptics cues compared to visual ones [139], but only to some extent. Indeed, the more signals to interpret, the more cognitive load – which needs to be addressed when giving guidance to a visually-impaired person [234]. A complex pattern

providing direction using vibration location and angle using vibration duration such as in [229] might lead to a higher cognitive load and/or a less intuitive understanding. Similarly, actuating two similar wristbands at the same time can be found redundant and produce more cognitive load and less comprehension of the guidance [121].

1.6.3 Usability

Another challenge regards the usability of wearable and handheld haptic systems for navigation, which is often reflected in the devices' evaluations. The most common protocol for usability is the SUS - *System Usability Scale* questionnaire [235], which was shrunk to four questions in the UMUX - *Usability Metric for User Experience* questionnaire [230].

Visual feedback for navigation guidance shows (non significant) better score using SUS than Haptic & Visual [138]. Similarly, using the SUS scale, auditory feedback was better perceived than haptics for providing directions to blindfolded participants [226]. Haptics was then suggested to assist users to keep straight directions and reduce their deviation while navigating. Similarly as the previous subsection, this usability is actually implementation-dependent. As an example, UMUX scores evaluating potential conceptual feedback modalities in [144] showed that audio feedback using headphones was perceived as the most usable. Yet, in practice, haptic feedback through vibrations and auditory feedback did not show a significant difference using SUS, and were both significantly more usable than visual feedback.

We indeed expect usability to significantly vary depending on the type of task considered, haptic feedback provided, and experience of the user, making the impact of the above results limited to the considered implementations.

1.6.4 Resolution & Accuracy

Even though haptics globally seems to reduce cognitive load for navigation guidance applications and is likely to be perceived as usable and viable, a compromise regarding resolution and accuracy error is also drawn [141], [144]. Indeed, when visual and auditory channels are available and free from other stimuli, accuracy seems to be higher than for haptic cues [138], [139], [218]. This might be justified as haptics need to be interpreted, and can often lead to more confusion in orientations, for instance. "Left and right" can be easily recognized (93% recognition rate for [208]), while "up/down" and "forward/backward" directions tend to be harder to interpret (70% recognition rate [208]). Absolute directions

are even trickier to communicate and ultimately interpret [152].

Some criticism needs to be added whilst analysing haptics accuracy results for navigation guidance. In fact, some evaluations are conducted with 2-Alternative Forced Choice, which can also increase the devices' results compared to asking the absolute perceived directions. Similarly, complex patterns might be tested with people sitting at the laboratory [139]. We can potentially imagine a drop in the devices performances considering the added cognitive load in an "in-the-field" experience, where participants are to be guided in real-time [236]. Finally, when multiple senses are compared, we have to consider the experiential designs of each condition: haptics might work better for guidance than an augmented reality map containing too many information, but not with a regular map [227]. The participants are also to be accounted for: wearable and handheld haptics for seeing, blindfolded or legally blind users might provide different results.

1.6.5 Discussion

Future deployment of wearable and handheld haptics for navigation guidance purposes will highly depend on the increase of its acceptability and usefulness. As an answer to a locomotion issue or physical disability, wearable and handheld haptics are indeed useful - though for global navigation guidance, it still is not perceived as the best modality to stimulate. Signals may seem too complicated to interpret - the same signal can for instance represent a "constraint", to force the user to follow its opposite direction as if a virtual wall was erected; or on the opposite, can represent the direction to follow. Even so, these directions are lacking referential. Indeed, spatial cognition heavily relies on referential to enable oneself's orientation and knowledge of a future direction to follow. For instance, a wearable haptic bracelet worn on the wrist, vibrating on its left, should indicate to turn left (or as mentioned before, turn right). Though, the wrist has many degrees of freedom, it could induce a change of orientation of the wearable device. In this configuration, will the user have to interpret the signal as an absolute direction or as related to the wrist relative position? This is also the same case for handheld haptic device: the directional cues from the device applied to the hand requires a short latency for the user to interpret and react. We could consider integrating wearable haptics for navigation guidance in body parts that could act like a compass, for instance on the torso or on the head. However, and as mentioned in our first dimension, comfort and sensitivity are to take into account. Moreover, sensitivity in the field - while navigating - has not been investigated yet: we might not perceive our phone vibrating in our pocket while walking or cycling. In the

same line of observations, current resolutions are still low. Real-life navigation does not only require binary directions, but most often many intersections or roundabouts where directions are to be communicated in a precise way. Globally, many compromises are to be drawn in order to design acceptable, useful, understandable, usable, accurate wearable and handheld haptics for navigation guidance. This enhancement in the deployment of wearable haptics for navigation guidance could be instantiated through the integration of more precepts from spatial cognition - to better answer to users requirement from their perspective.

1.7 Conclusions

In this introductory chapter, we provide the analysis of wearable and handheld haptic devices and technologies for navigation guidance according to two main dimensions: (1) their body area and (2) their associated stimulation and actuation technology. We then identify the main navigation guidance strategies using these haptic devices. Finally, we describe current challenges and potential limitations of wearable and handheld haptics in this context. These limitations are usually reflected through evaluation protocols: haptic cues seem to reduce cognitive load and are usable, but they are still not catering for future users expectations and increase error rates in guidance. We mainly reflect in this chapter how compromises need to be drawn when designing wearable and handheld haptics technology, notably for navigation guidance. The devices are to optimise the usability and sensitivity while understanding the requirements for specific users. Depending on the types of users and/or coupling with other multimodal interfaces, they need to communicate clear instructions without obstructing the cognitive workload or usability.

One step further, in Chapter 2, we present a prototype of a wearable cutaneous device able to provide position/location feedback for indoor navigation.

Chapter

2 Wearable Cutaneous Device for Position/location Haptic Feedback During Navigation

Contents

2.1 Introduction

This Chapter presents a 2-DoF wearable cutaneous device able to provide skin stretch and position/location haptic feedback in a 12×12 mm workspace. We evaluated the effectiveness of using location haptic feedback when the device is worn on the forehead, forearm, and back of the hand. In addition, we tested the device in a human navigation task. Users are asked to move along a target trajectory following the cutaneous location/position feedback provided by the device. Results show an average navigation error of 0.26 m, which is comparable to state-of-the-art vibrotactile guidance techniques using two vibrating armbands.

Two servomotors move a Cartesian-like structure, actuating a pin housing a small metallic sphere. The sphere can be either left free to rotate when the pin moves, providing location feedback about its absolute position, or kept fixed, providing skin stretch about its relative displacement. The device is worn using an elastic belt that can be easily adapted to many parts of the body. While the proposed device is also capable of providing skin stretch, we focus our evaluation on *position* feedback.

Wearable devices providing position feedback are quite rare. For example, Rossi et al. [237] developed a 1-D position-feedback device for the forearm, able to convey proprioceptive information about the aperture of a prosthetic hand, while Provancher et al. [238] developed a 2-D position-feedback device for the fingertip to render the contact location in telemanipulation and virtual reality applications. We present one the first wearable device capable of providing skin stretch and position feedback for guidance. The objective of this design is to study and explore the effectiveness of cutaneous stimuli in providing position/location feedback and for navigation guidance.

This Chapter is a revised version of the work published as

* **L. Kuang**, M. Aggravi, P. Robuffo Giordano. "Wearable cutaneous device for applying position/location haptic feedback in navigation applications." *Proc. IEEE Haptics Symposium (HAPTICS)*, Santa Barbara, USA, 2022.
  Video available at: https://youtu.be/38BHsYCQ6uM.

2.2 Device Design and Actuation

The CAD assembly of the device is shown in Fig. 2.1, while a detail of its actuated parts is shown in Fig. 2.4a. A video of the device is available at https://youtu.be/38BHsYCQ6uM.

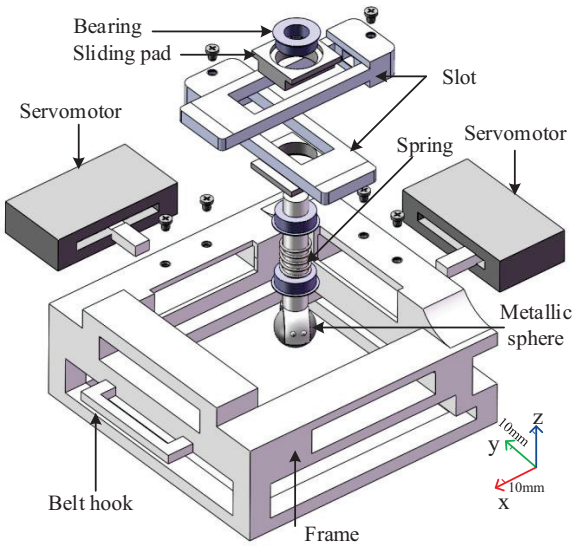

Figure 2.1 – Assembly of the 2-DoF wearable cutaneous device. A metallic sphere either provides position/location feedback or skin stretch in a 12×12 mm workspace. We tested the device at the forehead, forearm, and hand.

2.2.1 Mechanism and Structure

The cutaneous device is composed of a squared 60×60×30 mm ABS frame housing two linear servomotors that drive two intersecting guides. For our prototype, we used two VS-19 Linear Pico Servomotors (max. stall torque of 60 gf.cm at 3.7 VDC, yielding a theoretuca). A Maestro board (Pololu, USA) is in charge of controlling the motors. At the intersection of the guides, we fixed a cylindrical pin indenting the skin. It has a diameter of 6 mm and a length of 30 mm. A metallic sphere is housed at the end of the pin, in contact with the skin. When the pin moves, the sphere can be either left free to rotate or not. If it rotates freely on the skin, it provides position/location feedback about its absolute position; if it is blocked, it provides skin stretch about its relative motion. The behavior of the sphere, and thus the feedback provided, can be chosen by adjusting how strong the sphere is fastened to the pin. We also explored the possibility of employing a small electromagnet between the pin and the sphere to dynamically change the sphere's behavior without any manual intervention; however, this technique is not used in this work. Finally, a spring on the pin ensures that the sphere is always in contact with the skin, applying a constant pressure throughout the interaction.

2.2.2 Wearability

At two opposite sides of the ABS frame, we placed two hooks for fixing an elastic belt. In the following Sections, we evaluate the device around the forehead, forearm, and hand. However, the device can be easily worn in other parts of the body.

A thin layer of foam between the frame and the skin ensures a comfortable and firm fastening, enabling the user to focus on the feedback provided by the sphere. Figure 2.2 shows the device worn by a user. For attaining increased wearability, we can also directly attach the cutaneous device on the skin using a layer of adhesive silicone, without needing the elastic belt. We already used this technique for fixing a much heavier wearable haptic device on the back of a user's hand [28]. This approach enables to attach the device wherever needed, with very little impact on the user's mobility.

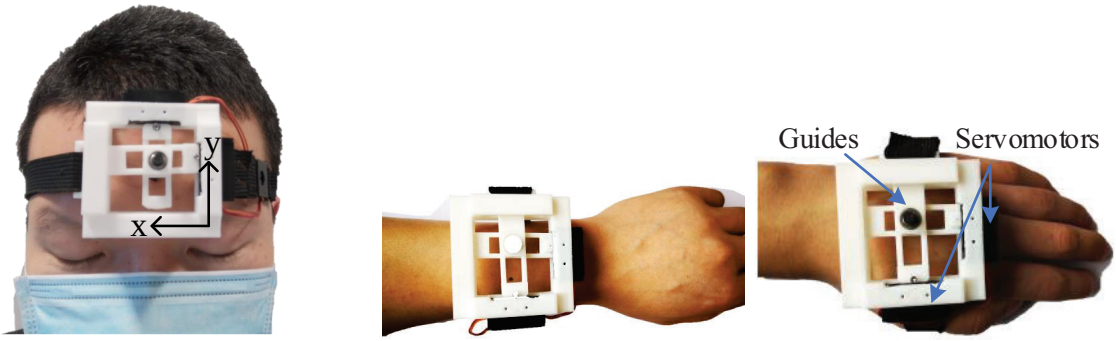

(a) Device on forehead **(b)** Device on forearm **(c)** Device on the hand

Figure 2.2 – The prototype of our wearable cutaneous device worn on the (a) forehead, (b) forearm, and (c) back of the hand.

2.3 Perceptual Evaluations

While research on skin stretch devices is well documented [239], [240], we focus on evaluating the effectiveness of our wearable cutaneous device in providing position/location feedback. We carried out two perceptual experiments. The first one evaluates the differential threshold for the location feedback (see Sec. 2.3.3), while the second one analyses the capability of recognizing different shapes/patterns (see Sec. 2.3.4). In both experiments, we tested the device when worn on the forehead, forearm, and back of the hand. As already discussed in Sec. 2.1, although the device is also capable of providing skin stretch, we focus our evaluation on position/location feedback.

2.3.1 Participants

Five subjects participated in the experiments (4 males, 1 females, age 27–34, right-handed). Two of them had previous experience with haptic interfaces. None of the participants reported any deficiencies in their haptic perception abilities. Participants received an information sheet with the experiment details and signed a consent form. The study has been approved by Inria's ethics committee (Saisine 513).

2.3.2 Setup

Users were asked to wear the wearable cutaneous device around the considered part of the body (forehead, forearm, or hand) in a comfortable yet firm way (see Sec. 2.2.2 for details). A picture of the device being worn is shown in Fig. 2.2. Then, the experimenter spent around two minutes ensuring that the device was worn correctly and that the end-effector contacted the skin. As the servomotors make some noise when actuated, users were also required to wear a pair of noise-cancelling headphones. Finally, the Maestro board commanding the servomotors was controlled by an external computer through ROS.

2.3.3 Differential Threshold or Just-Noticeable Difference (JND)

The Just-Noticeable Difference (JND) provides information about how different two displacements conveyed with our device need to be so as to be *perceived* as different. This information is important for correctly controlling the device's output and known the renderable range of information. It also reflects the fact that humans are usually more sensitive to changes in weak stimuli than they are to similar changes in stronger stimuli. E. Weber proposed the proportional law $JND = kI$, suggesting that the differential threshold increases with increasing intensity I of the stimulus. Constant k is thus referred to as "Weber's fraction".

In our experiment, subjects were asked to wear the device as indicated in Sec. 2.3.2 and shown in Fig. 2.2. We evaluated the JND for two directions of motion, vertical (y axis in Fig. 2.2a) and horizontal (x axis in Fig. 2.2a), using the method of limits adapted for finding JND values [241].

Subjects were required to tell the experimenter when the two provided stimuli felt different. We tested the JND at eleven standard/reference stimuli, from 1 mm to 11 mm, with a step-size of 0.1 mm (the minimum displacement the servomotors can actuate). Fig. 2.3 show the recorded JND and Weber's fraction for each standard stimuli and

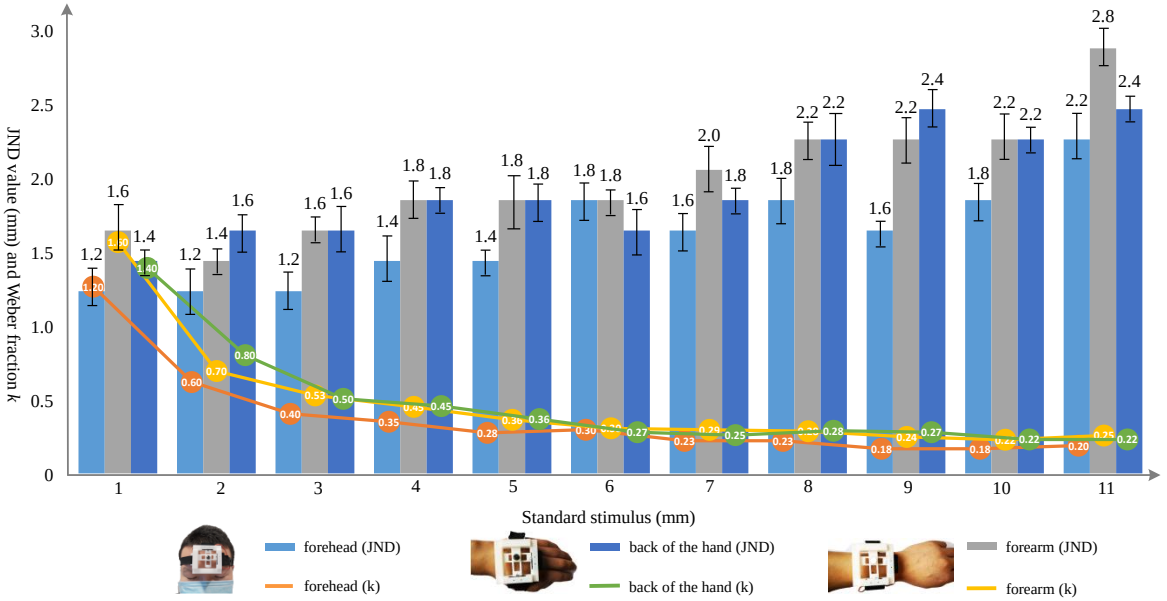

Figure 2.3 – Perceptual experiment: differential threshold. Results per each standard stimulus and considered location, considering the absolute JND value (mm) and the Weber fraction k.

considered location. Although further analysis is needed, we can already see that the forehead shows the highest recognition rates, followed by the forearm and the back of the hand, which shows little difference between each other. As expected, Weber fractions k are quite consistent across columns, except for the standard stimulus of 1 mm. We did not report separately the results of the two directions of motion as we did not find any relevant difference between them.

2.3.4 Shape Recognition

Our second experiment aimed at evaluating the capability of our device in rendering different shapes on the user's skin, once again when worn on the forehead, arm, and hand. As shown in Fig. 2.4(b)-(f), we considered five shapes: square, equilateral triangle, inverted equilateral triangle, vertical line, and horizontal line. We chose these shapes as they have edges, which are known to be salient features in haptic shape perception [242], and they could be used for navigation purposes, e.g., to indicate the user to stop, look up, look down, move up/down, move left/right, respectively. The pin moved at a speed of 12 mm/s. Subjects were again asked to wear the device as indicated in Sec. 2.3.2 and shown in Fig. 2.2. They were then given the possibility of trying/feeling each shape once before the beginning of the experiment. After that, subjects were presented with ten sequences

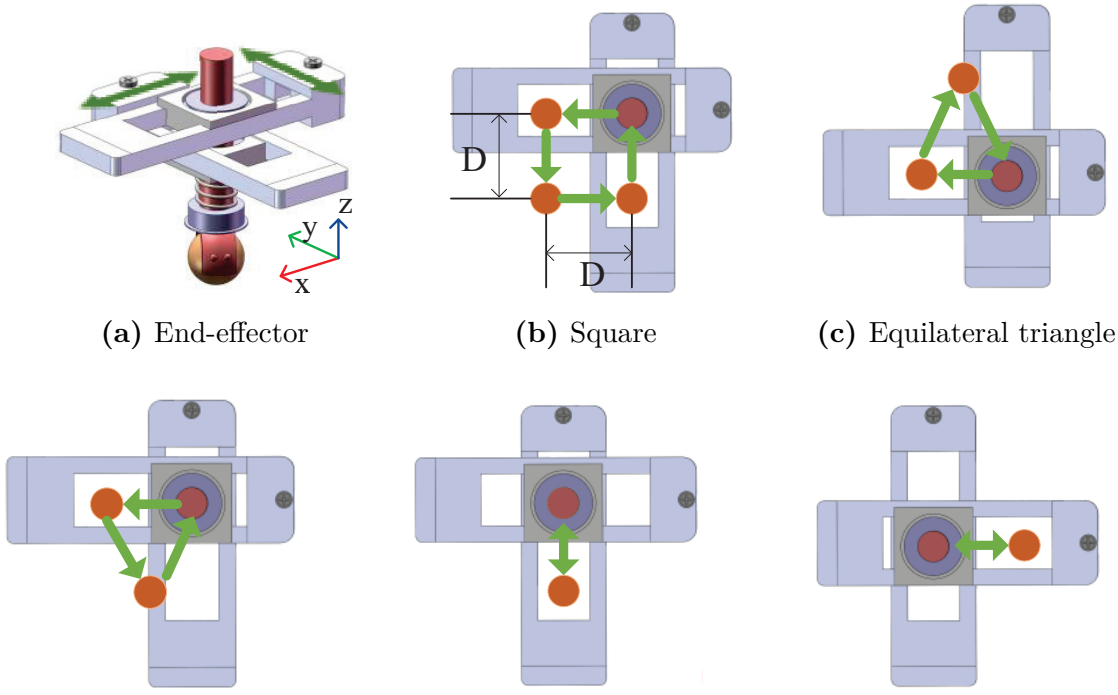

(a) End-effector **(b)** Square **(c)** Equilateral triangle

(d) Inverted equilateral triangle **(e)** Vertical line **(f)** Horizontal line

Figure 2.4 – Actuation principle. (a) The servomotors move two intersecting guides housing a cylindrical pin, that in turn houses a metallic sphere contacting the skin. The maximum displacement of each guide is D = 12 mm. (b)-(f) To evaluate the rendering capabilities of our device, we ask subjects to recognize five different shapes: (b) a square, (c) an equilateral triangle, (d) an inverted triangle, (e) a vertical line, and (f) a horizontal line.

of rendering, each sequence contains 15 rendering of shapes in a random order, i.e., each shape was repeated three times. After each sequence, subjects were asked to tell which shape they felt.

Figure 2.6 shows the results of this experiment for each shape and considered location. Confusion matrices indicate that subjects were able to well recognize the five shapes in all the considered situations. The lowest recognition rate, 62%, was registered when the equilateral triangle was rendered on the forehead, while the highest one, 88%, was registered when the horizontal line was rendered on the back of the forehead. As expected, more complex shapes (square and triangles) were harder to recognize than easier ones (lines).

Immediately after the experiment, participants were asked to fill in a six-item questionnaire using bipolar Likert-type 9-point scales, rating the following assertions:

1. (A1.1) It was comfortable to wear the device on the forehead.

2. (A1.2) It was comfortable to wear the device on the forearm.

3. (A1.3) It was comfortable to wear the device on the hand.

4. (A2.1) It was easy to identify the shapes when the device was worn on the forehead.

5. (A2.2) It was easy to identify the shapes when the device was worn on the forearm.

6. (A2.3) It was easy to identify the shapes when the device was worn on the hand.

A score of 9 indicated that the subjects fully agreed with the assertion, while a score of 1 indicated that they completely disagreed with it.

Fig. 2.5 shows the average evaluation of each question. A Friedman test showed a statistically significant difference between the means of the three locations in terms of effectiveness ($\chi^2(2) = 7.444$, $p = 0.024$, a $= 0.05$) but not in terms of comfort ($\chi^2(2) = 1.529$, $p > 0.05$, a $= 0.05$). The Friedman test is the non-parametric equivalent of the more popular repeated-measures ANOVA. The latter is not appropriate here since the dependent variable (i.e., the subjects' answer to the questionnaire) was measured at the ordinal level. Post hoc analysis with Bonferroni adjustments revealed a statistically significant difference in the perceived effectiveness when the device was worn on the forehead vs. forearm ($p = 0.034$).

In addition to this questionnaire, subjects were also asked which position of the device they preferred. Four out of six preferred when the device was placed on the forehead, one on the back of the hand, and one on the arm.

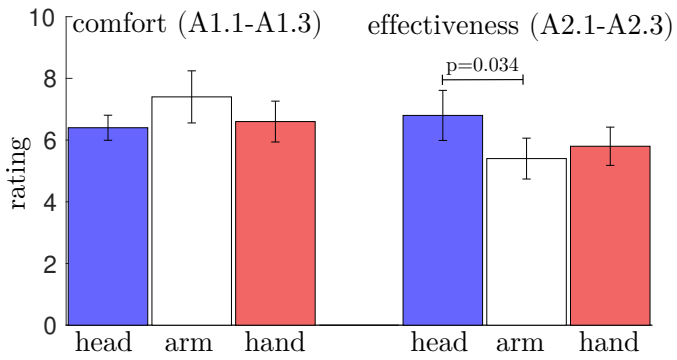

Figure 2.5 – Perceptual experiment: shape recognition. Mean and 95% confidence interval of the subjective ratings given by the subjects in the questionnaire, with noncontiguous Likert scale answer. They were asked to evaluate the comfort and effectiveness of wearing the device on the head, arm, and hand.

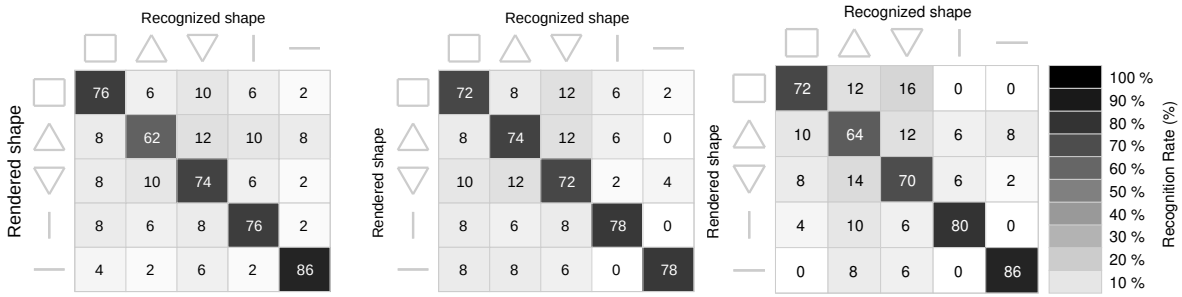

(a) Forehead **(b)** Forearm **(c)** Hand

Figure 2.6 – Perceptual experiment: shape recognition. Confusion matrices showing the recognition rates of five shapes (square, equilateral triangle, inverted equilateral triangle, vertical line, horizontal line) in the three tested location ((a) forehead, (b) forearm, (c) hand).

2.4 Navigation Use Case

After this perceptual evaluation, we tested the effectiveness of the proposed device in a human navigation task.

2.4.1 Experimental Setup

The navigation was carried out in an indoor 4×5 m room instrumented with twelve optical cameras (Vicon Motion Systems, UK) tracking the motion of the human users in real time. Such tracking system features little latency and it is suitable for the real-time tracking and guidance of human users, as already proven in [243], [244].

Participants wore the cutaneous device around the forehead in a comfortable yet firm way (see Sec. 2.2.2 for details). To avoid receiving any additional information about the environment, participants were also blindfolded and wearing headphones. We chose to wear the device on the forehead as it showed good performance and was the location most preferred by the subjects in Sec. 2.3. As before, the experimenter spent around two minutes ensuring that the device was worn correctly and that the end-effector contacted the skin. Users were required to wear a pair of noise-cancelling headphones. A computer, carried on a backpack by the user, controlled the device's Maestro board through ROS.

A video of the navigation experiment is available as supplemental material and at https://youtu.be/38BHsYCQ6uM. In the trial shown in the video, the subject does not wear the headphones so as to better show the device.

2.4.2 Subjects

Six subjects participated in this navigation experiment (4 males, 2 females, age 27–34, right-handed). Five of them had also participated in the shape recognition experiment. Two of them had previous experience with haptic interfaces. None of the participants reported any deficiencies in their haptic perception abilities.

2.4.3 Task and Methods

Inspired from our previous work [245], we considered three target paths, shown in red in Fig. 2.7. Participants were asked to wear the device on the forehead, keep their head pointed forward, and follow the provided guidance feedback as closely as possible. At the end of the indicated path, subjects were provided with three shape patterns in a randomized order, similarly to what we did in Sec. 2.3.4. The rendering of shapes at the end of the path can convey the user with information about additional tasks to carry, e.g., push a button, open a door, turn a valve. We decided to render the three most complex shapes for this use case, i.e., square, equilateral triangle, or inverted equilateral triangle. The area where subjects were provided with the target shape instead of guidance feedback is shown in light blue in Sec. 2.3.4 (an area of 1.4 m radius centered at the end of each path). While subjects knew they were going to receive a shape to identify at some point during the task, they did not know when it would happen. Each participant repeated the combined navigation/recognition task once per path, yielding to 18 navigation trials in total. Recorded paths are depicted in grey in Fig. 2.7. This task was inspired from industrial training tasks, where operators need to carry out a target movement and then execute a specific action, e.g., pushing a button, pulling a level, turning a knob.

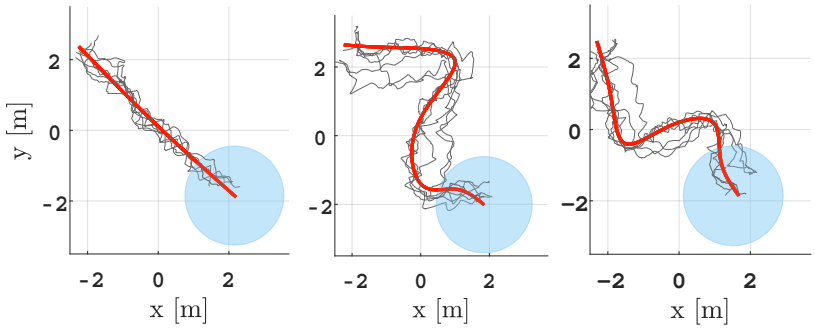

(a) path p_1 **(b)** path p_2 **(c)** path p_3

Figure 2.7 – Navigation use case. We considered three target paths (red), inspired from [245]. Six subjects carried out one navigation trial per path (grey).

We tried to use the simplest (i.e., fastest to render) and most intuitive sensations to follow, needing the least amount of training. Guidance feedback was conveyed through location/position feedback provided by the cutaneous device, indicating the direction toward the reference target path. Given the similarity between the human locomotion and the simplified kinematics of a unicycle robot [246], and considering that the user is moving forward, it is possible to indicate a desired rotation that would lead him or her to the desired path. This control approach has been described in [247] and has been used in [245], [248] for human navigation using vibrotactile haptic feedback. In our case, this rotation feedback was delivered through our position/location cutaneous system and it was proportional to the distance of the user from the path: if the person had to turn left, the pin end-effector would move the sphere toward the left, i.e., $P_{(x,y)} = [\,6 - \alpha,\ 6\,]^T$ with $0 \leq \alpha \leq 6$ proportional to the user error in following the path; conversely, if the person had to turn right, the pin would move toward the right, i.e., $P_{(x,y)} = [\,6 + \alpha,\ 6\,]^T$.

2.4.4 Results

As a measure of performance, we registered the error in following the target path, calculated as the average distance of the user from the path throughout the trial. We compare the performance of our device with a recent vibrotactile haptic guidance technique [245]. Aggravi et al. [245] evaluated the use of two vibrotactile armbands, one on each arm, to guide a human user along predefined paths very similar to the ones considered in this work. Each armband was composed of four vibrotactile motors positioned evenly around the arm. Figure 2.8 shows the results of the navigation experiment for each path, 1, 2, 3, and for each guidance methods, our position/location feedback technique and the state-of-the-art vibrotactile method of [245]. Figure 2.9 shows the recognition rate for the shape provided at the end of the path. Results show that, for all paths, the average walking speed in the navigation is 0.207 m/s, the navigation error was rather small (0.26 m in average) and comparable with that registered by Aggravi et al. [245]. However, with respect to [245], here we only use one device. Moreover, it is known that providing sustained vibrations becomes quickly uncomfortable [45], so other types of feedback might be preferable. Finally, the proposed device can be more easily worn wherever needed, especially in the version using adhesive silicon (see Sec. 2.2.2). All these considerations make the proposed navigation technique and device design rather promising.

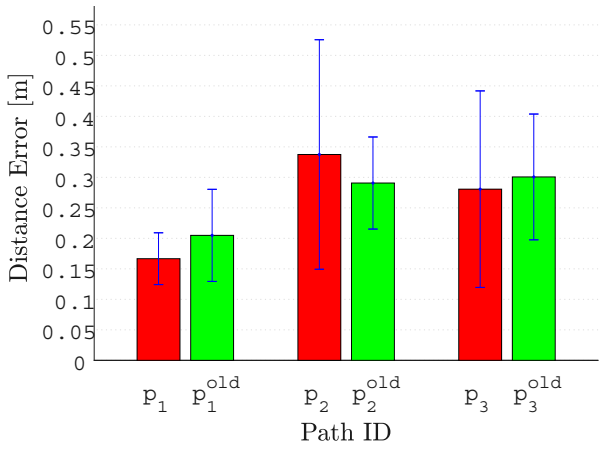

Figure 2.8 – Navigation use case. Mean and standard deviation of the error in following the target path for the three paths and two guidance methods: using position feedback provided by our device or vibrotactile feedback provided by two vibrotactile armbands from [245] (superscript "old").

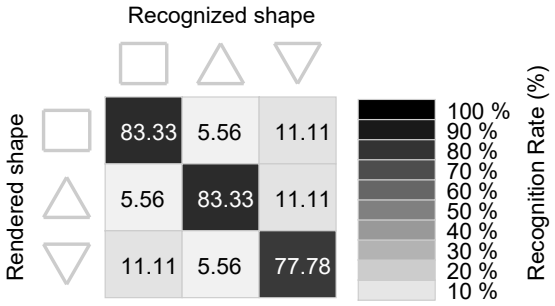

Figure 2.9 – Navigation use case. Recognition rate for the shape provided at the end of the path. Each shape was provided twice.

2.5 Discussion and Conclusions

This chapter presents a wearable cutaneous device able to apply 2D skin stretch and position/location haptic feedback on a workspace of 12×12 mm. Two linear servomotors actuate two intersecting guides housing a cylindrical pin at their intersection. By moving the guides, the motors can control the position of the pin within the workspace. At the end of the pin, in contact with the skin, we placed a metallic sphere, which can be either left free to rotate when the pin moves or not. In the first case, the sphere provides location feedback about its absolute position, while in the second case it provides skin stretch about its relative displacement. The device weighs 30 g for an overall encumbrance of 60×60×30 mm. It can be easily worn through an elastic band, similarly to an armband,

or using a layer of adhesive silicone, similarly to a gel patch. The device can be embedded in garments or other devices, such as a bike helmet.

This Chapter presents the device design, its actuation principle, and a series of experiments evaluating the position/location feedback it provides. First, we evaluate the differential threshold of the provided feedback when the device is worn on the forehead, forearm, and hand. The device showed the lowest JND (best performance) when worn on the forehead, but also the two other locations performed rather well, with a Weber fraction around 0.20. Then, we carried out a shape recognition experiment, where subjects were asked to recognize five shapes rendered by the device on the forehead, forearm, and hand. Recognition rates varied between 62% and 86%, well above the chance level. No striking difference between the three locations was observed, although further statistical analysis is needed. As expected, more complex shapes (square and the two triangles) were harder to recognize than simpler shapes (the two lines). Finally, we evaluate the performance of our device in guiding blindfolded users along three predefined paths. Users were asked to wear the device on the forehead and follow its guiding feedback while walking in an instrumented room.

Results show that users were able to follow the indicated paths rather well and that their performance is comparable with that registered in another work on human haptic guidance, where users were guided using two vibrotactile armbands. The results of our experimentation show that the proposed device and feedback is a viable approach for navigation, providing a more comfortable and flexible solution with respect to more popular vibrotactile solutions.

This study supports the development of using skin stretch device to apply position feedback to the hand, forehead and forearm, and motivates further application of wearable skin stretch device for indoor/outdoor navigation, both for commercial products and academia. From this work, we learnt that it was possible to render rich navigation information using skin stretch on the skin, even on the head, which can have practical applications in, e.g., guidance using helmets.

Chapter

3 Handles for Motion Guidance, Teleoperation, and Encounter-type Interaction

Contents

3.1 Introduction

In this Chapter, we aim to study the use of handheld devices (handles) with unidirectional and bilateral communication for human-robot interactions. Based on this, we presented three kinethestic devices which can be used as either grounded or ungrounded interfaces. In the experiments of these handles, we studied the application of (2-DoF) kinesthetic feedback on the hand for motion guidance, we evaluated the bilateral control implementation of the handle on a powered wheelchair, and we examined an encounter-type version of the handle with interchangeable end-effectors for virtual objects interactions. Indeed, haptic devices for motion guidance can guide the user using kinesthetic force feedack. In this respect, there are two main categories of kinesthetic devices: grounded and ungrounded. Grounded devices have their base placed on an external support, a representative device in this group is the Virtuose interface from Haption, which is often employed for teleoperation appications.

Kinesthetic haptics Kinesthetic haptic interfaces have been very popular in the past, for applications ranging from industrial to surgical robotics. Researchers have designed many different types of such interfaces, focusing on improving their, e.g., peak force, bandwidth, workspace, and/or price, according to the target field of application. In this respect, we can identify two main categories of kinesthetic interfaces: grounded and ungrounded. Grounded devices have their base placed on an external support, such as a table, while ungrounded devices have their base on the user's body [3]. Grounded kinesthetic devices include popular commercial kinesthetic systems such as the Virtuose (Haption, FR), Omega.x (Force Dimension, CH), Falcon (Novint Tech., USA) and the Phantom (Geomagic, 3D Systems, USA) series. More recently, in research, Jang et al. [249] presented a grounded isometric interaction device to induce whole-body interaction; Okui et al. [250] designed a delta-type 4-degrees-of-freedom (4-DoF) grounded haptic device actuated with a magnetorheological clutch, thus able to adjust its stiffness and viscosity; and Satler et al. [251] devised a portable interface composed of controlled wheel torques to render forces to a user handle placed on the top of the device.

On the other hand, ungrounded kinesthetic devices come in very different forms, spanning from hand-held devices for gaming and VR interaction [28], [252] or guidance [253], [254] to body-worn exoskeletons [7], [255].

Most common haptic devices are designed as robots of the impedance type, having small amounts of inertia and friction, enabling to freely and naturally move in space when

no force feedback is provided. In such systems, the user controls the position of the device that, in turn, provide a force feedback.

Grounded shape-changing haptics Actuated tangible user interfaces take advantage of our inherent spatial reasoning skills to haptically manipulate the environment around us. Among these interfaces, shape-changing devices are systems that allow for more general purpose shape change. Researchers have employed such systems for directly touching the (shape-changing) surface [256]–[258], manipulating tangible objects through said surface [259], and remotely interacting through gestures [260]. For example, Poupyrev et al. [257] proposed an electromechanical device consisting of a 2D array of movable light guides, whose height and color can be independently controlled to display images, shapes, and haptic sensations. Nakagaki et al. [258] presented a high-quality feedback 10×5 shape-changing display using linear actuators, able to both detect and apply dynamic force feedback at each pin. Follmer et al. [259] designed a shape display featuring dynamic affordances, constraints, and actuation of passive objects, using 30×30 actuated polystyrene pins in a 381×381 mm area. Blackshaw et al. [260] proposed an array of 120 actuated and instrumented pins, whose motion was controlled by the human user through a series of gestures captured by a depth camera installed above the array.

Encounter-type grounded haptics Encountered-type haptic systems convey haptic sensations by reactively positioning a (tangible) end-effector for the human user to encounter. This type of haptic display enables users to have unconstrained, free-hand contact with a tangible object provided by a robotic device, differently from more standard haptic devices in which users are required to always contact the end-effector. Mercado et al. [261] presented a comprehensive survey on this topic, proposing a taxonomy for classifying hardware types, as well as an analysis of haptic feedback most used in this context. For example, Mercado et al. [262] attached a cylindrical spinning tangible object to a robotic arm end-effector; the sensation of touching a virtual surface is achieved by coupling the movement of the robot with the sliding movement of the tangible object under the users' fingers. Similar recent approaches using a robotic arm to present a tangible prop to the user have been presented in [263]–[265]. Alternatively, Suzuki et al. [266] employed multiple tabletop-size ground mobile robots to recreate the sensation of interacting with a virtual environment. The mobile robots move on a table and can change their height and orientation to haptically render various surfaces and objects as the user contacts them. Similar recent approaches using ground mobile robots to present a tangible prop to the user have been presented in [267], [268].

The objective of this chapter is to study a parallel mechanism for a shape-changing haptic device, as well as the possibility of using flexible materials for encounter-type end-effectors. We also aim at exploring the performance of these designs in guidance, teleoperation, and encounter-type interaction in immersive virtual reality.

Sec. 3.2 presents the development of the handle for hand motion guidance. Sec. 3.3 then extends the the application scenario to bilateral guidance and teleoperation. Sec. 3.4 presents the shape-changing handle for encounter-type interactions.

This chapter is a revised version of the work published as

* **L. Kuang**, M. Marchal, P. Robuffo Giordano, C. Pacchierotti. "Rolling handle for hand motion guidance and teleoperation." *Short paper at Eurohaptics*, Hamburg, Germany, 2022. Video available at: https://youtu.be/38BHsYCQ6uM

* **L. Kuang**, M. Marchal, P. Robuffo Giordano, C. Pacchierotti. "Design of a 2-dof haptic device for motion guidance." *Regular paper at Eurohaptics*, Hamburg, Germany, 2022.

* **L. Kuang**, F. Chinello, P. Robuffo Giordano, M. Marchal, C. Pacchierotti. "Haptic Mushroom: a 3-DoF shape-changing encounter-type haptic device with interchangeable end-effectors." *Proc. IEEE World Haptics Conference*, 2023.

3.2 2-DoF Haptic Device for Motion Guidance

This section presents a 2-degrees-of-freedom (2-DoF) haptic device, which can be either used as a grounded or a hand-held device. It is composed of two platforms moving with respect to each other, actuated by two servomotors housed in one of structures. The device implements a rigid coupling mechanism between the two platforms, based on a threelegged 3-4R constrained parallel linkage, with the two servomotors actuating two of these legs. The device can apply position/kinesthetic haptic feedback to the user hand(s).

3.2.1 Device design and actuation

The proposed device is shown in Fig. 3.1. A video is available at https://youtu.be/vc6B-OOj590.

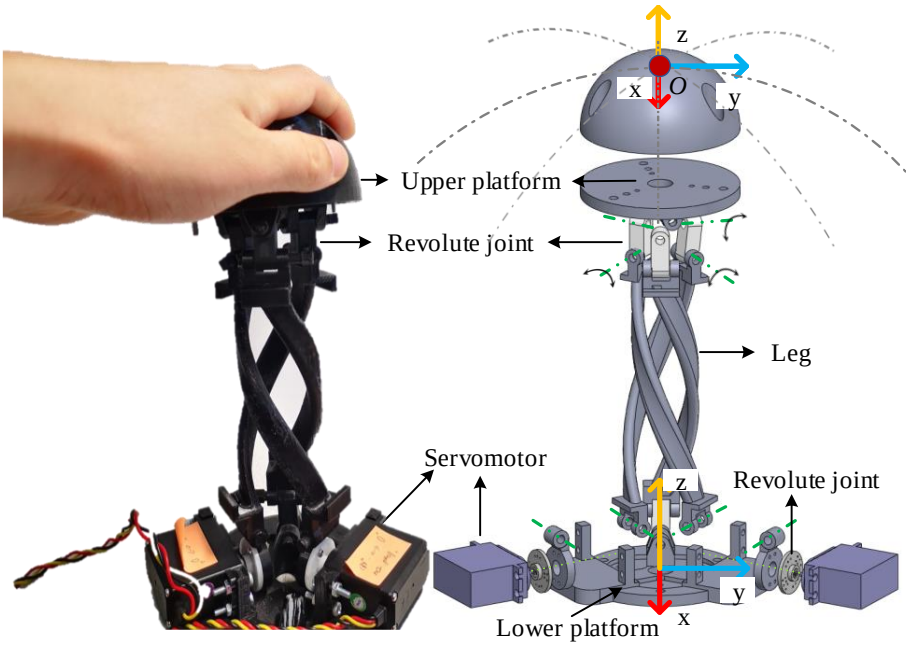

Figure 3.1 – The device is composed of two servo motors actuating an anti-parallelogram mechanism moving two platforms with respect to each other. (a) Device in its grounded configuration, with the lower platform secured to an external support and the user hand posed on the upper one. The device can be either used as a grounded interface, like in this figure and in our experiment of Sec. 3.2.3, or it can be held between the two hands (see the video for this configuration). (b) CAD of the device. The grey dotted lines show the surface of the sphere on which the upper platform moves. The spherical cap posed on the upper platform makes the interaction with the user hand more comfortable. Of course, it can be changed with other shapes according to the task at hand.

3.2.1.1 Mechanism and structure

The design of the proposed device is inspired by the principle of the anti-parallelogram mechanism [269], which consists of three identical supporting linkages forming an interlaced structure with no interference between them [270]. Compared to standard serial mechanisms, parallel mechanisms enable fast dynamics and high payload with relatively small size and low weight. Moreover, a large range of motion and uniform manipulability can be obtained by choosing appropriate dimensional parameters and actuation.

As shown in Fig. 3.1, the device consists of two platforms, a lower and an upper platforms, connected by three legs each having a spiral curved link. The device has dimensions of 15×15×23 cm and weighs 150 g. The two ends of each link are connected with two serial revolute joints to the platforms, forming a 3-4R coupling parallel mechanism which can move freely with 2 degrees of freedom, according to the orthogonal rolling motion

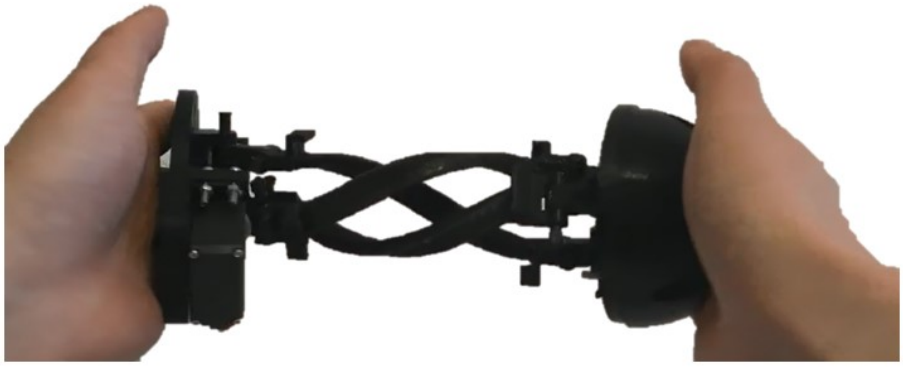

Figure 3.2 – The device in ungrounded (handheld) configuration.

on each leg [270]. If the lower platform is fixed on an external support (as in Fig. 3.1(a)), the motion of the upper platform is confined on the surface of a sphere centered in the center of the lower platform (see grey dotted lines in Fig. 3.1(b)). Two Hitech-625MG servo motors are attached to two legs on the lower platform. One revolute joint on the short linkage is mounted to the motor shaft, the other joint connects to the leg, as shown in Fig. 3.1. In this configuration, the two legs equipped with the servomotors have an active rotation on the lower joints and a passive rotation on the other three joints. By changing the actuation of the two motors, the upper platform can reach any point within its workspace (the surface of a sphere, as mentioned above). The graphical method using reciprocal screw system theory can be used [271] to analyze the mobility of the proposed parallel mechanism. The device can also be used in ungrounded (handheld) configuration, as shown in Fig. 3.2, two hands hold the two platforms of the device and receive the torque feedback.

3.2.2 Kinematics analysis

We study the kinematics of the device so as to evaluate the relationship between the motion of the servomotors and that of the upper platform with respect to the lower one. As illustrated in Figs. 3.1 and 3.3, three legs are regarded as individual open-chain manipulators. The connection points between the upper platform and legs 1, 2, 3 are defined as P_1, P_2, P_3, respectively, while the connection points between the lower platform and the legs is denoted by points B_1, B_2, B_3. Let us consider the device in its grounded configuration, with the base attached to an external support. The coordinate frames of the upper (mobile) and lower (static) platforms, $C_p(O_p - x_p y_p z_p)$ and $C_b(O_b - x_b y_b z_b)$,

are fixed on their geometric centers, O_p and O_b, respectively. The frames are defined as indicated in Figs. 3.1 and 3.3.

The plane where the z_b and z_p axes coexist is defined as the bending plane, which is always perpendicular to the surfaces of the two platforms. Here, the orientation angle θ and bending angle γ denote the angle between z_b and z_p on the bending plane and the angle from the x_b axis to the bending plane, respectively. Considering the bending and orientation angles, the homogeneous transformation from C_b to C_p is as follows:

$$
\begin{aligned}
{}^{b}_{p}T &= R(Z,\gamma)R(Y,\frac{\theta}{2})T(h)R(Y,\frac{\theta}{2})R(Z,-\gamma) \\
&= \begin{bmatrix}
1-2C^2(\gamma)S^2(\frac{\theta}{2}) & -S(2\gamma)S^2(\frac{\theta}{2}) & C(\gamma)S(\theta) & hC(\gamma)S(\frac{\theta}{2}) \\
-S(2\gamma)S^2(\frac{\theta}{2}) & 1-2S^2(\gamma)S^2(\frac{\theta}{2}) & S(\gamma)S(\theta) & hS(\gamma)S(\frac{\theta}{2}) \\
-C(\gamma)S(\theta) & -S(\gamma)S(\theta) & C(\theta) & hC(\frac{\theta}{2}) \\
0 & 0 & 0 & 1
\end{bmatrix}
\end{aligned}
\tag{3.1}
$$

where $S(x) = sin(x)$ and $C(x) = cos(x)$, $R(.,.)$ denotes a rotation, T an homogeneous transformation around the z axis, and h the distance between O_b and O_p, which is also the diameter of the sphere onto which the upper platform moves.

Geometrically, we can also derive the relationship (forward and inverse kinematics) between γ and θ with respect to the motor's inputs α_1 and α_2. As shown in Fig. 3.3b, motor 1 is mounted at B_1 with the motor shaft rotating along B_1O_b, while motor 2 is

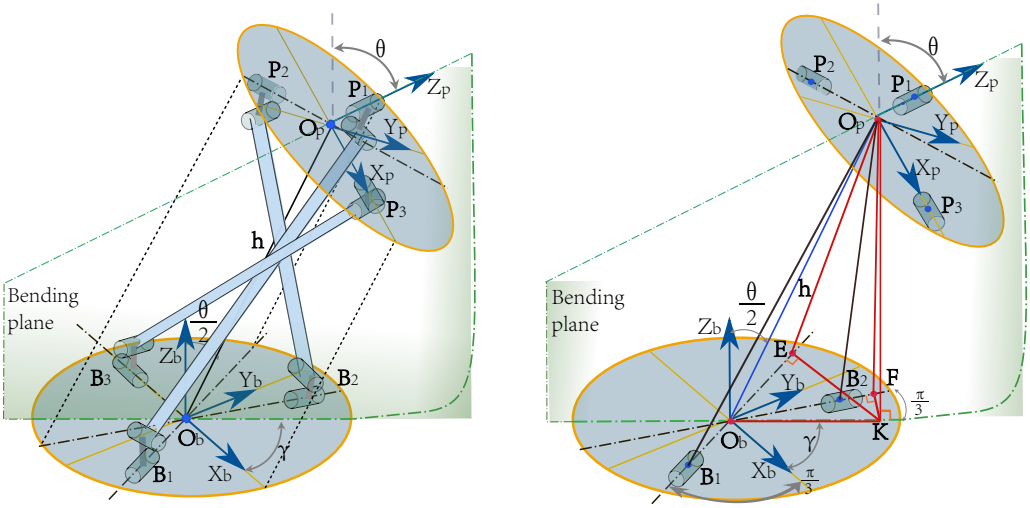

(a) Simplified schematic of the 3-4R mechanism.

(b) Kinematic model on the two actuating legs.

Figure 3.3 – Schematic of the proposed device.

mounted at B_2, with its shaft rotating along B_2O_b. The motor's rotating angle is limited within $(-\pi/2,\ \pi/2)$. For any bending pose of the upper platform, O_p has a projection point K in the plane $B_1B_2B_3$. Obviously, O_pK is perpendicular to B_1O_b and B_2O_b, and it is in the bending plane. Moving perpendicularly from K to B_1O_b and B_2O_b, we obtain two pedal points, E, F, which lie in the shaft axis of motor 1 and motor 2, respectively. Right-angled triangle $\triangle O_pKE$ and $\triangle O_pKF$ share the same edge O_pK. As O_pE and O_pB_1 lie in the same plane $O_pO_bB_1$, then the rotation angle of motor 1, α_1, is equal to $\angle O_pEK$, and that of motor 2, α_2, is equal to $\angle O_pFK$. From a simple geometrical derivation, we obtain

$$\begin{aligned}\tan(\alpha_1) = \tan(\angle O_pEK) &= \frac{O_pK}{EK} = \frac{O_pK}{O_bK\sin(\gamma+\frac{\pi}{3})} \\ &= \frac{h\cos\frac{\theta}{2}}{h\sin\frac{\theta}{2}\sin(\gamma+\frac{\pi}{3})} = \frac{1}{\tan\frac{\theta}{2}\sin(\gamma+\frac{\pi}{3})}\end{aligned} \tag{3.2}$$

$$\tan(\alpha_2) = \tan(\angle O_pFK) = \frac{O_pK}{FK} = \frac{1}{\tan\frac{\theta}{2}\sin(\gamma-\frac{\pi}{3})} \tag{3.3}$$

3.2.3 Experimental evaluation

We carried out an experiment evaluating the capabilities of the device in providing directional/motion information. The device renders a set of shapes with its end-effector, i.e., the moving upper platform, that users are asked to recognize.

3.2.3.1 Setup

The experimental setup is shown in Fig. 3.4. The device is used in its grounded configuration, with the lower platform attached to a table. Users are seated in front of the device and are asked to place their dominant hand on the device upper platform. A cardboard prevents the user from seeing his or her hand on the device during the experiment. A computer screen is also placed in front of the user, from which he or she can receive information about the experiment and answer the related questions.

3.2.3.2 Participants

Fourteen subjects (1 female and 13 males, aged from 23 to 33 years) participated in the experiment. Six are left-handed, eight are right-handed. Participants received an information sheet with the experiment details and signed a consent form. The study has been approved by Inria's ethics committee (Saisine 513).

3.2.3.3 Procedure

The experiment is divided in two blocks, carried out one after the other. In the first one, the device moves along eight linear patterns, shown in Figs. 3.5a and 3.5c. We recall that the center of the upper platform O_p moves across the surface of a sphere having diameter h and centered at the center of the lower platform O_b (see Sec. 3.2.2). Each linear pattern starts from the resting position of O_p, then moves towards its designated direction and back, along a circular arc with chord of 20 cm (see also the video). For example, the linear pattern referred to as "South" in Fig. 3.5, starts from the resting position of O_p, then moves towards the S (South) direction (see Fig. 3.5a), then back to the resting position of O_p, then moves towards the N (North) direction, and finishes in the resting position of O_p. All linear patterns start and finish in the resting position of O_p. The user sits on the South side of the device.

In the second block, the device moves along three shape patterns, shown in Figs. 3.6a and 3.6b. Similarly as before, these shapes are actuated over the surface of the sphere that is the workspace of our device. As indicated in Fig. 3.6a, they all start from a point located at the North of the resting position of O_p (named P in the Figure). Before starting the experiment, the experimenter explained the procedure to the user and spent about two minutes adjusting the chair armrest. Subjects placed their palm on the upper platform of the device and lean on the chair armrest to keep the forearm at the same level of the upper platform, ensuring maximum comfort. After each pattern was rendered, users were asked to select which pattern, in their opinion, the device just rendered. This choice was

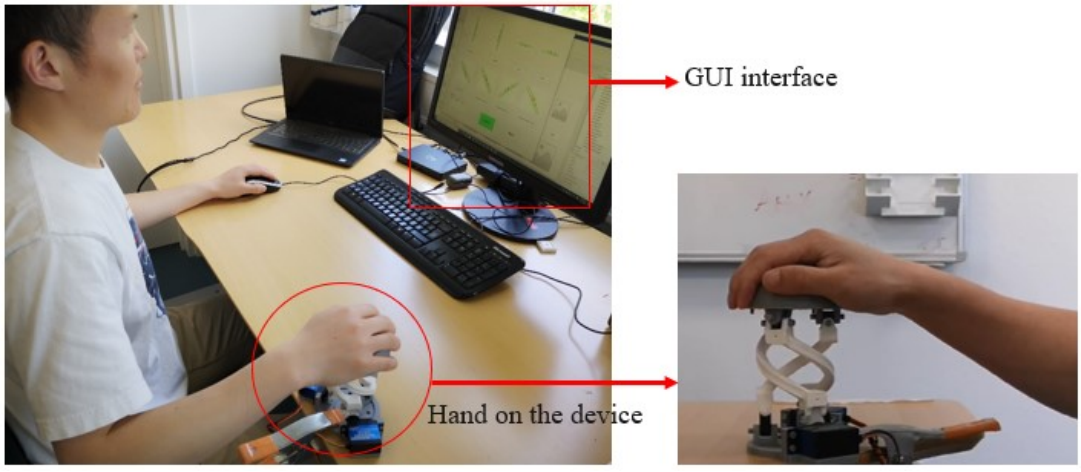

Figure 3.4 – Experiment setup

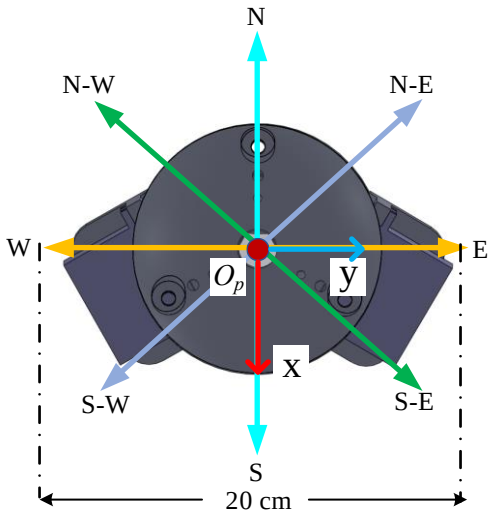

(a) View of the patterns from the top of the device.

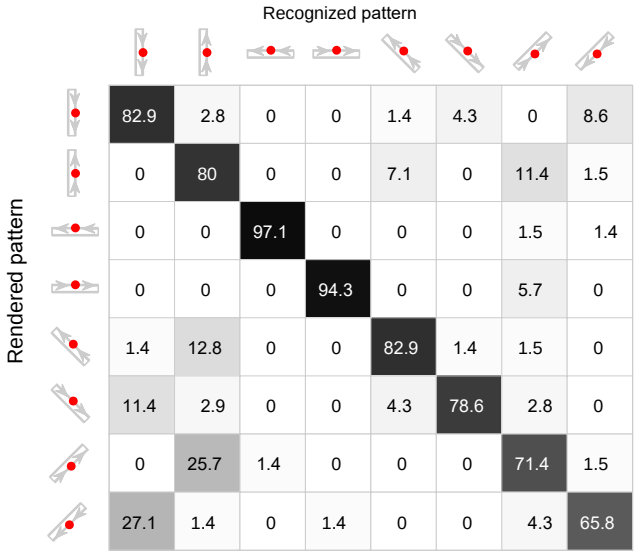

(b) Recognition rates.

(c) The linear patterns considered.

Figure 3.5 – Linear patterns. (a) The patterns as rendered by the device, view from the top of the upper platform; (b) recognition rates of linear patterns; (c) the linear patterns. All linear patterns start and finish in the resting position of O_p, moving along a circular arc having a chord of 20 cm.

made through a GUI on the computer screen in front of the user. The device actuating all the patterns is shown at https://youtu.be/vc6B-OOj590.

Each pattern was provided five times, yielding (8 linear patterns + 3 shape patterns)×5 = 55 repetitions of this pattern recognition task.

Immediately after the experiment, participants were asked to fill in a questionnaire where we asked which pattern was the harder/easier to recognize and if they had any further comment about the rendering and the experiment.

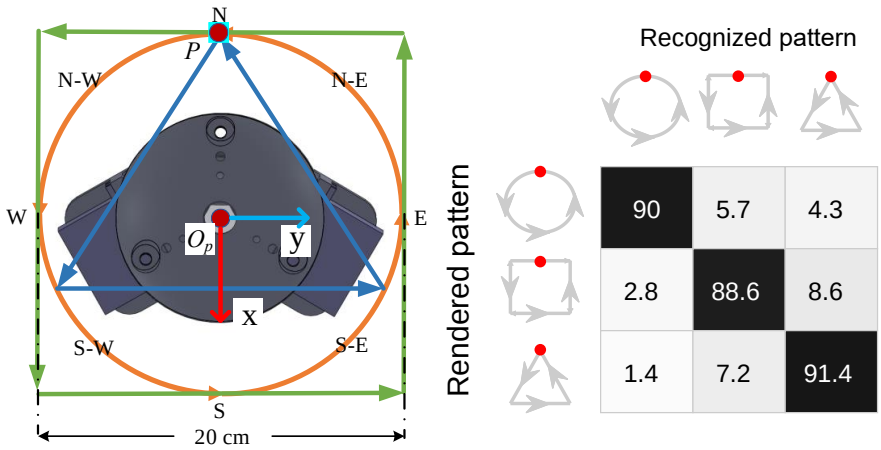

(a) View of the patterns from the top of the device.

(b) Recognition rates.

Figure 3.6 – Shape patterns. (a) The patterns as rendered by the device, view from the top of the upper platform. All shape patterns start and finish north of the resting position of O_p, in the point named P. (b) Recognition rates of shape patterns;

3.2.3.4 Results

Figs. 3.6a and 3.6b report the results of the experiment, in the form of two confusion matrices showing the percentage of recognition of the rendered vs. the recognized patterns. For the linear patterns the chance level is 1/8 (12.5%), while for the shape patterns the chance level is 1/3 (33.3%). The questionnaire showed that "East" and "West" linear patterns were considered as the easiest to identify, while the square shape pattern resulted to be the hardest. Diagonal linear patterns were reported to be harder to identify than other linear patterns.

3.2.4 Conclusions

This section presented a kinesthetic haptic device able to provide directional for hand motion guidance. We analyzed the device development, kinematics and control, as well as human-subjects experiment on the device. The device can be used both in a grounded or hand-held configuration, this section focused on the former. In this case, the lower base is firmly attached to an external support, and the upper platform moves so as to provide the user with haptic feedback. Experiments with 14 human subjects show that the device is able to provide distinguishable linear and shape directional patterns.

The design of this device shows also some limitations. First, in the current configuration, as we are using servo motors, the device is not backdrivable and cannot be used as a

standard impedance-type haptic interface. Second, the motors are both placed on the same platform, which is a good idea if the device is used in a grounded configuration, but not ideal if held between the two hands. In a hand-held configuration, it is better to distribute the weight equally between the two platform, which should be straightforward to do.

In the next future, we will also test the device when held between two hands, as well as the performance of the device in terms of resolution, precision, repeatability, and maximum output force. This device was developed within a larger effort to design a multi-modal haptic handle for various mobility aids, e.g., power wheelchairs, walkers, prewalkers. For this reason, we also plan to test this device effectiveness in rendering directional information when mounted on one of these mobility aids, similarly to [45].

3.3 Extension for Teleoperation Applications

Following Sec. 3.2, which presented and evaluated the device in a grounded configuration for hand motion guidance, this section extends the device to include a biaxial rocker module for teleoperation. The device is composed of a biaxial rocker module and a grounded base which houses two servomotors actuating a mobile platform through three constrained coupling structures. The mobile platform can apply kinesthetic haptic feedback to the user hand, while the biaxial rocker module has two analog channels which can be used to provide inputs to external systems.

3.3.1 The parallel mechanism

The design of the bilateral handle is inspired from [10], for which the mechanism was in turn originally inspired by [269]. Three identical supporting legs, as shown in Fig. 3.7, are evenly placed around the the z axis of the two platforms, forming an interlaced structure with no interference between them. Two revolute joints on the two sides of the leg generate reciprocal force and constrain the mobility between each linkage.

Gruebler–Kutzbach criterion (G–K criterion) or modified G-K can be used to analyze the mobility of the proposed handle, achieving a motion along 2 degrees of freedom (DoF). The motion of the upper platform is confined on the surface of a sphere centered in the center of the lower platform. Two servomotors are installed on the lower platform, with the motor shaft connected to the distal revolute joint on the leg, providing 2-DoF actuation. The two legs equipped with the servomotors have an active rotation on the lower joint and

a passive rotation on the other three joints. By varying the actuation of the servomotors, the upper platform can reach any position within its workspace (the surface of a sphere, as mentioned above and shown in Fig. 3.7).

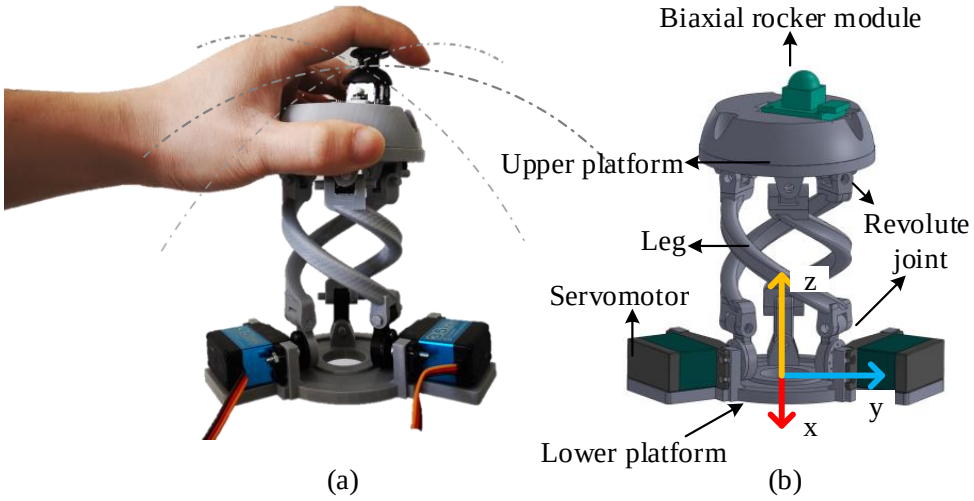

Figure 3.7 – (a) The device in its resting position, with the lower platform secured to an external support and the user hand posed on the upper one. (b) CAD of the device. The grey dotted lines show the surface of the sphere on which the upper platform moves. The user can provide directional input information through the biaxial rocker module.

3.3.2 User input for bilateral control

On the top of the upper platform, we installed a biaxial rocker module as to enable the user to provide directional 2-D input. This module has one button digital output and (X, Y) 2-axis analog output through rocker potentiometer. The two analog channels can also be used to represent the rotation angle about two mutually perpendicular axes, for instance, two of the Euler angles $(Roll - Pitch - Yaw)$ in 3D space. This input can also be used to control the free-space motion of the handle, similarly to a standard impedance-type haptic interface.

3.3.3 Use cases

We develop a goal-following game to test the effectiveness of the haptic force feedback generated by the handle as well as the intuitiveness of using the biaxial rocker module. A 2D GUI interface was developed with Matlab. The servomotors of the handle were controlled through an Arduino board.

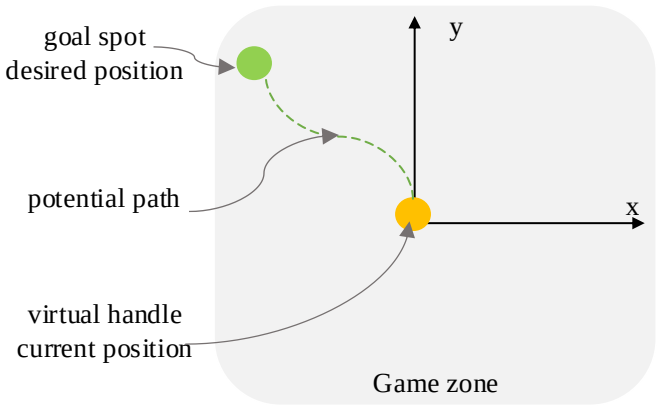

Figure 3.8 – The handle moves towards the goal point (in green, invisible to the user) to guide the user towards it. The closer the position of the user in the virtual environment (yellow point) to the goal spot, the smaller tilt of the handle with respect to its vertical resting position.

Fig. 3.8 shows the considered 2D environment. The current position of the user in the virtual environment is shown in yellow, controlled by the user through the biaxial rocker module. A random goal point, not visible by the user, is generated. The handle tilts toward the (invisible) goal point, guiding the user towards the objective position. The closer the position of the user in the virtual environment to the goal spot, the smaller tilt of the handle with respect to its vertical resting position. The task ends when the user reaches the goal point.

Preliminary tests indicated that the device is easy to use and intuitive to follow. An extensive human subjects will be subject of future work.

3.3.4 Conclusions

This section presents the extension of the handle in Sec. 3.2. We improved upon its design by including more powerful motors, able to provide force feedback to the user, a biaxial rocker module, to enable the user to provide 2D navigational input to the system, and making the design more ergonomic and comfortable to use.

In future work, we will integrate the proposed device in a powered wheelchair, so as to provide the driver with information about the presence of surrounding obstacles. This scenario is inspired by the collaborative Inria project DORNELL, where we aim at developing a multisensory haptic handle for helping disabled people using mobility aids such as power wheelchairs, white canes, and walkers.

3.4 Extension for Encounter-type Interaction

Following the work presented in Sec. 3.2 and Sec. 3.3, this section extends the handle to a 3-degrees-of-freedom (3-DoF) encounter-type kinesthetic device, which we called "Haptic Mushroom", as shown in Figs. 3.9 and 3.10. It is composed of two platforms, one fixed on an external support and one moving, connected by a three-leg parallel self-constrained mechanism. The Haptic Mushroom combines the characteristics of shape-changing displays and encounter-type systems; its modular design enables the easy and quick replacement of the end-effector to best fit the rendering requirements of the environment at hand. The end-effector can be designed according to the task at end, providing the necessary feedback information. In this chapter, as a representative example, we present a soft end-effector, able to render the sensations of interacting with different curvatures, and a rigid origami-like end-effector, able to render the sensations of interacting with different folding shapes.

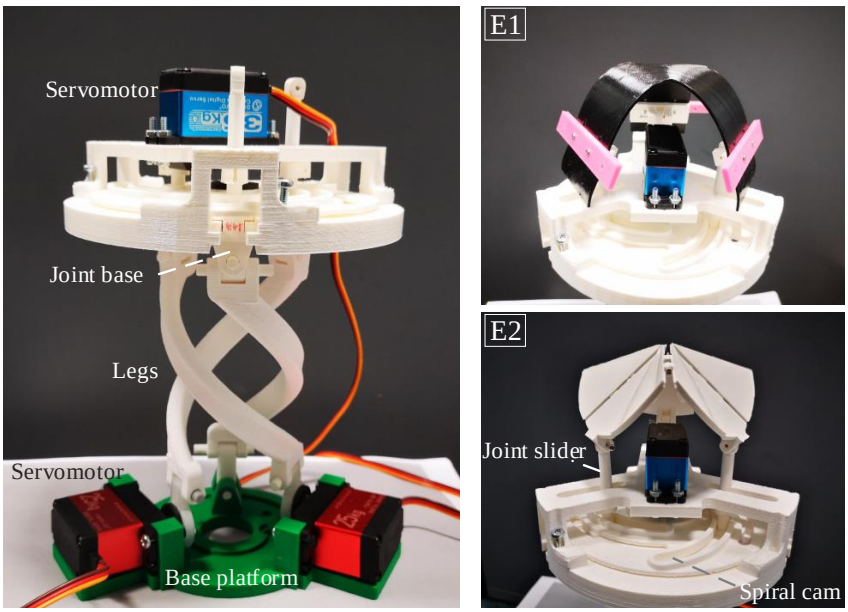

Figure 3.9 – The proposed 3-DoF shape-changing encounter-type haptic device. (Left) Main structure of the device (no end-effector attached yet). A video of the device in action is available as supplemental material and at https://youtu.be/vpC5s7-xXA8.

3.4.1 Device description and implementation

3.4.1.1 Device design and structure

The design of this device is inspired by the anti-parallelogram mechanism originally presented in [269] and later adopted in [10]. A prototype of the device is shown in Fig. 3.9, The lower/base platform (green in the Figure) is fixed, while the moving platform moves over the surface of a sphere. Two servomotors on the base actuate this motion through a three-leg parallel self-constrained mechanism. The legs are attached to the moving platform on joint bases, driven by an additional servomotor through a spiral cam. The chosen end-effector (E1, E2) is attached to the joint bases through three joint sliders, which moves towards/away from the center of the platform. As a representative example, we considered a (E1) soft end-effector, able to change its curvature, and (E2) a rigid origami-inspired end-effector, able to change its shape from flat to sharp.

Its schematic design is depicted in Fig. 3.10, and a set of representative movements are shown in Fig. 3.11, the three joint sliders are actuated within a circle (red) centered at the center of the moving platform. When the spiral cam rotates, the height of the platform and the radius of the abovementioned circle change. The blue dashed ellipses indicate the rolling motion of the platform. R_i represent the revolute joints of the three legs. In states a and b, the device is in a upright configuration and the spiral cam rotates to lower the moving platform and reduce the diameter of the slider circle. When equipped with the soft Y-shaped end-effector, this movement increases the curvature of the end-effector surface, as also shown in Fig. 3.12. In states c and d, the same movement as before but with the device in a bent configuration.

Three identical supporting legs are evenly placed around the the z axis of two platforms, forming an interlaced structure with no interference between them. The lower base platform is fixed on an external support and houses two servomotors, while the moving platform moves. The end of each leg is connected to the platforms through four serial revolute joints, indicated as $R_i, i = 1, 2, 3, 4$ in Fig. 3.11. Each 4R leg has 4 DoF, the three identical legs generate force and constraint to each other, forming 2 DoF mechanism to the device, which can freely move according to the orthogonal rolling motion on each leg. When the base platform is fixed on an external support (as in Fig. 3.10), the motion of the moving platform is confined on the surface of a sphere centered in the base platform center (see blue dotted lines in Fig. 3.11). The two servomotors have the motor shaft connected to the distal revolute joint on two legs, providing the above mentioned 2-DoF actuation. The legs

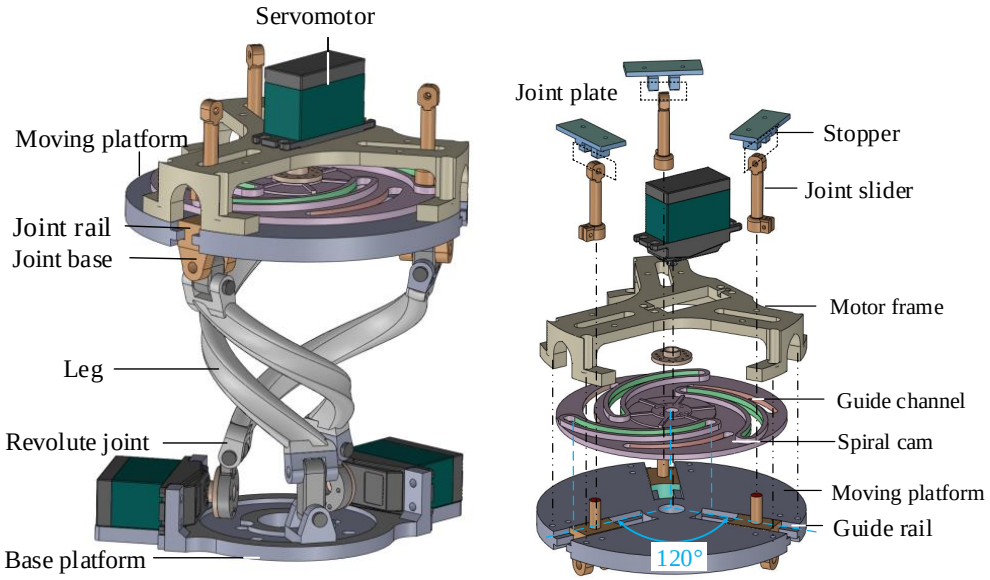

(a) CAD design **(b)** Upper moving platform

Figure 3.10 – Schematics of the proposed device. (a) CAD design. (b) Assembly view of the upper moving platform of the device, which includes the spiral cam mechanism that actuates the three joint sliders driving the end-effectors.

equipped with the servomotors have an active rotation on the lower joint and a passive rotation on the other three joints. By varying the actuation of the servomotors, the moving platform can reach any position within its workspace.

An additional servomotor is located on the moving platform, actuating a spiral-cam mechanism that in turn actuates the chosen end-effector through three joint plates on three joint sliders. The spiral cam is rigidly mounted to the servomotor shaft to effectively push the joint bases along their guide-rails. When the cam is turned, the joint bases slide radially, changing the overall diameter of the joint space, indicated as a red circle in Fig. 3.11. The guide channels allow the joint bases to reach a minimum diameter of 56 mm to a maximum of 106 mm. These dimensions are set by the mechanical constraints on the three legs; increasing the diameter would consequently reduce the height of the coupling parallel mechanism which, in turn, reduces the diameter of the spherical curve of the moving platform workspace (Fig. 3.11b). In addition, this handle can be used either in a grounded configuration, with the lower base on a table, or in an ungrounded configuration, with each base posed on the user's palm, similarly as shown in Fig. 3.2.

Table. 3.1 shows the main technical specifications of the device.

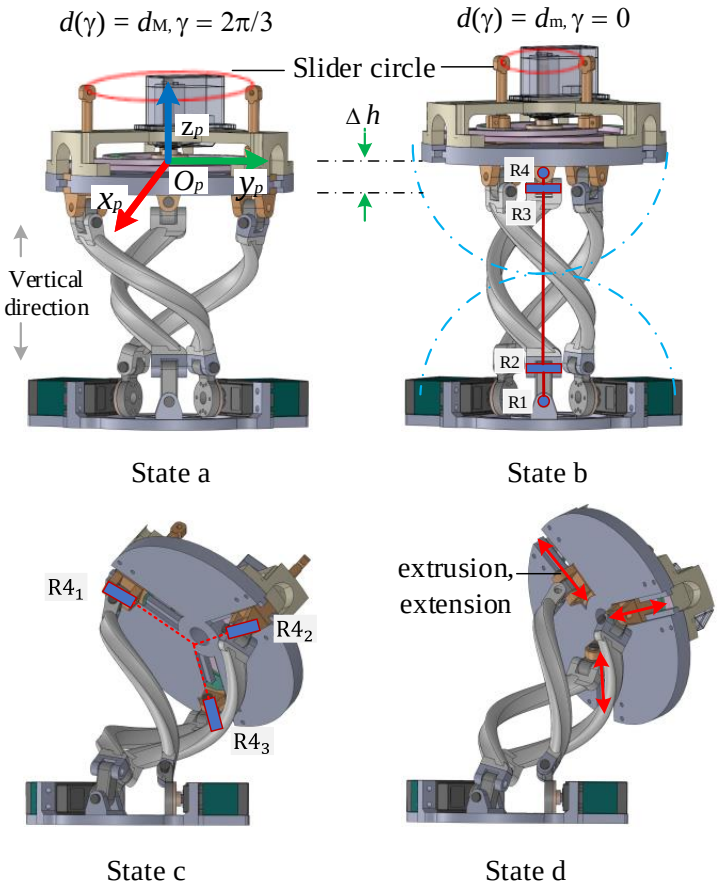

Figure 3.11 – Representative movements of the device.

3.4.1.2 The shape-changing end-effectors

As mentioned before, this device has been designed to support a wide range of end-effectors. As a representative example, we present two interchangeable end-effectors: a soft end-effector (E1 in Fig. 3.9), rendering different curvatures, and a rigid origami-like end-effector (E2 in Fig. 3.9), rendering different folding shapes. The end-effectors are installed on the joint sliders through passive revolute joints as shown in Fig. 3.10a and Fig. 3.10.

Soft Y-shaped end-effector This end-effector is composed of a flexible equilateral Y-shaped strip of PolyFlex TPU90, with a thickness of 1.5 mm. It is shown in Figs. 3.9 (E1) and 3.12. The end-effector strip is attached onto the joint plates through three stoppers (see Fig. 3.10). Because of the radial movement of the joint bases, the Y-shaped strip is forced to bend towards the vertical direction (positive z_p axis) when the spiral cam rotates.

Table 3.1 – Technical Specifications

Dimension Length × Width × Height	12 × 12 × 15 cm
Control system	M5Stack Core2, Atmega328
Operating voltage range	6.0 V
Operating joints speed	0.14 sec/60°
Workspace	Spherical curve, radius 13-15 cm

A mechanical stopper prevents the Y-shaped strip to deform in the downward direction. By adjusting the material characteristics of the Y-shaped strip (i.e, dimension, thickness), we can easily render different ranges of curvatures and stiffness.

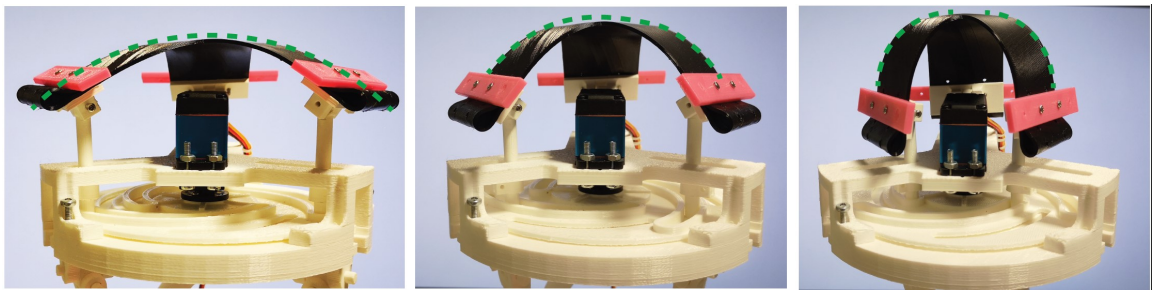

Figure 3.12 – Soft Y-shaped end-effector. It is composed of a 3D printed Y-shaped strip attached to the moving platform through three joint sliders actuated by the servomotor through a spiral cam. When the spiral cam rotates, the diameter of the circle encompassed by the joint sliders changes, controlling the curvature of the end-effector (in green).

Origami-inspired rigid end-effector The design of this end-effector is inspired by a modular origami structure. Such surface can fold/unfold to render specific reconfigurable structures. It is shown in Figs. 3.9 (E2), 3.13, and 3.14. To control the rendered shape, a kinematic-based description of the origami can be obtained [272]. We designed a structure composed of nine identical flat circle sectors (referred to as "panels" in Fig. 3.13), connected to each other with revolute joints, so as to bend into edges and one vertex in the center. Three of these panels are connected to the three actuated joint sliders through revolute joints. The sector angle per each actuated panel covers 40°, and it is linked to two passive panels as shown in Fig. 3.13.

When the joint sliders move, the active panels contract in unison approaching to the center of the spiral cam O_p (see Fig. 3.11). Doing so, the connection between the passive

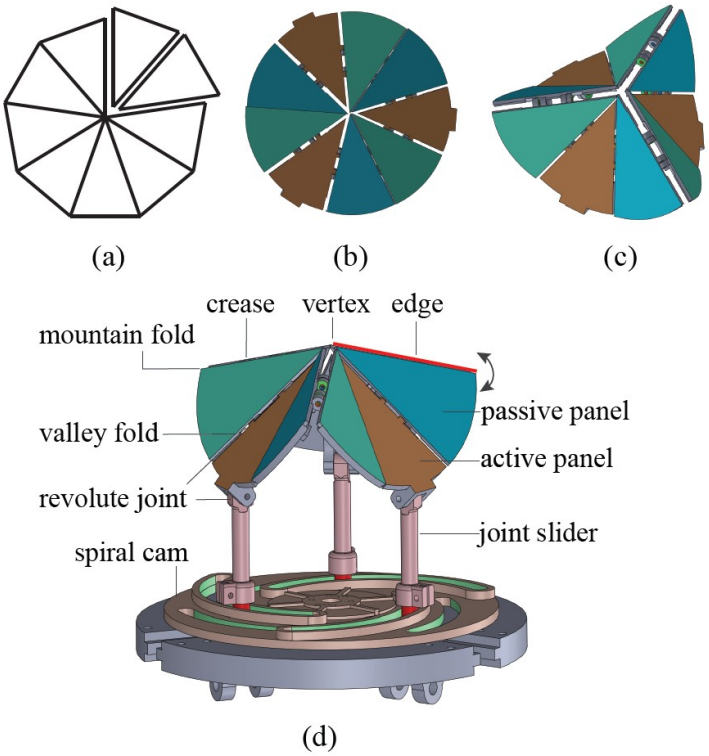

Figure 3.13 – Origami-inspired rigid end-effector: the design. (a) The single triangular panels are jointed together to form a modular re-configurable surface. Such a surface can render different edges as the spiral cam rotates. (b, c, d) The folding of the end-effector is controlled by rotating the spiral cam, which in turn moves the joint sliders towards the center of the platform. Doing so, the end-effector goes from flat to folded, rendering three edges and a center vertex. Of course, by changing the origami structure, we can render different reconfigurable shape sensations.

triangular elements folds them into a mountain-fold (creating an edge, see Fig. 3.13). Of course, different origami structure can lead to a wide range of reconfigurable surfaces.

3.4.1.3 Hardware

The device is realised using standard rapid prototyping techniques. All passive mechanical components on the device are 3D printed, using Polylactic Ascid lastic (PLA) and Thermoplastic Polyurethane (TPU) filament with Stratasys (F370) and PRUSA 3D printer.

The device is actuated by 6V position-controlled servomotors (ZOSKAY 35 kg·cm torque), two are rigidly mounted to the base platform while the motor shafts are connected to the revolute joints of two legs. The third servomotor is mounted on the moving platform, with the shaft aligned to Z_p and centered in O_p, and drives the spiral cam directly to

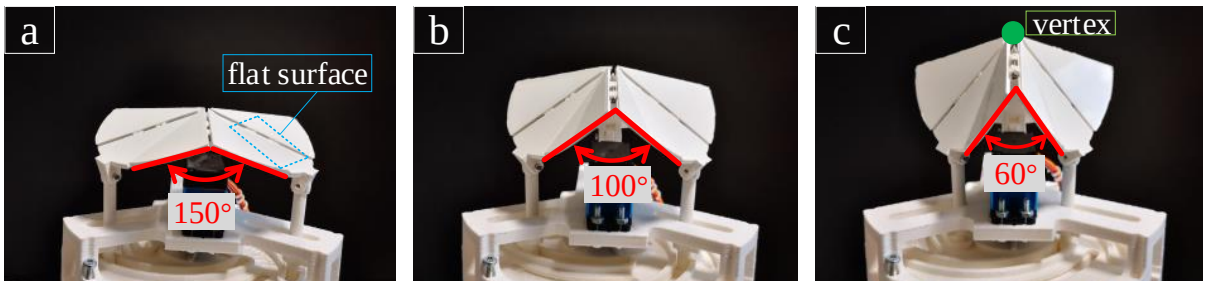

Figure 3.14 – Origami-inspired rigid end-effector: folding action. The folding of the end-effector is controlled by rotating the spiral cam, which in turn moves the joint sliders towards the center of the platform. Doing so, the end-effector goes from flat (150° angle between two adjacent passive panels, left figure) to folded (60° angle between two adjacent passive panels, right figure), rendering three edges and one vertex.

ensure a high torque transmission. A M5Stack integrated controller governs the actuation of all the servomotors, and directly manages the position control.

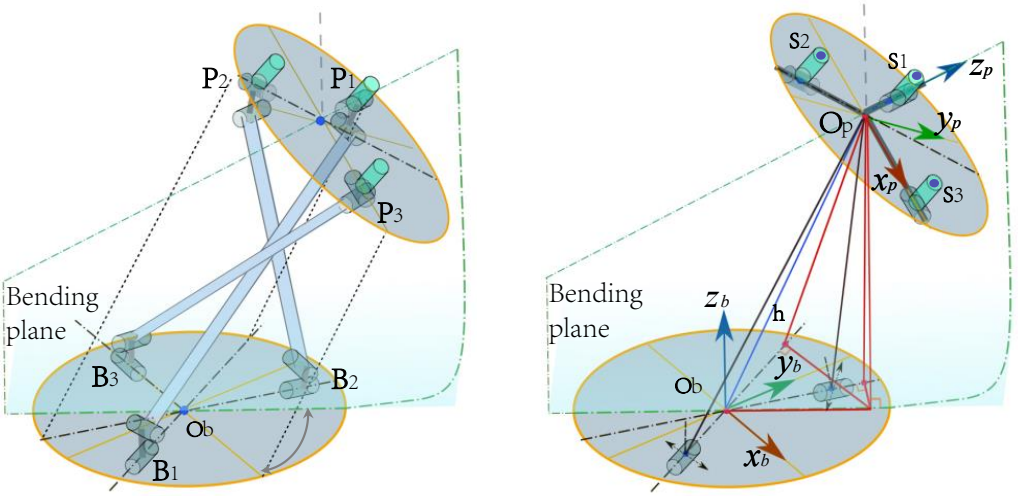

(a) Simplified schematic of the 3-4R mechanism.

(b) Kinematic model on the two actuating legs.

Figure 3.15 – Kinematic scheme of the proposed device (no end-effector).

3.4.2 Characterisation of the end-effectors

For the characterisation of the end-effectors, let us consider the center of the moving platform O_p, as shown in Figs. 3.11 and 3.15a. Observing the Fig. 3.15b, we called O_b the center of the base platform, which is connected in B_1, B_2, B_3 to the moving platform, through the three legs. The device enables points P_i to have variable reciprocal distance

dependant on the diameter $d(\gamma)$ of the slider circle (the circle encompassed by the joint sliders), where γ is the rotation angle of the spiral cam located at the center of the moving platform.

Since the joint sliders are constrained in the symmetrical guides of the spiral cam (see Fig. 3.10d), the positions of the sliders depend on the spiral-cam mechanism rotational angle γ, driven by the servomotor placed on the moving platform. As an example, when γ is zero, the distance of the joint sliders from the center is $d_m/2 = 28\,\text{mm}$. The spiral cam mechanism can rotate until reaching a maximum rotation of $2\pi/3$ by moving the joint sliders away from O_p, to a maximum distance of $d_M/2 = 53\,\text{mm}$ from O_p. This movement actuates the end-effector attached to the joint sliders according to its specific kinematics and characteristics.

Below we analyze how this motion affects the two representative end-effectors that we consider in this chapter. On the other hand, the direct and inverse kinematics of the three-legged parallel mechanism can be easily derived using reciprocal screw system theory, similarly to [10].

3.4.2.1 Soft Y-shaped end-effector

As the spiral cam rotates and the joint sliders get closer to each other and to the center of the platform, the end-effector bends, rendering spherical shapes of increasing curvatures. Let us consider a rendered curve $\mathcal{C}(x_{E_1}, R)$ having a curvature $1/R$ at the top of the bent end-effector.

The second order equation $\hat{f}(x_{E_1}) = ax_{E_1}^2 + bx_{E_1} + c$ (where b can be null) that best fits the rendered shape (for a limited sector) can be obtained as:

$$\min_{a,c} ||\mathcal{C}(x_{E_1}, R) - \hat{f}(x_{E_1})||^2.$$

The integral relation

$$\int_0^{\frac{x_{E_1}}{2}} \sqrt{1 + (d\hat{f}(x_{E_1})/dx_{E_1})^2} dx_{E_1} = d_M/2, \tag{3.4}$$

describes a generic parabolic curve with length $d_M/2$, where $d_M = 106$ mm is the maximum diameter for the slider circle. From there, we can directly obtain x_{E_1} using the Newton-Raphson method and, from $x_{E_1} = \frac{d(\gamma)}{2}$, we obtain γ.

This relationship enables us to render a given curvature by controlling the servomotor

placed on the moving platform.

3.4.2.2 Origami-inspired end-effector

Similarly as before, also the configuration of this end-effector depends on the distance of joint sliders from the O_p center and, consequently, by γ, i.e., the rotation angle of the servomotor on the moving platform. In particular, for the considered origami structure, shown in Figs. 3.13 and 3.14, the configuration is constrained at the three anchoring points located on the joint sliders. As the distance between the joint sliders and the center O_p decreases, the angle of the mountain-fold (edge) decreases towards a value of 60°, with $d(\gamma) = d_m$ when $\gamma = 0°$. The minimum value of the angle (so the "sharpest" configuration of the structure, as shown in Fig. 3.14c) is obtained when the vertex is raised 20 mm along the positive direction of z_p (as in Fig. 3.14c).

Note that as the spiral cam rotates and the joint sliders gets closer to each other, points P_i get closer to each other, lowering the moving platform. This behavior can be seen in the accompanying video.

3.4.3 User study on the soft Y-shaped end-effector

We carried out a user study to evaluate the rendering capabilities of the soft Y-shaped end-effector, evaluating its capabilities in generating distinguishable spherical shapes with variable curvatures.

Twelve subjects (10 males, 2 females, aged 22-31) were enrolled in the experiment. Ten of them had little experience with haptic devices (used once a year), two of them had extensive experience with haptic devices (used once a month). Participants used their dominant hand to interact with the device (seven right hand, five left hand).

3.4.3.1 Experimental setup

The static platform of the device is fixed on a table, as shown in Fig. 3.16. Participants sit in front of the table, able to comfortably reach the end-effector of the device. Participants were also asked to wear an eye mask to prevent the participant from seeing the movement of the end-effector. The experimenter controlled the device and recorded the answer given by the participants.

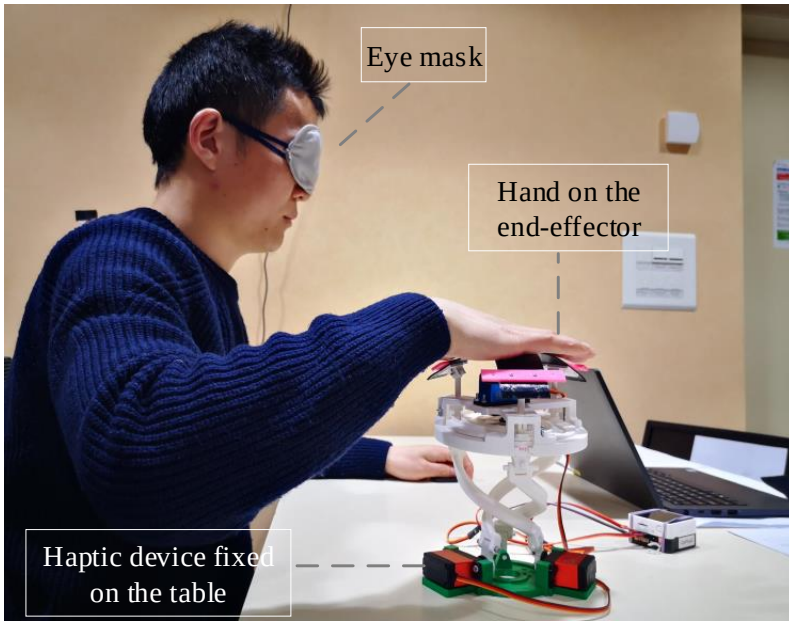

Figure 3.16 – User study. Experimental setup showing a user interacting with the end-effector. Users were not able to see the device moving.

3.4.3.2 Methods and protocol

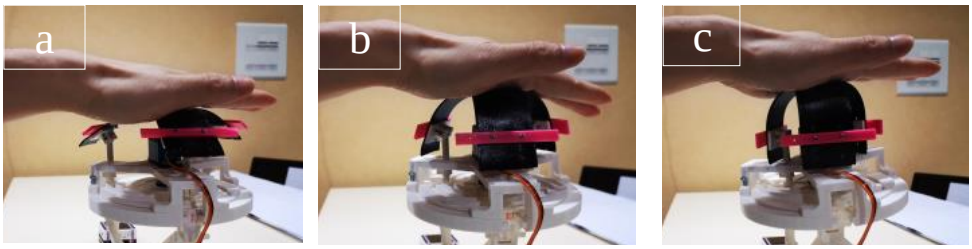

Figure 3.17 – User study. The soft Y-shaped end-effector render the sensation of interacting with three different curvatures. From (a) to (c), the rendered curvature increases (and its radius decreases).

We aim at exploring the difference in curvature participants can perceive when interacting with the soft Y-shaped end-effector. We considered a set of curvatures spanning the whole rendering workspace of the device. The spiral cam can move the joint sliders to encompass circles (see Fig. 3.11) with diameters from 56 mm to 106 mm, generating curvatures having radii from 30 to 100 mm on the soft end-effector surface (see Sec. 3.4.2.1). Using a standard two-alternative forced choice (2AFC) design, we proposed the participants to interact with two curvatures, one after the other, having differences in radii of 5, 10, 15, and 20 mm. Participants were asked to identify which one had the larger curvature.

We considered 40 comparisons, each repeated two times, listed in Table 3.2. For each comparison, participants were asked to touch the first surface with their palm for 5 seconds (see Fig. 3.17), then break contact with the surface, and then touch the second surface for another 5 seconds. Participants were allowed to interact with the surface as they liked during the 5-seconds interactions.

Table 3.2 – User study. Radii (mm) of the spherical surfaces rendered using the soft Y-shaped end-effector.

(40,45) (40,50) (40,55) (40,60)	(75,80) (75,85) (75,90) (75,95)
(45,40) (45,50) (45,55) (45,60)	(80,75) (80,85) (80,90) (80,95)
(50,40) (50,45) (50,55) (50,60)	(85,75) (85,80) (85,90) (85,95)
(55,40) (55,45) (55,50) (55,60)	(90,75) (90,80) (90,85) (90,95)
(60,40) (60,45) (60,50) (60,55)	(95,75) (95,80) (95,85) (95,90)

3.4.3.3 Results

Figure 3.18 shows the recognition accuracy registered during the experiment. As expected, as the difference between the curvatures increases, it is easier to correctly identify which one has the larger curvature.

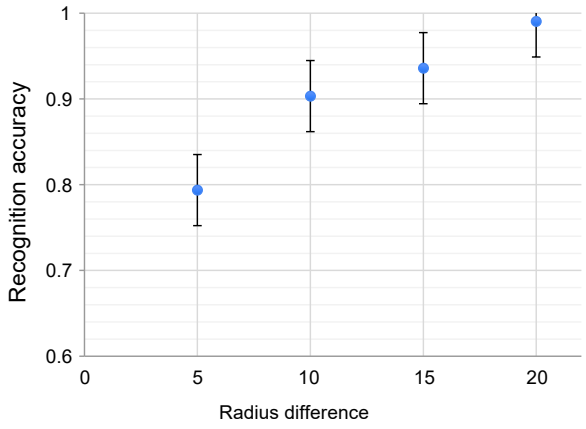

Figure 3.18 – User study on the soft Y-shaped end-effector. The accuracy of the recognition as a function of the difference in the presented curvatures radii difference (mm). Mean and standard deviations are plotted.

Figure 3.19 – Use case: encounter-type interaction with re-configurable surfaces. The motion of the user's hand was tracked by the HTC Vive motion system. The base platform of the device was fixed on a table and the moving platform follows the hand so as to always face the user's palm, ready for interaction.

3.4.4 Use case: encounter-type interaction with re-configurable surfaces

To showcase the device capabilities in delivering on-demand haptic touch sensations, we designed a use case study where participants interacted with virtual objects in a three-dimensional environment. The base platform of the device was fixed on a table as in the previous experiment. Participants were asked to wear a HTC Vive tracker on their wrist, so as to track the position of the hand. The experimental setup is shown in Fig. 3.19. The device follows the movement of the hand, so as to always face the palm of the user, ready for the interaction.

3.4.5 Conclusions

This section presents the Haptic Mushroom - a 3-DoF grounded shape-changing encounter-type haptic device designed for interchangeable end-effectors that can be easily and quickly exchanged to provide a wide range of haptic touch sensations. The device supports a wide range of end-effectors. As a representative example, we present two end-effectors in this chapter: a soft end-effector, able to change its curvature, and a rigid origami-inspired end-effector, able to change its shape from flat to sharp.

With respect to existing solutions, the proposed device combines the characteristics of encounter-type devices with those of shape-changing/reconfigurable interfaces. Moreover, the possibility of easily adapting the end-effector to the target haptic sensations makes the device quite flexible and applicable to a broad range of scenarios.

A user study enrolling 12 participants evaluated the performance of the soft end-effector in rendering different curvatures, showing over 90% recognition accuracy when rendering curvatures that differed 1.0 mm^{-1} or more. A use case scenario showed the potential of using the device in rendering virtual shapes during a free-hand encounter-type interaction. Work is in progress to integrate the device on robotic manipulator for large space surface exploration towards virtual reality.

3.5 Discussion and Conclusions

This Chapter presents the development of grounded and handheld kinethestic devices for motion guidance, teleoperation and encounter-type interaction. This work supports our hypothesis that grounded haptic device can be used as bilateral interfaces to provide the user with haptic feedback for navigation, and to transmit the user's command to a remote system. It also paves the way of exploring parallel-structured shape-changing devices for generating directional stimulation and encountered type devices for touch sensations.

Chapter 4

Wearable Ungrounded Device for Palmar-based Interactions: Rigid Foldable End-effector

Contents

4.1 Introduction

In Chapter 3, we presented the grounded and encountered type haptic devices for kinesthetic and touch sensation rendering. In this Chapter, we expand the work to hand-mounted devices which can apply touch sensation to the palm. Therefore, we present a 4-degrees-of-freedom (4-DoF) wearable haptic device for the palm, able to provide the sensation of interacting with slanted surfaces and edges. Our objective is to improve the immersiveness of interaction with virtual objects in VR.

As shown in Figs. 4.1 and 4.2. The device features a 4-degrees-of-freedom (4-DoF) end-effector that can move towards/away from the palm, sideways along the hand ulnar-radial direction, and fold in two. The device is therefore able to elicit the sensation of interacting with a wide range of slanted surfaces, curvatures, and even sharp edges through combined localized pressure and skin stretch sensations. A video of the device in action can be found as supplemental material and at `https://youtu.be/ZuB_JxwbB9s`.

With respect to other wearable haptic solutions for the palm, such as [273]–[278], the proposed device is able to provide a broader range of stimuli, i.e., slanted surfaces, edges, and variable curvature sensations. Moreover, it is accompanied by an in-depth mechanical analysis and evaluation which is missing in the aforementioned works. For example, Minamizawa et al. [273] used two motors to actuate two belts moving a flat end-effector on the palm, providing normal and shear forces. Trinitatova and Tsetserukou [274], [275] used a 3-DoF inverted delta mechanism consisting of three identical kinematic limbs to move a pin-like end-effector across the palm. Similarly, Dragusanu et al. [277] used a 3-DoF parallel tendon-based mechanical structure to actuate an interchangeable palmar end-effector. More recently, Cabrera et al. [276], [278] presented a device able to actuate three small contact points using an inverted five-bar linkages. The envisioned application for all these devices is manipulation in VR.

The Chapter presents the design of the wearable haptic device, together with its mobility, statics, and manipulability, as well as direct, inverse, and differential kinematics. We also present a position control scheme for the device, which is then quantitatively evaluated.

This Chapter is a revised version of the works under revision as

* **L. Kuang**, M. Malvezzi, M. Ferro, D. Prattichizzo, P. Robuffo Giordano, F. Chinello, C. Pacchierotti. "A 4-DoF Wearable Hand Device for Haptic Rendering of Surfaces and Edges." *Submitted to Mechatronics*, Elsevier, 2023.

Video available at: https://youtu.be/ZuB_JxwbB9s.

4.2 Design of the Wearable Haptic Device

The proposed 4-DoF wearable device was designed following the design guidelines for wearable haptics discussed in [3], with the objective of employing it in Virtual Reality and robotic teleoperation applications. The haptic system has been designed to:

1) minimize the impairment for users as well as be as lightweight and comfortable to wear as possible;
2) enable easy mechanical personalization and adaptation for different users [5];
3) render a wide range of haptic stimulation, including making/breaking contact, skin stretch, relative tangential motion, and edges [3].

A prototype of the wearable hand device is shown in Fig. 4.1, while its CAD design is shown in Fig. 4.2. Inspired by a dual-arm robot system, the device features a 4-DoF structure with two arms connecting a static upper body to the end-effector, constituting

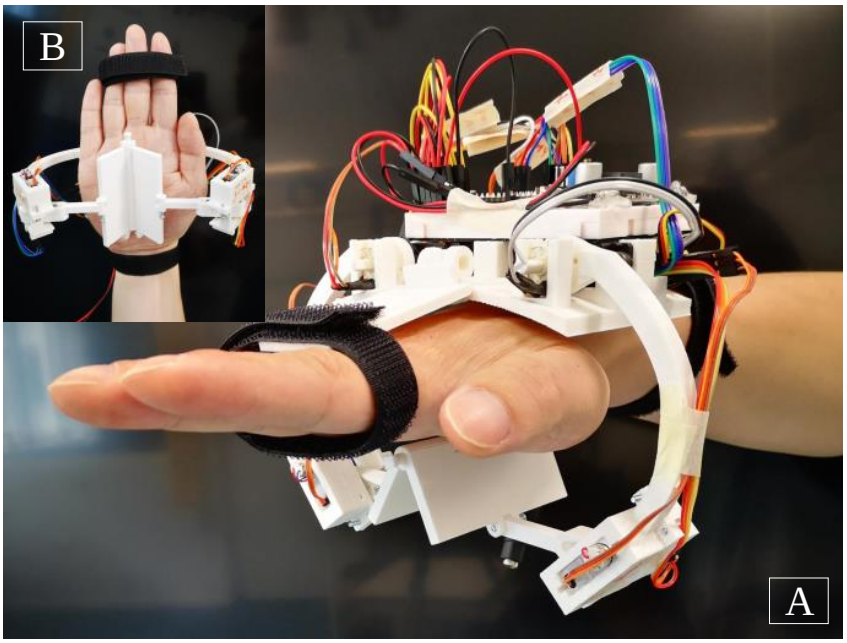

Figure 4.1 – Two views of the proposed 4-DoF wearable haptic device for the palm. The end-effector is composed of two plates connected in a hinge-like structure. Four motors enable the end-effector to move towards/away from the palm, sideways along the hand ulnar-radial direction, and fold in two.

a planar, parallel mechanism. The upper body is fastened to the back of the hand with velcro straps, while the end-effector applies the target haptic stimuli to the user's palm.

Each arm is composed of two rigid serial chains constrained to each other, including an arcuated link (L1 in Fig. 4.2) and a straight link (L2). Two upper revolute joints C and E connect the arcuated links of each arm to the upper body. Two lower revolute joints D and F connect the arcuated links of each arm to the corresponding straight links L2. The axes of the revolute joints are parallel to each other, making the whole mechanism planar. Finally, each straight link L2 is connected to the end-effector through a passive revolute joint, generating a 2-DoF planar articulated mechanism. The combined action of the two arms leads to the final 4 DoF of the system.

The end-effector is composed of two flat rectangular plates connected in a hinge-like fashion through a passive cylindrical bearing, allowing the folding of the two plates with respect to the z_0 direction (see Fig. 4.2). Actuated by the combined action of the two arms, the movement of the end-effector is constrained within the x_0–y_0 plane, referred to as plane Σ, constituted by the joints. In this way, the end-effector can be controlled to move vertically along the y_0 axis, sideways along the x_0 axis, fold, as well as roll. However,

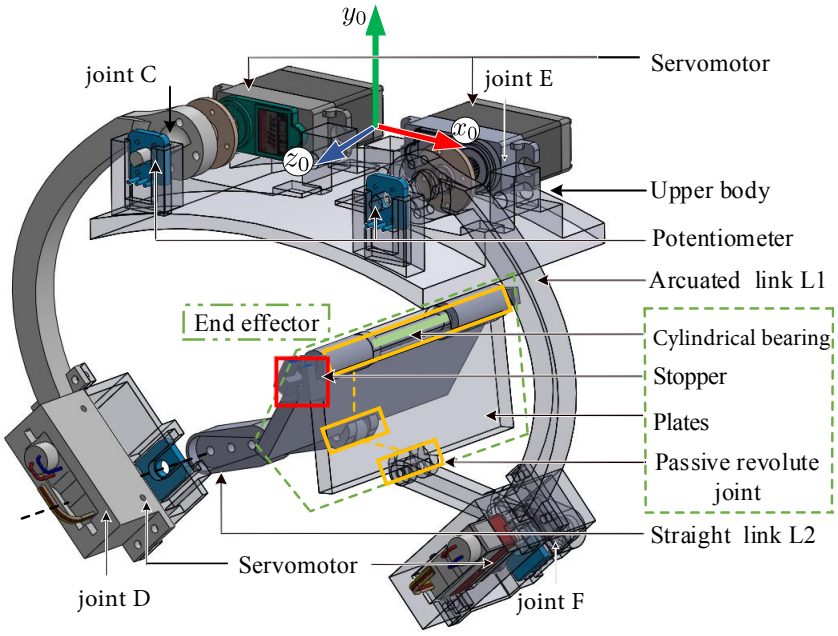

Figure 4.2 – CAD model of the proposed device. It is composed of a static upper body, located on the back of the hand, and a foldable two-piece end-effector placed in contact with the palm. Two articulated arms, composed of arcuated (L1) and straight (L2) sections, connect the two parts. Four servo motors, two on the upper body and two on the arms, actuate the end-effector, enabling it to move along the x_0 and y_0 axes, rotate with respect to z_0 axis, and fold.

Table 4.1 – Device specifications

Weight	160 g
Dimension Length × Width × Height	(13–18) × 18 × (12–15) cm
Maximum contact surface	42 cm^2
Control system	Arduino Uno, Atmega328
Communication latency	< 20 ms
Operating voltage range	4.8 to 6.0 V
Operating joints speed	0.14 sec/60°
Maximum normal force	7.33 N
Maximum horizontal displacement	9 cm
Maximum vertical displacement	5 cm

since the three joints on the end-effector are passive, we cannot control the direction of the folding, i.e., we cannot control whether the edge created by the folding points upwards or downwards. We included a stopper on the cylindrical bearing between the two plates to constraint the end-effector to fold with the edge pointing upwards, so as to generate the sensation of interacting with edges of different sharpness. Of course, the stopper can be easily adjusted to constraint the end-effector to fold in the other direction.

The electronics system consists of an Atmega328 controller mounted on an Arduino Uno Board. The actuation is provided by two HS-85MG servomotors, mounted on the upper body (in joint C, E), and actuating the arcuated links, and two KST-08H servomotors, mounted on the arms (joint D, F), and actuating the straight links. The torque provided by the servomotors allow the device to apply a force up to 7 N to the palm. The force that can be applied depends on device configuration, as detailed in Sec. 4.3. We also installed four rotatory Bourns potentiometer 3382H on each servomotor, so as to measure their current shaft rotation angle.

Figure 4.3 shows a series of representative motions that the device can actuate, while Table 4.1 summarizes the main characteristics of the device.

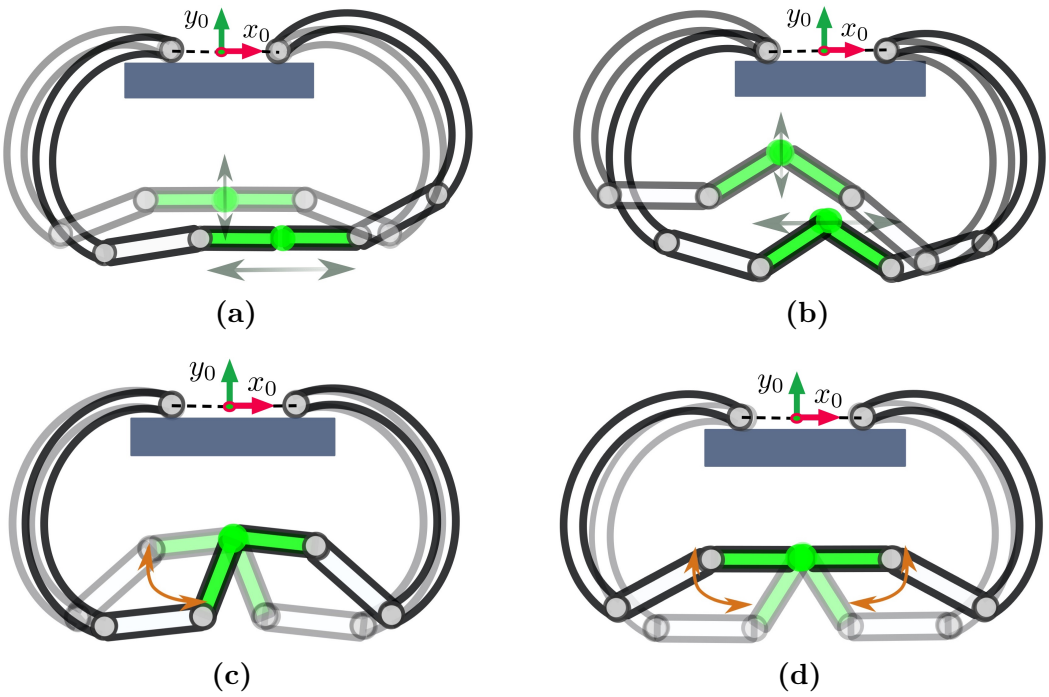

Figure 4.3 – Representative movements of the wearable 4-DoF device. The end-effector, depicted in green, is actuated by the joint action of the arcuated and straight links. (a) Horizontal/vertical movement while the end-effector is fully unfolded, providing variable pressure and skin stretch sensations through a flat surface; (b) Horizontal/vertical movement while the end-effector is partially folded, providing variable pressure and skin stretch sensations through a sharp edge; (c) Roll movement, providing the sensation of interacting with a slanted or uneven surface; (d) Folding/unfolding movement, providing the sensation of interacting with different edges.

4.3 Device Analysis

This Section presents the mechanical model of our device, including its mobility analysis as well as the forward and inverse kinematics analysis, necessary to derive the main structural parameters of the device and the kinematic and dynamic modeling.

As shown in Fig. 4.4, the revolute joints are parallel to each other and aligned in the same plane Σ. Let us indicate with $S_0 < O_0, x_0, y_0, z_0 >$ the reference frame attached to the upper body, in which O_0 is the origin and the center between revolute joints C and E. The x_0 axis is parallel to $\overrightarrow{CE}$, y_0 is in the same plane with x_0, C, and E (plane Σ), and z_0 is consequently defined (see also Fig. 4.2). The two lower revolute joints on the arcuated links, D and E, are also parallel to the each other and lie in the plane Σ. The two arcuated links L1 have the same structure, their configuration is defined by vectors $\overrightarrow{CD}$ and $\overrightarrow{EF}$, respectively, with length $|\overrightarrow{CD}| = |\overrightarrow{EF}| = l_1$. The straight links L2, connecting the arcuated links to the end-effector, are defined by the vectors $\overrightarrow{DA}$ and $\overrightarrow{FB}$, respectively,

with length $|\overrightarrow{DA}| = |\overrightarrow{FB}| = l_2$. Finally, the foldable end-effector is represented by vectors $\overrightarrow{AP}$ and $\overrightarrow{BP}$, with length $|\overrightarrow{AP}| = |\overrightarrow{BP}| = l_3$. The cylindrical bearing between the two plates of the end-effector intersects with the plane Σ at P, where we define the coordinate frame $S_p < O_p, x_p, y_p, z_p >$, with the origin O_p coinciding with P.

4.3.1 Mobility analysis

The mobility analysis of our device has similarities with dual arm manipulators and Delta-2 robots, i.e., with both serial and parallel robots. The device is actuated by two serial planar Revolute-Revolute (R-R) chains attached to the upper body, with a foldable two-plates end-effector constraining their movement. These two serial chains manipulate the two plates on the end-effector through passive joints, so as to control its position, orientation, and folding configuration along 4 DoF. A set of representative movements the device can actuate is shown in Fig. 4.3. Two DoF can be obtained by moving the end-effector within the $x_0 - y_0$ plane (as in Figs. 4.3a and 4.3b), one DoF comes when the end-effector rolls with respect to the z_0 direction (as in Fig. 4.3c), and another DoF lies in the folding movement of the two plates, constrained by the stopper (as in Fig. 4.3d). These four DoF can be represented by the four-dimensional vector $\mathbf{u} = [x_P, y_P, \theta, \alpha]^{\mathrm{T}}$, which includes P point coordinates (x_P, y_P) in the $x_0 - y_0$ (Σ) plane, the roll angle θ, and the folding angle α (see Fig. 4.4).

4.3.2 Direct kinematics

As shown in Fig. 4.4, let us indicate with $\mathbf{q} = [q_1, q_2, q_3, q_4]^{\mathrm{T}}$ the input variables, corresponding to the actuators' rotation angles of joints in C, D, E, and F, respectively, and with $\mathbf{u} = [x_P, y_P, \theta, \alpha]^{\mathrm{T}}$ the output control variables (see Sec. 4.3.1). Direct kinematics analysis aims at defining the relationship mapping $\mathbf{q}$ into $\mathbf{u}$, i.e.,

$$\mathbf{u} = f_d(\mathbf{q}). \tag{4.1}$$

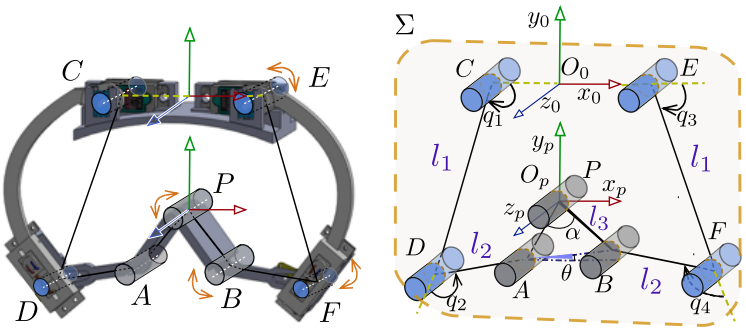

Figure 4.4 – Kinematic structure of the proposed 4-DoF wearable haptic device. Two planar Revolute-Revolute chains, actuated by four motors, move the end-effector of the device. The position (x_P, y_P) of the middle point of the cylindrical bearing on the end-effector P, the roll angle θ with respect to the $x_0 - z_0$ plane, and the folding angle α define the device active movements.

Given the input variables $\mathbf{q}$, the coordinates $A = (x_A, y_A)$ and $B = (x_B, y_B)$ can be evaluated as in standard planar RR robots, i.e.,

$$x_A = x_C + l_1 \cos(q_1) + l_2 \cos(q_1 + q_2) \tag{4.2}$$

$$y_A = y_C + l_1 \sin(q_1) + l_2 \sin(q_1 + q_2) \tag{4.3}$$

$$x_B = x_E + l_1 \cos(q_3) + l_2 \cos(q_3 + q_4) \tag{4.4}$$

$$y_B = y_E + l_1 \sin(q_3) + l_2 \sin(q_3 + q_4) \tag{4.5}$$

From these points, it is possible to evaluate angle θ as

$$\theta = \arctan\left(\frac{y_B - y_A}{x_B - x_A}\right), \tag{4.6}$$

and the distance between A and B as

$$L = \sqrt{(x_B - x_A)^2 + (y_B - y_A)^2}. \tag{4.7}$$

Since the considered device has a parallel structure, the input variables $\mathbf{q}$ are constrained by the structure. In particular, length L has to satisfy the following inequality:

$$L \leq 2l_3. \tag{4.8}$$

If this constraint is satisfied, the folding edge angle α can be evaluated as

$$\alpha = 2 \arcsin\left(\frac{L}{2l_3}\right). \tag{4.9}$$

Finally, P coordinates are given by:

$$x_P = x_A + l_3 \cos\left(\theta + \pi/2 - \alpha/2\right) \tag{4.10}$$

$$y_P = y_A + l_3 \sin\left(\theta + \pi/2 - \alpha/2\right) \tag{4.11}$$

Equations from (4.2) to (4.11) constitute the direct kinematics procedure f_d introduced in eq. (4.1), i.e., the set of operations allowing to evaluate the output variables $\mathbf{u}$ as a function of input variables $\mathbf{q}$.

4.3.3 Inverse kinematics

In the inverse kinematic problem, the actuator rotation angles $\mathbf{q}$ are evaluated as a function of a set of output variables $\mathbf{u}$, i.e.,

$$\mathbf{u} = f_i(\mathbf{u}) \tag{4.12}$$

We can start the procedure by evaluating the distance L between A and B as

$$L = 2l_3 \sin\frac{\alpha}{2}. \tag{4.13}$$

From P coordinates and α and θ angles, A coordinates can be calculated as follows

$$x_A = x_P - l_3 \cos\left(\theta + \pi/2 - \alpha/2\right) \tag{4.14}$$

$$y_A = y_P - l_3 \sin\left(\theta + \pi/2 - \alpha/2\right). \tag{4.15}$$

The B coordinates can be calculated in a similar way. Once A and B point positions are known, the problem can be solved as the inverse kinematics of two standard 2-DoF, R-R planar manipulators; see for instance [279].

4.3.4 Differential kinematics

In this subsection, we analyse the relationship between joint angular velocities $\dot{\mathbf{q}}$ and output variables velocity $\dot{\mathbf{u}}$. From the kinematic analysis of the mechanism, it results that such a relationship is linear and can be expressed as:

$$\dot{\mathbf{u}} = \mathbf{J}\dot{\mathbf{q}}, \tag{4.16}$$

where $\mathbf{J}$ is the mechanism Jacobian matrix, i.e., a 4×4 matrix whose elements depend on mechanism configuration $\mathbf{q}$. Following a straightforward kinematics analysis, it is possible to verify that the $\mathbf{J}$ matrix can be evaluated as:

$$\mathbf{J}(\mathbf{q}) = \begin{bmatrix} \mathbf{C} + \mathbf{D}\,[1\ 0]\,\mathbf{B}^{-1}\mathbf{A} \\ [1\ 1]\,\mathbf{B}^{-1}\mathbf{A} \\ [1\ -1]\,\mathbf{B}^{-1}\mathbf{A} \end{bmatrix} \tag{4.17}$$

with

$$\begin{aligned} \mathbf{A} &= \begin{bmatrix} -y_{AC} & -y_{AD} & y_{BE} & y_{BF} \\ x_{AC} & x_{AD} & -x_{BE} & -x_{BF} \end{bmatrix}, \\ \mathbf{B} &= \begin{bmatrix} y_{PA} & -y_{PB} \\ -x_{PA} & x_{PB} \end{bmatrix}, \\ \mathbf{C} &= \begin{bmatrix} -y_{AC} & -y_{AD} & 0 & 0 \\ x_{AC} & x_{AD} & 0 & 0 \end{bmatrix}, \\ \mathbf{D} &= \begin{bmatrix} -y_{PA} \\ x_{PA} \end{bmatrix}; \end{aligned}$$

where, for the sake of conciseness, the double-letter subscripts indicate the relative displacement components between two points, e.g., $y_{AC} = y_A - y_C$, $x_{AC} = x_A - x_C$, etc.

Recalling the definition of the output control variables $\mathbf{u}$, output velocities are defined as $\dot{\mathbf{u}} = \left[v_{Px}, v_{Py}, \dot{\theta}, \dot{\alpha}\right]$, i.e., the vector is composed of two linear velocities v_{Px}, v_{Py}, representing P velocity Cartesian components, and two angular velocities. Therefore, the device Jacobian matrix can be divided into two sub-matrices as follows:

$$\mathbf{J}(\mathbf{q}) = \begin{bmatrix} \mathbf{J}_P \\ \mathbf{J}_O \end{bmatrix}, \tag{4.18}$$

such that

$$\begin{bmatrix} v_{Px} \\ v_{Py} \end{bmatrix} = \mathbf{J}_P \dot{\mathbf{q}}, \quad \begin{bmatrix} \dot{\theta} \\ \dot{\alpha} \end{bmatrix} = \mathbf{J}_O \dot{\mathbf{q}}. \tag{4.19}$$

4.3.5 Statics

The transpose of the Jacobian matrix previously evaluated is also useful for the statics analysis of the mechanism. Let us consider a generic configuration defined by joint variables $\mathbf{q}$, and let us assume that, in such configuration, the device is in a static equilibrium condition under the action of an external interaction vector $\mathbf{w}$ and a vector of motor torques $\boldsymbol{\tau}$. The vector of motor torques has the same dimensions of $\mathbf{q}$ and contains the torques applied by each of the device motors $\boldsymbol{\tau} = [\tau_1, \cdots, \tau_4]^{\mathrm{T}}$, while $\mathbf{w}$ is defined on the basis of $\mathbf{u}$ components, as $\mathbf{w} = [f_x, f_y, \tau_\theta, \tau_\alpha]^{\mathrm{T}}$, where f_x, f_y are the components of the interaction force that the environment applies on P, τ_θ is an external torque that corresponds to a rotation θ (as in Fig. 4.3c), while τ_α is an external torque that corresponds to a rotation α (as in Fig. 4.3d).

In statics equilibrium conditions, by applying the Principle of Virtual Works to the device, it is straightforward to verify that

$$\boldsymbol{\tau} = -\mathbf{J}^{\mathrm{T}} \mathbf{w}. \tag{4.20}$$

This relationship allows to evaluate the set of motor torques $\boldsymbol{\tau}$ that have to be applied to balance an external interaction vector $\mathbf{w}$.

It is also worth noticing that the relationship between the motor torques $\boldsymbol{\tau}$ and the interaction vector $\mathbf{w}$ depends on $\mathbf{q}$, since the Jacobian matrix $\mathbf{J}^{\mathrm{T}}$ depends on the mechanism configuration. To estimate the sensitivity of the actuator torques with respect to the mechanism configuration, let us consider an arbitrary reference configuration $\mathbf{q}_0$. In such a configuration, if an external interaction $\mathbf{w}_0$ is applied, the corresponding set of torques required to maintain the mechanism in the equilibrium configuration is $\boldsymbol{\tau}_0 = -\mathbf{J}(\mathbf{q}_0)^{\mathrm{T}} \mathbf{w}_0$. Let us consider an arbitrarily small perturbation with respect to this equilibrium configuration, i.e., $\mathbf{w} = \mathbf{w}_0 + \delta\mathbf{w}$, $\mathbf{q} = \mathbf{q}_0 + \delta\mathbf{q}$, $\boldsymbol{\tau} = \boldsymbol{\tau}_0 + \delta\boldsymbol{\tau}$. If the new configuration is still an equilibrium one, by neglecting higher order infinitesimal terms, it is possible to verify that

$$\delta\boldsymbol{\tau} = -\mathbf{J}(\mathbf{q}_0)^{\mathrm{T}} \delta\mathbf{w} - \left[\frac{\partial (\mathbf{J}(\mathbf{q})^{\mathrm{T}} \mathbf{w}_0)}{\partial \mathbf{q}} \right] \delta\mathbf{q}, \tag{4.21}$$

where the term

$$\mathbf{K}_q = \left[\frac{\partial(\mathbf{J}(\mathbf{q})^{\mathrm{T}}\mathbf{w}_0)}{\partial \mathbf{q}}\right] \tag{4.22}$$

allows to estimate the sensitivity of actuators torques with respect to errors or disturbance in the mechanism configuration estimation. This term is useful to understand the impact of the position tracking and position control errors on the actuators torques. Even if $\mathbf{K}_q$ elements are dimensionally a stiffness, these terms do not represent physical stiffness elements, but rather they take into account the dependence of the Jacobian on the configuration. For this reason, they are usually referred to as geometric terms [280]. Furthermore, even if $\mathbf{K}_q$ is square (4×4), it is in general nonsymmetric [281] and depends on $\mathbf{w}_0$. The analytical expression of $\mathbf{K}_q$ has not been reported for the sake of space; its evaluation is available in the MATLAB script included as supplemental material.

4.3.6 Manipulability

Manipulability analysis is widely adopted in robotics and mechanics to evaluate the effectiveness of a mechanism to transmit velocities and forces [282]. The kinematic manipulability index, in particular, is defined in each configuration as

$$\kappa = \sqrt{\det(\mathbf{J}\mathbf{J}^{\mathrm{T}})}. \tag{4.23}$$

It is worth noticing that this expression cannot be directly evaluated since the elements of $\mathbf{J}$ are not dimensionally homogeneous. In fact, the elements on the first two rows are lengths (they relate a linear velocity to an angular velocity), while the elements of the last two rows are dimensionless. To avoid this problem, we defined two different manipulability indices (see also eq. 4.18):

$$\kappa_P = \sqrt{\det(\mathbf{J}_P{\mathbf{J}_P}^{\mathrm{T}})}, \tag{4.24}$$

$$\kappa_O = \sqrt{\det(\mathbf{J}_O{\mathbf{J}_O}^{\mathrm{T}})}. \tag{4.25}$$

More in general, in each configuration, manipulability analysis defines how a unit sphere in the joint-velocity space, i.e., $\dot{\mathbf{q}}^{\mathrm{T}}\dot{\mathbf{q}} = 1$, is mapped in the end-effector velocity sphere. Given the linear and configuration-dependent relationship between joints and end-effector velocities $\dot{\mathbf{u}}$ established in eq. (4.16), it is straightforward to see that the sphere is mapped into an ellipsoid, whose equation is $\dot{\mathbf{u}}^{\mathrm{T}}\mathbf{J}^{-\mathrm{T}}\mathbf{J}^{-1}\dot{\mathbf{u}} = 1$. The semi-axes of such an ellipsoid are oriented as the eigenvectors of the matrix $\mathbf{J}\mathbf{J}^{\mathrm{T}}$; the square-root of its eigenvalues returns, instead, their lengths.

The analysis of the manipulability ellipsoid provides some interesting information on the mechanism properties. In particular, it is clear that, when the mechanism approaches a singular configuration, the ellipsoids volume drops to zero. Furthermore, a sphere-shaped ellipsoid indicates a rather isotropic transmission behavior, i.e., the mechanism can move in any direction with approximately the same joint velocities. On the other side, a flatten ellipsoid indicates that, in such configuration, the mechanism can move more efficiently in the direction corresponding to the larger semi-axes, while moving in the directions corresponding to the smaller semi-axes requires higher joint velocities. In the analysed mechanism, both $\dot{\mathbf{q}}$ and $\dot{\mathbf{u}}$ are $\mathbb{R}^4$ vectors, so the ellipsoid is four-dimensional. Furthermore, the dimensions of $\dot{\mathbf{u}}$ vector elements are not homogeneous, since it contains two linear and two angular velocities. For the sake of clarity, in this analysis we only considered the linear velocities, i.e., we evaluate the two-dimensional projection of the manipulability ellipsoid in the v_{Px}-v_{Py} plane, that is an ellipse.

Fig. 4.5 shows how the position kinematic manipulability ellipse varies during two representative trajectories. The first three figures (I, II, III) have been realized by moving the end-effector horizontally along a direction parallel to x_0 axis, the second three (IV, V, VI) by moving it vertically along the y_0 axis. The analysis has been carried out on a wider set of configurations, spanning the operative device workspace, verifying that the manipulability index is, in all the analysed cases, sufficiently far from zero and that the device is sufficiently far from singularities. Such results can be verified by running the MATLAB script included as supplemental material.

Manipulability analysis is also useful for carrying out a preliminary evaluation of the force feedback capabilities of the device. In particular, similarly to the kinematic manipulability index, the *force* manipulability index is defined as the ratio of a performance measure in the space of forces exchanged with the environment and an effort measure in the space of actuated joint torques, i.e.,

$$\kappa_f = \frac{\delta \mathbf{w}^{\mathrm{T}} \mathbf{W}_w \delta \mathbf{w}}{\delta \boldsymbol{\tau}^{\mathrm{T}} \mathbf{W}_\tau \delta \boldsymbol{\tau}}, \tag{4.26}$$

where $\mathbf{W}_w$ and $\mathbf{W}_\tau$ are weight matrices that can be defined for properly weighting the different components and for adjusting the dimension units of $\mathbf{w}$ and $\boldsymbol{\tau}$, respectively. By considering eq. (4.20), it is possible to verify that, also in this case, a unit sphere in the actuator torque space is mapped into an ellipsoid in the end-effector force space. Assuming $\mathbf{W}_w$ and $\mathbf{W}_\tau$ as identity matrices for the sake of simplicity, lengths of the

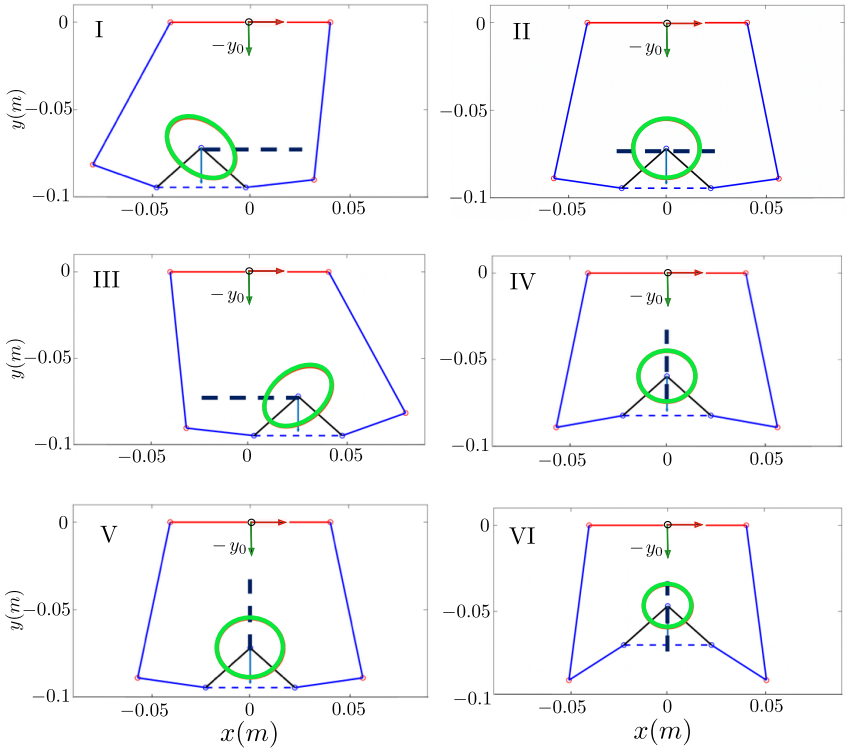

Figure 4.5 – Manipulability analysis. Position kinematic manipulability ellipses for x and y velocity components in six representative device configurations. In each subfigure, a scheme of the device is reported. The red link represent the static upper body, the blue lines represent the links driven by the motors, the black lines represent the passive links on the end-effector, the manipulability ellipse is reported in thick green, centered on the end-effector middle point P. Subplots I-III show a horizontal trajectory (black, thick, dashed line), subplots IV-VI show a vertical trajectory.

ellipsoid semi-axes can be evaluated as the square-root of the eigenvalues of $\left(\mathbf{J}\mathbf{J}^{\mathrm{T}}\right)^{-1}$, and their orientations are given by its eigenvectors. It is straightforward to verify that the semiaxes of the kinematic and force manipulability ellipsoids have the same orientation, while the lengths of the first one are the reciprocal of the second one.

4.3.7 Numerical simulations

Figures 4.6–4.10 report the results of a series of numerical simulations. They aim at testing whether the device can operate with suitable manipulability levels during a set of six representative movements for haptic applications.

Subfigures (a) of Figs. 4.6–4.10 show a translation of P along the x_0 direction, with a 26 mm stroke. The trajectory is travelled, with constant speed, in 10 s, while θ and α are

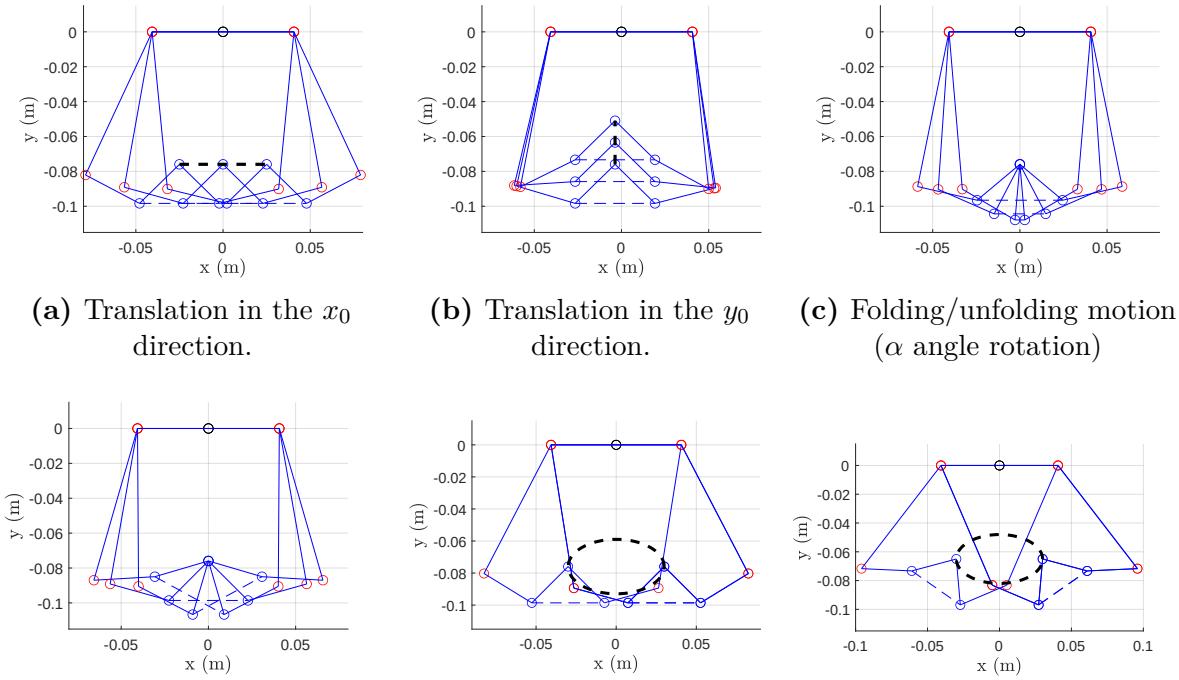

(a) Translation in the x_0 direction.

(b) Translation in the y_0 direction.

(c) Folding/unfolding motion (α angle rotation)

(d) Rolling motion (θ angle rotation)

(e) Translation of P along an ellipse trajectory

(f) Translation of P along an ellipse trajectory and θ roll movement

Figure 4.6 – Numerical simulations: Kinematic scheme of the device in the initial and final configurations of the considered movements. Blue lines represent the mechanism links, black dashed lines represent the trajectory of P.

maintained constant. Subfigures (b) show a translation of P along the y_0 direction, with a 16 mm stroke. Also in this case, the speed is constant and the trajectory is travelled in 10 s, while θ and α are maintained constant. Subfigures (c) show a roll movement in which the θ angle decreases linearly from 15° to 0° in the first 5 s and then increases from 0° to 15° in the remaining 5 s. The α angle and the position of P are maintained constant. Subfigures (d) show a folding/unfolding movement in which the α angle decreases linearly from 110° to 20° in the first 5 s and then increases from 20° to 110° in the remaining 5 s. The θ angle and the position of P position are maintained constant. Subfigures (e) show a translation movement of P that follows an ellipse with semi-axes 30 mm and 17 mm in the x_0 and y_0 directions, respectively, during 10 s. θ and α angles are maintained constant. Finally, subfigures (f) show the same ellipse trajectory travelled by P in 10 s, but this time coupled with a roll movement θ, which varies from $-35°$ to 35°. The α angle is maintained constant.

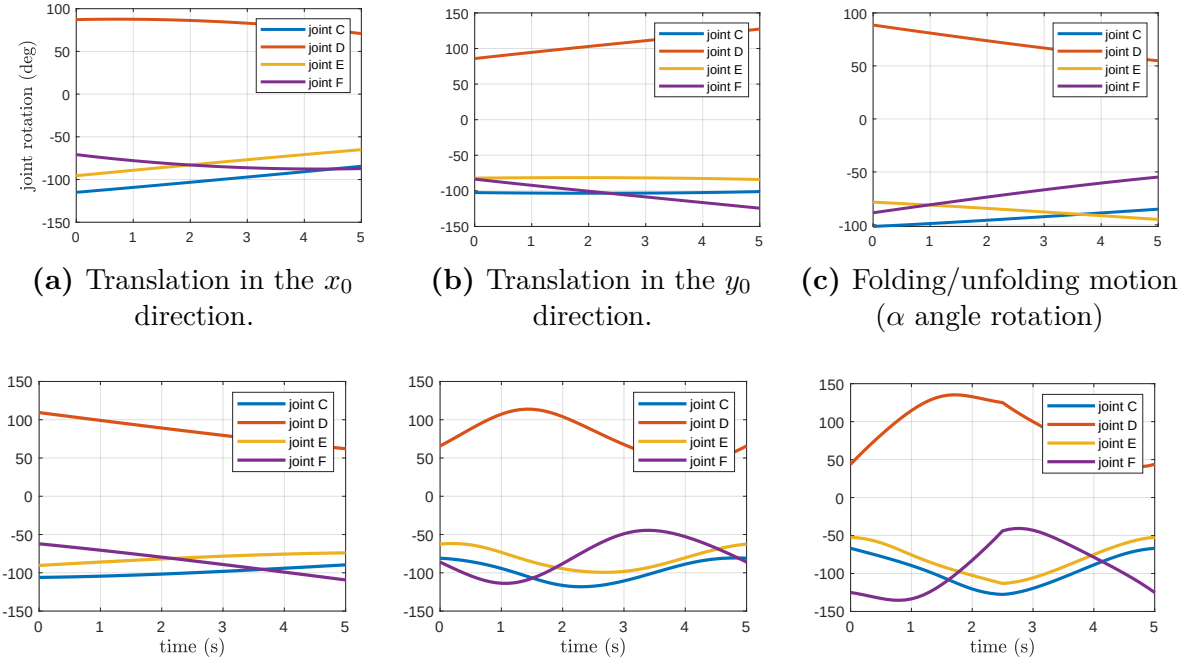

(a) Translation in the x_0 direction.

(b) Translation in the y_0 direction.

(c) Folding/unfolding motion (α angle rotation)

(d) Rolling motion (θ angle rotation)

(e) Translation of P along an ellipse trajectory

(f) Translation of P along an ellipse trajectory and θ roll movement

Figure 4.7 – Numerical simulations: Rotation angles of actuated joints C, D, E, F as a function of time.

Fig. 4.6 reports the kinematics scheme of the device in the initial and final configurations (blue, thin lines) of the above movements, as well as the trajectory of point P (black, thick dashed line). Fig. 4.7 shows the rotation angles of the actuated joints C, D, E, F (see Fig. 4.2). To obtain these angles, we performed the inverse kinematic analysis (see Sec. 4.3.3), starting from the trajectory defined in the workspace. Fig. 4.8 shows the joint torques the motors need to apply to resist a representative constant force of 2 N applied on P towards the $-y_0$ direction. Finally, Figs. 4.9 and 4.10 show the kinematic manipulability indices κ_P and κ_O, evaluated from eq. (4.24) and (4.25). Results relative to force manipulability have not been reported here for the sake of space, however, assuming that the interaction vector contains the interaction force only, i.e., $\mathbf{w} = [f_x, f_y, 0, 0]^{\mathrm{T}}$, the force manipulability index κ_f can be evaluated straightforwardly as $\kappa_f = 1/\kappa_P$. Each subfigure (a)-(f) in Figs. 4.6–4.10 refers to one of the six movements described at the beginning of this subsection.

Results show that device workspace is compatible with design requirements for haptic interactions on hand palm. In all the simulated cases, the inverse kinematics procedure

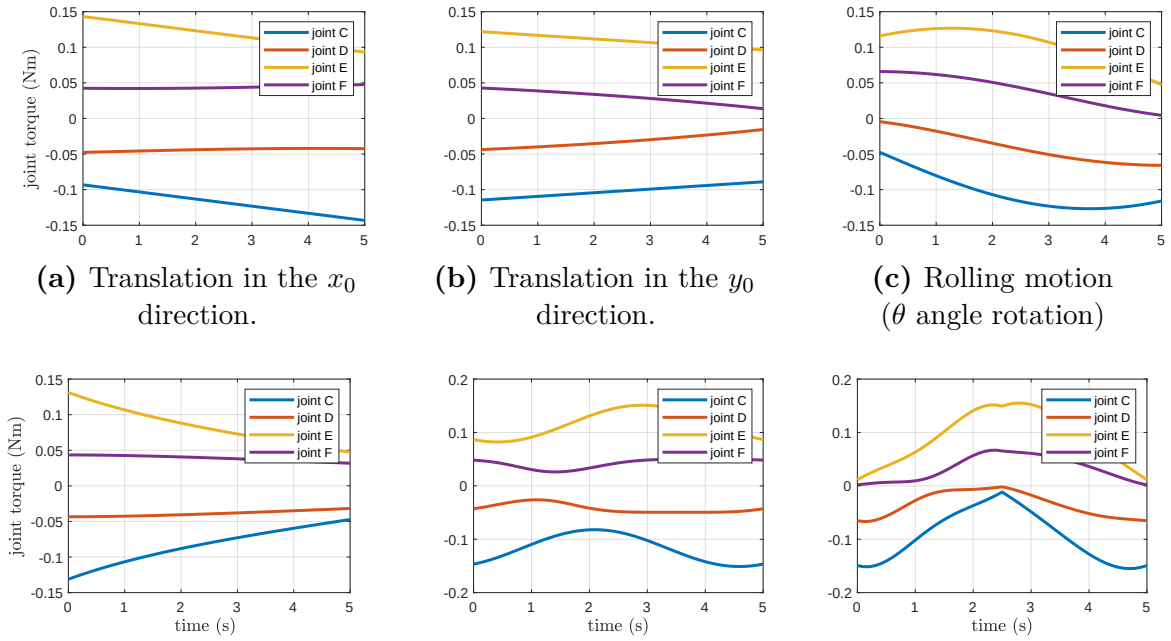

(a) Translation in the x_0 direction.

(b) Translation in the y_0 direction.

(c) Rolling motion (θ angle rotation)

(d) Folding/unfolding motion (α angle rotation)

(e) Translation of P along an ellipse trajectory

(f) Translation of P along an ellipse trajectory and θ roll movement

Figure 4.8 – Numerical simulations: Joint torques applied by the motors in joints C, D, E, F as a function of time, when a 2 N force is applied on P towards the $-y_0$ direction.

provides physically feasible solutions. The torques necessary to resist a force applied on P with magnitude 2N are clearly configuration-dependent, but always compatible with the motor characteristics in all the simulated cases. Manipulability indices κ_P and κ_O vary according to the different simulated configurations, but their values are sufficiently far from zero, reflecting that there are no singularity issues.

A wider set of simulations can be carried out using the MATLAB script included as supplemental material (see also Sec. 4.3.8).

4.3.8 CoppeliaSim kinematic model

We also present a simulated model of the device, which replicates its kinematic structure and mechanics as described in the previous Sections. Each link of the kinematic chain is realized through the composition of three objects: i) the virtual joint that is responsible of the link motion, ii) a simple cuboid shape defining the kinematic connection between the same joint and the subsequent one along the chain, iii) a visual mesh extracted from

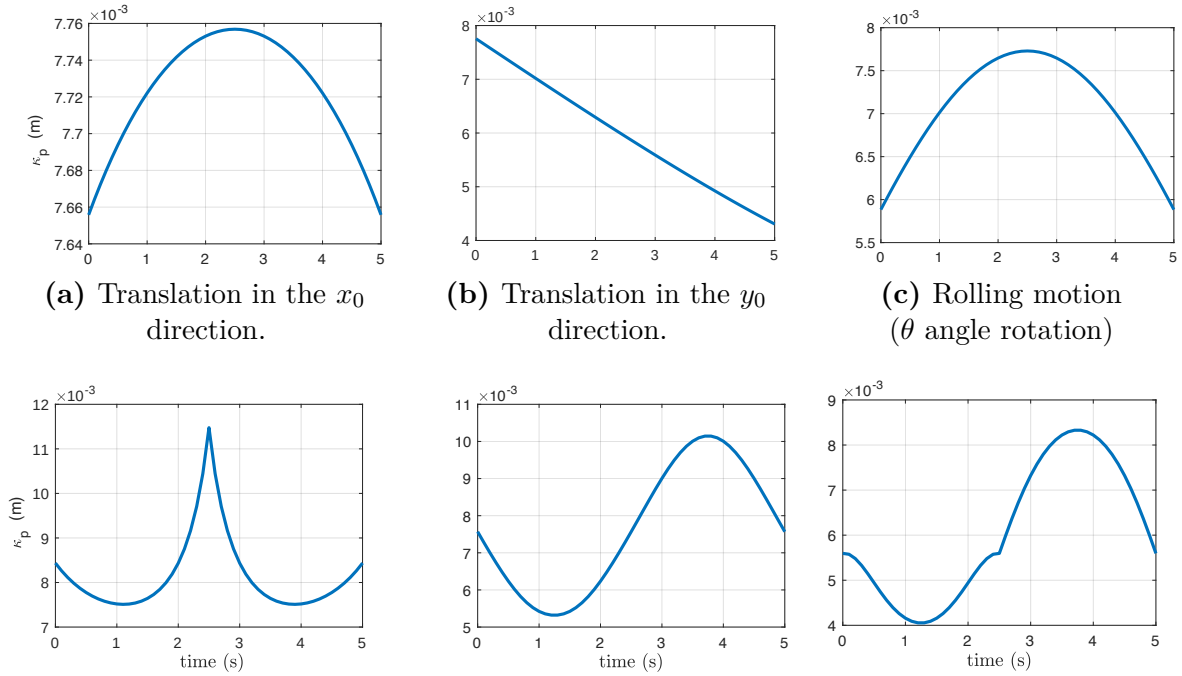

(a) Translation in the x_0 direction.

(b) Translation in the y_0 direction.

(c) Rolling motion (θ angle rotation)

(d) Folding/unfolding motion (α angle rotation)

(e) Translation of P along an ellipse trajectory

(f) Translation of P along an ellipse trajectory and θ roll movement

Figure 4.9 – Numerical simulations: Kinematic manipulability index κ_p evaluated considering the position Jacobian matrix $\mathbf{J}_p$.

the device CAD model, with the same structure of the corresponding link of the real device. Each joint is commanded through position inputs: in particular, given an arbitrary configuration of the two serial arms, specified through the vector $\mathbf{q}$ of the active joints C, D, E and F, the closed-chain structure is guaranteed by forcing the position of the passive joints A and P as

$$\begin{aligned} q_A &= \theta + (\pi - \alpha)/2 - q_1 - q_2 \\ q_P &= q_A + \alpha. \end{aligned} \tag{4.27}$$

The CoppeliaSim scene containing this model, along with a MATLAB script computing the appropriate joint configuration vector $\mathbf{q}$ for a set of representative trajectories (see also Sec. 4.5.3), are available as supplemental material.

4.4 Control Implementation

According to the device mechanism and type of interaction to be rendered, our device can be controlled in different ways. We present here a position control scheme, along with its evaluation.

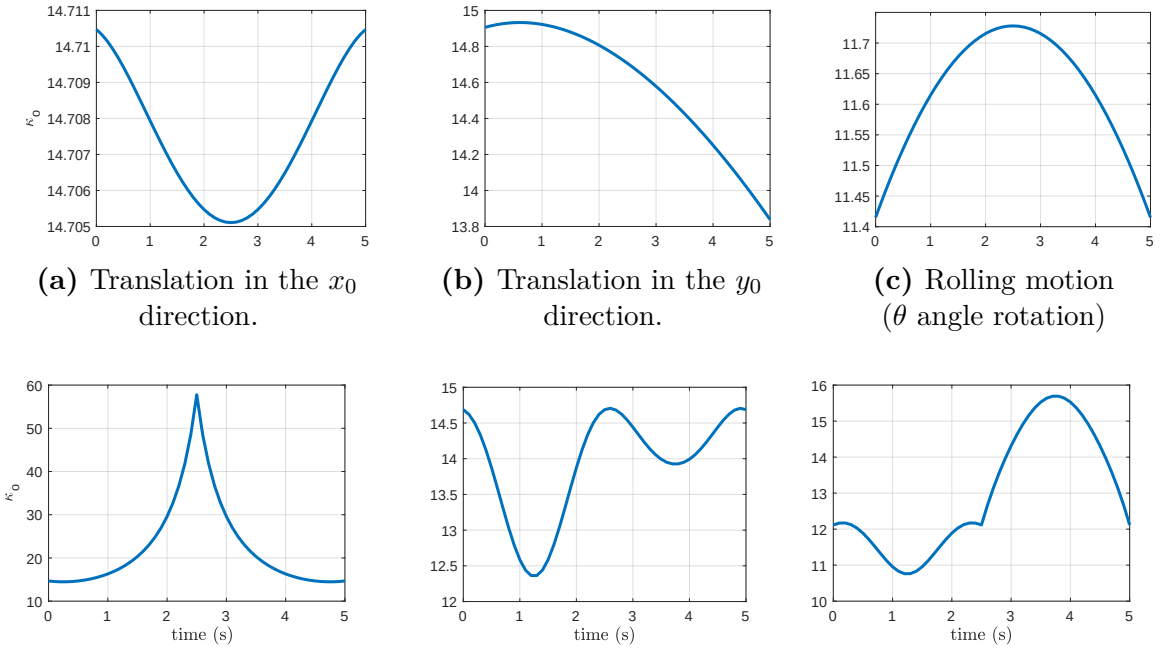

(a) Translation in the x_0 direction.

(b) Translation in the y_0 direction.

(c) Rolling motion (θ angle rotation)

(d) Folding/unfolding motion (α angle rotation)

(e) Translation of P along an ellipse trajectory

(f) Translation of P along an ellipse trajectory and θ roll movement

Figure 4.10 – Numerical simulations: Kinematic manipulability index κ_o evaluated considering the orientation Jacobian matrix $\mathbf{J}_o$.

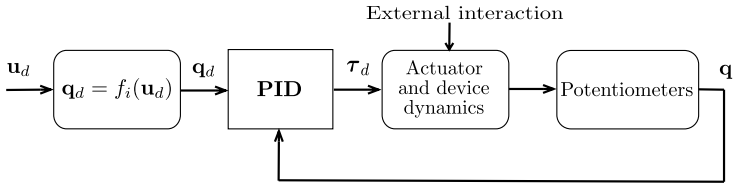

Figure 4.11 – Position control system. The reference configuration is provided in the end-effector configuration space $\mathbf{u_d}$. The inverse kinematics procedure described in Sec. 4.3 allows to convert the desired configuration in the joint space. Finally, a PID controller is implemented, providing the desired motor torque $\boldsymbol{\tau}_d$. The actual joint configuration is measured by the potentiometers placed on the device active joints (C, D, E, F – see Fig. 4.2).

4.4.1 Device position control

The device position control focuses on controlling the position and orientation of the end-effector. This can be implemented in two ways. The first is to manipulate the end-effector as a rigid fixed-shaped object: in this case, its orientation and folding angle are kept constant, while its position with respect to the upper body coordinate $S_0 < x_0, y_0, z_0 >$ is modified by the two articulated arms. The second is to manipulate the end-effector as a flexible coupling hinge by rotating the two plates composing the end-effector: in this case, its position with respect to the upper body coordinate $S_0 < x_0, y_0, z_0 >$ is kept constant, while the orientation of the end-effector and the angle between its two plates varies. By combining these two levels, the two arms can move and orient the end-effector within its allowed workspace. Both the levels can be schematised and managed as shown in Fig. 4.11, where the task can be defined in the end-effector configuration space as a sequence of desired configurations $\mathbf{u}_d$. The inverse kinematics procedure detailed in Sec. 4.3 allows to pass from the end-effector space to the joint space, i.e.,

$$\mathbf{q}_d = f_i(\mathbf{u}_d) \tag{4.28}$$

The position control is therefore managed at the joint level by means of a PID controller, in which the actual joint configuration $\mathbf{q}$ is provided by the potentiometers.

4.4.2 Control Evaluation

To evaluate the performance of each actuated joint (C, D, E, F), we commanded step and sinusoidal inputs and analyzed the actual actuated movement. Each actuated joint was tested separately, with the other joints free to move. Each movement was repeated 10 times and their results were averaged.

We considered three step reference inputs, with target amplitudes of 20°, 40°, and 60°, all of which starting from 0°. The rise time is defined as the time required for the signal, i.e., the actual rotation of the joint, to rise from 10 to 90% of its steady value. Fig. 4.12 and Tab. 4.4.2 present the results, showing very little overshooting, a maximum rise time of 0.17 s (on joint E), and a maximum error at steady state of 1.0% (on joint F).

We considered three sinusoidal reference inputs, $r(t) = A\sin(0.4\pi t)$ with amplitudes $A = 10°$, 20°, and 30°. Fig. 4.13 present the results. The worst performance was registered on joint D when actuating the sinusoid with A =30°, showing an average tracking error of 6.7% of the amplitude; while the best performance was registered on joints C when

actuating the sinusoid with A =10°, showing an average tracking error of 5.1% of the amplitude.

4.5 Device Performance Evaluation

We evaluate the performance of the proposed device in actuating a set of representative movements.

4.5.1 Target movements for the end-effector

We considered five representative patterns of motions for the end-effector (see Figs. 4.3 and 4.4 for reference):

M1. a horizontal movement of the end-effector while it is partially folded: P moves of 26 mm along x_0, with $\alpha = 100°$ (see https://youtu.be/ZuB_JxwbB9s?t=20);

M2. a vertical movement of the end-effector while it is partially folded: P moves of 16 mm along y_0, with $\alpha = 100°$ (see https://youtu.be/ZuB_JxwbB9s?t=44);

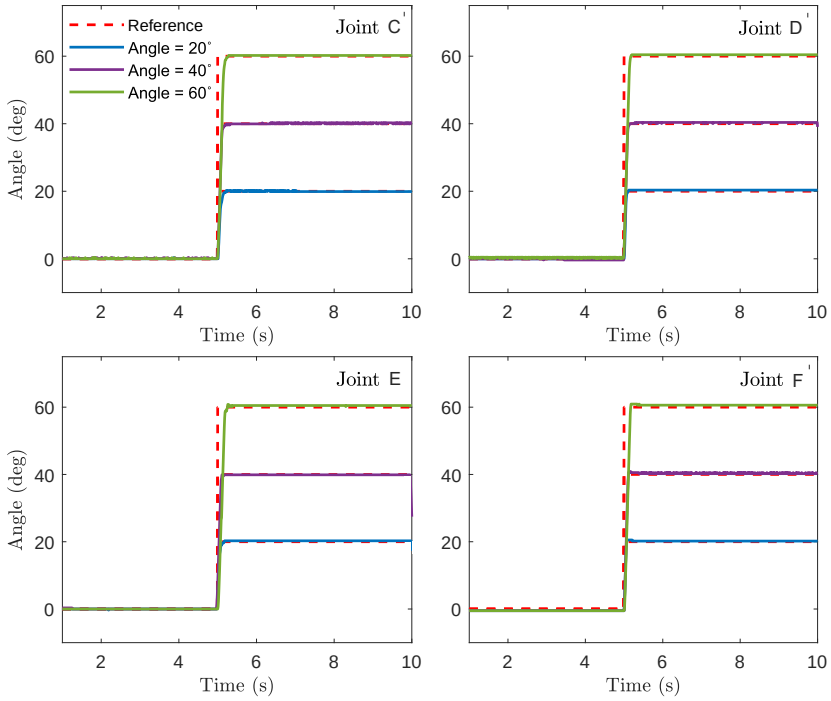

Figure 4.12 – Step response. We commanded the four actuated joints to follow a step command, rotating from 0°to 20°, 40°, or 60°.

Table 4.2 – Step response. Rise time and tracking errors.

	Angle	joint C	joint D	joint E	joint F
Rise time (s)	20°	0.08	0.06	0.07	0.06
	40°	0.14	0.09	0.09	0.11
	60°	0.16	0.15	0.17	0.16
Error (deg)	20°	0.229	0.341	0.273	0.193
	40°	0.270	0.377	0.118	0.558
	60°	0.216	0.429	0.497	0.595

M3. a roll movement of the end-effector while it is partially folded: P is stationary, while θ rolls in [0, 15]° (see https://youtu.be/ZuB_JxwbB9s?t=69);

M4. a folding/unfolding movement of the end-effector: P is stationary, while α changes in [20, 110]° (see https://youtu.be/ZuB_JxwbB9s?t=94);

M5. a combined planar/roll movement of the end-effector while it is partially folded: P moves along an ellipse with axes 34 mm and 60 mm (combination of M1 and M2), while θ rotates in [0, 35]° (similar to M3) and α is stationary at 100° (see https://youtu.be/ZuB_JxwbB9s?t=121).

These are the same movements also considered in the numerical simulations of Sec. 4.3.7.

4.5.2 Tracking of the end-effector

To evaluate the error in tracking the target set of movements, we measured the pose of the end-effector using the external optical tracking system OptiTrack (NaturalPoint Corp). It is composed of six infrared cameras (Optitrack Flex-3) sampling the position of six passive markers installed over the two moving plates of the end-effector. The tracking system is connected to a desktop computer (Alienware AURORA R8, Intel Core i7, 16 GB RAM, NVIDIA GeForce 1080), which enable to record the position of the markers and reconstruct the pose and configuration of the end-effector at 100 Hz.

4.5.3 Results

We compared the five target patterns of motion, described in Sec. 4.5.1 and implemented using the position control of Sec. 4.4, with the actuated motions, registered using the

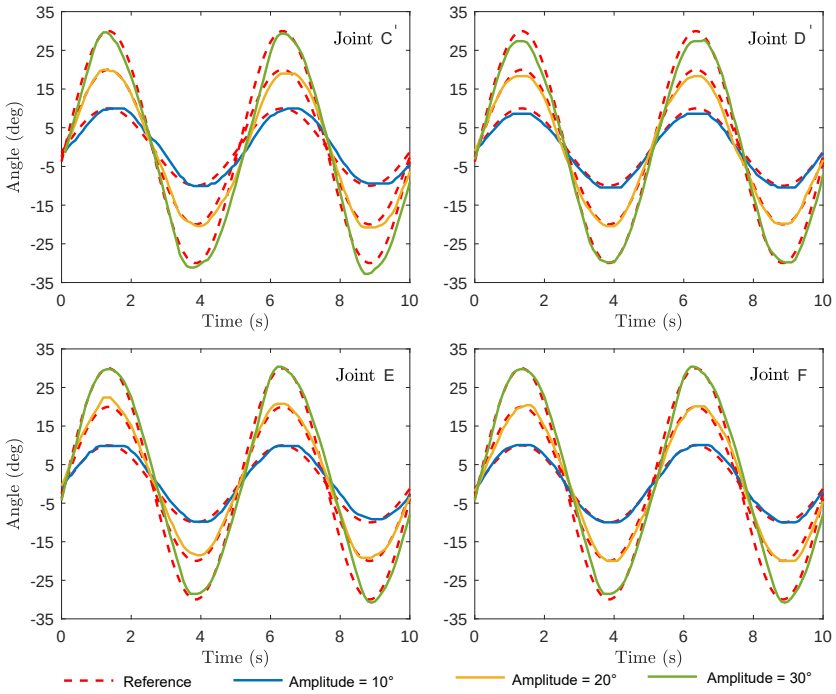

Figure 4.13 – Sine response in tracking response of the four active joints. Sinusoidal inputs with different amplitudes (10°, 20°and 30°).

optical tracking system described in Sec. 4.5.2.

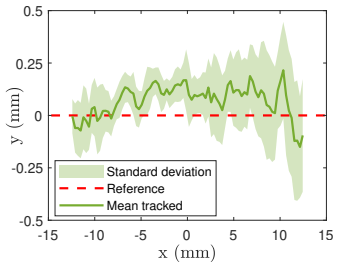

Figure 4.14 – M1: horizontal mov. of P, $x_P \in$[-13, 13] mm.

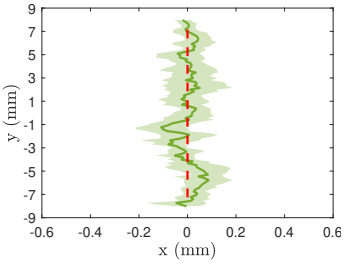

Figure 4.15 – M2: vertical mov. of P, $y_P \in$[-8, 8] mm.

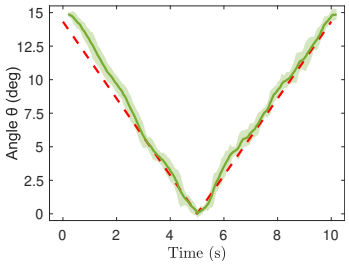

Figure 4.16 – M3: roll movement of $\theta \in$ [0,15]°.

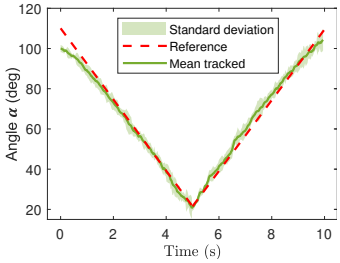

Figure 4.17 – M4: folding movement of $\alpha \in$ [20,110]°.

Figures 4.14, 4.15, 4.16, 4.17, and 4.18 report the commanded and tracked mean

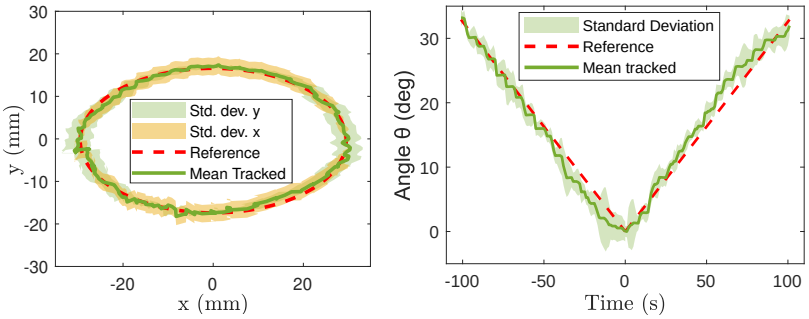

(a) elliptical movement of P, with $x_P \in$[-30, 30] mm and $y_P \in$[-17, 17] mm

(b) roll movement of $\theta \in$ [0,35]°

Figure 4.18 – M5: combined ellipse and roll movement.

Table 4.3 – Results of the device performance evaluation.

Pattern (Sec. 4.5.1)	Error (mean)
M1 (horizontal)	P along x: 1.678 mm (5.60% wrt reference) P along y: 0.057 mm (should be 0)
M2 (vertical)	P along x: 0.056 mm (should be 0) P along y: 1.537 mm (4.90% wrt reference)
M3 (roll)	θ: 0.686° (4.57% wrt reference)
M4 (folding)	α: 2.305° (2.71% wrt reference)
M5 (ellipse + roll)	P along x: 2.538 mm (4.23% wrt reference) P along y: 1.793 (5.26% wrt reference) θ: 1.323° (3.34% wrt reference)

movements for motions M1, M2, M3, M4, and M5, respectively. Each movement was repeated ten times. Table 4.3 reports the registered errors, computed as the mean difference between the commanded and tracket motions.

4.6 Human Subjects Evaluation

We carried out a human subjects study to test the device capabilities of delivering haptic sensations. Twelve participants (10 males, 2 females, age 22-32, all right-handed) were enrolled in the study. None of the participants reported any visual or haptic perception

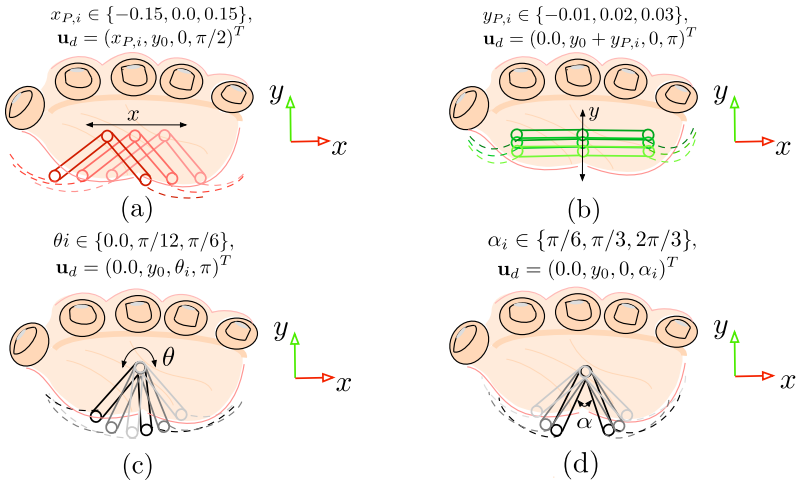

Figure 4.19 – Human subjects evaluation. The device applied a series of haptic patterns, spanning the full rendering space of the device along the four controlled variables of the end-effector: three movements per variable, changing (a) x_p, (b) y_p, (c) θ, and (d) α. Subjects had to recognize which haptic stimulation they were provided.

deficiencies. The experimenter explained the procedures and spent about three minutes adjusting the setup to be comfortable before the subject began the experiment. Due to the different dimension of the hands, for each participant, the device is calibrated to define the make/break contact configuration. Users were asked to wear the device and recognize a series of haptic patterns, spanning the full rendering space of the device along the four controlled variables of the end-effector, i.e., x_P, y_P, θ and α (see Sec. 4.4). As detailed in Table 4.4, for the four variables, we rendered twelve different configurations of the device, considering three variations of each parameter: variations of x_p provided sharp contacts at different points on the palm (see Fig. 4.19a), variations of y_p provided contacts with different applied forces (see Fig. 4.19b), variations of θ provides contacts at different orientations (see Fig. 4.19c), and variations of α provides contact at different sharpness levels (see Fig. 4.19d). For each configuration, the device end-effector moves towards the user's palm, stays in contact for 2 s, and then breaks contact and moves away. After each interaction, participants are asked to describe what they felt, identifying which sensation/configuration was just provided to them among the different choices reported in Table 4.4. To avoid order effects, the interactions where randomized using a Latin square design, dividing the interactions in four blocks (one per control variable).

Results showed an overall recognition rate of 68.75%, with specific rates of 83.3%, 50%, 75% and 66.7% for the sets of control variables x_P, y_P, θ and α, respectively, which is well above the chance level.

Table 4.4 – Device configurations rendered during the human subjects evaluation, spanning the full rendering space along the 4 controlled parameters. y_0 represents the standard vertical height of the end-effector, calibrated for each subject to ensure good contact.

Ctrl. var.	Considered set	Rendered configuration
x_P	$x_{P,i} \in \{-0.15, 0.0, 0.15\}$ [m]	$\mathbf{u}_d = (x_{P,i}, y_0, 0, \pi/2)^T$
y_P	$y_{P,i} \in \{0.01, 0.02, 0.03\}$ [m]	$\mathbf{u}_d = (0.0, y_0 + y_{P,i}, 0, \pi)^T$
θ	$\theta_i \in \{0.0, \pi/12, \pi/6\}$ [rad]	$\mathbf{u}_d = (0.0, y_0, \theta_i, \pi)^T$
α	$\alpha_i \in \left\{\pi/6, \pi/3, \frac{2}{3}\pi\right\}$ [rad]	$\mathbf{u}_d = (0.0, y_0, 0, \alpha_i)^T$

4.7 Discussion and Conclusions

This Chapter presented a 4-DoF wearable haptic device for the palm. The end-effector is a foldable two-pieces flat surface that can make/break contact with the palm to provide variable pressure stimuli, move sideways to provide skin stretch and tangential motion stimuli, as well as fold to elicit the sensation of interacting with edges of varied nature. With respect to other wearable interfaces for the palm, the proposed device is able to provide a wider range of haptic stimuli, including the rendering of edge sensations, which is rather innovative. It weighs 310 g and features an adjustable structure to adapt to different hand types and sizes. Together with the design of the device, we present its mobility, statics, and manipulability analyses as well as direct, inverse, and differential kinematics, which are in turn used to implement a position control algorithm. The simulated model of the device, both for MATLAB and CoppeliaSim, is available as supplemental material, enabling the reader to further study its structure and rendering capabilities.

Results of our device performance evaluation show that the device is well capable of actuating a wide range of patterns of motion with reduced error and good repeatability. The registered *maximum* error across the considered movements is 2.538 mm (4.23% wrt reference) for displacements and 0.686° (4.57% wrt reference) for rotations. A human subjects study also showed that users are well capable of understanding and recognizing the provided sensations, especially when rendering slanted surfaces and curvatures. On the other hand, vertical movements, i.e., moving the end-effector towards/away from the palm, were found harder to recognize (but still well above the chance level). This latter result can be explained by the fact that, in such interactions, the control of the *force* applied to the palm is more important than the displacement. Future work will address the force

control and characterization of the device.

We envision the use of this device for applications of Virtual Reality (VR) and robotic teleoperation, which have been proven to significantly benefit from cutaneous haptics [283]. In this respect, we have already carried out a series of human subjects experiments using the proposed hand device in immersive. The device has been adapted to support other end-effectors in addition to the one presented in this Chapter, so as to able to simulate the sensation of interacting with an even broader range of surfaces, having different curvatures, stiffness, local shape, and texture. Twelve participants were asked to wear the device and interact with a series of objects in VR, evaluating the immersiveness of the interaction and the realism of the rendering. Results show a rather good performance of the device, e.g., realism was ranked 8.4 out of 10 for the hinge-like end-effector when interacting with rigid objects with different edges, proving the viability of the proposed device for VR applications.

From this work, we learnt that it is possible to recreate rich touch sensations to the palm with rigid reconfigurable end-effectors, which can have applications in immersiveness virtual interaction. However, as the end-effector developed is rigid, we could only apply limited mechanical sensation to the skin. For this reason, in the next chapter, we will extend the design of the device to consider interchangeable (soft) end-effectors for more diverse stimulation.

Chapter 5

Wearable Ungrounded Device for Palmar-based Interactions: Interchangeable End-effectors

Contents

5.1 Introduction

This chapter is a generalization of the work presented in Chapter 4. Here, we develop multiple end-effectors for the same hand-mounted device for generating diverse stimulation with varying stiffness and deformability characteristics. Similarly, this chapter summarizes the design and kinematics of the wearable haptic device and presents a position control scheme able to actuate generic end-effectors. A human-subjects evaluation in immersive VR shows the broad applicability of the device, able to render rich interactions with a diverse set of virtual objects. Our objective is to study and explore the possibility of using flexible materials for deformable soft end-effectors, as well as advancing the line of research on *modular* haptic devices.

The device, as shown in Fig. 5.1, features a 4-degrees-of-freedom (4-DoF) mechanism controlling the motion of two articulated legs that, in turn, actuate the end-effector. The device is designed to support a broad range of end-effectors that can be easily customized and exchanged for each considered scenario, so as to best render the target sensations. As a representative example, we describe five end-effectors, which are capable of providing the sensations of breaking/making contact with rigid and soft surfaces, interacting with objects having different stiffness, curvature, local shape, texture as well as variable edges or slanted surfaces. Nonetheless, the device structure and control support the use of many other types of end-effectors, not limited to those presented here. Three of these end-effectors are quantitatively evaluated in a human-subjects experiment in immersive VR, proving the viability and flexibility of the proposed system in rendering a wide range of different sensations. A video of the device in action can be found as supplemental material and at `https://youtu.be/1rs0s9UN2fI`.

With respect to other wearable haptic solutions for the palm [273]–[278], the proposed device can convey a significantly broader and more customizable range of stimuli. Indeed, it is rare to see reconfigurable haptic interfaces. One of the few examples is the Haptic Revolver [284], which is a hand-held VR controller actuating an interchangeable wheel that raises and lowers underneath the user's finger to render contact with different textures. More recently, we presented a 3-DoF parallel tendon-based palm device able to actuate a set of rigid tactors that can have different shapes [277]. To the best of our knowledge, no wearable reconfigurable haptic solution for the palm have been presented in the literature. A preliminary version of our device, featuring a rigid non-changeable end-effector, has been presented in [18]. Here we improve the device design and control to support interchangeable

end-effectors, discuss the rendering characteristics of five end-effectors, and present a human-subjects evaluation on three of them in VR.

This Chapter is a revised version of the works under revision as

* **L. Kuang**, M. Ferro, M. Malvezzi, D. Prattichizzo, P. Robuffo Giordano, F. Chinello, C. Pacchierotti. "A Wearable Haptic Device for the Hand with Interchangeable End-Effectors." *Submitted to IEEE Transactions on Haptics*, 2023.
  Video available at: https://youtu.be/1rs0s9UN2fI.

5.2 Wearable Device and Interchangeable End-effectors

The general design of the wearable haptic device, together with its mobility, statics, and manipulability, as well as direct, inverse, and differential kinematics is presented in [18]. Here we summarize the main aspects, focusing on the improvements made to enable the support of interchangeable end-effectors. We also describe the three representative end-effectors that we have chosen to display the features of the device. The prototype of the wearable device is shown in Fig. 5.1, the static upper body is fixed to the back of the hand, housing two motors. Two articulated legs, housing two additional motors, connect the upper body with the end-effector, that can be changed according to the target interaction. Here we present five end-effectors, able to simulate the sensations of interacting with: (E1) rigid slanted surfaces and sharp edges having different orientations, (E2) U-shaped soft surfaces having different curvatures, and soft surfaces having different (E3) stiffness, (E4) local shape, or (E5) texture. The first three of these end-effectors are tested in a human subjects study in VR. Of course, more end-effectors can be easily designed according to the target environment to render. The CAD design in presented in Fig. 5.2. The device features a 4-DoF structure with two symmetric serial arms connecting the chosen end-effector to the static upper body, which is in turn fastened to the back of the hand with velcro straps. Each arm consists of an arcuated link (L1 in Fig. 5.2) and a straight link (L2), forming a rigid serial chain constrained to each other. The arcuated links of each arm connect to the upper body with joints C and E, as well as to the corresponding straight links L2 through two lower revolute joint D and F. Joints C, E, D, and F are actuated by servomotors. The axes of the revolute joints are parallel to each other, making the whole mechanism planar. Finally, each straight link L2 is connected to the chosen end-effector through a passive

revolute joint, generating a 2-DoF planar articulated mechanism. The combined action of the two arms leads to the final 4 DoF of the system, making the two end points of the legs, A and B, move vertically and horizontally across the plane defined by axes x_0–y_0 in Fig. 5.2.

Given the above kinematics constraints, it is possible to design end-effectors that cover a wide range of interactions, according to the task at hand. The end-effectors can be attached to the straight links of the device, between the joints indicated with A and B in Fig. 5.2.

In our prototype, we controlled the device using an Atmega328 controller on an Arduino Uno Board. We used two HS-85MG (Hitech RCD, US) servomotors on the upper body, actuating joints C, E, and two KST-08H (KST servos, HK) servomotors on the arms, actuating joints D, F. Rotatory Bourns potentiometers 3382H (Bourns, CA, US) are installed in each servomotor shaft, so as to measure the motor's rotation angle. Fig. 5.3

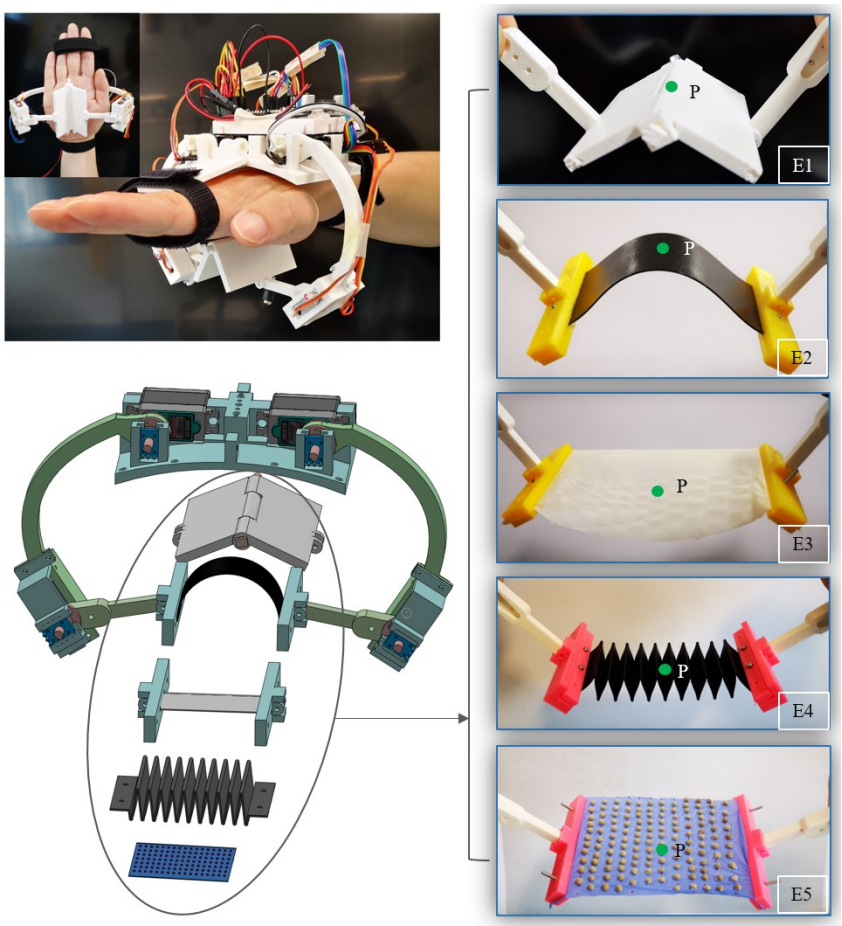

Figure 5.1 – The proposed 4-DoF wearable haptic device for the palm.

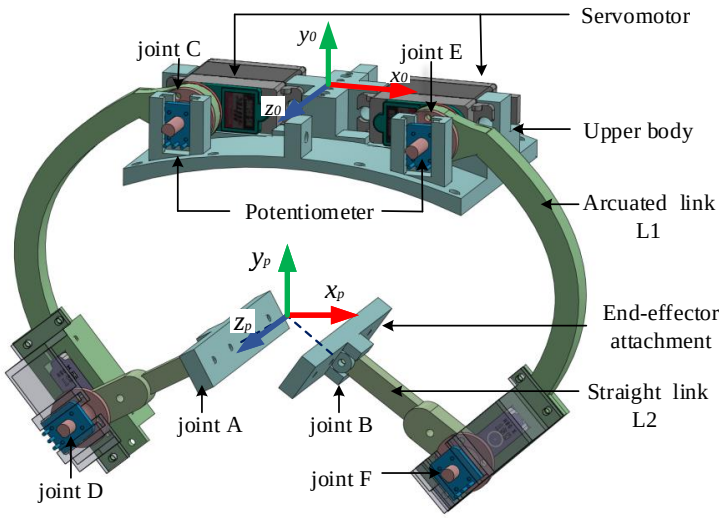

Figure 5.2 – CAD scheme of the proposed wearable device. It is composed of a static upper body, located on the back of the hand, and an interchangeable end-effector, placed in contact with the palm. Two articulated arms, composed of arcuated (L1) and straight (L2) sections, connect the two parts. Four servo motors, two on the upper body and two on the arms, actuate the end-effector.

shows a series of representative motions that the device can actuate, while Table 5.1 summarizes its main characteristics.

Table 5.1 – Device specifications

Weight	160 g
Dimension Length × Width × Height	(13–18) × 18 × (12–15) cm
Maximum contact surface	42 cm^2
Control system	Arduino Uno, Atmega328
Operating voltage range	4.8 to 6.0 V
Operating joints speed	0.14 sec/60°
Maximum horizontal displacement	9 cm
Maximum vertical displacement	5 cm

5.2.1 Five representative end-effectors

As a proof of concept, we designed five end-effectors (E1–E5), able to render different sets of sensations. The first three end-effectors are then evaluated in the human subjects

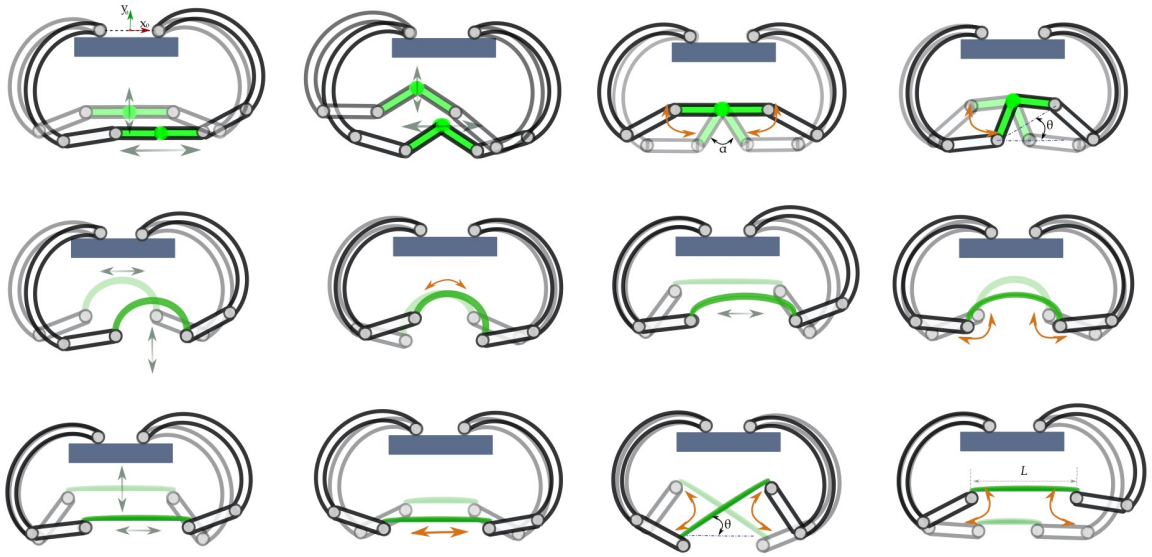

Figure 5.3 – Representative movements of the wearable device when equipped with end-effectors E1 (top), E2 (middle), and E3 (bottom). The end-effectors, in green, are actuated by the joint action of the arcuated and straight links, rolling and moving horizontally/vertically on a plane. In addition to these motions, E1 can fold and unfold, simulating the interaction with rigid slated surfaces and edges; E2 can adjust the local curvature, simulating the interaction with soft slanted surfaces having different curvatures; and E3 can stretch, simulating the interaction with soft slanted surfaces having different stiffness characteristics.

experiment of Sec. 5.4.

5.2.1.1 Rigid hinge-like end-effector

As shown in Fig. 5.1-E1, the end-effector is composed of two flat rectangular plates connected in a hinge-like fashion through a passive revolute joint, allowing the folding of the two plates around the z_0 direction (see Fig. 5.2). Actuated by the combined action of the two arms, the movement of the end-effector is constrained within the x_0–y_0 plane, constituted by the joints. In this way, the end-effector can be controlled to move vertically along the y_0 axis, sideways along the x_0 axis, fold, and roll. However, since the three joints on the end-effector are passive, we cannot control the direction of the folding, i.e., we cannot control whether the edge created by the folding points upwards or downwards. We included a stopper on the revolute joint between the two plates to constraint the end-effector to fold with the edge pointing upwards, so as to generate the sensation of interacting with edges of different sharpness. Of course, the stopper can be easily adjusted to constraint the end-effector to fold in the other direction. This end-effector can provide

the sensation of interacting with rigid slanted surfaces and edges. A preliminary version of this end-effector was used in [18], where its kinematic model is described in detail.

5.2.1.2 Soft U-shaped end-effector

As shown in Fig. 5.1-E2, the end-effector is composed of a flexible rectangular strip of PolyFlex TPU90 (thermoplastic polyurethane), having dimensions 40×110×1.2 mm (width×length×thickness).

As for all end-effectors, its short ends are rigidly clamped to the distal parts of the device's straight links L2 (A and B in Fig. 5.2). Actuated by the combined action of the two arms, the movement of the end-effector is again constrained within the x_0–y_0 plane, creating reversed U-shapes with different curvatures as the two arms move closer/farther from each other (see Sec. 5.3.1 for its model). The clamping structure forces the end-effector to bend in the upper direction, similarly to how the rigid hinge-like end-effector E1 folds. This second end-effector can render 4 DoF movements vertically along the y_0 axis, sideways along the x_0 axis, as well as roll, and bend in a reversed U shape, providing the sensation of interacting with soft shapes having different curvatures and orientations. Changing the thickness of the TPU strip, we can adjust the stiffness of the end-effector to the target task and environment.

5.2.1.3 Elastic rubber end-effector

As shown in Fig. 5.1-E3, the end-effector is composed of a flexible rectangular strip of latex rubber, having dimensions 40×110×0.1 mm (width×length×thickness). This material has a 4.69 Mpa Young Modules and 18.36 Mpa tensile strength, making it rather flexible yet very resistant. Actuated by the combined action of the two arms, the end-effector can stretch and roll, creating the sensation of interacting with soft surfaces having different stiffness and orientation. The more it is stretched, the stiffer it is (see Sec. 5.5 for its characterization).

5.2.1.4 Triangular origami end-effector

As shown in Fig. 5.1-E4, the end-effector is composed of a flexible rectangular origami structure made of PolyFlex TPU90, having dimensions 40×70×0.8 mm (width×lengthspan×thickness). The structure folds in a series of triangular shapes whose edges get farther to each other as the end-effector is stretched out. Actuated by the com-

bined action of the two arms, the end-effector can stretch and roll, creating the sensation of interacting with surfaces having different local patterns, i.e., variable spaced ridges in this case, and orientation.

5.2.1.5 Texture elastic end-effector

As shown in Fig. 5.1-E5, the end-effector is composed of a flexible rectangular strip of Nitrile rubber, having dimensions 40×110×0.1 mm (width×length×thickness). This material has a 2.10 Mpa Young Modules and 22 Mpa tensile strength. Small plastic grains of 1 mm diameter are homogeneously glued to the surface so as to render the sensation of interacting with a rough surface. As the elastic end-effector is stretched, the grains become more distant from each other, lowering their local density and, in turn, the perceived roughness of the surface. Actuated by the combined action of the two arms, the end-effector can stretch and roll, creating the sensation of interacting with soft surfaces having different texture and orientation.

5.3 Device Kinematic Analysis

This Section describes the mechanical model of the device, including its mobility analysis as well as the forward and inverse kinematics analysis, necessary to derive the main structural parameters of the device and for the definition of position control algorithms. As shown in Figs. 5.2 and 5.5, the revolute joints are parallel to each other and perpendicular to the reference plane Σ, defined by x_0 and y_0. Let us indicate with C, D, E, and F the intersection points between the revolute joint axes and the Σ plane. Let us indicate with $S_0 < O_0, x_0, y_0, z_0 >$ the reference frame attached to the upper body, in which O_0 is the origin located in the midpoint between C and E points. The x_0 axis is parallel to $\overrightarrow{CE}$, y_0 is in the same plane with x_0, C, and E (plane Σ), and z_0 is consequently defined (see also Fig. 5.2). The two arcuated links L1 have the same structure, their configuration is defined by vectors $\overrightarrow{CD}$ and $\overrightarrow{EF}$, respectively, with length $|\overrightarrow{CD}| = |\overrightarrow{EF}| = l_1$. The straight links L2, connecting the arcuated links to the end-effector, are defined by the vectors $\overrightarrow{DA}$ and $\overrightarrow{FB}$, respectively, with length $|\overrightarrow{DA}| = |\overrightarrow{FB}| = l_2$.

The device can be represented by two symmetrical serial planar Revolute-Revolute (R-R) chains sharing the same base, represented by the upper body, and the interchangeable rigid/deformable end-effector, constraining their movement and defining a closed-loop planar mechanism. The analysis of the mechanism can be divided in two main parts, as

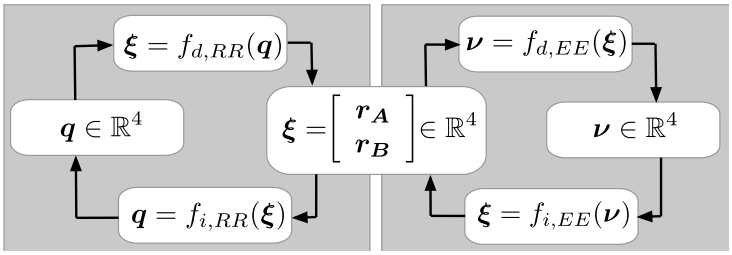

Figure 5.4 – Kinematic analysis scheme. We can identify two main parts. The first one relates joint rotation angles $\mathbf{q}$ with A and B point positions, collected in the vector $\boldsymbol{\xi}$, and it is independent from the end-effector. The second one relates A and B point positions to the output vector $\boldsymbol{\nu}$, and it depends on the specific end-effector characteristics.

summarized in Fig. 5.4. The first part is independent from the end-effector in use, relating joint rotation angles $\mathbf{q}$ with A and B point positions. The second part depends on the characteristics of the end-effector, relating A and B point positions to the end-effector output vector $\boldsymbol{\nu}$. For this reason, we introduce an intermediate set of variables, defining the state between the serial R-R mechanisms and the end-effector. Let us indicate with $\mathbf{q} = [q_1, q_2, q_3, q_4]^{\mathrm{T}} \in \mathbb{R}^4$ the vector containing the input variables, corresponding to the actuators' rotation angles of joints in C, D, E, and F, respectively. Let us also indicate with $\boldsymbol{\nu}$ the vector containing the output variables, whose definition depends on the specific end-effector, and with $\boldsymbol{\xi} = [x_A, y_A, x_B, y_B]^{\mathrm{T}} \in \mathbb{R}^4$ the intermediate state defining the position of A and B points, respectively. While $\mathbf{q}$ and $\boldsymbol{\xi}$ are the same regardless the end-effector in use, $\boldsymbol{\nu}$ depends on the end-effector employed. Specifically, for the end-effectors considered in this Chapter, the following output vectors can be defined for E1, ..., E5:

$$\boldsymbol{\nu}_{E1} = [x_P, y_P, \theta, \alpha]^{\mathrm{T}}, \tag{5.1}$$

where x_P, y_P are the coordinates of the middle point of the revolute joint in the end-effector edge (see Fig. 5.1-E1 and [18]), θ is the tilt angle (i.e., the angle between $\overline{AB}$ and x_0, see Fig. 5.3-top), and α is the folding angle of the end-effector (see again Fig. 5.3-top);

$$\boldsymbol{\nu}_{E2} = [x_P, y_P, \theta, R]^{\mathrm{T}}, \tag{5.2}$$

where x_P, y_P are the coordinates of the midpoint of the AB arc (see Figs. 5.1-E2 and 5.5b), θ is again the tilt angle (see Fig. 5.5b), and R is the curvature radius of the end-effector at P;

$$\boldsymbol{\nu}_{E3} = \boldsymbol{\nu}_{E4} = \boldsymbol{\nu}_{E5} = [x_P, y_P, \theta, L]^{\mathrm{T}}, \tag{5.3}$$

where x_P, y_P are the coordinates of the midpoint of the AB segment (see Figs. 5.1-E3, 5.1-E4, 5.1-E5), θ is again the tilt angle (see Fig. 5.3-bottom), and L is the distance between A and B (see again Fig. 5.3-bottom).

Direct kinematics analysis aims at defining the relationship mapping $\mathbf{q}$ into $\boldsymbol{\nu}$, i.e.,

$$\boldsymbol{\nu} = f_d(\mathbf{q}). \tag{5.4}$$

while inverse kinematics analysis defines the relationship mapping $\boldsymbol{\nu}$ into $\mathbf{q}$, i.e.,

$$\mathbf{q} = f_i(\boldsymbol{\nu}), \tag{5.5}$$

By introducing the intermediate state $\boldsymbol{\xi}$ these functions can be further expressed as

$$\boldsymbol{\nu} = f_{d,EE}(\boldsymbol{\xi}) = f_{d,EE}(f_{d,RR}(\mathbf{q})), \tag{5.6}$$

and

$$\mathbf{q} = f_{i,RR}(\boldsymbol{\xi}) = f_{i,RR}(f_{i,EE}(\boldsymbol{\nu})), \tag{5.7}$$

where $f_{d,RR}$ and $f_{i,RR}$ represent the direct and inverse kinematics functions for the two planar R-R mechanisms, that are the same for all the configurations, while $f_{d,EE}$ and $f_{i,EE}$ are the direct and inverse kinematics functions specific to the end-effectors.

5.3.1 From joint variables q to A and B position and vice-versa

Given the input variables $\mathbf{q}$, the coordinates $A = (x_A, y_A)$ and $B = (x_B, y_B)$ can be evaluated as in standard planar R-R robots, i.e.,

$$x_A = x_C + l_1 \cos(q_1) + l_2 \cos(q_1 + q_2) \tag{5.8}$$
$$y_A = y_C + l_1 \sin(q_1) + l_2 \sin(q_1 + q_2) \tag{5.9}$$
$$x_B = x_E + l_1 \cos(q_3) + l_2 \cos(q_3 + q_4) \tag{5.10}$$
$$y_B = y_E + l_1 \sin(q_3) + l_2 \sin(q_3 + q_4) \tag{5.11}$$

Eqs. (5.8), ..., (5.11) define the direct kinematic function $f_{d,RR}$. On the other hand, to define $f_{i,RR}$, we need to find $\mathbf{q}$ vector when A and B point positions are known. The problem consists in solving the inverse kinematics of two standard 2-DoF R-R planar manipulators. For the sake of brevity, the procedure is not reported here but the reader

can refer to, e.g., [279].

5.3.2 Direct and inverse kinematics for the end-effectors

This Section reports the direct and inverse kinematics functions for the three end-effectors E1, E2, and E3 considered in our evaluation. A similar reasoning can be used to evaluate the direct and inverse kinematics functions for other end-effectors.

5.3.2.1 Rigid hinge-like end-effector

In the direct kinematic problem for this end-effector [18], from A and B coordinates, it is possible to evaluate angle θ as

$$\theta = \arctan\left(\frac{y_B - y_A}{x_B - x_A}\right), \tag{5.12}$$

and the distance between A and B as

$$L = \sqrt{(x_B - x_A)^2 + (y_B - y_A)^2}. \tag{5.13}$$

Since the considered device has a parallel structure, the input variables $\mathbf{q}$ are constrained by the structure. In particular, length L has to satisfy the following inequality:

$$L \leq 2l_3. \tag{5.14}$$

If this constraint is satisfied, the folding edge angle α can be evaluated as

$$\alpha = 2\arcsin\left(\frac{L}{2l_3}\right).$$

Finally, P coordinates are given by:

$$x_P = x_A + l_3\cos(\theta + \pi/2 - \alpha/2) \tag{5.15}$$

$$y_P = y_A + l_3\sin(\theta + \pi/2 - \alpha/2) \tag{5.16}$$

According to the output variable definition in eq. (5.1), equations from (5.12) to (5.16) constitute the direct kinematics procedure $f_{d,EE}$ introduced in eq. (5.6), i.e., the set of operations allowing to evaluate the output variables $\boldsymbol{\nu}_{E1}$ as a function of the intermediate variables $\boldsymbol{\xi}$.

In the inverse kinematic problem for this end-effector, vector $\boldsymbol{\xi}$ components are evaluated as a function of a set of output variables $\boldsymbol{\nu}_{E1}$, i.e.,

$$\boldsymbol{\xi} = \mathrm{f}_{\mathrm{i,EE}}(\boldsymbol{\nu}_{\mathrm{E1}}).$$

We can start the procedure by evaluating the distance L between A and B as

$$L = 2\mathrm{l}_3 \sin\frac{\alpha}{2}. \tag{5.17}$$

From P coordinates and α and θ angles, A and B coordinates can be calculated as follows

$$x_A = x_P - l_3\cos(\theta + \pi/2 - \alpha/2) \tag{5.18}$$
$$y_A = y_P - l_3\sin(\theta + \pi/2 - \alpha/2) \tag{5.19}$$
$$x_B = x_P + l_3\cos(\theta + \pi/2 - \alpha/2) \tag{5.20}$$
$$y_B = y_P + l_3\sin(\theta + \pi/2 - \alpha/2) \tag{5.21}$$

eq. (5.17), ..., (5.21) define the inverse kinematic function $f_{i,EE}$ for this end-effector.

5.3.2.2 Soft U-shaped end-effector

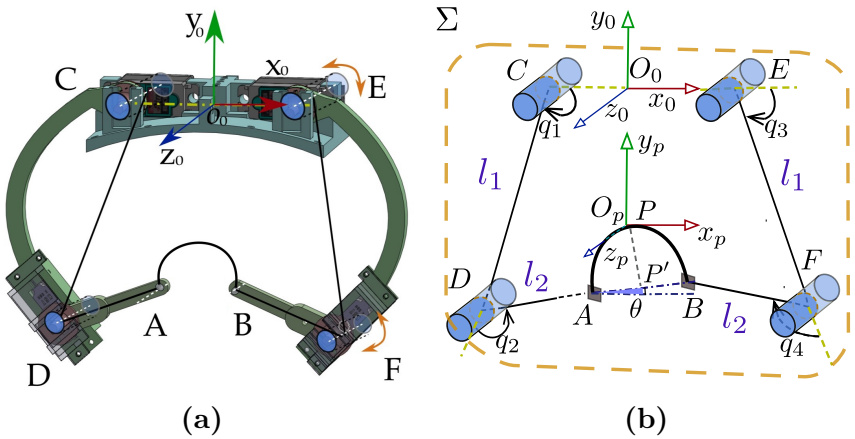

(a) **(b)**

Figure 5.5 – Kinematic structure of the proposed device when equipped with the soft U-shaped end-effector (E2). Point P is placed at the vertex of the bent end-effector, which has fixed length and is attached to points A and B. Point P' is placed at the middle between $\overline{AB}$. Two planar Revolute-Revolute (R-R) chains, actuated by four motors, move the end-effector, providing the user with the sensation of interacting with soft objects having different curvatures.

As before, in the direct kinematic problem for this end-effector, given vector $\boldsymbol{\xi}$, θ angle can be evaluated by eq. (5.12), while L can be evaluated by eq. (5.13). However, for this end-effector, the congruence control reported in eq. (5.14) should be substituted by

$$L_m \leq L \leq L_0,$$

where L_m represents a lower limit defined according to the end-effector mechanical properties, while L_0 is the upper limit, corresponding to a flatten end-effector. In the case of our implementation of E2, $L_m = 40$ mm and $L_0 = 115$ mm. The curvature radius R, assumed constant across the end-effector, can be evaluated by solving the following nonlinear equation:

$$2R \sin\left(\frac{L_0}{2R}\right) = L.$$

Finally, the coordinates of P, representing the midpoint on the U-shape end-effector, can be calculated as

$$\begin{aligned} x_P &= x_{P'} - R\left(1 - \cos\left(\frac{L_0}{2R}\right)\right)\sin(\theta) \\ y_P &= y_{P'} + R\left(1 - \cos\left(\frac{L_0}{2R}\right)\right)\cos(\theta), \end{aligned}$$

where P' is the midpoint of $\overline{AB}$.

In the inverse kinematic problem for this end-effector, we assume that the target curvature is known and can be approximated by a quadratic function.

We then consider generic quadratic set of functions $f(x) = ax^2 + bx + c$, where b can be zero. To obtain the $\hat{f}(x)$ fitting the simulated curvature $1/R$, with R being the radius, a least square fitting method can be applied,

$$\min_{a,c} ||\mathcal{C}(x, R) - \hat{f}(x)||^2,$$

where $\mathcal{C}(x, R)$ is the curve resembling the target U shape, which depends on R. In Fig. 5.5b, the kinematic scheme of our device equipped with E2 is shown. When vector $\boldsymbol{\nu}_{E2} = [x_P, y_P, \theta, R]$ is known, x_B can be obtained through the Newton-Raphson method as solution of the integral equation

$$\int_0^{x_B} \sqrt{1 + (d\hat{f}(x)/dx)^2}dx = L_0/2, \tag{5.22}$$

where L_0 is the maximum extension possible for the flexible strip and corresponds to the maximum distance between A and B, i.e., when the end-effector E2 is flat. Finally, coordinates A and B can be obtained as

$$\begin{aligned} x_A &= x_P + |\overline{PP'}|\sin(\theta) - (x_P - x_A)\cos(\theta) \\ y_A &= y_P - |\overline{PP'}|\cos(\theta) - (x_P - x_A)\sin(\theta) \\ x_B &= x_P + |\overline{PP'}|\sin(\theta) + (x_P - x_A)\cos(\theta) \\ y_B &= y_P - |\overline{PP'}|\cos(\theta) + (x_P - x_A)\sin(\theta). \end{aligned}$$

5.3.2.3 Elastic rubber end-effector

In the direct kinematic problem for this end-effector, recalling the definition of the output vector $\boldsymbol{\nu}_{E3}$ of eq. (5.3) and indicating the midpoint of $\overline{AB}$ as P, we can evaluate its coordinates as a function of $\boldsymbol{\xi}$,

$$x_P = (x_A + x_B)/2, \tag{5.23}$$

$$y_P = (y_A + y_B)/2. \tag{5.24}$$

Then, θ can be evaluated as in eq. (5.12), while L can be evaluated as in eq. (5.13). In this case, the congruence control originally introduced in eq. (5.14) should be substituted by

$$L_0 \leq L \leq L_M, \tag{5.25}$$

where L_M represents an upper limit defined on the basis of end-effector material and device structure, i.e., the maximum the end-effector can be stretched, while L_0 is a lower limit necessary to guarantee that the end-effector is taut, i.e., the minimum the end-effector should be stretched to keep it straight. Note that the L_0 parameter represents, both for E2 and E3 end effectors, the length of $\overline{AB}$ when the end-effector is straight and unstretched. This value represents the upper limit for E2 end-effector and the lower one for E3. In the case of our implementation of E3, $L_M = 170$ mm and $L_0 = 134$ mm. Finally, by controlling the stretch applied to the end-effector

$$\delta = L - L_0, \tag{5.26}$$

we can control its stiffness k. This relationship between the stretch and the stiffness of the material is experimentally evaluated and modelled in the Appendix. Eqs. (5.23), (5.24), (5.12), and (5.13) define the direct kinematics function $f_{d,EE}$ for end-effector E3.

In the inverse kinematic problem for this end-effector, given $\boldsymbol{\nu}_{E3}$ from eq. (5.3), A and B coordinates can be straightforward calculated as

$$x_A = x_P - \frac{L}{2}\cos\theta, \tag{5.27}$$

$$y_A = x_P - \frac{L}{2}\sin\theta, \tag{5.28}$$

$$x_B = x_P + \frac{L}{2}\cos\theta, \tag{5.29}$$

$$y_B = x_P + \frac{L}{2}\sin\theta. \tag{5.30}$$

Eqs. (5.27), ..., (5.30) define the inverse kinematics function $f_{i,EE}$ for the end-effector E3. This procedure can also be extended to end-effectors E4 and E5.

5.3.3 Control

The control system of the device can also be divided in two parts, similarly to the kinematics analysis. As shown on the left-hand side of Fig. 5.6, one part consists of the definition of the control input and depends on the specific end-effector. In this block, the task is defined in the end-effector space, providing the end-effector-dependent target output vector $\boldsymbol{\nu}_d$. Through the inverse kinematic relationships described before, the correspondent value of $\boldsymbol{\xi}_d$ vector can be evaluated. As shown on the right-hand side of Fig. 5.6, the second part of the control scheme is independent from the specific end-effector. From $\boldsymbol{\xi}_d$, we evaluate the corresponding reference values $\mathbf{q}_d$ for actuating the joint angles. Then, a standard PID-based position control is used to control each actuator.

5.4 Experimental Evaluation

We evaluated the effectiveness of our device in rendering diverse contact interactions in immersive Virtual Reality. As a proof of concept, as mentioned before, we considered interactions with three of the five end-effectors described in Sec. 5.2.1, i.e., E1, E2, and E3 (see also Fig. 5.1).

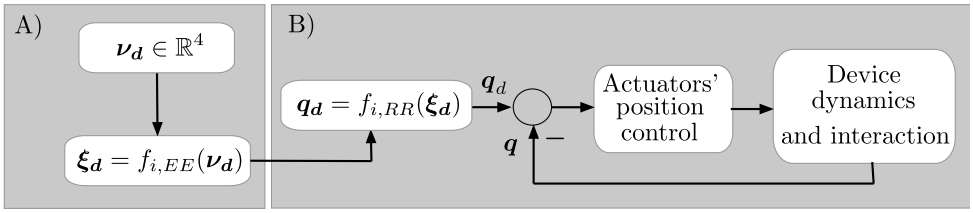

Figure 5.6 – Control system. According to the definitions provided in the kinematics analysis of Sec. 5.3, the control system can be divided in two main parts. Part A) consists of the definition of the control input and depends on the specific end-effector. The task is defined in the end-effector space, providing the target output vector $\boldsymbol{\nu}_d$. Through the inverse kinematics, the intermediate vector $\boldsymbol{\xi}_d$ can be evaluated. Part B) is relative to the actuators' position control and is independent from the end-effector. Starting from $\boldsymbol{\xi}_d$, we evaluate the corresponding reference values $\mathbf{q}_d$ for actuating the joint angles. Finally, a PID position control can be employed to actuate each actuator.

Table 5.2 – Main characteristics of the virtual objects on the carousel

Object	**Main characteristics**
1 - rigid red dice	10×10×10 cm, flat surface on top
2 - rigid blue dice	10×10×10 cm, 90° edge on top
3 - rigid house rooftop	8×15×20 cm, 50° edge on top
4 - "watermelon" shape	curvature κ=3 cm^{-1}
5 - "8-ball" shape	curvature κ=5 cm^{-1}
6 - "onion" shape	curvature κ=7 cm^{-1}
7 - soft green cube	5×5×5 cm, isotropic stiffness k=26 N/mm
8 - soft yellow cube	5×5×5 cm, isotropic stiffness k=31 N/mm
9 - soft red cube	5×5×5 cm, isotropic stiffness k=36 N/mm

5.4.1 Participants

Twelve subjects participated in the study (10 males, 2 females, all right-handed). None of the participants reported any deficiencies in their visual or haptic perception abilities. The experimenter explained the procedures and spent about three minutes adjusting the setup to be comfortable before the subject began the experiment.

5.4.2 Experimental setup and protocol

Participants were asked to wear the proposed haptic device on their right hand, as shown in Figs. 5.1 and 5.7b. On top of the haptic device, we mounted an HTC Vive tracker,

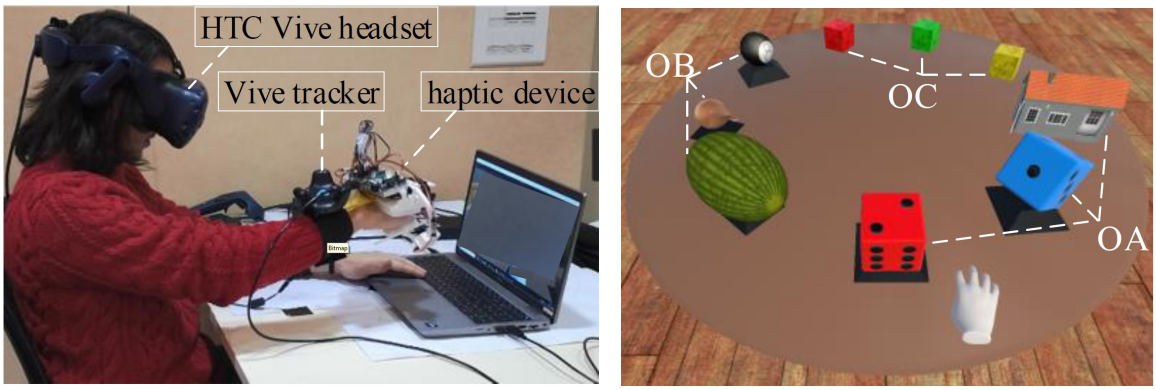

(a) **(b)**

Figure 5.7 – (a) Experimental setup showing a user wearing the HTC Vive headset and the proposed haptic device, while interacting with the objects in the virtual environment. (b) The carousel of objects rendered in the virtual environment, divided into three main groups according to their characteristics.

so as to track the position of the user's hand. Finally, participants were asked to wear an HTC Vive headset and sit comfortably on a chair.

The virtual environment was composed of a rotating carousel, inspired from [285] and shown in Fig. 5.7a, which presented the user with nine different objects to interact with. The objects were designed to present a wide range of diverse physical characteristics, which can rarely be rendered by a single haptic device or end-effector: three objects have rigid edges, three are curved, and three are soft. Their main characteristics are reported in Table 5.2.

The participants interacted with each object on the carousel using the wearable device equipped with all the three considered end-effectors, leading to 3 (end-effectors) $\times$ 9 (objects) $\times$ 12 (participants) $=$ 324 total interactions. Participants could touch each object how many times and how long they wanted. On average, they spent 10 s on each object. A button next to the carousel enabled the participant to rotate the carousel, so as to interact with a new object. For each object and for each end-effector, participants were asked to answer the question: "How realistic was the interaction with this virtual object?," yielding to 27 ratings per participant. At the end of the whole experiment, participants were also asked four additional questions: "How comfortable was the interaction with this end-effector?", "How accurate was the contact rendering with this end-effector?" and "How tired are you?". Participants could answer the questions using a slider that went from 1 "not at all" to 10 "very much".

Table 5.3 – Ratings evaluating the realism of the interaction

	OA: objs. 1–3	OB: objs. 4–6	OC: objs. 7–9
E1	8.4	5.3	4.5
E2	5.5	6.8	5.9
E3	6.7	6.4	8.3

5.4.3 Results

Table 5.3 shows the ratings given by the participants when interacting with the three sets of objects through end-effectors E1, E2, and E3 regarding the question "How realistic was the interaction with this virtual object?". The first set gathers the three rigid objects featuring different edges and slanted surfaces (OA: objects 1–3 in Table 5.2 and Fig. 5.7a), the second set the three objects featuring different curvature characteristics (OB: objects 4–6), and the third set the three objects featuring different stiffness characteristics (OC: objects 7–9). To compare the ratings, we ran a two-way repeated-measures ANOVA test. The type of end-effector (E1, E2, E3) and the sets of objects (OA, OB, OC) were treated as within-subject factors. Transformed data passed the Shapiro–Wilk normality test and Mauchly's Test of Sphericity. The two-way repeated-measure ANOVA revealed a statistically significant two-way interaction between the end-effector and the sets of objects variables ($F(4, 44) = 18.958, p < 0.001$). When a statistically significant interaction between variables is found, we need to analyze the simple main effects. Interpreting the simple main effects for the end-effector variable, we found a statistically significant difference (E1-OA vs. E1-OB vs. E1-OC: $F(2, 22) = 13.964, p < 0.001$; E2-OA vs. E2-OB vs. E2-OC: $F(2, 22) = 4.220, p = 0.028$; E3-OA vs. E3-OB vs. E3-OC: $F(2, 22) = 17.236, p < 0.001$). Interpreting the simple main effects for the objects variable, we found a statistically significant difference (E1-OA vs. E2-OA vs. E3-OA: $F(2, 22) = 20.421, p < 0.001$; E1-OC vs. E2-OC vs. E3-OC: $F(2, 22) = 15.419, p < 0.001$). Results of post hoc analysis with Bonferroni adjustments are reported in Table 5.4 (only significant p values are shown).

Similarly, we ran a one-way repeated-measures ANOVA test regarding the questions "How comfortable was the interaction?" and "How accurate was the interaction?". Transformed data passed the Shapiro–Wilk normality test and Mauchly's Test of Sphericity. The ANOVA revealed no statistically significant difference between end-effectors for both questions.

Table 5.4 – Experimental evaluation

Subjects	12 (2 females, 10 males)
Task	Interact with nine virtual objects using the considered three end-effectors.
Conditions	Type of end-effector E1 (rigid hinge-like end-eff.), E2 (soft U-shaped end-eff.), E3 (elastic rubber end-eff.) Sets of objects OA (objs. 1–3), OB (objs. 4–6), OC (objs. 7–9)

"How realistic was the interaction with this virtual object?"

Statistical analysis (only significant p values)

Simple main effect of the type of end-effector

E1-OA vs. E1-OB	$p < 0.001$	E1-OA vs. E1-OC	$p = 0.016$
E2-OA vs. E2-OB	$p = 0.034$	E3-OA vs. E3-OB	$p = 0.025$
E3-OA vs. E3-OC	$p = 0.001$	E3-OB vs. E3-OC	$p = 0.033$

Simple main effect of the sets of objects

E1-OA vs. E2-OA	$p < 0.001$	E1-OA vs. E3-OA	$p < 0.001$
E1-OC vs. E2-OC	$p = 0.025$	E1-OC vs. E3-OC	$p = 0.007$
E2-OC vs. E3-OC	$p = 0.025$		

"How comfortable was the interaction?"

Ratings were 7.7/10, 6.5/10, and 8.0/10 for end-effectors E1, E2, and E3, respectively.

"How accurate was the interaction?"

Average ratings were 7.8/10, 6.3/10, and 7.1/10 for end-effectors E1, E2, and E3, respectively.

"How tired are you?"

The average rating was 3.1/10.

5.5 Force Characterization for the Elastic Rubber End-effector

As detailed in Sec. 5.3.2.3, the elastic rubber end-effector (E3) can be stretched by moving the two arms endpoints A and B farther from each other, enabling the device to control the stiffness of the end-effector surface. This Section analyzes and evaluates the relationship between the stretch δ applied to the end-effector, defined in eq. (5.26), and its stiffness. For the sake of simplicity, we consider a simplified elastic model for our end-effector, assuming a direct coupling between the horizontal stretch of the elastic strip

(axis x in Fig. 5.2) and its stiffness along the vertical direction (axis y). Of course, more complex models can be employed, so as to better characterize the stiffness coefficients of the strip along the different directions [286], [287].

Fig. 5.8 presents the experimental setup we used for this identification procedure. A force sensor Nano43 (ATI Industrial Automation, US) is attached right below the upper body of the device, while a 3D-printed spherical shape is mounted between the sensor and the end-effector, mimicking the user's palm. We model the interaction force f between the spherical shape and the end-effector as a linear function of the movement along the vertical axis, Δy (see Fig. 5.8):

$$f = k(\delta)\Delta y \tag{5.31}$$

where $k(\delta)$ represents the dependence of the stiffness coefficient k on the stretch δ of the elastic rubber end-effector, and Δy is the relative displacement along the vertical axis y between the current position of the end-effector and the rest/baseline position, i.e., when the end-effector is barely in contact with the spherical shape.

We consider a set of 18 stretches $\mathcal{D} = \{\delta_1, \ldots, \delta_i, \ldots, \delta_{18}\}$, satisfying eq. (5.25) and actuated following the control presented in Sec. 5.3.3. For each stretch configuration $i = 1, \ldots, 18$, we moved the end-effector upwards, from its rest/baseline position until the maximum possible offset (see Fig. 5.8), and back. Throughout these movements, we

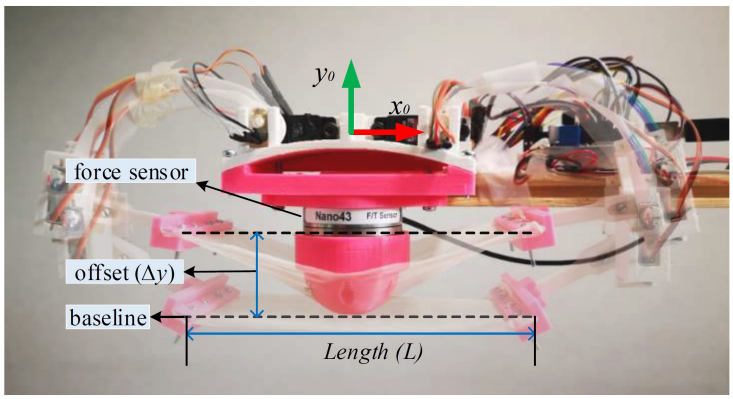

Figure 5.8 – Force characterization for the elastic rubber end-effector (E3): experimental setup. The force sensor is fixed right below the upper body of the device, while a 3D-printed spherical shape is mounted between the sensor and the end-effector. The figure shows two configurations of the device. In the first one, the end-effector barely touches the spherical shape (i.e., the baseline position); in the second one, the end-effector applies a force to the spherical shape and, in turn, to the sensor (i.e., its moves upwards of a certain offset Δy with respect to the baseline position). Increasing the distance L between A and B, i.e., horizontally stretching the end-effector, we can control its stiffness during the interaction.

registered the position of the end-effector and the corresponding forces applied to the force sensor along the vertical axis y. From the collected data, we can define the i-th estimated stiffness coefficient related to the end-effector stretch δ_i as

$$k_i = \hat{k}(\delta_i) = \mathbf{\Delta}\mathrm{y}_i^{\#}\mathrm{f}_i, \tag{5.32}$$

where f_i and $\mathbf{\Delta}\mathrm{y}_i$ denote the corresponding vectors of measurements acquired during the motion, and $(\cdot)^{\#}$ is the least-square pseudo-inverse operator. Finally, we use sets (δ_i, k_i) to fit a quadratic polynomial regression, i.e., a vector of coefficients $(a, b, c)^T$ such that $\delta(k) = ak^2 + bk + c$, given the estimated stiffness coefficients k, best fits the measured stretch δ for the considered measurements.

Results of this stiffness identification across different stretch values of the end-effector are summarised in Fig. 5.9a. For each stretch δ_i, the force-displacement relationship is displayed, comparing the force $\hat{\mathrm{f}}_i = \hat{k}(\delta_i)\mathbf{\Delta}\mathrm{y}_i$ resulting from eq. (5.32) (dashed red lines) with the force measured by the sensor (blue lines). Results show that the range of renderable stiffness is $[26, 36]$ N/m. Fig. 5.9b shows the quadratic polynomial regression fit, with the estimated coefficients being $(a, b, c)^T = (0.0002, -0.0120, 0.1478)^T$.

These results show that, to a certain extent, we can adjust the stiffness of the end-effector surface by stretching it. Sections 5.3.2.3 and 5.3.3 details how to control this parameter during the interaction with virtual or remote environments.

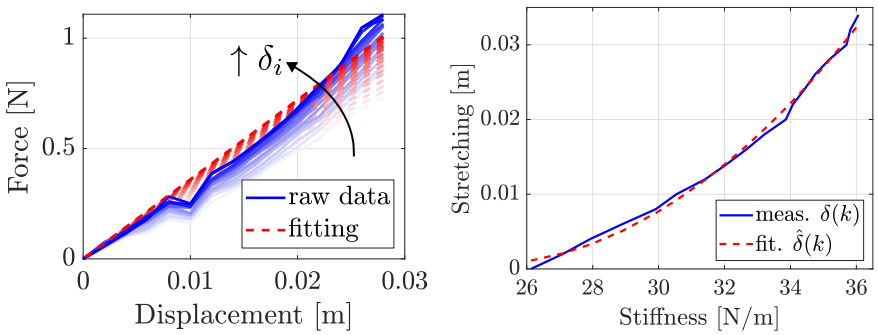

Figure 5.9 – Force characterization for the elastic rubber end-effector (E3): results. (a) Stiffness identification along the considered stretch configurations. Opacity of the plots increases as the stretch δ_i increases. (b) Results of the quadratic polynomial regression fit to estimate the function $\delta(k)$ relating the end-effector stiffness k along the normal direction with its stretch δ.

5.6 Discussion and Conclusions

We have presented a 4-DoF hand wearable haptic device for interacting in Virtual Reality (VR). The device has been designed to support different end-effectors, that can be easily and quickly exchanged to provide a wide range of haptic sensations. The device is composed of a static upper body, secured to the back of the hand, and the (changeable) end-effector, placed in contact with the palm. The two parts of the device are connected by two articulated arms, actuated by four servo motors housed on the upper body and along the arms. The end-effector can be changed without doffing the device. This wearable device has been designed to address one of the main limitations of wearable haptic interfaces, i.e., the limited range of sensations they can provide. With respect to existing solutions, the proposed device can provide a significantly wider range of sensations. The Chapter presented the design and kinematics of the proposed haptic device together with a position control scheme able to actuate generic end-effectors during VR interaction. The Chapter also discusses, as a proof of concept, five representative end-effectors, able to render the sensation of interacting (E1) with rigid slanted surfaces and sharp edges having different orientations, (E2) with curved surfaces having different curvatures, and with soft surfaces having different (E3) stiffness characteristics, (E4) local shape, and (E5) texture.

The first three of these end-effectors, E1, E2, and E3, have been evaluated in a human-subjects study in immersive VR. The 12 participants proved that the considered end-effectors are capable to render rather realistic interactions in VR. Participants also found the device comfortable to wear and use, and they were not too tired at the end of the experiment. As expected, end-effectors performed significantly better when rendering virtual objects showing appropriate haptic characteristics, i.e., E1 was better at rendering objects featuring different edges and slanted surfaces, E2 at rendering objects featuring different curvature characteristics, and E3 at rendering objects featuring different stiffness characteristics. This result shows that is indeed important to tailor the end-effector to the interaction at hand, supporting the need for such modular haptic interfaces.

As we studied in Chapter 1, haptic palmar devices is a family of devices which stimulate the palm of the hand, these interfaces allow larger surface exploration, objects recognition, texture and collision detection in VR and teleoperation. Our work expand the research of using interchangeable end-effectors with diverse materials for varying deformation generation and stimulation, it provides us inspiration for the development of hand mounted palmar devices for human robot interaction.

Chapter

6 Hand-held Vibrotactile Device for Motor Skill Training

Contents

6.1 Introduction

Chapter 2 and Chapter 3 studied the effectiveness of employing cutaneous feedback in navigation and hand motion guidance. In this Chapter we study the effectiveness of vibrotactile, kinesthetic and visual feedback in human motor skill training. We compare the motor skill performance under the conditions 1) Visual feedback only, 2) Visual and kinesthetic haptic feedback, and 3) Visual and vibrotactile haptic feedback.

As extensively discussed in Chapter 1, haptic stimuli play a fundamental role in enhancing the performance in navigation and guidance scenarios. Vibrotactile stimulation for guidance and rendering can be applied in various modes, e.g,. leader-follower and collision avoidance. Along these rationale, researchers have proposed a great variety of handheld devices [288] and for navigation and rehabilitation [97], [289].

Virtual Reality (VR) training is gaining popularity in medicine, rehabilitation, and industry, addressing various psychomotor, procedural, spatial, and decision-making skills [290], [291]. VR training proviices virtual environments where trainees receive consistent and replicable training, allowing for an objective assessment of skills. However, evidence for supporting the advantages of VR training over other methods is mixed. For example, in a cochrane meta-analysis of VR-based endoscopy training literature, Khan et al. [292] found that though VR training is better than no training, it is not better than conventional training, whereas Mekbib et al. [293] in a meta-analysis of upper limb rehabilitation literature found that VR was better than conventional therapy. The effectiveness of VR for training may be enhanced by improving the sensory fidelity of VR, i.e., the "immersion" provided by the system through the use of head mounted displays (HMDs) or CAVE Automatic Virtual Environments (CAVEs) [294]. A more immersive and interactive VR system may indeed lead to higher perceived presence (the subjective response to immersion) [294], which in turn positively affects the effectiveness of VR training [295]. For the same reasons, haptic feedback in VR may increase presence and potentially training performance [296], [297].

However, employing haptics remains relatively unexplored in motor skill training literature in immersive VR (IVR) outside the surgical and rehabilitation domains. Therefore, further investigation, not only on the haptic feedback, but also on its modalities and variations can aid the discussion of how VR training might be enhanced [291]). Inspired by examples of motor skill training from immersive VR. [298], [299], this Chapter focuses on a buzzwire (or wire loop) task, where the aim is to move a metallic loop across a wire

without touching it. This setup is used to investigate the following research questions:
***RQ 1**: Can vibrotactile or kinesthetic feedback influence VR training performance in a buzzwire motor skill task?*
***RQ 2**: Can motor skill training in VR with different haptic feedback (kinesthetic vs. vibrotactile) cause variations in arousal levels during training? Is there a link between physiological arousal during training and improvements in performance afterward?*
***RQ 3**: Can motor skill training in VR with different haptic feedback (kinesthetic vs. vibrotactile) cause variations in reported presence, task load, and self-efficacy?*

This Chapter is a revised version of the works under revision as

* U. Radhakrishnan, **L. Kuang**, K. Koumaditis, F. Chinello, C. Pacchierotti. "Haptic Feedback, Performance and Arousal: A Comparison Study in an Immersive VR Motor Skill Training Task." *Submitted to IEEE Transactions on Haptics*, 2023.

6.2 Related Works

6.2.1 Haptics in immersive VR training

In a systematic review and meta-analysis of the use of different types of haptic feedback on VR and box trainers in laparoscopic surgical skills, Overtoom et al. [300] found that the addition of haptics provides only a small positive effect on task performance while providing a better learning curve at the beginning of training as compared to no haptics conditions. Similarly, Rangarajan et al. found that haptics enhanced surgical training further than training without haptics [301]. They also found that the addition of haptic feedback reduced the learning curve for novice trainees. In this Chapter, we focus on kinesthetic and vibrotactile feedback modalities as they are suitable for providing relevant information regarding mistakes in the buzzwire task. Kinesthetic feedback is closest to recreating real-world physical forces using grounded haptic devices.

VR training literature has compared vibrotactile and kinesthetic feedback against each other and other modalities. Researchers have proved that vibrotactile feedback, used either alone or along with other feedback modalities was effective in most motor skill training applications in VR [302], Similarly, kinesthetic feedback led to better immediate outcomes in terms of task time completion in physical training tests and better performance on a delayed post-test in VR group [303]. In between-subjects comparisons, vibrotactile combined with audio feedback led to the greatest increase in performance, whereas the

addition of kinesthetic feedback did not improve performance [304]. While in a within-subjects study, kinesthetic feedback (plus visual) led to better task performance compared to vibrotactile feedback (plus visual) and visual only (no haptics). These work illustrate the need for further research into investigating the effectiveness of different haptic feedback modalities.

6.2.2 Haptic feedback and physiological arousal

The term "arousal" refers to the increase in alertness and attention in response to external or mental stimuli. Subjective methods to measure arousal include questionnaires like the Self-Assessment Manikin (SAM) [305] and the Affective Slider (AS) [306]. Physiological measures of arousal are obtained by measuring signals from the autonomic nervous system (ANS) including EDA (electrodermal activity) caused by sweating in response to arousal, HRV (Heart Rate Variability), respiration volume/rate, pupil diameter variation, and brain activity [307]. The relationship between arousal and task performance has been hypothesized to be linked to performance in an inverted U-shaped curve according to Yerkes-Dodson law [308], this has not been conclusively established by literature due to other factors like task complexity and personality factors [309], [310]. Increases in arousal can affect memory and cause retrieval of task-irrelevant information, which may affect training outcomes [311]. Though as discussed, both haptic feedback and arousal may affect task performance, the relationships between these three factors are not well established. There are few explorations linking arousal to haptic feedback in literature [312], [313], Gatti et al. [314] used a Geomagic Touch (3D Systems, US) to render viscous forces onto participants' hands while they viewed emotional pictures where they found an effect of haptics on subjective arousal (SAM) but not on physiological arousal (EDA, HRV, respiratory rate, and temperature). Akshita et al. [315] similarly linked an emotional pictures dataset with vibrotactile haptics and subjective arousal (SAM), finding that high-intensity haptic feedback on the fingers contributes to increases in subjective arousal.

In addition to measures of performance and arousal, subjective measures of presence, and task load among others add additional insight into designing more effective haptics-enabled VR training. Gibbs et al. [316] and Cooper et al. [317] found that multimodal (i.e., combinations of haptics with audio or visuals) feedback led to better presence as compared to providing feedback in any one modality alone. However, it is not clear which feedback modality, between kinesthetic and vibrotactile can cause the greatest increase in presence. Additionally, research has pointed to the links between task load and haptic modality. For

example, kinesthetic feedback has been linked to lower task load in surgical VR training [318] and VR motor skills therapy scenarios [319]. Weber et al. [320] in a desktop VR peg-in-hole experiment found that kinesthetic feedback led to a lesser overall task load compared to vibrotactile and visual (no haptic feedback) conditions. It remains an open question if this pattern holds for the buzzwire task in immersive VR which requires finer motor skill control.

6.3 Methods

We designed an experiment to address the research questions addressed in Sec. 6.1. As a representative example of fine motor skill task, we considered a buzzwire (or wire loop) task, where the aim is to move a metallic loop across a wire without touching it, as shown in Fig. 6.1, (a) Physical experimental environment, where the participant moves the loop across the real wire. The participant wears an Electrodermal Activity (EDA) sensor (Shimmer GSR+). The Heart Rate Variability sensor (Polar H10) is worn around the chest, in contact with the skin (not visible in the picture). (b) The custom handle held by a participant. It houses six vibrotactile motors able to provide distributed vibrations when a mistake happens, i.e., the wire touches the loop. It was attached to a real metallic loop during the physical tasks (as in (a)) and to a Geomagic kinesthetic interface during the VR tasks (as in Fig. 6.5). (c) CAD representation of the custom handle, highlighting the positioning of the vibrotactile actuators, L: left, U: up, R: right, D: down, F: front, B:

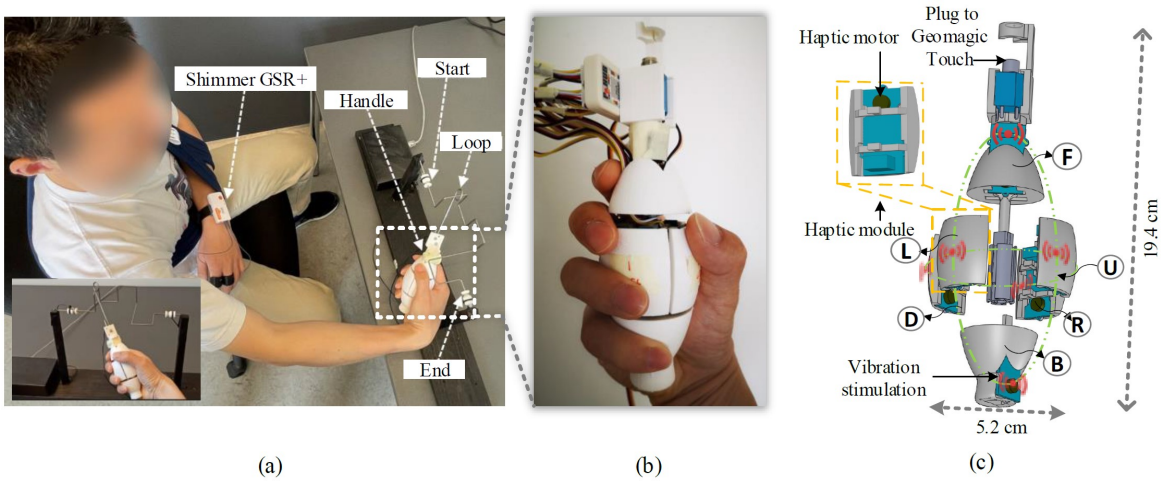

Figure 6.1 – Experimental setup (physical tasks).

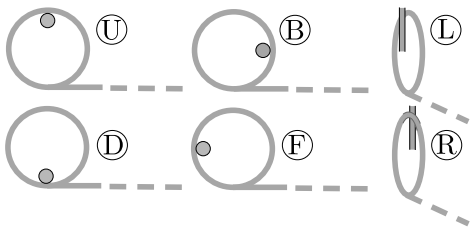

Figure 6.2 – Vibrotactile motor activation: related to the contact between the rod and the wire in the virtual scenario the corresponding motor is activated on the handle.

back. As an example, if the contact happened in the superior part of the ring (Fig. 6.2 position U) the U motor was activated. The same, correspondent for the other sides.

6.3.1 Flow of the experiment

The flow of the experiment is shown in Fig. 6.3, from left to right wire. First, all participants are asked to perform the buzzwire task in a physical environment, called "pretest". During this task, participants hold a handle attached to a metal loop, which they move from one end of a physical wire to the other, as fast as possible and with the least number of mistakes. Then, participants are given training in an immersive VR environment to improve their task performance, called "VR Training (Phase 1)". The VR training environment consists of multiple virtual buzzwires, similar to the one in the pretest environment, but featuring different levels of difficulty. This time, participants hold the handle attached to a Geomagic grounded haptic interface. Similarly as before, they had to move the loop across the considered virtual buzzwire as fast as possible and with the least number of mistakes. During this VR training, participants receive different types of feedback about the contacts of the loop with the wire, according to the group they have been assigned to: one group of participants receives visual feedback only, one receives visual and kinesthetic feedback, and one receives visual and vibrotactile feedback. After this VR training, all participants are asked again to perform the buzzwire task in the physical environment, called "intermediate test". Finally, this experimental protocol is repeated, with the participants once again receiving training in an immersive VR environment, called "VR Training (Phase 2)" and subsequently analyzing the change in their performance in a final buzzwire physical task, called "post-test" (see the right-hand part of Fig. 6.3). The two phases of VR training ("Phase 1" and "Phase 2") provide the participants with different intensities of feedback, as detailed in Sec. 6.3.5, enabling us to also analyze whether the intensity of the feedback affect the user's performance.

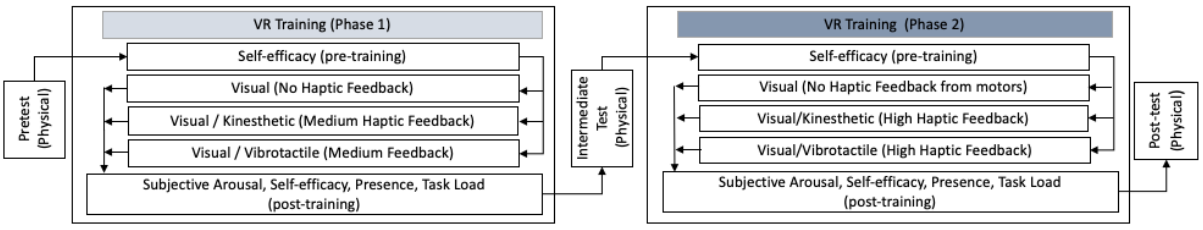

Figure 6.3 – Flow of the experiment.

6.3.2 Physical experimental environment

The physical environment is shown in Fig. 6.1. It is an adaptation of the physical test of motor skills used by Radhakrishnan et al. [299]. The metal wire is long 52 cm and rests on two 20 cm-high pillars. The start and end positions are denoted by grooves on two white plastic cylinders on either side of the wire, designed so that the loop can rest on them. An Arduino UNO is used to detect the mistake signals, i.e., when the loop touches the wire, and transmit them to an external computer through a serial connection. Similar circuits are used to detect when the loop is lifted off the groove at the beginning of the task as well as when the loop reaches the groove at the end of the wire. A video showing the physical setup can be found at `https://youtu.be/qZ6fBP-poAs?t=106`.

Participants were asked to carry out the task in this physical environment three times throughout the overall experience ("pretest" "intermediate test" and "post-test"), as described before and summarized in Fig. 6.3.

6.3.3 Custom vibrotactile handle

Figure 6.1 shows the custom handle designed to provide vibrotactile sensations about the (undesired) contacts between the loop and the wire, according to the feedback condition at hand. It is shaped as an ellipsoid and houses six vibrotactile modules, inspired from [321], [322]. The vibrotactile modules are positioned around the handle: four are placed symmetrically around the plane perpendicular to the main axis, and two are placed at the ends of the main axis (see Fig. 6.1). Small gaps around where the haptic modules are positioned weaken the transmission of vibrations, making it easier to recognize the source of the vibration. In this regards, we conducted a tests on vibration propagation distribution the handle, located on the desk. During such a test, each haptic module has been sequentially activated at the maximum nominal power and vibration amplitude. An accelerometer was located, and connected, to the non-vibrating haptic module measuring

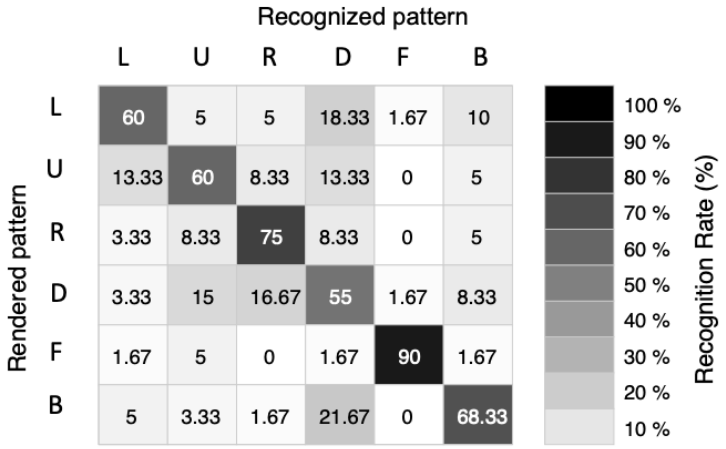

Figure 6.4 – Custom vibrotactile handle: perceptual experiment. Confusion matrix showing the recognition rates when activating each of the six motors (see also Fig. 6.1).

the vibration propagation effect. It resulted that the vibration amplitude in the passive modules was in average reduced of 67.19% ± 4.78% respect to the one active.

We carried out a perceptual experiment, enrolling 12 participants, to evaluate the capability of the handle to provide spatialized vibrotactile sensations. The participants hold the handle with the haptic module 'U' pointed upwards, this is also the grip gesture when the handle was used in the training experiment. We activated one random motor at a time and asked the participants to indicate which one was vibrating (30 trials in total, 5 per motor). Participants were able to correctly recognize the activated motor 68.0% of the times (see Fig. 6.4). On the other hand, 13.6% of the times participants confused adjacent motors, while 18.4% they confused motors located further away.

6.3.4 VR training environment

The VR training environment is shown in Fig. 6.5. It was composed of three virtual buzzwires levels, shown in Level 1 was 57 cm long (end to end) with a horizontal span of 21 cm and eighteen 90° bends level 2 was designed to be the mirrored version of level 1 so that the beginning and the end were inverted, and level 3 was designed to be the same as level 1 but tilted 45° around the main axis of the wire (Fig. 6.5d).

Participants were asked to wear a Oculus Rift Head Mounted Display (HMD) and hold the custom handle attached to a Geomagic Touch interface, as shown in Fig. 6.5a. The latter is used to track the movement of the user to animate the virtual loop in all feedback conditions. It is also used to provide kinesthetic feedback in the dedicated

feedback condition.

6.3.5 Feedback conditions during VR training

Participants undergo two training phases in VR to become better at the buzzwire task. They are randomly assigned to one of the three VR training conditions: visual feedback only, visual and kinesthetic feedback, and visual and vibrotactile feedback about the contacts between the loop and the wire, that users are asked to minimize. Each subject carries out the VR training in only *one* feedback condition.

Across the two VR training phases ("Phase 1" and "Phase 2") the intensity of the haptic feedback, kinesthetic and vibrotactile, changes. Haptic feedback provided during Phase 2 is 50% stronger than that provided during Phase 1, as detailed in Secs. 6.3.5.2 and 6.3.5.3 for kinesthetic and vibrotactile feedback, respectively. Visual feedback does not change across the two VR training phases.

We carried out a short preliminary experiment to ensure that this difference in haptic intensity was noticeable. The change was indicated as "clearly noticeable" by the 12 participants of the preliminary test, who were asked to carry out the VR buzzwire task four times, one per feedback intensity (medium, high) and type of haptic feedback

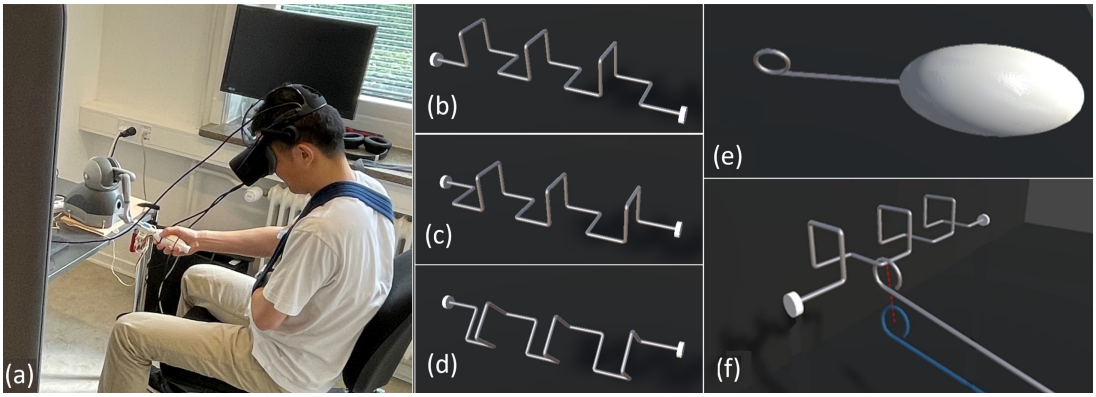

Figure 6.5 – Experimental setup (Virtual Reality training). (a) The Virtual Reality (VR) training environment, where participant holds the custom handle attached to the Geomagic Touch haptic device. (b) Level 1, (c) level 2, and (d) level 3 of the buzzwire task, presented during the two phases of the VR training. (e) Detail of the the loop and handle avatars in VR, which have the same dimensions of their physical counterparts. (f) Visual feedback provided to the users when the loop contacts the wire: a semi-transparent blue loop indicates the true position of the loop as commanded by the user, while the standard opaque grey loop indicates the proxy/ideal position of the loop inside the wire. Visual feedback is provided in all the feedback conditions.

(kinesthetic, vibrotactile), and describe their experience. The indications and results of this preliminary study have been used to set the parameters of the provided feedback as well, as detailed in the following Sections.

6.3.5.1 Visual feedback only

In this feedback condition, only visual feedback is provided, whenever the loop touches the wire, the virtual representation of the loop doubles, as shown in Fig. 6.5f and at https://youtu.be/qZ6fBP-poAs?t=65. A semi-transparent blue loop indicates the true position of the loop as commanded by the user, while the standard opaque grey loop indicates the proxy/ideal position of the loop, still inside the wire. During the contact situation, the opacity of the semi-transparent blue loop increases as it moves away from the proxy position of the loop inside the wire. Finally, a dotted line indicates the direction where the user should move to rejoin the wire and continue the task; the color of the line changes from black to red as the user moves the loop away from its proxy position inside the wire.

6.3.5.2 Visual and kinesthetic haptic feedback

In this case, visual and kinesthetic feedback are provided, whenever the loop touches the wire, participants receive the visual feedback as well as kinesthetic feedback forces provided by the Geomagic Touch interface. Specifically, the loop-wire haptic interaction was rendered using a simple elastic model with stiffness 56.7 N/m and 85 N/m for the two phases of the VR training, respectively. The linear damping was kept constant in both phases at 8 Ns/m.

6.3.5.3 Visual and vibrotactile haptic feedback

In this case, visual and vibrotactile feedback are provided, whenever the loop touches the wire, participants receive the visual feedback as well as vibrotactile feedback stimuli provided by the custom handle. Vibrations were provided along the direction where the contact between the virtual loop and wire happened, e.g., if the loop touched the wire in its upper sector (as in Fig. 6.5f), the vibration was provided by the motor U (up); if the loop touched the wire in its lower sector, motor D (down) would be activated.

The vibration amplitude was fixed and set to 0.33 g for phase 1 and 0.49 g for phase 2 of VR training.

6.3.6 Metrics

6.3.6.1 Objective performance metrics

Three types of metrics that can be used to objectively measure performance, i.e., spatial, temporal, and spatiotemporal metrics. We considered three metrics [323]:

1. task completion time (TCT), which is the time taken to move the loop from start to end;
2. loop-wire contact time (CT), which is the time spent by the wire in contact with the wire.
3. the improvement score (IS), which is calculated by rank ordering improvements among all participants into ten equal quantiles for TCT and CT separately. A rank order of 1 denotes the least improvement in performance while a rank order of 10 denotes the most improvement. Subsequently, IS for a participant is defined as the sum of the ranks for TCT and CT, e.g., a participant who has improved the most in both TCT (rank order = 10) and CT (rank order = 10) would get an IS of 20.

6.3.6.2 Subjective measures

We considered subjective metrics related to perceived task load, self-efficacy, subjective arousal and presence. To measure task load, we used NASA-TLX [324], across the six standard dimensions - Mental Demand, Physical Demand, Temporal Demand, Performance, Effort, and Frustration. A combined task load score was then taken by averaging all six dimensions. To measure self-efficacy, the participants are asked the question *"How confident are you that you can perform a similar task effectively (go from start to finish as fast as you can with minimal mistakes) on a scale from 1 to 7?"*, both before and after the training. To measure subjective arousal, we combined the arousal sub-scale of Self-Assessment Manikin (SAM) [305] with the Affective Slider [306], [325]. To measure presence, we used the five dimensions in the physical subscale of the Multimodal Presence Scale [326].

6.3.6.3 Physiological arousal metrics

To investigate the participants' arousal levels, heart rate variability, and electrodermal activity, we used the Polar H10 (Polar Electro Oy, Finland) and Shimmer GSR+ (Shimmer Research Ltd., Ireland) sensors. Baseline values were subtracted where applicable from the physiological arousal metrics to control for individual physiological differences [327]. All

Table 6.1 – Relationship between increases in physiological arousal and EDA and ECG metrics.

Effect of Arousal (↑: increase, ↓: decrease)	
EDA	Skin Conductance (SC) ↑
	Skin Conductance Response Amplitude (SCRAmp) ↑
	Skin Conductance Response Peaks Rate (SCRPeaks) ↑
ECG	Heart Rate (HR) ↑
	Inter-Beat Interval (IBI) ↓
	Root Mean Square of Successive Differences (RMSSD) ↓
	Standard Deviation of NN Intervals (SDNN) ↓
	Normalized High-Frequency Component (HFN) ↓
	LF/HF (Low Frequency/High Frequency) Ratio ↑

physiological sensor data were streamed and stored using the iMotions platform (iMotions A/S, Denmark).

Heart Rate Variability The Polar H10 is an Electrocardiogram (ECG) heart rate monitor often used in VR studies [299]. Based on the raw R-R interval data, different measures of heart rate variability, including time and frequency domain metrics, were calculated using the hrv-analysis Python library [1]. Table 6.1 shows the link between increases in arousal and its effect on ECG based metrics. Increases in arousal are indicated by increases in Heart Rate and Low Frequency/High Frequency (LF/HF) Ratio [328]. Decreases in HRV measures like IBI (Inter-Beat Interval), SDNN (Standard Deviation of NN Intervals), RMSSD (Root Mean Square of Successive Difference), and the frequency domain measure HFN (Normalized High-Frequency Component), indicate an increase in arousal [329].

Electrodermal activity (EDA) The Shimmer GSR+ (Galvanic Skin Resistance) measures EDA by passing a small current through electrodes placed on the index and middle fingers in the left hand [299]. EDA measures used in this study include SC (Skin Conductance), which increases in response to an increase in arousal [330]. Table 6.1 also shows the link between increases in arousal and its effect on EDA metrics. An increase

1. https://github.com/Aura-healthcare/hrv-analysis

in arousal also leads to a higher rate of Skin Conductance Response Peaks per minute (SCRPeaks) which are peaks in the SC amplitude lasting between 1-5 seconds after onset [331]. Similarly, the mean peak amplitude of all SCR peaks (SCRAmp) is also a positive measure of arousal [331].

6.3.7 Experimental procedure and participants

Participants signed up for the study using the University online participant recruitment system and were randomly assigned to one of the three feedback conditions (see Sec. 6.3.5). They had to satisfy these criteria: (a) right-handed (to minimize variation in the setup), (b) normal vision or corrected-to-normal vision with contact lenses (no glasses), and c) no mental illnesses or sensitivity to nausea. Participants signed up for 35-minutes time slots of their choosing and were paid the equivalent of 12 EUR. Approval for this experiment was obtained from the Cognition and Behavior Lab's Human Subjects Committee (approval code: 339), Aarhus University.

After reading and signing the consent forms, participants were familiarized with the experimental task by an experimenter, who demonstrated the task. Thereafter, participants were given privacy to place the Polar H10 around their chest. The Shimmer GSR electrodes were placed on the index and middle fingers of the participant's left hand. Then participants were assisted in wearing a sling around the neck so that they could rest their left hand with the fingers relaxed. Participants were asked to keep their left hand still, so as to minimize the noise in the recorded signals. The signal quality for both sensors was verified before the experiment started. Baseline data from these biosensors were measured with the participants seated quietly, with their eyes closed, breathing normally, and without wearing the HMD.

6.4 Results

6.4.1 Participants and data analysis

73 participants enrolled in the study, randomly divided between visual/kinesthetic (n=26), visual/vibrotactile (n=22), and visual only (n=25) feedback conditions. 37 participants identified themselves as female, 35 as male, and 1 as other. 36 participants indicated their age group in the 25-34 range, 33 in the range 18-24, and 4 in the range 35–44. More than half of the participants in the study (49) indicated that they had tried VR using a

head-mounted display more than once, while 24 reported never having used it before the experiment. An analysis of the quality of the HRV and EDA data using iMotions led to dicarding of HRV and EDA data from 3 and 20 participants, respectively, Shapiro-Wilk tests for normality were applied to all the variables, and if a variable was found to violate assumptions of normality, non-parametric statistical alternatives were used. A significance level of 0.05 was selected while interpreting the results of the statistical tests.

6.4.2 Objective performance

We analyzed the task completion time (TCT), contact time (CT), and improvement scores (IS), as described in Sec. 6.3.6.1. Improvements in performance metrics due to training are evaluated as changes

1. from the pretest to the post-test physical tasks (referred to as "overall training");
2. from the pretest to the intermediate test physical tasks (referred to as "Phase 1 training");
3. from the intermediate test to the post-test physical tasks (referred to as "Phase 2 training").

Table 6.2 – Summary of Two-way Mixed ANOVA Results for Task Completion Time and Contact time by Feedback Condition (between-subjects) and Test Iteration (within-subjects)

Dependent variable	Source of variation	Sum of Squares	Degrees of Freedom	Mean Squares	F-value	p-value
Task Completion Time	Feedback condition	2883.949	2	1441.974	1.930	.153
	Test iteration	1060.274	1.473	719.692	7.582	.003*
	Feedback condition * Test iteration	181.935	2.946	61.747	.650	.582
Contact Time	Feedback condition	32.951	2	16.476	.992	.376
	Test iteration	95.662	2	47.831	18.113	<.001*
	Feedback condition * Test iteration	7.940	4	1.985	.752	.559

* denotes significant difference at α=0.05

Task completion time (TCT) A two-way mixed ANOVA was conducted to analyse the differences between "feedback conditions" (between-subjects factor: visual, visual/kinesthetic, visual/vibrotactile) and "test iterations" (within-subjects factor: pretest, intermediate, and post-test physical tests) on this metrics. Table 6.2 summarizes the results of the following analysis. Mauchly's test of sphericity indicated that the assumption of sphericity was violated for the two-way interaction, $\chi^2(2)$=30.089, p<.001.

Therefore, a Greenhouse-Geisser correction was applied (ε=0.737). There was no statistically significant interaction between the feedback condition and test iteration on TCT, F(2.946, 101.653)=.650, p=.582, partial η^2=.019. The main effect of time showed a statistically significant decrease in TCT over the three test iterations, F(1.473, 101.653)=7.582, p=.003, partial η^2=.099, with TCT decreasing from 31.53 ± 21.57 s (mean ± standard deviation) in the pretest, to 27.98 ± 15.64 s in the intermediate test and to 26.2 ± 13.97 s in the post-test. Post hoc analysis with a Bonferroni adjustment revealed that TCT decreased significantly from pretest to intermediate test (3.63 s, p=.024), and from pretest to post-test (5.34 s, p=.01) but not from intermediate test to post-test (1.7 s, p=.304). The main effect of group showed that there was no statistically significant difference in task completion time between feedback conditions F(2, 69)=1.93, p=.153, partial η^2=.053.

Contact time (CT) As before, a two-way mixed ANOVA was conducted to analyse the differences between feedback conditions and test iteration for this metrics (see Table 6.2 a summary of the results). Mauchly's test of sphericity indicated that the assumption of sphericity was met for the two-way interaction, $\chi^2(2)$=4.754, p=.093 There was no statistically significant interaction between the feedback condition and test on CT, F(4, 138)=0.75, p=.559, partial η^2=.021. The main effect of time showed a statistically significant difference in CT over the test iterations, F(2,138)=18.11, p<.001, partial η^2=.208, with CT decreasing from 7.25 ± 2.49 s (mean ± standard deviation) during the pretest, to 6.18 ± 2.99 s in the intermediate test, and to 5.68 ± 2.58 s in the post-test. Post-hoc analysis with a Bonferroni adjustment revealed that CT decreased significantly from pretest to intermediate test (1.07 s, p=.002), and from pretest to post-test (1.61 s, p<.001) but not from intermediate test to post-test (0.53 s, p=.153). The main effect of feedback condition showed that there was no statistically significant difference in contact time between the feedback conditions, F(2,69)=0.992, p=.376, partial η^2=.028.

Improvement Score (IS) A one-way ANOVA was performed to compare the improvement score between the three feedback conditions, which revealed no statistically significant difference (F(2,69)=0.047, p=0.95).

6.4.3 Self-Efficacy, Task load, Presence

A two-way mixed ANOVA was conducted to analyse the effect of feedback condition (between-subjects factor: visual, visual/kinesthetic, visual/vibrotactile)) and test iteration

(within-subjects factor: pre-phase 1 training, post-phase 1 training, pre-phase 2 training, post-phase 2 training) on self-efficacy (SE). Mauchly's test of sphericity indicated that the assumption of sphericity was violated for the two-way interaction, $\chi^2(5)=32.45$, $p<.001$. Therefore, a Greenhouse-Geisser correction was applied ($\varepsilon=0.788$). There was no statistically significant interaction between the feedback condition and time on self-efficacy, $F(4.729,165.52)=1.143$, $p=.339$, partial $\eta^2=.032$. The main effect of time did not show a statistically significant difference in mean SE at the different time points, $F(2.365,165.52)=1.549$, $p<.0005$, partial $\eta^2=.022$. The main effect of feedback condition showed that there was no statistically significant difference in mean SE between feedback conditions $F(2,70)=1.135$, $p=.327$, partial $\eta^2=.031$.

Fig. 6.6a shows the overall NASA-TLX score obtained by calculating the average of the six NASA-TLX task load dimensions (mental demand, physical demand, temporal demand, performance, effort, and frustration) reported by the participants. One-way ANOVAs/Kruskal-Wallis tests were performed to compare the effect of feedback condition on the individual NASA-TLX dimensions revealing no significant differences between the feedback conditions. However, posthoc pairwise comparisons (Mann-Whitney U tests) revealed a near statistically significant difference in temporal demand between visual/vibrotactile condition where participants reported on average a score of 10.02, and visual/kinesthetic condition where participants reported 11.94 ($p=0.07$, $U=371.5$).

Fig. 6.6b shows the overall presence score reported by the participants, calculated by taking the average of the responses to the five questions in the presence questionnaire. A Kruskal-Wallis test revealed no significant difference in the presence score between the feedback conditions ($F(2,70)=1.5$, $p=0.22$).

6.4.4 Physiological arousal

Arousal and feedback condition One-way ANOVAs performed on SAM (Self-Assessment Manikin) reported by participants did not reveal an effect of feedback condition on subjective arousal during training ($H(2)=0.47$, $p=0.79$). One-way ANOVAs performed on each of the EDA and HRV metrics also did not show any significant effect of feedback condition on those metrics. However, posthoc pairwise comparisons (Mann-Whitney U tests) showed that participants in the visual/kinesthetic condition had a higher baseline corrected LF/HF ratio (-0.15) compared to participants in the visual/vibrotactile condition (-2.59) ($p=0.028$, $U=349$). To measure differences in arousal immediately after the participants commit a mistake during VR training, the physiological arousal levels were

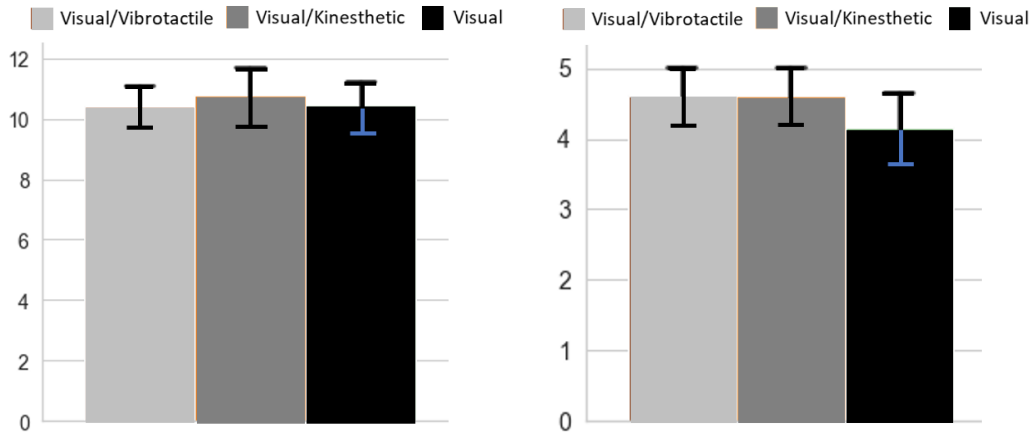

(a) NASA TLX **(b)** Presence

Figure 6.6 – (a) NASA TLX and (b) Presence scores across Visual/Vibrotactile, Visual/Kinesthetic, and Visual conditions. Mean and 95% confidence interval are reported.

averaged for 10-seconds windows starting at the moment of contact between the loop at the wire. One-way ANOVAs/Kruskal-Wallis tests performed to compare the effect of feedback condition on all of these "immediate" arousal metrics did not show any significant difference between the three feedback conditions.

Arousal and task performance The link between task performance and arousal was assessed using co-relation tests between improvement score (IS) and arousal, as measured by both subjective (SAM) and physiological (EDA, HRV) measures. Statistically significant (but weak) negative correlations were observed between Improvement Score (IS) and three HRV metrics: RMSSD (ρ=-0.35, p=0.003), SDNN (ρ=-0.32, p=0.008) and HR (ρ=0.245, p=0.043). As decreases in RMSSD and SDNN, and increases in HR, are correlated with increases in arousal (see Sec. 6.3.6.3 and Table 6.1), the results of the correlations tests show that improvements in performance are correlated with increases in arousal. To further investigate this point, we grouped participants into two groups: high-improvement (n=15) and low-improvement (n=15), respectively. Following the technique described by Radhakrishnan et al. [299], the high-improvement group was defined as participants who had an improvement score (IS) above the upper range of the inter-quartile range (i.e., above the 75% mark) and the low-improvement group had participants from the lower quartile range (i.e., below the 25% mark). As shown in Table 6.3, Mann-Whitney U tests were performed for HRV and EDA metrics between these two groups. It can be observed that participants in the high-performance group had a higher baseline adjusted

Table 6.3 – Physiological Arousal Metrics across High (n=15) and Low Improvement groups (n=16).

Arousal Metric		High Improvement(Mean±SD)	Low Improvement (Mean±SD)	p-value
HRV	HR	4.82±5.59	-1.16±3.28	0.002*
	IBI	-42.27±55.81	4.7±34.69	0.02*
	RMSSD	-58.41±101.15	17.68±35.54	0.001*
	SDNN	-47.91±63.07	4.08±32.14	0.003*
	LF/HF Ratio	-1.47±3.97	-1.44±4.97	0.98
	HFN	1.33±17.83	7.41±14.89	0.35
EDA	SC	2.35±3.18	1.84±1.81	1.0
	SCRAmp	0.14±0.22	0.14±0.16	0.99
	SCRPeaks	10.37±4.76	8.84±1.84	0.36

* denotes significant difference at α=0.05

heart rate (HR) of 4.82, as compared to -1.16 of the low-performance group (p=0.002, U=178). In terms of inter-beat interval (IBI), the high-performance group had a lower baseline-adjusted IBI (-42.27) compared to the low-performance group with an IBI of 4.7 (p=0.02, U=51). Participants in the high-performance group showed a lower baseline adjusted RMSSD (Root Squared Mean of Successive Differences) of -58.41 compared to the RMSSD of 17.68 for the low-performance group (p=0.001, U=30). Similarly, participants in the high-performance group also showed a lower baseline-adjusted SDNN (Standard Deviation of NN intervals) of -47.91, compared to an SDNN of 4.08 for the low-performance group (p=0.003, U=37). This result supports the patterns observed in the correlation tests, i.e., improvements in performance are correlated with increases in arousal.

To further investigate the trends in the relationship between arousal and performance, participants were also divided into high-arousal and low-arousal groups regarding, separately, the HRV and EDA metrics. This split followed the same principle we used for splitting the participants into high and low-performance groups, i.e., according to their position in the inter-quartile range. Subsequently, the improvement scores (IS) were compared for each of these pairs of high and low-arousal groups using Mann-Whitney U tests. In terms of high and low-arousal groups split according to RMSSD, participants in the high-arousal group had an IS of 9.06, which was lower than the IS of 12.06 observed in the low-arousal group (p=0.01, U=66). Similarly, for groups split according to SDNN,

participants in the high-arousal group were observed to have an IS of 9.06, which was lower than the IS of 12.31 observed in the low-arousal group (p=0.017, U=70). Among groups split according to HR, participants in the high-arousal group had an HR of 12.39 as compared to the HR of 9.78 observed in the low-arousal group, and this difference approached the threshold of statistical significance (p=0.09, U=221). This further confirms the trends observed earlier of performance improvement as arousal increases.

6.5 Discussion

Here we discuss the results from Sec. 6.4 in the context of the three research questions introduced at the end of Sec. 6.1.

6.5.1 Kinesthetic and vibrotactile feedback for VR training

Improvements (i.e., reductions) in task completion time were seen after overall training (pretest to post-test) as well as Phase 1 training (pretest to intermediate test) for all participants. Similarly, concerning contact time, participants in all feedback conditions showed improvements (i.e., reductions) after overall training (pretest to post-test). Furthermore, statistical tests comparing the improvement scores across the three feedback conditions were inconclusive in finding any difference between them. This implies that, while IVR training with vibrotactile and kinesthetic feedback improves performance, it is not clear which haptic modality is better or if they are better than visual feedback only. However, analysis described in Sec. 6.5.2 points to the potential for further investigation on the use of haptic feedback to modulate arousal and thereby improve performance. Furthermore, alternate uses of haptic feedback could be explored in the context of training in the buzzwire task, for example in the form of virtual fixtures or guidance [9], [45], [332], [333].

6.5.2 Kinesthetic and vibrotactile feedback for arousal level

Analysis of the data revealed no effect of feedback condition on EDA and HRV. Analysis of SAM responses did not reveal any effect of feedback on subjective arousal. However, pairwise comparisons of EDA and HRV metrics across feedback conditions revealed a higher arousal level (for the HRV metric LF/HF Ratio) among participants receiving kinesthetic feedback compared to those receiving vibrotactile feedback during

training. This finding is similar to that of Krogmeier et al. [331] where it was observed in a scenario in which participants received haptic feedback (on the torso) from a vest, that the most realistic haptic feedback condition resulted in greater arousal compared to the least realistic. These links between arousal and haptic feedback offer opportunities for further investigation, especially in light of indications from our study that certain arousal levels are correlated with performance improvements. Specifically, correlation tests revealed a weak negative correlation between improvements in performance and two HRV metrics (RMSSD, SDNN), i.e., as arousal increased (decrease in RMSSD and SDNN is correlated with increases in arousal) during VR training, so did performance. This link was further supported by statistical tests which showed higher arousal levels indicated by four HRV metrics (HR, IBI, RMSSD, and SDNN) in the high-improvement group as compared to the arousal levels of participants in the low-improvement group. This trend was again confirmed by statistical tests comparing performance between groups of participants split according to the degree of arousal, which showed that participants in high-arousal groups (defined by the HRV metrics RMSSD and SDNN) demonstrated greater improvement scores compared to those in low-arousal groups. These two findings, that kinesthetic feedback resulted in more arousal (compared to vibrotactile feedback) and that increases in arousal were corelated with increases in performance, inspire future research on the potential for increasing training performance by varying arousal with the help of haptic feedback. Even though our study points to higher levels of arousal linked to better improvements in performance, we also acknowledge the view that increasing arousal or stress may have detrimental effects on performance. For example, in a buzzwire training scenario, Radhakrishnan et al. [299] found that participants across VR and physical training conditions who had the highest arousal levels during training showed the lowest improvements in performance (and vice-versa). Though the motor task is similar (a buzzwire scenario), that study had participants undergo training in a different setup, i.e., physical training and VR training with simple non-directional vibrotactile feedback from the Oculus Touch controller. There are also non-VR studies that point out that high-arousal levels may lead to lower performance [334], [335]. Wu et al. [336] in their VR driving scenario found that moderate arousal levels (neither too high nor too low) correlated with the best performance. Perhaps, such contradictions may be solved if variables in addition to performance and arousal are considered. For example, a high-arousal level may be linked to higher enjoyment or motivation, which in turn affects performance positively, but similar arousal levels due to anxiety may negatively affect performance.

6.5.3 Kinesthetic and vibrotactile feedback for recognition variations

The analysis showed no effect of feedback condition on overall presence. This might be caused by the subjective experience of presence being dominated in this study by the visual aspect which were the same across the three feedback conditions. As Grassini et al. [337] had linked increased presence to better training outcomes, the lack of an effect of feedback condition on improvements in performance may thus be partially explained by the lack of differences in terms of presence. However, there are inspirations from literature for further investigation into improving presence and thereby training outcomes. For example, some studies have found vibrotactile feedback coupled with visual feedback to result in better-reported presence compared to visual alone [316] or kinesthetic feedback alone [296].

The analysis also revealed no effect of feedback condition on overall task load. This is important as increases in workload have been linked to decreased motor skill performance as described by Yurko et al. [338] in their study on simulator based laparascopy training. In light of this, the lack of differences in performance metrics between the feedback conditions in our study maybe linked to the lack of differences in perceived task load. However, it was also observed that there was a near statistically significant trend towards participants in the visual/kinesthetic condition reporting more temporal demand, i.e. they felt the training to be more rushed/hurried compared to those in the visual/vibrotactile condition. This is interesting as ultimately the outcome of the training in terms of performance were indistinguishable across the feedback conditions in spite of this difference. In a study using a similar buzzwire test setup, Radhakrishnan et al. [299] found participants who received physical training to report more temporal demand than those who underwent IVR training (with non-directional vibrotactile feedback), and similar to our study, overall task load and performance improvements were indistinguishable between the training conditions. On the other hand, Weber et al. [320], in a peg-in-hole task using desktop VR, found that vibrotactile feedback resulted in a higher task load compared to kinesthetic feedback, and the authors attributed this to "feedback ambiguity" arising from the design of the vibrotactile feedback. Therefore, it is possible that the lack of differences in overall task load between the kinesthetic and vibrotactile feedback conditions in our study may arise from the lack of directional ambiguity as shown in the perceptual experiment described in Sec. 6.3.3.

There were no statistically significant changes in self-efficacy during VR training for all

the feedback conditions. This is surprising, as prior literature points to the links between self-efficacy and learning/training performance [295], [339]. Our study has shown that there is improvement in performance across all the feedback conditions, in spite of this lack of increase in self-efficacy. Radhakrishnan et al. [299] presents a contrasting example with a similar buzzwire motor skill task, where it was found that significant improvements in self-efficacy during VR training was accompanied by corresponding improvements in performance. Stevens et al. [340] in a motor skill training task showed that increased task-difficulty level is one factor which leads to impairments in both self-efficacy and performance. Therefore future research could consider methods to improve self-efficacy, for example by adapting the difficulty level of training.

6.5.4 Summary

In summary, VR training is effective in improving performance regardless of the considered haptic feedback modality. So one may wonder if kinesthetic or vibrotactile feedback were to be used, are they interchangeable, or should additional parameters be considered? Our analysis of the data showed that (1) participants in the kinesthetic feedback condition showed higher arousal than those in the vibrotactile feedback condition, and that (2) there is a correlation between higher arousal levels and higher performance across feedback conditions. These findings should encourage further research in using different types of haptic feedback to potentially affect arousal levels and performance. Future research could explore variations of kinesthetic feedback, for example with wearable exoskeletons, which might also combine aspects of cutaneous feedback to provide a good trade-off between cost and performance [8]. With regards to investigating the relationship between haptic feedback and arousal, additional physiological metrics can be considered, such as EEG (electroencephalography), EMG (electromyography), and pupil dilation, particularly since biosensors to measure these signals are being increasingly integrated into commercial VR head-mounted displays.

6.6 Conclusions

In this study, a fine motor skill training buzzwire task in immersive VR was used to investigate the effect of haptic feedback and physiological arousal on performance. The experiment revealed the effectiveness of motor skill training in VR regardless of the

haptic feedback. The investigation into physiological arousal levels between three feedback conditions revealed that training with kinesthetic feedback resulted in higher arousal compared to training with vibrotactile feedback. Links between arousal and performance were also found, with increases in arousal being accompanied by increases in performance. The inclusion of haptic feedback thus holds potential for motor skill training in VR, though further research is needed to explore the trade-offs between kinesthetic feedback and varieties of cutaneous feedback, such as the vibrotactile feedback considered here.

From this work, we have learnt that motor skill training performance was improved in all the three feedback conditions after a training session. In addition, training with kinesthetic feedback resulted in higher arousal compared to training with vibrotactile feedback. Thus, this work contributes to the research on using haptics for motor skill training with and without VR, it also paves the way of exploring the potential of haptic stimulation for human motor rehabilitation.

Conclusion

The human neurosensory system is a complex network that enables us to perceive, process, and respond to environmental stimuli. It also plays a crucial role in our perception of touch sensations. Although advances in science and technology have allowed for deeper investigation into the human neurosensory system, manipulating and interacting with it directly remains a difficult challenge. Our haptic interfaces stimulate the touch receptors the same way our environment does, by applying the target stimuli through mechanical end-effectors that deforms our skin. However, there are still many unanswered questions, starting from understanding which information is most important to deliver through haptic technology given a certain interaction task, the multisensory modelling of touch sensations, and the challenges in developing unobtrusive interfaces.

In this respect, the Chinese old parable called "the blind men touching an elephant" tells a story of a group of blind men who have never come across an elephant before and who learn and imagine what the elephant is like by touching it. Each blind man feels a different part of the elephant's body, but only one part, such as the side or the tusk. They then describe the elephant based on their limited experience, and their descriptions of the elephant are different from each other. One touches the elephant's trunk and thinks it similar to a snake, another touches its ear and thinks it is similar to a fan, another touches its leg and thinks it is similar to a tree trunk, and another thinks it is like a urn by touching the belly. This parable well illustrates the limitations of perception and the importance of considering multiple perspectives, as well as the importance of integrating different sensory information to form a coherent understanding of the world.

In this thesis, my research has centered on two primary areas: the development of ungrounded haptic devices to facilitate haptic interaction, and the examination of haptic stimulation in relation to human navigation and environmental rendering. The devices we developed have prompted us to enter into various design considerations, such as the wearable and portable mechanical mechanisms needed to generate force and torque for haptic feedback and the use of new compliant materials as end-effectors to deliver the target

sensations. In Chapter 3, we propose a parallel mechanism for generating kinesthetic forces and validate its efficacy in guiding hand motion. Additionally, we introduce an origami-inspired end-effector capable of generating a range of encounter-type touch sensations. In Chapter 5, we evaluated compliant materials for the implementation of deformable end-effectors to create soft and shape touch sensations of virtual objects[341]. We developed these devices borrowing the mechatronics structures and techniques from the robotics field. Our work showed promising results in using emerging compliant materials and fast fabrication tools for developing low-cost, accessible, modular, and easy-to-build haptic interfaces. The diverse haptic stimulations we employed showed effectiveness in immersive virtual interaction and in navigation applications. The systematic use of human subjects evaluations for the validation of our systems has proven the viability and effectiveness of ungrounded cutaneous solutions, showing once more that - in many cases - simple haptic solutions are able to convey rich interaction sensations.

Despite the extensive research being conducted in the field of haptics, there is still ample opportunity for enhancing the efficacy and usability of this technology as well as for using it in a broad new range of applications. To address this, we must focus on overcoming a series of important challenges, including:

* Haptic perception and rendering: how to generate rich sensations in a way that is interpretable and intuitive for user.
* Design of haptic systems: how to design effective haptic devices that are compact, inexpensive, and comfortable.

Perspectives

In the perspective of my work in the field, multimodal sensory aspects need to be taken into consideration when developing ungrounded haptic devices similar to those I have worked on these past three years.

Haptic devices must prioritize user-centered design, accounting for individual needs, preferences, and abilities. Beyond ergonomics and placement, designers should consider multimodal feedback, combining haptic sensations with audio and visual cues to increase immersion and engagement with virtual environments. Similarly, we should consider multimodal *haptic* feedback, considering the multiple aspects of haptic sensations, e.g., vibrations, pressure, skin stretch. Indeed, in Chapter 6, our research demonstrated the efficacy of visual and haptic feedback for improving motor skill training in VR. Additionally,

advancements in artificial intelligence and information science can improve adaptive feedback algorithms that adjust the intensity, frequency, and type of haptic feedback based on user behavior and preferences, reducing the risk of sensory overload. To further expand functionality, haptic devices frequently integrate with other technologies such as virtual reality headsets and motion tracking systems, fostering intuitive and natural interaction. In this respect, motion tracking is particularly critical to provide precise haptic sensations. Durability and portability are also critical design considerations to facilitate widespread use in diverse settings. Thus, designers must contemplate materials, battery life, repair and maintenance procedures to create a robust and portable devices, especially for applications of everyday use (e.g., gaming, rehabilitation).

From an engineering perspective, the design should ensure accurate and precise haptic feedback by implementing stabilization mechanisms that reduce unwanted vibrations and oscillations. These mechanisms may include passive damping materials, active feedback control systems, or gyroscopic stabilization. Moreover, the design should aim to decrease the size, cost, and weight of the device while maintaining the bandwidth, force output, range of motion, and degrees of freedom of the haptic actuators. To ensure user comfort and mobility, the device should be lightweight, portable, and energy efficient, allowing users to wear or carry it for extended periods without discomfort or hindering their movements. Finally, designers should remain updated on new technologies developed in related fields, such as smart materials used in soft robotics and novel actuators used in wearable robotics, to continuously improve and innovate the design of ungrounded haptic devices.

As I mentioned in the introduction, the goal of haptic rendering is to create a sense of realism and immersion for the user, allowing them to feel as though they are actually interacting with the virtual or remote environment at hand. To achieve this goal, it is important to develop rendering algorithms that take into account both the perceptual meaning of the haptic feedback (i.e., what sensation is being delivered) and its semantic congruence with the user's actions and the environment in which they are interacting. For example, if a user is interacting with a virtual object that is supposed to be hard and rigid, the haptic feedback should reflect this by providing a sensation of resistance or stiffness. If the virtual object is supposed to be soft and pliable, the haptic feedback should be correspondingly softer and more yielding, and this is studied in chapter 5, where we developed multiple end-effectors with varying stiffness and deformation to create the touch sensations of curvatures and softness. In addition to the perceptual and semantic aspects of haptic rendering, it is also important to consider the dynamics of the interaction.

Haptic rendering algorithms must be able to respond quickly and accurately to changes in the user's actions and the environment, providing haptic feedback that is both realistic and responsive. Achieving this level of performance requires sophisticated algorithms and hardware, as well as careful attention to the details of the interaction and the user's perceptual and cognitive abilities.

In the near future, it is promising to create predictive models of human perception and cognition surrounding touch feedback, in order to decrease reliance on exhaustive human user studies. Past psychophysics studies have mainly focused on touch perception on certain parts of the body, particularly the hands. There is a need to better expand our understanding of how touch is perceived on other parts of the body, such as the feet or torso. In addition, there is currently no standardized metric for evaluating the output characteristics of haptic devices. This means that different devices may provide different types and levels of feedback, making it difficult to compare and evaluate their effectiveness, which now heavily relies on human user studies. Developing a standardized metric for evaluating haptic devices could help to ensure that they are optimized for their intended use and provide consistent and reliable feedback.

With the advances in AI, mechatronics, and neuroscience, it is increasingly clear that we are on the cusp of a new era where haptic technology will become an integral part of our bodies and everyday interactions. With rich available information channels and unrestricted opportunities to interact with the world, haptic technology will enable us to experience the world in ways previously unimaginable.

Bibliography

[1] D. Prattichizzo, C. Pacchierotti, and G. Rosati, « Cutaneous force feedback as a sensory subtraction technique in haptics », *IEEE Transactions on Haptics*, vol. 5, *4*, pp. 289–300, 2012.

[2] C. Pacchierotti, D. Prattichizzo, and K. J. Kuchenbecker, « Cutaneous feedback of fingertip deformation and vibration for palpation in robotic surgery », *IEEE Trans. Biomedical Engineering*, vol. 63, *2*, pp. 278–287, 2015.

[3] C. Pacchierotti, S. Sinclair, M. Solazzi, A. Frisoli, V. Hayward, and D. Prattichizzo, « Wearable haptic systems for the fingertip and the hand: taxonomy, review, and perspectives », *IEEE Trans. haptics*, vol. 10, *4*, pp. 580–600, 2017.

[4] M. Marchal and C. Pacchierotti, « Virtual reality and haptics », *in Robotics Goes MOOC*, B. Siciliano, Ed., 2022.

[5] M. Malvezzi, F. Chinello, D. Prattichizzo, and C. Pacchierotti, « Design of personalized wearable haptic interfaces to account for fingertip size and shape », *IEEE Trans. Haptics*, 2021.

[6] E. M. Young, D. Gueorguiev, K. J. Kuchenbecker, and C. Pacchierotti, « Compensating for fingertip size to render tactile cues more accurately », *IEEE Transactions on Haptics*, vol. 13, *1*, pp. 144–151, 2020.

[7] F. Chinello, M. Malvezzi, D. Prattichizzo, and C. Pacchierotti, « A modular wearable finger interface for cutaneous and kinesthetic interaction: control and evaluation », *IEEE Trans. Industrial Electronics*, vol. 67, *1*, pp. 706–716, 2019.

[8] C. Pacchierotti, « Cutaneous haptic feedback for robotics and Virtual Reality », Habilitation à diriger des recherches, Université de Rennes 1, Rennes, 2022.

[9] L. Kuang, M. Aggravi, P. R. Giordano, and C. Pacchierotti, « Wearable cutaneous device for applying position/location haptic feedback in navigation applications », *in Proc. IEEE Haptics Symposium*, 2022, pp. 1–6.

[10] L. Kuang, M. Marchal, M. Aggravi, P. R. Giordano, and C. Pacchierotti, « Design of a 2-dof haptic device for motion guidance », *in International Conference on Human Haptic Sensing and Touch Enabled Computer Applications*, 2022, pp. 198–206.

[11] D. Prattichizzo, C. Pacchierotti, S. Cenci, K. Minamizawa, and G. Rosati, « Using a fingertip tactile device to substitute kinesthetic feedback in haptic interaction », *Haptics: Generating and Perceiving Tangible Sensations*, pp. 125–130, 2010.

[12] C. Pacchierotti, A. Tirmizi, G. Bianchini, and D. Prattichizzo, « Improving transparency in passive teleoperation by combining cutaneous and kinesthetic force feedback », *in 2013 IEEE/RSJ International Conference on Intelligent Robots and Systems*, IEEE, 2013, pp. 4958–4963.

[13] C. Pacchierotti, A. Tirmizi, and D. Prattichizzo, « Improving transparency in teleoperation by means of cutaneous tactile force feedback », *ACM Transactions on Applied Perception*, vol. 11, *1*, p. 4, 2014.

[14] I. Hussain, G. Spagnoletti, G. Salvietti, and D. Prattichizzo, « Toward wearable supernumerary robotic fingers to compensate missing grasping abilities in hemiparetic upper limb », *The International Journal of Robotics Research*, vol. 36, *13-14*, pp. 1414–1436, 2017.

[15] C. Pacchierotti, E. M. Young, and K. J. Kuchenbecker, « Task-driven pca-based design optimization of wearable cutaneous devices », *IEEE Robotics and Automation Letters*, vol. 3, *3*, pp. 2214–2221, 2018.

[16] L. Kuang, M. Marchal, P. R. Giordano, and C. Pacchierotti, « Rolling handle for hand motion guidance and teleoperation », *in EuroHaptics 2022-International Conference on Haptics: Science, Technology, Applications*, 2022.

[17] L. Kuang, F. Chinello, P. R. Giordano, M. Marchal, and C. Pacchierotti, « Haptic mushroom: a 3-dof shape-changing encounter-type haptic device with interchangeable end-effectors », *in Proc. IEEE World Haptics Conference (WHC)*, 2023.

[18] L. Kuang, M. Malvezzi, M. Ferro, *et al.*, « A 4-dof wearable hand device for haptic rendering of surfaces and edges », 2023.

[19] A. M. Kappers, M. F. S. Oen, T. J. Junggeburth, and M. A. Plaisier, « Hand-held haptic navigation devices for actual walking », *IEEE Transactions on Haptics*, vol. 15, *4*, pp. 655–666, 2022.

[20] J. Bimbo, C. Pacchierotti, M. Aggravi, N. Tsagarakis, and D. Prattichizzo, « Teleoperation in cluttered environments using wearable haptic feedback », *in Proc. IEEE/RSJ Int. Conf. on Intelligent Robots and Systems*, 2017, pp. 3401–3408.

[21] D. Ryu, C.-S. Hwang, S. Kang, M. Kim, and J.-B. Song, « Wearable haptic-based multi-modal teleoperation of field mobile manipulator for explosive ordnance disposal », *in IEEE International Safety, Security and Rescue Rototics, Workshop, 2005.*, IEEE, 2005, pp. 75–80.

[22] C. Pacchierotti, F. Chinello, M. Malvezzi, L. Meli, and D. Prattichizzo, « Two finger grasping simulation with cutaneous and kinesthetic force feedback », *Haptics: Perception, Devices, Mobility, and Communication*, pp. 373–382, 2012.

[23] L. Meli, C. Pacchierotti, G. Salvietti, *et al.*, « Combining wearable finger haptics and augmented reality: user evaluation using an external camera and the microsoft hololens », *IEEE Robotics and Automation Letters*, vol. 3, *4*, pp. 4297–4304, 2018.

[24] F. Gosselin, T. Jouan, J. Brisset, and C. Andriot, « Design of a wearable haptic interface for precise finger interactions in large virtual environments », *in First Joint Eurohaptics Conference and Symposium on Haptic Interfaces for Virtual Environment and Teleoperator Systems. World Haptics Conference*, 2005, pp. 202–207.

[25] F. Chinello, M. Malvezzi, C. Pacchierotti, and D. Prattichizzo, « A three dofs wearable tactile display for exploration and manipulation of virtual objects », *in 2012 IEEE Haptics Symposium (HAPTICS)*, IEEE, 2012, pp. 71–76.

[26] L. Meli, S. Scheggi, C. Pacchierotti, and D. Prattichizzo, « Wearable haptics and hand tracking via an rgb-d camera for immersive tactile experiences », *in Proc. ACM SIGGRAPH Posters*, 2014.

[27] S. Scheggi, L. Meli, C. Pacchierotti, and D. Prattichizzo, « Touch the virtual reality: using the leap motion controller for hand tracking and wearable tactile devices for immersive haptic rendering », *in ACM SIGGRAPH 2015 Posters*, 2015, pp. 1–1.

[28] X. de Tinguy, T. Howard, C. Pacchierotti, M. Marchal, and A. Lécuyer, « Weatavix: wearable actuated tangibles for virtual reality experiences », *in International Conference on Human Haptic Sensing and Touch Enabled Computer Applications*, 2020, pp. 262–270.

[29] I. Bortone, D. Leonardis, N. Mastronicola, *et al.*, « Wearable haptics and immersive virtual reality rehabilitation training in children with neuromotor impairments », *IEEE Trans. Neural Systems and Rehabilitation Engineering*, vol. 26, *7*, pp. 1469–1478, 2018.

[30] I. Hussain, G. Spagnoletti, C. Pacchierotti, and D. Prattichizzo, « A wearable haptic ring for the control of extra robotic fingers », *in International AsiaHaptics conference*, 2016, pp. 323–325.

[31] G. Rosati, F. Oscari, C. Pacchierotti, and D. Prattichizzo, « Effects of kinesthetic and cutaneous stimulation during the learning of a viscous force field », *IEEE Transactions on Haptics*, vol. 7, *2*, pp. 251–263, 2014.

[32] I. Hussain, L. Meli, C. Pacchierotti, G. Salvietti, and D. Prattichizzo, « Vibrotactile haptic feedback for intuitive control of robotic extra fingers. », *in World Haptics*, 2015, pp. 394–399.

[33] I. Hussain, G. Spagnoletti, C. Pacchierotti, and D. Prattichizzo, « A wearable haptic ring for the control of extra robotic fingers », *in Haptic Interaction: Science, Engineering and Design 2*, Springer, 2018, pp. 323–325.

[34] I. Hussain, L. Meli, C. Pacchierotti, and D. Prattichizzo, « A soft robotic supernumerary finger and a wearable cutaneous finger interface to compensate the missing grasping capabilities in chronic stroke patients », *in 2017 IEEE World Haptics Conference (WHC)*, IEEE, 2017, pp. 183–188.

[35] S. Condino, R. M. Viglialoro, S. Fani, *et al.*, « Tactile augmented reality for arteries palpation in open surgery training », *in Proc.International Conference on Medical Imaging and Augmented Reality*, 2016, pp. 186–197.

[36] X. De Tinguy, C. Pacchierotti, M. Marchal, and A. Lécuyer, « Enhancing the stiffness perception of tangible objects in mixed reality using wearable haptics », *in Proc. IEEE Conference on Virtual Reality and 3D User Interfaces (VR)*, 2018, pp. 81–90.

[37] L. Meli, C. Pacchierotti, and D. Prattichizzo, « Sensory subtraction in robot-assisted surgery: fingertip skin deformation feedback to ensure safety and improve transparency in bimanual haptic interaction. », *IEEE Transactions on Biomedical Engineering*, vol. 61, *4*, pp. 1318–1327, 2014.

[38] A. C. Abad, D. Reid, and A. Ranasinghe, « A Novel Untethered Hand Wearable with Fine-Grained Cutaneous Haptic Feedback », en, *Sensors*, vol. 22, *5*, p. 1924, Mar. 2022.

[39] C. Pacchierotti, F. Chinello, and D. Prattichizzo, « Cutaneous device for teleoperated needle insertion », *in Proc. IEEE RAS & EMBS International Conf. Biomedical Robotics and Biomechatronics*, 2012, pp. 32–37.

[40] C. Pacchierotti, M. Abayazid, S. Misra, and D. Prattichizzo, « Teleoperation of steerable flexible needles by combining kinesthetic and vibratory feedback », *IEEE Transactions on Haptics*, vol. 7, *4*, pp. 551–556, 2014.

[41] C. Pacchierotti, M. Abayazid, S. Misra, and D. Prattichizzo, « Steering of flexible needles combining kinesthetic and vibratory force feedback », *in 2014 IEEE/RSJ International Conference on Intelligent Robots and Systems*, IEEE, 2014, pp. 1202–1207.

[42] J. D. Brown, M. Ibrahim, E. D. Chase, C. Pacchierotti, and K. J. Kuchenbecker, « Data-driven comparison of four cutaneous displays for pinching palpation in robotic surgery », *in 2016 IEEE Haptics Symposium (HAPTICS)*, 2016, pp. 147–154.

[43] F. Sorgini, R. Caliò, M. C. Carrozza, and C. M. Oddo, « Haptic-assistive technologies for audition and vision sensory disabilities », *Disability and Rehabilitation: Assistive Technology*, vol. 13, *4*, pp. 394–421, 2018.

[44] L. Masia, I. Hussain, M. Xiloyannis, *et al.*, « Soft wearable assistive robotics: exosuits and supernumerary limbs », *in Wearable Exoskeleton Systems: Design, control and applications*, 2018, pp. 219–254.

[45] L. Devigne, M. Aggravi, M. Bivaud, *et al.*, « Power wheelchair navigation assistance using wearable vibrotactile haptics », *IEEE Trans. Haptics*, vol. 13, *1*, pp. 52–58, 2020.

[46] D. Prattichizzo, F. Chinello, C. Pacchierotti, and K. Minamizawa, « Remotouch: a system for remote touch experience », *in Proc. IEEE International Workshop on Robot and Human Interactive Communication*, 2010, pp. 676–679.

[47] F. Chinello, M. Aurilio, C. Pacchierotti, and D. Prattichizzo, « The hapband: a cutaneous device for remote tactile interaction », *in Haptics: Neuroscience, Devices, Modeling, and Applications: 9th International Conference, EuroHaptics 2014, Versailles, France, June 24-26, 2014, Proceedings, Part I 9*, Springer, 2014, pp. 284–291.

[48] C. Pacchierotti, D. Prattichizzo, and K. J. Kuchenbecker, « A data-driven approach to remote tactile interaction: from a biotac sensor to any fingertip cutaneous device », *in Haptics: Neuroscience, Devices, Modeling, and Applications: 9th International Conference, EuroHaptics 2014, Versailles, France, June 24-26, 2014, Proceedings, Part I 9*, Springer, 2014, pp. 418–424.

[49] S. Azenkot, R. E. Ladner, and J. O. Wobbrock, « Smartphone haptic feedback for nonvisual wayfinding », *in The proceedings of the 13th international ACM SIGACCESS conference on Computers and accessibility*, 2011, pp. 281–282.

[50] M. Prasad, P. Taele, D. Goldberg, and T. A. Hammond, « HaptiMoto: turn-by-turn haptic route guidance interface for motorcyclists », en, *in Proc. SIGCHI Conference on Human Factors in Computing Systems*, 2014, pp. 3597–3606.

[51] Y. Mo, A. Song, and H. Qin, « A Lightweight Accessible Wearable Robotic Interface for Bimanual Haptic Manipulations », *IEEE Trans. Haptics*, pp. 1–1, 2021, Conference Name: IEEE Trans. Haptics.

[52] F. Abi-Farraj, C. Pacchierotti, O. Arenz, G. Neumann, and P. R. Giordano, « A haptic shared-control architecture for guided multi-target robotic grasping », *IEEE Transactions on Haptics*, 2019.

[53] F. Chinello, C. Pacchierotti, N. G. Tsagarakis, and D. Prattichizzo, « Design of a wearable skin stretch cutaneous device for the upper limb », *in 2016 IEEE Haptics Symposium (HAPTICS)*, IEEE, 2016, pp. 14–20.

[54] F. Abi-Farraj, C. Pacchierotti, and P. R. Giordano, « User evaluation of a haptic-enabled shared-control approach for robotic telemanipulation », *in Proc. IEEE/RSJ International Conf. Intelligent Robots and Systems*, 2018, pp. 1–9.

[55] M. Selvaggio, F. Abi-Farraj, C. Pacchierotti, P. R. Giordano, and B. Siciliano, « Haptic-based shared-control methods for a dual-arm system », *IEEE Robotics and Automation Letters*, vol. 3, *4*, pp. 4249–4256, 2018.

[56] R. Rahal, F. Abi-Farraj, P. Robuffo Giordano, and C. Pacchierotti, « Haptic shared-control methods for robotic cutting under nonholonomic constraints », *in Submitted to Robotics & Automation Letters*, 2019.

[57] R. Rahal, G. Matarese, M. Gabiccini, *et al.*, « Caring about the human operator: haptic shared control for enhanced user comfort in robotic telemanipulation », *IEEE Trans. haptics*, vol. 13, *1*, pp. 197–203, 2020.

[58] M. Abayazid, C. Pacchierotti, P. Moreira, R. Alterovitz, D. Prattichizzo, and S. Misra, « Experimental evaluation of co-manipulated ultrasound-guided flexible needle steering », *The International Journal of Medical Robotics and Computer Assisted Surgery*, vol. 12, *2*, pp. 219–230, 2016.

[59] A. R. Peon, C. Pacchierotti, and D. Prattichizzo, « Vibrotactile stimuli for augmented haptic feedback in robot-assisted surgery », *in Proc. World Haptics Conference (WHC)*, 2013, pp. 473–478.

[60] P. Preechayasomboon, A. Israr, and M. Samad, « Chasm: A Screw Based Expressive Compact Haptic Actuator », en, *in Proc. CHI Conference on Human Factors in Computing Systems*, 2020, p. 13.

[61] Y. Zhao, C. L. Bennett, H. Benko, *et al.*, « Enabling People with Visual Impairments to Navigate Virtual Reality with a Haptic and Auditory Cane Simulation », en, *in Proc. CHI Conference on Human Factors in Computing Systems*, 2018, pp. 1–14.

[62] I. Birznieks, P. Jenmalm, A. W. Goodwin, and R. S. Johansson, « Encoding of direction of fingertip forces by human tactile afferents », *The Journal of Neuroscience*, vol. 21, *20*, pp. 8222–8237, 2001.

[63] K. O. Johnson, « The roles and functions of cutaneous mechanoreceptors », *Current opinion in neurobiology*, vol. 11, *4*, pp. 455–461, 2001.

[64] H. Yousef, M. Boukallel, and K. Althoefer, « Tactile sensing for dexterous in-hand manipulation in robotics—a review », *Sensors and Actuators A: physical*, vol. 167, *2*, pp. 171–187, 2011.

[65] S. M. Lephart, D. M. Pincivero, J. L. Giraido, and F. H. Fu, « The role of proprioception in the management and rehabilitation of athletic injuries », *The American journal of sports medicine*, vol. 25, *1*, pp. 130–137, 1997.

[66] E. Kim and O. Schneider, « Defining Haptic Experience: Foundations for Understanding, Communicating, and Evaluating HX », en, *in Proc. CHI Conference on Human Factors in Computing Systems*, 2020, pp. 1–13, ISBN: 978-1-4503-6708-0.

[67] A. Talvas, M. Marchal, and A. Lecuyer, « A Survey on Bimanual Haptic Interaction », *IEEE Trans. Haptics*, vol. 7, *3*, pp. 285–300, 2014.

[68] D. Wang, Y. Guo, S. Liu, Y. Zhang, W. Xu, and J. Xiao, « Haptic display for virtual reality: progress and challenges », en, *Virtual Reality & Intelligent Hardware*, vol. 1, *2*, pp. 136–162, 2019.

[69] V. R. Mercado, M. Marchal, and A. Lecuyer, « "Haptics On-Demand": A Survey on Encountered-Type Haptic Displays », *IEEE Trans. Haptics*, vol. 14, *3*, pp. 449–464, 2021.

[70] I. Rakkolainen, E. Freeman, A. Sand, R. Raisamo, and S. Brewster, « A Survey of Mid-Air Ultrasound Haptics and Its Applications », *IEEE Trans. Haptics*, vol. 14, *1*, pp. 2–19, 2020.

[71] K. Rangarajan, H. Davis, and P. H. Pucher, « Systematic Review of Virtual Haptics in Surgical Simulation: A Valid Educational Tool? », en, *Journal of Surgical Education*, vol. 77, *2*, pp. 337–347, 2020.

[72] D. Escobar-Castillejos, J. Noguez, L. Neri, A. Magana, and B. Benes, « A Review of Simulators with Haptic Devices for Medical Training », *Journal of Medical Systems*, vol. 40, *4*, pp. 1–22, 2016.

[73] T. R. Coles, D. Meglan, and N. W. John, « The Role of Haptics in Medical Training Simulators: A Survey of the State of the Art », *IEEE Trans. Haptics*, vol. 4, *1*, pp. 51–66, 2011.

[74] C. Bermejo and P. Hui, « A survey on haptic technologies for mobile augmented reality », *arXiv:1709.00698 [cs]*, Sep. 2017, arXiv: 1709.00698.

[75] D. Wang, K. Ohnishi, and W. Xu, « Multimodal Haptic Display for Virtual Reality: A Survey », *IEEE Trans. Industrial Electronics*, vol. 67, *1*, pp. 610–623, Jan. 2020.

[76] E. Bouzbib, G. Bailly, S. Haliyo, and P. Frey, « "Can I Touch This?": Survey of Virtual Reality Interactions via Haptic Solutions », *in Proc. Conférence Francophone sur l'Interaction Homme-Machine*, 2021.

[77] P. Galambos, « Vibrotactile Feedback for Haptics and Telemanipulation: Survey, Concept and Experiment », en, *Acta Polytechnica Hungarica*, vol. 9, *1*, p. 25, 2012.

[78] P. Xia, « Haptics for Product Design and Manufacturing Simulation », *IEEE Trans. Haptics*, vol. 9, *3*, pp. 358–375, 2016.

[79] Varalakshmi, Thriveni, Venugopal, and Patnaik, « Haptics: State of the Art Survey », *IJCSI International Journal of Computer Science Issues*, vol. 9, *3*, pp. 234–244, 5 2012.

[80] M. E. Berglund, J. Duvall, and L. E. Dunne, « A survey of the historical scope and current trends of wearable technology applications », *in Proc. ACM International Symposium on Wearable Computers*, 2016, pp. 40–43.

[81] S. Seneviratne, Y. Hu, T. Nguyen, *et al.*, « A Survey of Wearable Devices and Challenges », *IEEE Communications Surveys Tutorials*, vol. 19, *4*, pp. 2573–2620, 2017.

[82] Y. Chen, Y. Yang, M. Li, *et al.*, « Wearable Actuators: An Overview », *Textiles*, vol. 1, *2*, pp. 283–321, 2021.

[83] A. Ometov, V. Shubina, L. Klus, *et al.*, « A Survey on Wearable Technology: History, State-of-the-Art and Current Challenges », *Computer Networks*, vol. 193, p. 108 074, 2021.

[84] T. Luczak, R. Burch, E. Lewis, H. Chander, and J. Ball, « State-of-the-art review of athletic wearable technology: What 113 strength and conditioning coaches and athletic trainers from the USA said about technology in sports », *International Journal of Sports Science & Coaching*, vol. 15, *1*, pp. 26–40, 2020.

[85] A. Pantelopoulos and N. Bourbakis, « A survey on wearable biosensor systems for health monitoring », *in Proc. International Conference of the IEEE Engineering in Medicine and Biology Society*, 2008, pp. 4887–4890.

[86] S. F. Memon, M. Memon, and S. Bhatti, « Wearable technology for infant health monitoring: a survey », *IET Circuits, Devices & Systems*, vol. 14, *2*, pp. 115–129, 2020.

[87] P. B. Shull and D. D. Damian, « Haptic wearables as sensory replacement, sensory augmentation and trainer – a review », *Journal of NeuroEngineering and Rehabilitation*, vol. 12, *1*, p. 59, 2015.

[88] Q. Wang, P. Markopoulos, B. Yu, W. Chen, and A. Timmermans, « Interactive wearable systems for upper body rehabilitation: a systematic review », *Journal of NeuroEngineering and Rehabilitation*, vol. 14, *1*, p. 20, 2017.

[89] C. Fang, Y. Zhang, M. Dworman, and C. Harrison, « Wireality: Enabling Complex Tangible Geometries in Virtual Reality with Worn Multi-String Haptics », en, p. 10, 2020.

[90] J. Perret and E. V. Poorten, « Touching Virtual Reality: a Review of Haptic Gloves », en, *in Proc. International Conference on New Actuators*, 2018, p. 6.

[91] R. L. Koslover, B. T. Gleeson, J. T. De Bever, and W. R. Provancher, « Mobile navigation using haptic, audio, and visual direction cues with a handheld test platform », *IEEE Trans. Haptics*, vol. 5, *1*, pp. 33–38, 2011.

[92] A. F. Siu, M. Sinclair, R. Kovacs, E. Ofek, C. Holz, and E. Cutrell, « Virtual reality without vision: a haptic and auditory white cane to navigate complex virtual worlds », *in Proceedings of the 2020 CHI Conference on Human Factors in Computing Systems*, 2020, pp. 1–13.

[93] H. Kawaguchi and T. Nojima, « Stravigation: a vibrotactile mobile navigation for exploration-like sightseeing », *in Advances in Computer Entertainment: 9th International Conference, ACE 2012, Kathmandu, Nepal, November 3-5, 2012. Proceedings 9*, Springer, 2012, pp. 517–520.

[94] D. K. Chen, J.-B. Chossat, and P. B. Shull, « Haptivec: presenting haptic feedback vectors in handheld controllers using embedded tactile pin arrays », *in Proceedings of the 2019 CHI Conference on Human Factors in Computing Systems*, 2019, pp. 1–11.

[95] A. J. Spiers, J. van der Linden, S. Wiseman, and M. Oshodi, « Testing a shape-changing haptic navigation device with vision-impaired and sighted audiences in an immersive theater setting », *IEEE Trans. Human-Machine Systems*, vol. 48, *6*, pp. 614–625, 2018.

[96] A. J. Spiers, J. van Der Linden, M. Oshodi, and A. M. Dollar, « Development and experimental validation of a minimalistic shape-changing haptic navigation device », *in 2016 IEEE International Conference on Robotics and Automation*, IEEE, 2016, pp. 2688–2695.

[97] A. J. Spiers and A. M. Dollar, « Outdoor pedestrian navigation assistance with a shape-changing haptic interface and comparison with a vibrotactile device », *in 2016 IEEE Haptics Symposium (HAPTICS)*, IEEE, 2016, pp. 34–40.

[98] S. Rümelin, E. Rukzio, and R. Hardy, « Naviradar: a novel tactile information display for pedestrian navigation », *in Proceedings of the 24th annual ACM symposium on User interface software and technology*, 2011, pp. 293–302.

[99] T. Sokoler, L. Nelson, and E. R. Pedersen, « Low-resolution supplementary tactile cues for navigational assistance », *in Human Computer Interaction with Mobile Devices: 4th International Symposium, Mobile HCI 2002 Pisa, Italy, September 18–20, 2002 Proceedings*, Springer, 2002, pp. 369–372.

[100] A. Nasser, K.-N. Keng, and K. Zhu, « Thermalcane: exploring thermotactile directional cues on cane-grip for non-visual navigation », *in Proceedings of the 22nd international ACM SIGACCESS conference on computers and accessibility*, 2020, pp. 1–12.

[101] T. Amemiya and H. Sugiyama, « Orienting kinesthetically: a haptic handheld wayfinder for people with visual impairments », *ACM Transactions on Accessible Computing (TACCESS)*, vol. 3, *2*, pp. 1–23, 2010.

[102] J.-P. Choiniere and C. Gosselin, « Development and experimental validation of a haptic compass based on asymmetric torque stimuli », *IEEE transactions on haptics*, vol. 10, *1*, pp. 29–39, 2016.

[103] T. Amemiya and H. Sugiyama, « Navigation in eight cardinal directions with pseudo-attraction force for the visually impaired », *in 2009 IEEE International Conference on Systems, Man and Cybernetics*, IEEE, 2009, pp. 27–32.

[104] M. Pielot, B. Poppinga, W. Heuten, and S. Boll, « Pocketnavigator: studying tactile navigation systems in-situ », *in Proceedings of the SIGCHI Conference on Human Factors in Computing Systems*, 2012, pp. 3131–3140.

[105] D. Montello, « Spatial cognition », *in International Encyclopedia of the Social & Behavioral Sciences*, N. J. Smelser and P. B. Baltes, Eds., Oxford: Pergamon, 2001, pp. 14 771–14 775.

[106] J. J. LaViola, E. Kruijff, R. P. McMahan, D. A. Bowman, and I. Poupyrev, *3D user interfaces: theory and practice* (Addison-Wesley usability and HCI series). 2017.

[107] A. S. Devlin, « 41 Environmental Perception: Wayfinding and Spatial Cognition », *in The Oxford Handbook of Environmental and Conservation Psychology*, Oxford University Press, Sep. 2012.

[108] J. M. Wiener, S. J. Büchner, and C. Hölscher, « Taxonomy of human wayfinding tasks: a knowledge-based approach », *Spatial Cognition and Computation*, vol. 9, *2*, pp. 152–165, 2009.

[109] A. W. Siegel and S. H. White, « The development of spatial representations of large-scale environments », *in* ser. Advances in Child Development and Behavior, H. W. Reese, Ed., vol. 10, JAI, 1975, pp. 9–55.

[110] H. Gacem, G. Bailly, J. Eagan, and E. Lecolinet, « A design space of guidance techniques for large and dense physical environments », *in Proc. Conference on l'Interaction Homme-Machine*, G. Casiez, T. Pietrzak, O. Chapuis, and S. Conversy, Eds., 2014, pp. 9–17.

[111] S. Paneels, M. Anastassova, S. Strachan, S. P. Van, S. Sivacoumarane, and C. Bolzmacher, « What's around me? multi-actuator haptic feedback on the wrist », *in 2013 World Haptics Conference (WHC)*, IEEE, 2013, pp. 407–412.

[112] J. Hong, A. Pradhan, J. E. Froehlich, and L. Findlater, « Evaluating Wrist-Based Haptic Feedback for Non-Visual Target Finding and Path Tracing on a 2D Surface », *in Proc. International ACM SIGACCESS Conference on Computers and Accessibility*, Baltimore Maryland USA, 2017, pp. 210–219.

[113] P. Kapur, M. Jensen, L. J. Buxbaum, S. A. Jax, and K. J. Kuchenbecker, « Spatially distributed tactile feedback for kinesthetic motion guidance », *in 2010 IEEE Haptics Symposium*, 2010, pp. 519–526.

[114] C. Pacchierotti, G. Salvietti, I. Hussain, L. Meli, and D. Prattichizzo, « The hring: a wearable haptic device to avoid occlusions in hand tracking », *in 2016 IEEE Haptics Symposium (HAPTICS)*, 2016, pp. 134–139.

[115] S. Razzaque, *Redirected walking*. The University of North Carolina at Chapel Hill, 2005.

[116] A. Khan, A. Khan, and M. Waleed, « Wearable navigation assistance system for the blind and visually impaired », *in 2018 International Conference on Innovation and Intelligence for Informatics, Computing, and Technologies (3ICT)*, IEEE, 2018, pp. 1–6.

[117] N. A.-h. Hamdan, A. Wagner, S. Voelker, J. Steimle, and J. Borchers, « Springlets: Expressive, Flexible and Silent On-Skin Tactile Interfaces », en, *in Proc. CHI Conference on Human Factors in Computing Systems*, 2019, pp. 1–14.

[118] L. Devigne, M. Aggravi, M. Bivaud, *et al.*, « Power Wheelchair Navigation Assistance Using Wearable Vibrotactile Haptics », *IEEE Trans. Haptics*, vol. 13, *1*, pp. 52–58, 2020.

[119] H. Kajimoto, Y. Kanno, and S. Tachi, « Forehead electro-tactile display for vision substitution », *in Proc. EuroHaptics*, 2006.

[120] S. Günther, F. Müller, M. Funk, J. Kirchner, N. Dezfuli, and M. Mühlhäuser, « Tactileglove: assistive spatial guidance in 3d space through vibrotactile navigation », *in Proceedings of the 11th PErvasive Technologies Related to Assistive Environments Conference*, 2018, pp. 273–280.

[121] G. Mori, C. Santoro, and F. Paternò, « Understanding indoor orientation through wearable vibrotactile feedback », *in Proceedings of the 18th International Conference on Mobile and Ubiquitous Multimedia*, 2019, pp. 1–5.

[122] G. D. Schott, « Penfield's homunculus: a note on cerebral cartography. », *Journal of Neurology, Neurosurgery, and Psychiatry*, vol. 56, *4*, pp. 329–333, 1993.

[123] V. Vechev, J. Zarate, D. Lindlbauer, R. Hinchet, H. Shea, and O. Hilliges, « Tactiles: dual-mode low-power electromagnetic actuators for rendering continuous contact and spatial haptic patterns in vr », *in 2019 IEEE Conference on Virtual Reality and 3D User Interfaces (VR)*, IEEE, 2019, pp. 312–320.

[124] N. Dunkelberger, J. L. Sullivan, J. Bradley, *et al.*, « A multi-sensory approach to present phonemes as language through a wearable haptic device », *IEEE Transactions on Haptics*, 2020.

[125] R. M. Khurshid, N. Fitter, E. Fedalei, and K. Kuchenbecker, « Effects of grip-force, contact, and acceleration feedback on a teleoperated pick-and-place task », *IEEE Transactions on Haptics*, May 2016.

[126] G. A. Gescheider, *Psychophysics: the fundamentals*. Psychology Press, 2013.

[127] K. Pickett and J. Konczak, « Measuring kinaesthetic sensitivity in typically developing children », en, *Developmental Medicine and Child Neurology*, vol. 51, *9*, pp. 711–716, 2009.

[128] S. Weinstein, « Intensive and Extensive Aspects of Tactile Sensitivity as a Function of Body Part, Sex, and Laterality », English, *in The Skin Senses*, D. Kenshalo, Ed., OCLC: 239118, 1968.

[129] K. Myles and M. S. Binseel, « The Tactile Modality: A Review of Tactile Sensitivity and Human Tactile Interfaces », en, *Technical report*, p. 27, 2007.

[130] J. M. Loomis and C. C. Collins, « Sensitivity to shifts of a point stimulus: An instance of tactile hyperacuity », *Perception & Psychophysics*, vol. 24, *6*, pp. 487–492, 1978.

[131] A. Nasser, K. Zhu, and S. Wiseman, « Thermo-haptic earable display for the hearing and visually impaired », *in The 21st International ACM SIGACCESS Conference on Computers and Accessibility*, 2019, pp. 630–632.

[132] T. Machida, N. K. Dim, and X. Ren, « Suitable body parts for vibration feedback in walking navigation systems », *in Proceedings of the Third International Symposium of Chinese CHI*, 2015, pp. 32–36.

[133] K. A. Morrow, « The neck as a potential site for vestibular tactile sensory substitution », en, *Northern Michigan University theses*, p. 59, 2016.

[134] M. Bikah, M. S. Hallbeck, and J. H. Flowers, « Supracutaneous vibrotactile perception threshold at various non-glabrous body loci », *Ergonomics*, vol. 51, *6*, pp. 920–934, 2008.

[135] S. Schaack, G. Chernyshov, K. Ragozin, B. Tag, R. Peiris, and K. Kunze, « Haptic Collar: Vibrotactile Feedback around the Neck for Guidance Applications », en, *in Proc. 10th Augmented Human International Conference 2019*, Reims France, 2019, pp. 1–4.

[136] M. Lee, S. Je, W. Lee, D. Ashbrook, and A. Bianchi, « Activearring: spatiotemporal haptic cues on the ears », *IEEE Trans. haptics*, vol. 12, *4*, pp. 554–562, 2019.

[137] M. Hoppe, D. Oskina, A. Schmidt, and T. Kosch, « Odin's Helmet: A Head-Worn Haptic Feedback Device to Simulate G-Forces on the Human Body in Virtual Reality », *Proc. ACM on Human-Computer Interaction*, vol. 5, *EICS*, pp. 1–15, 2021.

[138] J. Szczerba, R. Hersberger, and R. Mathieu, « A wearable vibrotactile display for automotive route guidance: evaluating usability, workload, performance and preference », *in Proceedings of the Human Factors and Ergonomics Society Annual Meeting*, SAGE Publications Sage CA: Los Angeles, CA, vol. 59, 2015, pp. 1027–1031.

[139] T. Nukarinen, J. Rantala, A. Farooq, and R. Raisamo, « Delivering directional haptic cues through eyeglasses and a seat », *in Proc. IEEE World Haptics Conference (WHC)*, 2015, pp. 345–350.

[140] S. Mann, J. Huang, R. Janzen, *et al.*, « Blind navigation with a wearable range camera and vibrotactile helmet », *in Proceedings of the 19th ACM international conference on Multimedia*, 2011, pp. 1325–1328.

[141] H. Kerdegari, Y. Kim, and T. J. Prescott, « Head-mounted sensory augmentation device: comparing haptic and audio modality », *in Conf. Biomimetic and Biohybrid Systems*, 2016, pp. 107–118.

[142] C. Bertram, M. H. Evans, M. Javaid, T. Stafford, and T. Prescott, « Sensory augmentation with distal touch: the tactile helmet project », *in Conf. on Biomimetic and Biohybrid Systems*, 2013, pp. 24–35.

[143] H. Tobita and T. Kuzi, « Smartwig: wig-based wearable computing device for communication and entertainment », *in Proceedings of the International Working Conference on Advanced Visual Interfaces*, 2012, pp. 299–302.

[144] M. P. Woźniak, J. Dominiak, K. Grudzień, *et al.*, « Gapeau: Enhancing the Sense of Distance to Others with a Head-Mounted Sensor », *in Sixteenth International Conference on Tangible, Embedded, and Embodied Interaction*, Daejeon Republic of Korea, 2022, pp. 1–19.

[145] O. B. Kaul and M. Rohs, « Haptichead: a spherical vibrotactile grid around the head for 3d guidance in virtual and augmented reality », *in Proceedings of the 2017 CHI Conference on Human Factors in Computing Systems*, 2017, pp. 3729–3740.

[146] O. B. Kaul and M. Rohs, « Haptichead: 3d guidance and target acquisition through a vibrotactile grid », *in Proceedings of the 2016 CHI Conference Extended Abstracts on Human Factors in Computing Systems*, 2016, pp. 2533–2539.

[147] O. Spakov, J. Rantala, and P. Isokoski, « Sequential and simultaneous tactile stimulation with multiple actuators on head, neck and back for gaze cuing », *in IEEE World Haptics Conference*, 2015, pp. 333–338.

[148] V. A. de Jesus Oliveira, L. Brayda, L. Nedel, and A. Maciel, « Experiencing guidance in 3d spaces with a vibrotactile head-mounted display », *in Proc. IEEE Virtual Reality (VR)*, 2017, pp. 453–454.

[149] B. Dunbar, J. Hynes-Bruell, E. Shi, *et al.*, « Augmenting human spatial navigation via sensory substitution », *in 2017 IEEE MIT Undergraduate Research Technology Conference (URTC)*, IEEE, 2017, pp. 1–4.

[150] M. Luo, Z. Wang, H. Zhang, *et al.*, « High-density thermal sensitivity maps of the human body », *Building and Environment*, vol. 167, p. 106 435, 2020.

[151] H. Tang and D. J. Beebe, « An oral tactile interface for blind navigation », *IEEE Trans. Neural Systems and Rehabilitation Engineering*, vol. 14, *1*, pp. 116–123, 2006.

[152] V. Buchmann, M. Billinghurst, and A. Cockburn, « Directional interfaces for wearable augmented reality », *in Proceedings of the 9th ACM SIGCHI New Zealand Chapter's International Conference on Human-Computer Interaction: Design Centered HCI*, 2008, pp. 47–54.

[153] E. Piateski and L. Jones, « Vibrotactile pattern recognition on the arm and torso », *in First Joint Eurohaptics Conference and Symposium on Haptic Interfaces for Virtual Environment and Teleoperator Systems. World Haptics Conference*, IEEE, 2005, pp. 90–95.

[154] U. Norrsell and H. Olausson, « Human, tactile, directional sensibility and its peripheral origins », *Acta Physiologica Scandinavica*, vol. 144, *2*, pp. 155–161, 1992.

[155] S. Das and Y. Kurita, « Providing navigation assistance through forcehand: a wearable force-feedback glove », *in 2019 IEEE Global Conference on Signal and Information Processing (GlobalSIP)*, IEEE, 2019, pp. 1–5.

[156] H.-R. Tsai, Y.-C. Chang, T.-Y. Wei, *et al.*, « Guideband: intuitive 3d multilevel force guidance on a wristband in virtual reality », *in Proceedings of the 2021 CHI Conference on Human Factors in Computing Systems*, 2021, pp. 1–13.

[157] N. Henze, W. Heuten, and S. Boll, « Non-intrusive somatosensory navigation support for blind pedestrians », *in Proc. of Eurohaptics*, vol. 2006, 2006.

[158] L. Jones, « Kinesthetic Sensing », *Human and Machine Haptics*, 2000.

[159] G. O. Gibson and J. C. Craig, « Tactile spatial sensitivity and anisotropy », *Perception & Psychophysics*, vol. 67, *6*, pp. 1061–1079, 2005.

[160] P. Lopes, A. Ion, and P. Baudisch, « Impacto: Simulating Physical Impact by Combining Tactile Stimulation with Electrical Muscle Stimulation », *in Proc. UIST ACM Symposium on User Interface Software & Technology*, Daegu, Kyungpook, Republic of Korea, 2015, pp. 11–19.

[161] Z. Bauer, A. Dominguez, E. Cruz, F. Gomez-Donoso, S. Orts-Escolano, and M. Cazorla, « Enhancing perception for the visually impaired with deep learning techniques and low-cost wearable sensors », *Pattern Recognition Letters*, 2019.

[162] D. Croce, P. Gallo, D. Garlisi, L. Giarré, S. Mangione, and I. Tinnirello, « Arianna: a smartphone-based navigation system with human in the loop », *in 22nd Mediterranean Conference on Control and Automation*, IEEE, 2014, pp. 8–13.

[163] R. C. Me, G. Andreoni, A. Biamonti, and M. R. M. Saad, « Wearable haptic-feedback navigational assistance for people with dementia: preliminary assessment », *Technology and Disability*, vol. 29, *1-2*, pp. 35–46, 2017.

[164] C. Rosalam, B. Alessandro, A. Giuseppe, R. Antonio, and M. M. Rashid, « Haptic modality for assistive navigation system of elderly with alzheimer's disease »,

[165] F. E. Brown, J. Sutton, H. M. Yuen, *et al.*, « A novel, wearable, electronic visual aid to assist those with reduced peripheral vision », *Plos one*, vol. 14, *10*, e0223755, 2019.

[166] E. Demircan, « A pilot study on locomotion training via biomechanical models and a wearable haptic feedback system », *ROBOMECH Journal*, vol. 7, pp. 1–13, 2020.

[167] S. Stock, A. Bertemes, M. Stang, M. Sommer, D. Grimm, and W. Stork, « FEEDI - A Smart Wearable Foot-Band for Navigation and Guidance Using Haptic Feedback », *in Proc. International Conference on Human Interaction and Emerging Technologies: Future Applications*, 2020, pp. 349–355.

[168] M. Schirmer, J. Hartmann, S. Bertel, and F. Echtler, « Shoe me the way: a shoe-based tactile interface for eyes-free urban navigation », *in Proceedings of the 17th International Conference on Human-Computer Interaction with Mobile Devices and Services*, 2015, pp. 327–336.

[169] Q. Xu, T. Gan, S. C. Chia, L. Li, J.-H. Lim, and P. K. Kyaw, « Design and evaluation of vibrating footwear for navigation assistance to visually impaired people », *in Proc. IEEE Int. Conf. on Internet of Things (iThings) and IEEE Green Computing and Communications (GreenCom) and IEEE Cyber, Physical and Social Computing (CPSCom) and IEEE Smart Data (SmartData)*, IEEE, 2016, pp. 305–310.

[170] A. Meier, D. J. Matthies, B. Urban, and R. Wettach, « Exploring vibrotactile feedback on the body and foot for the purpose of pedestrian navigation », *in Proceedings of the 2nd international Workshop on Sensor-based Activity Recognition and Interaction*, 2015, pp. 1–11.

[171] R. Velãzquez, O. Bazán, and M. Magaña, « A shoe-integrated tactile display for directional navigation », *in 2009 IEEE/RSJ International Conference on Intelligent Robots and Systems*, IEEE, 2009, pp. 1235–1240.

[172] A. Wilska, « On the Vibrational Sensitivity in Different Regions of the Body Surface », en, *Acta Physiologica Scandinavica*, vol. 31, *2-3*, pp. 285–289, 1954.

[173] E. H. Weber and H. E. Ross, *The sense of touch*. Academic Press for [the] Experimental Psychology Society, 1978.

[174] E. H. Skorina, M. Luo, and C. D. Onal, « A soft robotic wearable wrist device for kinesthetic haptic feedback », *Frontiers in Robotics and AI*, vol. 5, p. 83, 2018.

[175] E. Knoop and J. Rossiter, « The tickler: a compliant wearable tactile display for stroking and tickling », *in Proceedings of the 33rd Annual ACM Conference Extended Abstracts on Human Factors in Computing Systems*, 2015, pp. 1133–1138.

[176] M. Aggravi, G. Salvietti, and D. Prattichizzo, « Haptic wrist guidance using vibrations for human-robot teams », *in 2016 25th IEEE International Symposium on Robot and Human Interactive Communication (RO-MAN)*, 2016, pp. 113–118.

[177] B. B. Edin and N. Johansson, « Skin strain patterns provide kinaesthetic information to the human central nervous system », *Journal of Physiology*, vol. 487, pp. 243–251, 1995.

[178] D. F. Collins, K. M. Refshauge, G. Todd, and S. C. Gandevia, « Cutaneous receptors contribute to kinesthesia at the index finger, elbow, and knee », *Journal of Neurophysiology*, vol. 94, *3*, pp. 1699–1706, 2005.

[179] K. Shikata, Y. Makino, and H. Shinoda, « Inducing elbow joint flexion by shear deformation of arm skin », *in Proc. World Haptics Conference*, 2015.

[180] E. López-Larraz, A. Sarasola-Sanz, N. Irastorza-Landa, N. Birbaumer, and A. Ramos-Murguialday, « Brain-machine interfaces for rehabilitation in stroke: A review », en, *NeuroRehabilitation*, vol. 43, *1*, pp. 77–97, 2018.

[181] J. Auda, M. Pascher, and S. Schneegass, « Around the (Virtual) World: Infinite Walking in Virtual Reality Using Electrical Muscle Stimulation », *in Proc. CHI Conference on Human Factors in Computing Systems*, ACM Press, 2019, pp. 1–8.

[182] M. Pfeiffer, T. Dünte, S. Schneegass, F. Alt, and M. Rohs, « Cruise Control for Pedestrians: Controlling Walking Direction using Electrical Muscle Stimulation », en, *in Proc. ACM Conference on Human Factors in Computing Systems*, Seoul Republic of Korea, 2015, pp. 2505–2514.

[183] M. Raitor, J. M. Walker, A. M. Okamura, and H. Culbertson, « WRAP: Wearable, restricted-aperture pneumatics for haptic guidance », *in Proc. IEEE International Conference on Robotics and Automation (ICRA)*, 2017, pp. 427–432.

[184] K. Aqeel, U. Naveed, F. Fatima, *et al.*, « Skin stroking haptic feedback glove for assisting blinds in navigation », *in Proc. IEEE International Conference on Robotics and Biomimetics (ROBIO)*, 2017, pp. 177–182.

[185] K. Bark, J. Wheeler, P. Shull, J. Savall, and M. Cutkosky, « Rotational skin stretch feedback: a wearable haptic display for motion », *IEEE Trans. Haptics*, vol. 3, *3*, pp. 166–176, 2010.

[186] A. A. Stanley and K. J. Kuchenbecker, « Evaluation of tactile feedback methods for wrist rotation guidance », *IEEE Trans. Haptics*, vol. 5, *3*, pp. 240–251, 2012.

[187] O. Kayhan and E. Samur, « A wearable haptic guidance system based on skin stretch around the waist for visually-impaired runners », *in Proc. IEEE Haptics Symposium*, 2022, pp. 1–6.

[188] E. Pezent, S. Fani, J. Clark, M. Bianchi, and M. K. O'Malley, « Spatially separating haptic guidance from task dynamics through wearable devices », *IEEE Transactions on Haptics*, 2019.

[189] B. T. Gleeson, S. K. Horschel, and W. R. Provancher, « Design of a fingertip-mounted tactile display with tangential skin displacement feedback », *IEEE Trans. Haptics*, vol. 3, *4*, pp. 297–301, 2010.

[190] Y. S. Jin, H. Y. Chun, E. T. Kim, and S. Kang, « VT-ware: A wearable tactile device for upper extremity motion guidance », *in Proc. IEEE International Symposium on Robot and Human Interactive Communication*, 2014, pp. 335–340.

[191] J. R. Alayon, V. G. D. Corciega, N. M. L. Genebago, A. B. A. Hernandez, C. R. C. Labitoria, and R. E. Tolentino, « Design of wearable wrist haptic device for blind navigation using microsoft kinect for xbox 360 », *in 2020 4th International Conference on Trends in Electronics and Informatics (ICOEI)(48184)*, IEEE, 2020, pp. 1005–1010.

[192] J. H. Kirman, « Tactile apparent movement: the effects of interstimulus onset interval and stimulus duration », *Perception & Psychophysics*, vol. 15, *1*, pp. 1–6, 1974.

[193] M. N. Selzer, J. A. Biondi, F. Gamboa, and S. Escarza, « Braille messages in a haptic wearable device for visually impaired people »,

[194] F. A. Geldard and C. E. Sherrick, « The cutaneous" rabbit": a perceptual illusion », *Science*, vol. 178, *4057*, pp. 178–179, 1972.

[195] E. Strasnick, J. R. Cauchard, and J. A. Landay, « Brushtouch: exploring an alternative tactile method for wearable haptics », *in Proceedings of the 2017 CHI Conference on Human Factors in Computing Systems*, 2017, pp. 3120–3125.

[196] R. L. Peiris, W. Peng, Z. Chen, L. Chan, and K. Minamizawa, « Thermovr: exploring integrated thermal haptic feedback with head mounted displays », *in Proceedings of the 2017 CHI Conference on Human Factors in Computing Systems*, 2017, pp. 5452–5456.

[197] J. Tewell, J. Bird, and G. R. Buchanan, « Heat-nav: using temperature changes as navigation cues », *in Proc. CHI Conf. on Human Factors in Computing Systems*, 2017, pp. 1131–1135.

[198] R. L. Peiris, W. Peng, Z. Chen, and K. Minamizawa, « Exploration of cuing methods for localization of spatial cues using thermal haptic feedback on the forehead », *in Proc. IEEE World Haptics Conference (WHC)*, 2017, pp. 400–405.

[199] R. L. Peiris, Y.-L. Feng, L. Chan, and K. Minamizawa, « Thermalbracelet: exploring thermal haptic feedback around the wrist », *in Proceedings of the 2019 CHI Conference on Human Factors in Computing Systems*, 2019, pp. 1–11.

[200] T. Narumi, A. Tomohiro, Y. A. Seong, and M. Hirose, « Characterizing the space by thermal feedback through a wearable device », *in International Conference on Virtual and Mixed Reality*, Springer, 2009, pp. 355–364.

[201] D. S. Pamungkas and W. Caesarendra, « Overview Electrotactile Feedback for Enhancing Human Computer Interface », *Journal of Physics: Conference Series*, vol. 1007, p. 012 001, 2018.

[202] S. Meers and K. Ward, « A substitute vision system for providing 3D perception and GPS navigation via electro-tactile stimulation », *in Proc. International Conference on Sensing Technology*, 2005, p. 8.

[203] H. Tang and D. Beebe, « An oral tactile interface for two-way communication », *in 1st Annual International IEEE-EMBS Special Topic Conference on Microtechnologies in Medicine and Biology. Proceedings (Cat. No. 00EX451)*, IEEE, 2000, pp. 639–643.

[204] J. B. Van Erp, « Guidelines for the use of vibro-tactile displays in human computer interaction », *in Proc. Eurohaptics*, vol. 2002, 2002, pp. 18–22.

[205] A. Bloomfield and N. I. Badler, « Collision awareness using vibrotactile arrays », *in 2007 IEEE Virtual Reality Conference*, IEEE, 2007, pp. 163–170.

[206] A. Cassinelli, C. Reynolds, and M. Ishikawa, « Augmenting spatial awareness with haptic radar », *in Proc. IEEE International Symposium on Wearable Computers*, 2006, pp. 61–64.

[207] H.-C. Wang, R. K. Katzschmann, S. Teng, B. Araki, L. Giarré, and D. Rus, « Enabling independent navigation for visually impaired people through a wearable vision-based feedback system », *in Proc. IEEE Int. Conf. on robotics and automation*, IEEE, 2017, pp. 6533–6540.

[208] H. Culbertson, J. M. Walker, M. Raitor, and A. M. Okamura, « Waves: a wearable asymmetric vibration excitation system for presenting three-dimensional translation and rotation cues », *in Proc. CHI Conf. on Human Factors in Computing Systems*, 2017, pp. 4972–4982.

[209] F. Sorgini, A. Mazzoni, L. Massari, *et al.*, « Encapsulation of Piezoelectric Transducers for Sensory Augmentation and Substitution with Wearable Haptic Devices », *Micromachines*, vol. 8, *9*, p. 270, 2017.

[210] I. M. Koo, K. Jung, J. C. Koo, J.-D. Nam, Y. K. Lee, and H. R. Choi, « Development of Soft-Actuator-Based Wearable Tactile Display », *IEEE Trans. Robotics*, vol. 24, *3*, pp. 549–558, 2008.

[211] N. K. Dim and X. Ren, « Investigation of suitable body parts for wearable vibration feedback in walking navigation », *International Journal of Human-Computer Studies*, vol. 97, pp. 34–44, 2017.

[212] P. Kourtesis, F. Argelaguet, S. Vizcay, M. Marchal, and C. Pacchierotti, « Electrotactile feedback for hand interactions: a systematic review, meta-analysis, and future directions », *arXiv preprint arXiv:2105.05343*, 2021.

[213] S. Bosman, B. Groenendaal, J.-W. Findlater, T. Visser, M. de Graaf, and P. Markopoulos, « Gentleguide: an exploration of haptic output for indoors pedestrian guidance », *in International Conference on Mobile Human-Computer Interaction*, Springer, 2003, pp. 358–362.

[214] O. B. Kaul, M. Rohs, B. Simon, K. C. Demir, and K. Ferry, « Vibrotactile funneling illusion and localization performance on the head », *in Proc. 2020 CHI Conference on Human Factors in Computing Systems*. 2020, pp. 1–13.

[215] J. R. Marston, J. M. Loomis, R. L. Klatzky, and R. G. Golledge, « Nonvisual route following with guidance from a simple haptic or auditory display », *Journal of Visual Impairment & Blindness*, vol. 101, *4*, pp. 203–211, 2007.

[216] F. Kiss, R. Boldt, B. Pfleging, and S. Schneegass, « Navigation systems for motorcyclists: exploring wearable tactile feedback for route guidance in the real world », *in Proceedings of the 2018 CHI Conference on Human Factors in Computing Systems*, 2018, pp. 1–7.

[217] M. E. Alarcon and F. Ferrise, « Design of a wearable haptic navigation tool for cyclists », *in Int. Conf. on Innovative Design and Manufacturing*, 2017, pp. 1–6.

[218] A. Brock, S. Kammoun, M. Macé, and C. Jouffrais, « Using wrist vibrations to guide hand movement and whole body navigation », *i-com*, vol. 13, *3*, pp. 19–28, 2014.

[219] D. Bial, D. Kern, F. Alt, and A. Schmidt, « Enhancing outdoor navigation systems through vibrotactile feedback », *in CHI'11 Extended Abstracts on Human Factors in Computing Systems*, 2011, pp. 1273–1278.

[220] D. Dakopoulos and N. G. Bourbakis, « Wearable obstacle avoidance electronic travel aids for blind: a survey », *IEEE Trans. Systems, Man, and Cybernetics, Part C (Applications and Reviews)*, vol. 40, *1*, pp. 25–35, 2009.

[221] L. He, R. Wang, and X. Xu, « Pneufetch: supporting blind and visually impaired people to fetch nearby objects via light haptic cues », *in Extended Abstracts of the 2020 CHI Conference on Human Factors in Computing Systems*, 2020, pp. 1–9.

[222] G. Ghiani, B. Leporini, and F. Paternò, « Vibrotactile feedback to aid blind users of mobile guides », *Journal of Visual Languages & Computing*, vol. 20, *5*, pp. 305–317, 2009.

[223] A. Gibson, A. Webb, and L. Stirling, « Analysis of a wearable, multi-modal information presentation device for obstacle avoidance », *in 2017 IEEE Aerospace Conference*, IEEE, 2017, pp. 1–9.

[224] B. T. Gleeson, S. K. Horschel, and W. R. Provancher, « Perception of Direction for Applied Tangential Skin Displacement: Effects of Speed, Displacement, and Repetition », *IEEE Trans. Haptics*, vol. 3, *3*, pp. 177–188, 2010.

[225] S. Bhatlawande, M. Mahadevappa, and J. Mukhopadhyay, « Way-finding electronic bracelet for visually impaired people », *in 2013 IEEE Point-of-Care Healthcare Technologies (PHT)*, IEEE, 2013, pp. 260–263.

[226] A. Brock, S. Kammoun, M. Macé, and C. Jouffrais, « Using wrist vibrations to guide hand movement and whole body navigation », *I-com*, vol. 13, *3*, pp. 19–28, 2014.

[227] A. Montuwy, A. Dommes, and B. Cahour, « What Sensory Pedestrian Navigation Aids For The Future?: A Survey Study », *in Proc. CHI Extended Abstracts Conference on Human Factors in Computing Systems*, 2018, pp. 1–6.

[228] H. Profita, R. Albaghli, L. Findlater, P. Jaeger, and S. K. Kane, « The AT Effect: How Disability Affects the Perceived Social Acceptability of Head-Mounted Display Use », *in Proc. 2016 CHI Conference on Human Factors in Computing Systems*, 2016, pp. 4884–4895.

[229] O. Gustafson-Pearce, E. Billett, and F. Cecelja, « Tugs–the tactile user guidance system », 2005.

[230] K. Finstad, « The Usability Metric for User Experience », *Interacting with Computers*, vol. 22, *5*, pp. 323–327, 2010.

[231] E. Bouzbib and G. Bailly, « "Let's Meet and Work it Out": Understanding and Mitigating Encountered-Type of Haptic Devices Failure Modes in VR », *in Proc. IEEE Conference on Virtual Reality*, 2022, pp. 1–10.

[232] S. G. Hart and L. E. Staveland, « Development of NASA-TLX (Task Load Index): Results of Empirical and Theoretical Research », *in Advances in Psychology*, vol. 52, 1988, pp. 139–183.

[233] S. Fani, S. Ciotti, and M. Bianchi, « Multi-cue haptic guidance through wearables for enhancing human ergonomics », *IEEE Trans. Haptics*, pp. 115–120, 2021.

[234] S. Khusro, B. Shah, I. Khan, and S. Rahman, « Haptic Feedback to Assist Blind People in Indoor Environment Using Vibration Patterns », *Sensors*, vol. 22, *1*, p. 361, 2022.

[235] J. Brooke *et al.*, « Sus-a quick and dirty usability scale », *Usability evaluation in industry*, vol. 189, *194*, pp. 4–7, 1996.

[236] N. K. Dim and X. Ren, « Investigation of suitable body parts for wearable vibration feedback in walking navigation », *International Journal of Human-Computer Studies*, vol. 97, pp. 34–44, 2017.

[237] M. Rossi, M. Bianchi, E. Battaglia, M. G. Catalano, and A. Bicchi, « Happro: a wearable haptic device for proprioceptive feedback », *IEEE Trans. Biomedical Engineering*, vol. 66, *1*, pp. 138–149, 2018.

[238] W. R. Provancher, M. R. Cutkosky, K. J. Kuchenbecker, and G. Niemeyer, « Contact location display for haptic perception of curvature and object motion », *The International Journal of Robotics Research*, vol. 24, *9*, pp. 691–702, 2005.

[239] S. Kanjanapas, C. M. Nunez, S. R. Williams, A. M. Okamura, and M. Luo, « Design and analysis of pneumatic 2-dof soft haptic devices for shear display », *IEEE Robotics and Automation Letters*, vol. 4, *2*, pp. 1365–1371, 2019.

[240] K. T. Yoshida, C. M. Nunez, S. R. Williams, A. M. Okamura, and M. Luo, « 3-dof wearable, pneumatic haptic device to deliver normal, shear, vibration, and torsion feedback », *in Proc. IEEE World Haptics Conf.*, 2019, pp. 97–102.

[241] A. Tirmizi, C. Pacchierotti, I. Hussain, G. Alberico, and D. Prattichizzo, « A perceptually-motivated deadband compression approach for cutaneous haptic feedback », *in Proc. IEEE Haptics Symposium (HAPTICS)*, 2016, pp. 223–228.

[242] M. A. Plaisier, W. M. B. Tiest, and A. M. Kappers, « Salient features in 3-d haptic shape perception », *Attention, Perception, & Psychophysics*, vol. 71, *2*, pp. 421–430, 2009.

[243] M. Aggravi, G. Sirignano, P. Robuffo Giordano, and C. Pacchierotti, « Decentralized control of a heterogeneous human-robot team for exploration and patrolling », *IEEE Trans. Automation Science and Engineering*, 2021.

[244] M. Aggravi, A. A. S. Elsherif, P. Robuffo Giordano, and C. Pacchierotti, « Haptic-enabled decentralized control of a heterogeneous human-robot team for search and rescue in partially-known environments », *IEEE Robotics and Automation Letters*, vol. 6, *3*, pp. 4843–4850, 2021.

[245] M. Aggravi, S. Scheggi, and D. Prattichizzo, « Evaluation of a predictive approach in steering the human locomotion via haptic feedback », *in Proc. IEEE/RSJ Int. Conf. Intelligent Robots and Systems*, 2015, pp. 597–602.

[246] G. Arechavaleta, J.-P. Laumond, H. Hicheur, and A. Berthoz, « On the nonholonomic nature of human locomotion », *Autonomous Robots*, vol. 25, *1-2*, pp. 25–35, 2008.

[247] C. De Wit, G. Bastin, and B. Siciliano, *Theory of robot control*. Springer-Verlag New York, Inc, 1996.

[248] S. Scheggi, M. Aggravi, and D. Prattichizzo, « Cooperative navigation for mixed human–robot teams using haptic feedback », *IEEE Trans. Human-Machine Systems*, vol. 47, *4*, pp. 462–473, 2016.

[249] B.-g. Jang and G. J. Kim, « Evaluation of grounded isometric interface for whole-body navigation in virtual environments », *Computer Animation and Virtual Worlds*, vol. 25, *5-6*, pp. 561–575, 2014.

[250] M. Okui, M. Kobayashi, Y. Yamada, and T. Nakamura, « Delta-type four-dof force-feedback device composed of pneumatic artificial muscles and magnetorheological clutch and its application to lid opening », *Smart Materials and Structures*, vol. 28, *6*, p. 064 003, 2019.

[251] M. Satler, C. A. Avizzano, and E. Ruffaldi, « Control of a desktop mobile haptic interface », *in IEEE World Haptics Conference (WHC)*, 2011, pp. 415–420.

[252] R. Kovacs, E. Ofek, M. Gonzalez Franco, *et al.*, « Haptic pivot: on-demand handhelds in vr », *in Proc.Annual ACM Symposium on User Interface Software and Technology*, 2020, pp. 1046–1059.

[253] A. J. Spiers and A. M. Dollar, « Design and evaluation of shape-changing haptic interfaces for pedestrian navigation assistance », *IEEE Trans. Haptics*, vol. 10, *1*, pp. 17–28, 2016.

[254] J. M. Walker, N. Zemiti, P. Poignet, and A. M. Okamura, « Holdable haptic device for 4-dof motion guidance », *in IEEE World Haptics Conference (WHC)*, 2019, pp. 109–114.

[255] M. Sarac, M. Solazzi, and A. Frisoli, « Design requirements of generic hand exoskeletons and survey of hand exoskeletons for rehabilitation, assistive, or haptic use », *IEEE Trans. haptics*, vol. 12, *4*, pp. 400–413, 2019.

[256] H. Iwata, H. Yano, F. Nakaizumi, and R. Kawamura, « Project feelex: adding haptic surface to graphics », *in Proc. the 28th annual conference on Computer graphics and interactive techniques*, 2001, pp. 469–476.

[257] I. Poupyrev, T. Nashida, S. Maruyama, J. Rekimoto, and Y. Yamaji, « Lumen: interactive visual and shape display for calm computing », *in ACM SIGGRAPH 2004 emerging technologies*, 2004, p. 17.

[258] K. Nakagaki, D. Fitzgerald, Z. Ma, L. Vink, D. Levine, and H. Ishii, « Inforce: bi-directional force/shape display for haptic interaction », *in Proc. the thirteenth international conference on tangible, embedded, and embodied interaction*, 2019, pp. 615–623.

[259] S. Follmer, D. Leithinger, A. Olwal, A. Hogge, and H. Ishii, « Inform: dynamic physical affordances and constraints through shape and object actuation. », *in Uist*, vol. 13, 2013, pp. 2501–988.

[260] M. Blackshaw, A. DeVincenzi, D. Lakatos, D. Leithinger, and H. Ishii, « Recompose: direct and gestural interaction with an actuated surface », *in Proc. Extended Abstracts on Human Factors in Computing Systems*, 2011, pp. 1237–1242.

[261] V. R. Mercado, M. Marchal, and A. Lécuyer, « "Haptics On-Demand": a survey on encountered-type haptic displays », *IEEE Trans. Haptics*, vol. 14, *3*, pp. 449–464, 2021.

[262] V. Mercado, M. Marchal, and A. Lécuyer, « Entropia: towards infinite surface haptic displays in virtual reality using encountered-type rotating props », *IEEE Trans. visualization and computer graphics*, vol. 27, *3*, pp. 2237–2243, 2019.

[263] R. Meguro, P. Ratsamee, T. Mashita, Y. Uranishi, and H. Takemura, « Frictionhaptics: encountered-type haptic device fortangential friction emulation », *in 2019 IEEE International Symposium on Mixed and Augmented Reality Adjunct (ISMAR-Adjunct)*, 2019, pp. 382–383.

[264] B. Araujo, R. Jota, V. Perumal, J. X. Yao, K. Singh, and D. Wigdor, « Snake charmer: physically enabling virtual objects », *in Proc. the TEI'16: Tenth International Conference on Tangible, Embedded, and Embodied Interaction*, 2016, pp. 218–226.

[265] L. Zhang, Y. Liu, H. Bai, *et al.*, « Robot-enabled tangible virtual assembly with coordinated midair object placement », *Robotics and Computer-Integrated Manufacturing*, vol. 79, p. 102 434, 2023.

[266] R. Suzuki, E. Ofek, M. Sinclair, D. Leithinger, and M. Gonzalez-Franco, « Hapticbots: distributed encountered-type haptics for vr with multiple shape-changing mobile robots », *in Proc. ACM Symposium on User Interface Software and Technology*, 2021, pp. 1269–1281.

[267] E. J. Gonzalez, P. Abtahi, and S. Follmer, « Reach+ extending the reachability of encountered-type haptics devices through dynamic redirection in vr », *in Proc. the 33rd Annual ACM Symposium on User Interface Software and Technology*, 2020, pp. 236–248.

[268] L. H. Kim and S. Follmer, « Swarmhaptics: haptic display with swarm robots », *in Proc. the 2019 CHI conference on human factors in computing systems*, 2019, pp. 1–13.

[269] M. Okada and Y. Nakamura, « Development of a cybernetic shoulder-a 3-dof mechanism that imitates biological shoulder motion », *IEEE Trans. Robotics*, vol. 21, *3*, pp. 438–444, 2005.

[270] Y.-J. Kim, J.-I. Kim, and W. Jang, « Quaternion joint: dexterous 3-dof joint representing quaternion motion for high-speed safe interaction », *in 2018 IEEE/RSJ International Conference on Intelligent Robots and Systems (IROS)*, IEEE, 2018, pp. 935–942.

[271] J. Yu, X. Dong, X. Pei, and X. Kong, « Mobility and singularity analysis of a class of two degrees of freedom rotational parallel mechanisms using a visual graphic approach », *Journal of Mechanisms and Robotics*, vol. 4, *4*, 2012.

[272] R. L. P. Barreto, F. V. Morlin, M. B. de Souza, A. P. Carboni, and D. Martins, « Multiloop origami inspired spherical mechanisms », *Mechanism and Machine Theory*, vol. 155, p. 104 063, 2021.

[273] K. Minamizawa, S. Kamuro, N. Kawakami, and S. Tachi, « A palm-worn haptic display for bimanual operations in virtual environments », *in Proc. Intl. Conf. Human Haptic Sensing and Touch Enabled Computer Applications*, 2008, pp. 458–463.

[274] D. Trinitatova and D. Tsetserukou, « Touchvr: a wearable haptic interface for vr aimed at delivering multi-modal stimuli at the user's palm », *in Proc, SIGGRAPH Asia XR*, 2019, pp. 42–43.

[275] D. Trinitatova and D. Tsetserukou, « Deltatouch: a 3d haptic display for delivering multimodal tactile stimuli at the palm », *in Proc. IEEE World Haptics Conference (WHC)*, 2019, pp. 73–78.

[276] M. Altamirano Cabrera and D. Tsetserukou, « Linkglide: a wearable haptic display with inverted five-bar linkages for delivering multi-contact and multi-modal tactile stimuli », *in Proc. International AsiaHaptics Conference*, 2018, pp. 149–154.

[277] M. Dragusanu, A. Villani, D. Prattichizzo, and M. Malvezzi, « Design of a wearable haptic device for hand palm cutaneous feedback », *Frontiers in Robotics and AI*, p. 254, 2021.

[278] M. A. Cabrera, J. Tirado, J. Heredia, and D. Tsetserukou, « Linkglide-s: a wearable multi-contact tactile display aimed at rendering object softness at the palm with impedance control in vr and telemanipulation », *arXiv preprint arXiv:2208.14149*, 2022.

[279] L. Sciavicco and B. Siciliano, *Modelling and control of robot manipulators*. Springer Science & Business Media, 2001.

[280] S.-F. Chen and I. Kao, « Conservative congruence transformation for joint and cartesian stiffness matrices of robotic hands and fingers », *The International Journal of Robotics Research*, vol. 19, *9*, pp. 835–847, 2000.

[281] N. Ciblak and H. Lipkin, « Asymmetric cartesian stiffness for the modelling of compliant robotic systems », *in International Design Engineering Technical Conferences and Computers and Information in Engineering Conference*, American Society of Mechanical Engineers, vol. 12860, 1994, pp. 197–204.

[282] J. P. Merlet, « Jacobian, Manipulability, Condition Number, and Accuracy of Parallel Robots », *Journal of Mechanical Design*, vol. 128, *1*, pp. 199–206, 2005.

[283] M. Marchal and C. Pacchierotti, « Virtual reality and haptics », *in Robotics Goes MOOC*, B. Siciliano, Ed., Springer Cham, 2023.

[284] E. Whitmire, H. Benko, C. Holz, E. Ofek, and M. Sinclair, « Haptic revolver: touch, shear, texture, and shape rendering on a reconfigurable virtual reality controller », *in Proc. CHI conference on human factors in computing systems*, 2018, pp. 1–12.

[285] X. de Tinguy, C. Pacchierotti, M. Marchal, and A. Lecuyer, « Toward universal tangible objects: optimizing haptic pinching sensations in 3d interaction », *in Proc. IEEE Conference on Virtual Reality and 3D User Interfaces (VR)*, 2019, pp. 321–330.

[286] B. Woodward and M. Kashtalyan, « Three-dimensional elasticity solution for bending of transversely isotropic functionally graded plates », *European J. Mechanics-A/Solids*, vol. 30, *5*, pp. 705–718, 2011.

[287] L. Kuang, Y. Lou, and S. Song, « Design and fabrication of a novel force sensor for robot grippers », *IEEE Sensors Journal*, vol. 18, *4*, pp. 1410–1418, 2017.

[288] S. Robinson, P. Eslambolchilar, and M. Jones, « Evaluating haptics for information discovery while walking », *People and Computers XXIII Celebrating People and Technology*, pp. 93–102, 2009.

[289] D. Gallo, S. Shreepriya, and J. Willamowski, « Runahead: exploring head scanning based navigation for runners », *in Proceedings of the 2020 CHI Conference on Human Factors in Computing Systems*, 2020, pp. 1–13.

[290] J. Abich, J. Parker, J. S. Murphy, and M. Eudy, « A review of the evidence for training effectiveness with virtual reality technology », *Virtual Reality*, vol. 25, *4*, pp. 919–933, 2021.

[291] U. Radhakrishnan, K. Koumaditis, and F. Chinello, « A systematic review of immersive virtual reality for industrial skills training », *Behaviour & Information Technology*, vol. 40, *12*, pp. 1310–1339, 2021.

[292] R. Khan, J. Plahouras, B. C. Johnston, M. A. Scaffidi, S. C. Grover, and C. M. Walsh, « Virtual reality simulation training in endoscopy: a cochrane review and meta-analysis », *Endoscopy*, vol. 51, *07*, pp. 653–664, 2019.

[293] D. B. Mekbib, J. Han, L. Zhang, *et al.*, « Virtual reality therapy for upper limb rehabilitation in patients with stroke: a meta-analysis of randomized clinical trials », *Brain injury*, vol. 34, *4*, pp. 456–465, 2020.

[294] M. Slater, « Immersion and the illusion of presence in virtual reality », *British Journal of Psychology*, vol. 109, *3*, pp. 431–433, 2018.

[295] G. Makransky and G. B. Petersen, « The cognitive affective model of immersive learning (camil): a theoretical research-based model of learning in immersive virtual reality », *Educational Psychology Review*, vol. 33, *3*, pp. 937–958, 2021.

[296] J. Kreimeier, S. Hammer, D. Friedmann, *et al.*, « Evaluation of different types of haptic feedback influencing the task-based presence and performance in virtual reality », *in Proc. 12th ACM International Conference on Pervasive Technologies Related to Assistive Environments*, 2019, pp. 289–298.

[297] T. Howard, M. Marchal, A. Lécuyer, and C. Pacchierotti, « Pumah: pan-tilt ultrasound mid-air haptics for larger interaction workspace in virtual reality », *IEEE Trans. Haptics*, vol. 13, *1*, pp. 38–44, 2019.

[298] C. G. Christou, D. Michael-Grigoriou, D. Sokratous, and M. Tsiakoulia, « Buzzwirevr: an immersive game to supplement fine-motor movement therapy. », *in ICAT-EGVE*, 2018, pp. 149–156.

[299] U. Radhakrishnan, F. Chinello, and K. Koumaditis, « Investigating the effectiveness of immersive vr skill training and its link to physiological arousal », *Virtual Reality*, pp. 1–25, 2022.

[300] E. M. Overtoom, T. Horeman, F.-W. Jansen, J. Dankelman, and H. W. Schreuder, « Haptic feedback, force feedback, and force-sensing in simulation training for laparoscopy: a systematic overview », *Journal of surgical education*, vol. 76, *1*, pp. 242–261, 2019.

[301] K. Rangarajan, H. Davis, and P. H. Pucher, « Systematic review of virtual haptics in surgical simulation: a valid educational tool? », *Journal of surgical education*, vol. 77, *2*, pp. 337–347, 2020.

[302] M. S. Islam and S. Lim, « Vibrotactile feedback in virtual motor learning: a systematic review », *Applied Ergonomics*, vol. 101, 2022.

[303] P. Carlson, A. Peters, S. B. Gilbert, J. M. Vance, and A. Luse, « Virtual training: learning transfer of assembly tasks », *IEEE Trans. Visualization and Computer Graphics*, vol. 21, *6*, pp. 770–782, 2015.

[304] G. Yin, M. J.-D. Otis, P. E. Fortin, and J. R. Cooperstock, « Evaluating multimodal feedback for assembly tasks in a virtual environment », *Proc. ACM on Human-Computer Interaction*, vol. 3, *EICS*, pp. 1–11, 2019.

[305] M. M. Bradley and P. J. Lang, « Measuring emotion: the self-assessment manikin and the semantic differential », *Journal of behavior therapy and experimental psychiatry*, vol. 25, *1*, pp. 49–59, 1994.

[306] A. Betella and P. F. Verschure, « The affective slider: a digital self-assessment scale for the measurement of human emotions », *PloS one*, vol. 11, *2*, 2016.

[307] J. T. Cacioppo, L. G. Tassinary, and G. Berntson, *Handbook of psychophysiology*. Cambridge university press, 2007.

[308] R. M. Yerkes and J. D. Dodson, « The relation of strength of stimulus to rapidity of habit-formation », *Journal of Comparative Neurology and Psychology*, vol. 18, *5*, pp. 459–482, 1908.

[309] J. Storbeck and G. L. Clore, « Affective arousal as information: how affective arousal influences judgments, learning, and memory », *Social and personality psychology compass*, vol. 2, *5*, pp. 1824–1843, 2008.

[310] J. A. Bargh and J. L. Cohen, « Mediating factors in the arousal-performance relationship », *Motivation and Emotion*, vol. 2, *3*, pp. 243–257, 1978.

[311] J. L. Plass and S. Kalyuga, « Four ways of considering emotion in cognitive load theory », *Educational Psychology Review*, vol. 31, *2*, pp. 339–359, 2019.

[312] K. Koumaditis, F. Chinello, and S. Venckute, « Design of a virtual reality and haptic setup linking arousals to training scenarios: a preliminary stage », *in IEEE Conference on Virtual Reality and 3D User Interfaces (VR)*, 2018, pp. 1–2.

[313] U. Radhakrishnan, K. Koumaditis, and F. Chinello, « Investigating haptic feedback and arousal for motor skill training in virtual reality », *in Haptics: Science, Technology, Applications: 13th International Conference on Human Haptic Sensing and Touch Enabled Computer Applications (EuroHaptics), Proceedings*, Springer Nature, 2022, p. 472.

[314] E. Gatti, G. Caruso, M. Bordegoni, and C. Spence, « Can the feel of the haptic interaction modify a user's emotional state? », *in World Haptics Conference (WHC)*, 2013, pp. 247–252.

[315] Akshita, H. Alagarai Sampath, B. Indurkhya, E. Lee, and Y. Bae, « Towards multimodal affective feedback: interaction between visual and haptic modalities », *in Proc. 33rd Annual ACM Conference on Human Factors in Computing Systems*, Seoul, Republic of Korea, 2015, pp. 2043–2052.

[316] J. K. Gibbs, M. Gillies, and X. Pan, « A comparison of the effects of haptic and visual feedback on presence in virtual reality », *International Journal of Human-Computer Studies*, vol. 157, 2022.

[317] N. Cooper, F. Milella, C. Pinto, I. Cant, M. White, and G. Meyer, « The effects of substitute multisensory feedback on task performance and the sense of presence in a virtual reality environment », *PloS one*, vol. 13, *2*, 2018.

[318] M. Zhou, D. Jones, S. Schwaitzberg, and C. Cao, « Role of haptic feedback and cognitive load in surgical skill acquisition », *in Proc. Human Factors and Ergonomics Society Annual Meeting*, vol. 51, 2007, pp. 631–635.

[319] C. Ramırez-Fernández, A. L. Morán, and E. Garcıa-Canseco, « Haptic feedback in motor hand virtual therapy increases precision and generates less mental workload », *in Conf. Pervasive Computing Technologies for Healthcare (PervasiveHealth)*, 2015, pp. 280–286.

[320] B. Weber, M. Sagardia, T. Hulin, and C. Preusche, « Visual, vibrotactile, and force feedback of collisions in virtual environments: effects on performance, mental workload and spatial orientation », *in International Conference on Virtual, Augmented and Mixed Reality*, 2013, pp. 241–250.

[321] P.-A. Cabaret, T. Howard, C. Pacchierotti, M. Babel, and M. Marchal, « Perception of spatialized vibrotactile impacts in a hand-held tangible for virtual reality », *in International Conference on Human Haptic Sensing and Touch Enabled Computer Applications*, 2022, pp. 264–273.

[322] M. Aggravi, F. Pausé, P. R. Giordano, and C. Pacchierotti, « Design and evaluation of a wearable haptic device for skin stretch, pressure, and vibrotactile stimuli », *IEEE Robotics and Automation Letters*, vol. 3, *3*, pp. 2166–2173, 2018.

[323] E. Basalp, P. Wolf, and L. Marchal-Crespo, « Haptic training: which types facilitate (re) learning of which motor task and for whom answers by a review », *IEEE Trans. Haptics*, 2021.

[324] S. G. Hart and L. E. Staveland, « Development of nasa-tlx (task load index): results of empirical and theoretical research », *in Advances in psychology*, vol. 52, Elsevier, 1988, pp. 139–183.

[325] M. Granato, D. Gadia, D. Maggiorini, and L. A. Ripamonti, « Software and hardware setup for emotion recognition during video game fruition », *in Proc. 4th EAI International Conference on Smart Objects and Technologies for Social Good*, 2018, pp. 19–24.

[326] G. Makransky, L. Lilleholt, and A. Aaby, « Development and validation of the multimodal presence scale for virtual reality environments: a confirmatory factor analysis and item response theory approach », *Computers in Human Behavior*, vol. 72, pp. 276–285, 2017.

[327] J. J. Braithwaite, D. G. Watson, R. Jones, and M. Rowe, « A guide for analysing electrodermal activity (eda) & skin conductance responses (scrs) for psychological experiments », *Psychophysiology*, vol. 49, *1*, pp. 1017–1034, 2013.

[328] R. Orsila, M. Virtanen, T. Luukkaala, *et al.*, « Perceived mental stress and reactions in heart rate variability—a pilot study among employees of an electronics company », *International Journal of Occupational Safety and Ergonomics*, vol. 14, *3*, pp. 275–283, 2008.

[329] D. Narciso, M. Melo, J. V. Raposo, J. Cunha, and M. Bessa, « Virtual reality in training: an experimental study with firefighters », *Multimedia Tools and Applications*, vol. 79, *9*, pp. 6227–6245, 2020.

[330] C. Collet, C. Petit, A. Priez, and A. Dittmar, « Stroop color–word test, arousal, electrodermal activity and performance in a critical driving situation », *Biological psychology*, vol. 69, *2*, pp. 195–203, 2005.

[331] C. Krogmeier, C. Mousas, and D. Whittinghill, « Human–virtual character interaction: toward understanding the influence of haptic feedback », *Computer Animation and Virtual Worlds*, vol. 30, *3-4*, 2019.

[332] J. J. Abbott, P. Marayong, and A. M. Okamura, « Haptic virtual fixtures for robot-assisted manipulation », *in Robotics research*, 2007, pp. 49–64.

[333] F. Chinello, C. Pacchierotti, J. Bimbo, N. G. Tsagarakis, and D. Prattichizzo, « Design and evaluation of a wearable skin stretch device for haptic guidance », *IEEE Robotics and Automation Letters*, vol. 3, *1*, pp. 524–531, 2017.

[334] A. Prabhu, W. Smith, Y. Yurko, C. Acker, and D. Stefanidis, « Increased stress levels may explain the incomplete transfer of simulator-acquired skill to the operating room », *Surgery*, vol. 147, *5*, pp. 640–645, 2010.

[335] J. A. Quick, A. D. Bukoski, J. Doty, B. J. Bennett, M. Crane, and S. L. Barnes, « Objective measurement of clinical competency in surgical education using electrodermal activity », *Journal of Surgical Education*, vol. 74, *4*, pp. 674–680, 2017.

[336] D. Wu, C. G. Courtney, B. J. Lance, *et al.*, « Optimal arousal identification and classification for affective computing using physiological signals: virtual reality stroop task », *IEEE Trans. Affective Computing*, vol. 1, *2*, pp. 109–118, 2010.

[337] S. Grassini, K. Laumann, and M. Rasmussen Skogstad, « The use of virtual reality alone does not promote training performance (but sense of presence does) », *Frontiers in psychology*, vol. 11, p. 1743, 2020.

[338] Y. Y. Yurko, M. W. Scerbo, A. S. Prabhu, C. E. Acker, and D. Stefanidis, « Higher mental workload is associated with poorer laparoscopic performance as measured by the nasa-tlx tool », *Simulation in healthcare*, vol. 5, *5*, pp. 267–271, 2010.

[339] A. Bandura, « The explanatory and predictive scope of self-efficacy theory », *J. social and clinical psychology*, vol. 4, *3*, p. 359, 1986.

[340] D. Stevens, D. I. Anderson, N. J. O'Dwyer, and A. M. Williams, « Does self-efficacy mediate transfer effects in the learning of easy and difficult motor skills? », *Consciousness and cognition*, vol. 21, *3*, pp. 1122–1128, 2012.

[341] L. Kuang, M. Ferro, M. Malvezzi, *et al.*, « A wearable haptic device for the hand with interchangeable end-effectors », *IEEE Transactions on Haptics*, 2023.

COLLEGE DOCTORAL BRETAGNE
MATHS, TELECOMS
INFORMATIQUE, SIGNAL
SYSTEMES, ELECTRONIQUE

Université de Rennes

Titre : Interfaces haptiques non fondées pour le guidage et le rendu d'interaction

Mot clés : haptique, l' interaction, le rendu

Résumé : Les systèmes haptiques de terrain jouent un rôle clé dans l'interaction homme-robot-environnement, les défis résident dans le développement de ces dispositifs, y compris la conception mécatronique, les algorithmes de rendu haptique, et la compréhension de la perception haptique. Dans cette thèse, nous présentons la conception de plusieurs dispositifs haptiques non ancrés (portables et de poche) capables de générer diverses sensations tactiles pour les humains dans le cadre d'applications de navigation et de rendu de l'environnement. Dans la première contribution, nous explorons le développement d'un dispositif cutané de port de positions corporelles multiples pour l'application d'un retour d'information sur la position et l'emplacement dans des scénarios de navigation. Dans la deuxième contribution, nous présentons la conception d'un mécanisme parallèle contraint pour le rendu haptique kinesthésique pour le guidage des mouvements de la main et le rendu tactile de type rencontre. Dans la troisième contribution, nous présentons un ensemble de dispositifs palmaires montés sur la main avec des effecteurs terminaux interchangeables, qui inspirent également l'exploration de matériaux souples et déformables pour le rendu des sensations tactiles. Enfin, nous étudions l'efficacité du retour haptique pour l'entraînement des capacités motrices en réalité virtuelle.

Title: Ungrounded Haptic Interfaces for Guidance and Interaction Rendering

Keywords: haptics, interaction, rendering

Abstract: Unground haptic systems play a key role in the human-robot-environment interaction, the challenges lie in the development of these devices, including the mechatronic design, haptic rendering algorithms, and the understanding of haptic perception. In this thesis, we present the design of multiple ungrounded (wearable and handheld) haptic devices able to generate diverse touch sensations for the human for the application of navigation and rendering environment. In the first contribution, we explore the development of multiple-body-position wear cutaneous device for applying position/location feedback in navigation scenarios. In the second contribution, we present the design of constrained parallel mechanism for kinesthetic haptic rendering for hand motion guidance and encounter-type touch rendering. In the third contribution, we present a set of hand-mounted palmar devices with interchangeable end-effectors, which also inspire the exploration of soft and deformable materials for touch sensation rendering. Finally, we study the effectiveness of haptic feedback for motor skill training in virtual reality.